UNIVERSITEIT VAN PRETORIA
UNIVERSITY OF PRETORIA
YUNIBESITHI YA PRETORIA
Denkleiers • Leading Minds • Dikgopolo tša Dihlalefi

Characterisation of semi-volatile hydrocarbon emissions from diesel engines

By

Amanda Sonto Mahlangu

Submitted in partial fulfilment of the requirements for the degree

Master of Science (Chemistry)

In the Department of Chemistry, Faculty of Natural & Agricultural Sciences
University of Pretoria

October 2021

Supervisor: Prof P.B.C. Forbes
Co Supervisor: Mr P.W. Schaberg

Declaration

I, Amanda Sonto Mahlangu, declare that the dissertation, which I hereby submit for the degree Master of Science at the University of Pretoria, is my own work and has not previously been submitted by me for a degree at this or any other tertiary institution.

Signature: 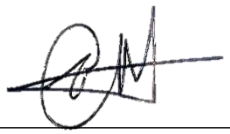 Date: 2021-07-09

Summary

Diesel exhaust emissions from vehicles have been receiving global attention, due to the potential human health and negative environmental effects associated with exposure to emitted pollutants. Air pollutants emitted by diesel engines include hydrocarbons which, despite very low concentrations in the exhaust, may act as precursors in the formation of secondary pollutants such as photochemical ozone and secondary organic aerosols, which play a vital role in photochemical smog pollution.

The environmental impact of diesel engines is poorly quantified and understood, with much debate on the role played by emitted semi-volatile organic compounds (SVOCs). Research shows that while short chain hydrocarbons (HCs), typically emitted by petrol vehicles, are easier to characterise and have been successfully reduced in many cities, longer chain semi-volatile hydrocarbons, such as those emitted by diesel vehicles, are typically not considered as part of air quality control strategies, and a limited range of these hydrocarbons have been studied.

Development of an ideal method for collection, analysis and characterisation of SVOCs emitted by diesel engines is thus necessary to determine the link between these emissions and photochemical smog. The implementation of increasingly stringent emission limits also brings about the need for a method to determine the effect of emissions control technology, i.e. fuel formulation, catalytic systems and engine technology. An emissions monitoring campaign was therefore conducted in this study under controlled laboratory conditions, using a Euro 3 compliant 1.6 L passenger car diesel engine, operating over a standard test cycle typical of urban driving conditions. Cold and hot start emissions tests were performed using three different fuels (a paraffinic diesel, a South African market diesel, and a European reference diesel). Changes in emissions at different speed phases as well as the role played by exhaust aftertreatment technology on emissions control was also investigated.

During testing, a portion (1/100) of the exhaust was diluted with compressed air within a partial flow dilution system, and simultaneous sampling of the diluted gaseous and particulate exhaust emissions was achieved by means of portable denuder sampling

devices consisting of a quartz fibre filter sandwiched between two multi-channel polydimethylsiloxane traps. Instrumental analysis of the traps was performed by thermal desorption-two dimensional gas chromatography-time of flight mass spectrometry and targeted analysis of 43 compounds (30 aromatic HCs and 13 n-alkanes) was conducted.

It was found that the South African market diesel had the highest total n-alkane emissions (26.91 – 255.71 mg/km from the extra high to the low phase), followed by the paraffinic diesel (34.77 – 162.05 mg/km) and the European reference diesel (21.63 – 63.97 mg/km). Qualitative analysis of the fuels' alkylbenzene emissions was conducted and the European reference diesel had the highest emission factors followed by the South African market diesel and paraffinic diesel, respectively. In addition, for the fuels containing aromatic compounds (SAM10 and EUR10), 1-methyl-3-ethylbenzene, 1-methyl-4-ethylbenzene, 1,3,5-trimethylbenzene, 1-methyl-2-ethylbenzene, 1,2,4-trimethylbenzene, 1,2,4,5-tetramethylbenzene, 1-methyl-3n-propylbenzene and n-butylbenzene were found in high abundance in the emissions, which was strongly reflective of the fuels which contained 6% and 4% of C_9 and C_{10} compounds respectively. A decrease in emissions was observed with increasing periods of engine operation (low to extra high speed phases). The presence of exhaust aftertreatment technology, such as a diesel oxidation catalyst and diesel particulate filter, resulted in lower hydrocarbon emissions, particularly in the high and extra high speed phases. The observed changes in emissions could be correlated to the fuel composition, fuel physical properties and engine operating conditions.

The developed method illustrated the suitability of denuder samplers and thermal desorption-two dimensional gas chromatography-mass spectrometry for the collection and analysis of photochemical smog forming SVOCs in dilute exhaust emissions. Emission factors were successfully calculated and it was illustrated how the ozone formation potential of emissions can be estimated from the calculated emission factors, which is critical in understanding elevated ozone levels in urban environments.

Acknowledgements

- I would like to express my deepest appreciation to my supervisor Prof Patricia Forbes for her expert guidance, constant encouragement and support throughout my project as well as being a model figure who played an integral role in my development as a young scientist from my undergraduate years. A special thanks to my co-supervisor Mr Paul Schaberg for your invaluable insight, coordinating our sampling campaigns and warm hospitality during our visits. My appreciation goes to Mr Mark Wattrus for his tireless assistance during the sampling campaigns.

- Many thanks to Dr Yvette Naude for her assistance during instrumental analysis and, Mr David Masemula for constructing the PDMS traps, and always preparing consumables to insure smooth running of the instrument, especially when I needed to work on weekends. I also wish to thank Genna-Leigh Schoonraad for her assistance with my preliminary study and answering all my questions with great enthusiasm.

- I would like to extend my appreciation to Sasol and the National Research Foundation for generously funding the study. I am grateful to the University of Pretoria for awarding me with a study bursary in the second year of my study. The Sasol Fuels Application Centre is thanked for kindly granting the use of their engine test facility and providing the necessary resources for testing. Sponsorships from Anatech and the International Mass Spectrometry Foundation, which allowed me to attend the Analitika conference and the International Mass Spectrometry School are highly appreciated.

- Thank you to my colleagues at the student office for lending a listening ear, their willingness to always assist and great office laughter. A special thanks to Kedibone Mashale for being a supportive friend, daily reminders to take breaks and leaving treats on my desk.

- To Clement Mashaba, I cannot begin to explain your importance in my life. Thank you for always standing by my side.

- Lastly I would like to thank my family for constantly supporting and checking up on me. uGogo for being my source of comfort, and to my loving mom, Annah Mtsweni; I am so thankful for your prayers, support and encouragement. You taught me from a very young age that “ifundo yiskhiya saksasa”. I am where I am today because of you.

Research outputs

Publications

- Mahlangu, A.S., Schaberg, P.W., Wattrus, M.C. & Forbes P.B.C 2020. Characterisation of semi-volatile hydrocarbon emissions from diesel engines. *Clean Air Journal*, 30 (1), 1-8. DOI: https://doi.org/10.17159/caj/2020/30/1.7672

Conference presentations

- Oral presentation: A.S., Mahlangu, P.W., Schaberg, M.C., Wattrus, and P.B.C., Forbes, “Characterisation of semi-volatile hydrocarbon emissions from diesel engines”, 2019 Conference of the National Association for Clean Air, 3-4 October 2019, Stellenbosch, South Africa (*Received prize for Best Student Paper*).

- Oral presentation: A.S., Mahlangu, P.W., Schaberg, M.C., Wattrus, and P.B.C., Forbes, “Characterisation of semi-volatile hydrocarbon emissions from diesel engines”, 2019 ChromSA Postgraduate Student Seminar, 26 September 2019, University of Johannesburg.

- Poster presentation: A.S., Mahlangu, G., Schoonraad, P.W., Schaberg, M.C., Wattrus, C., Munyeza, C., Pretorius, and PBC Forbes, “Hydrocarbon emissions from diesel engines under different load conditions”, 4th International Mass Spectrometry School, 15-20 September 2019, Barcelona, Spain.

- Poster presentation: A.S., Mahlangu, G., Schoonraad, P.W., Schaberg, M.C., Wattrus, C., Munyeza, C., Pretorius, and P.B.C., Forbes, “Hydrocarbon emissions from diesel engines under different load conditions”, 2018 Analitika Conference, 22-25 July 2018, Limpopo.

Table of Contents

Declaration i
Summary ii
Acknowledgements iv
Research outputs vi
Publications vi
Conference proceedings vi
List of figures x
List of tables xiv
Abbreviations xv
Chapter 1: Introduction 1
1.1 Photochemical smog 2
1.1.1 Photochemical ozone 2
1.1.2 Secondary organic aerosols 3
1.2 The role played by vehicular engine emissions 4
1.3 Problem statement 5
1.4 Justification for study 5
1.5 Aim and objectives of study 5
1.5.1 Aim 5
1.5.2 Objectives 5
1.6 Dissertation outline 6
1.7 References 7
Chapter 2: Literature Review 9
2.1 Introduction 9
2.2 The diesel combustion engine 10
2.3 Diesel exhaust emissions 11
2.4 Diesel exhaust aftertreatment systems 14
2.5 Consequences of diesel exhaust emissions 15
2.5.1 Health effects 15
2.5.2 Environmental effects 16
2.5.2.1 Secondary organic aerosols 17
2.5.2.2 Photochemical ozone 19
2.6 Statistics on diesel use in South Africa 22
2.7 Regulation of air pollutants in South Africa 24

2.8 Hydrocarbon classes relevant to this study 28
2.8.1 Review of previous work on sampling and analysis of SVOCs 28
2.8.2 Estimating the ozone formation potential of diesel exhaust hydrocarbons 30
2.9 Characterising engine exhaust emissions 34
2.9.1 Engine emission test procedures 34
2.9.2 Techniques used for sampling of PM and SVOC exhaust emissions 36
2.10 Techniques for the compositional analysis of organic compounds in diesel exhaust emissions 38
2.10.1 Sample introduction methods 38
2.10.2 Separation and detection methods 40
2.11 References 43
Chapter 3: Experimental methods and materials 49
3.1 Identifying semi-volatile hydrocarbons of relevance to the study: hydrocarbons that play a role in photochemical ozone formation 49
3.1.1 Selecting target hydrocarbons 49
3.1.2 Preliminary study: Identifying hydrocarbons in diesel exhaust samples 49
3.2 Emissions testing 51
3.2.1 Test cell setup 51
3.2.2 Driving cycle and test fuels 55
3.2.3 Sampling campaign one 58
3.2.3.1 Preparation of PDMS traps and quartz fibre filters 58
3.2.3.2 Collection of background air samples 59
3.2.3.3 Steady state tests: optimization studies 59
3.2.3.4 Transient cycle tests 61
3.2.3.5 Low phase emissions tests 62
3.2.4 Sampling campaign two 64
3.2.4.1 Background air samples 64
3.2.4.2 Cold start transient tests 64
3.2.4.3 Investigating the effect of exhaust aftertreatment systems 65
3.3 Instrumental analysis 66
3.4 Characterisation of target hydrocarbons 69
3.4.1 n-Alkane hydrocarbons 69
3.4.1.1 Preparation of n-alkane calibration solutions and internal standards 69
3.4.1.2 Linear regression analysis and determination of detection and quantification limits. 69
3.4.2 Alkylbenzene hydrocarbons 72
3.5 Identification of target analytes 73
3.6 Calculation of hydrocarbon emission factors and ozone-formation potentials . 73
3.7 References 75
Chapter 4: Results and Discussion 76
4.1 Preliminary study: Identifying target hydrocarbons in diesel exhaust samples 76
4.2 Method validation 81
4.3 Comparison of engine exhaust hydrocarbon emissions 87

4.3.1 Optimization studies: Steady state tests 87
4.3.1.1 Breakthrough studies and selection of sampler configuration 87
4.3.1.2 Optimization of the instrumental analysis method 91
4.4 The role of two dimensional gas chromatography and mass spectrometry for engine exhaust emission speciation 94
4.5 Comparison of exhaust emissions from different fuels 100
4.5.1 Cold start emissions testing using different fuels 101
4.5.1.1 n-Alkane emissions 101
4.5.1.2 Aromatic hydrocarbon emissions 103
4.5.2 Hydrocarbon emissions at different speed phases of the WLTC test cycle 115
4.5.3 Target hydrocarbon emissions compared to other gaseous emissions 120
4.5.4 Comparison of cold start and hot start hydrocarbon emissions 122
4.5.5 The effect of exhaust aftertreatment technology 127
4.6 Ozone formation potential of different fuels 132
4.7 References 135
Chapter 5: Conclusions and future work 137
5.1 Limitations of the study 139
5.2 Recommendations for future work 140
Appendices 142
Appendix A: Example 2D and 3D chromatograms of test fuel emissions 142
Appendix B: The Unresolved Complex mixture 148
Appendix C: Example sampling information sheet 150
Appendix D: Certificates Of Analysis 151
(i) C_8-C_{20} n-alkane standard solution COA 151
(ii) D_{34}-hexadecane internal standard COA 152
(iii) DHA aromatic standard COA 153
Appendix E: Calibration curves for PDMS trap 156
Appendix F: Poster presentation 158
Appendix G: Publication 159

List of figures

Figure 1.1. National Ambient Air Quality monitoring network consisting of 136 national, provincial and municipal monitoring stations. 2
Figure 2.1 Regions of pollutant production in a combustion chamber with a heterogeneous air/fuel mixture 14
Figure 2.2 Products of atmospheric oxidation reactions that are constituents of photochemical smog 17
Figure 2.3 Competing atmospheric oxidative pathways for the toluene-OH adduct . 22
Figure 2.4 Total number of new vehicle sales in South Africa from 2007-2016..... 23
Figure 2.5 The petrol and diesel consumption in South Africa from 2007-2016. 23
Figure 2.6 The total fuel sales in South Africa for the year 2018. 24
Figure 2.7 Change in $PM_{2.5}$ levels from the year 2007 to 2016 in the Vaal Triangle Priority Area. 27
Figure 2.8 Change in O_3 levels monitored from December 2016 to May 2018 in the Vaal Triangle Priority Area. 28
Figure 3.1 Process of selecting the target compounds relevant for the study. 51
Figure 3.2 Schematic diagram showing the denuder setup employed during exhaust emission sampling. 53
Figure 3.3 Test cell setup. 54
Figure 3.4 Schematic diagram of the test cell setup *(*not drawn to scale)*. 55
Figure 3.5 Speed profile of the WLTC driving cycle used during emissions testing. 56
Figure 3.6 Chemical composition of the test fuels. The paraffinic (blue) and aromatic (orange) fractions of each fuel have been illustrated. 57
Figure 3.7 Sampler setup during the steady state emissions tests. 60
Figure 3.8 Sampler setup during the transient cycle emissions tests. 62
Figure 3.9 Outline of methods used to prepare calibration standards and internal standard solutions. 70
Figure 4.1 A comparison of the tentatively identified HC peak areas from the exhaust engine emissions of a 1.6 L test engine, fuelled with ultra-low sulphur (ULS) diesel. 77
Figure 4.2 Extracted ion 2D chromatogram (m/z = 57) showing the aliphatic hydrocarbon region observed from the analysis of primary traps used to sample diesel engine exhaust emissions during operating modes M1-M5 (a-e). 79

Figure 4.3 Six point calibration curves obtained for octane, nonane, hexadecane and eicosane (injected onto PDMS traps) with the respective linear equation and correlation coefficient indicated as well as the error bars calculated as the standard deviation between the two replicate standard solutions. 83
Figure 4.4 A comparison of the hydrocarbon levels found on the primary and secondary traps during the 5,10 and 30 min breakthrough studies for both the denuder and trap-trap sampler configurations where exhaust emissions were sampled with the test engine being operated under steady state conditions. 90
Figure 4.5 Extracted ion (m/z = 57, 91) 2D chromatograms of exhaust emissions collected onto PDMS traps from the steady state tests, analysed at a split ratio of 50:1 (a), and 100:1 (b). 92
Figure 4.6 Typical extracted ion (m/z = 57, 91) 2D chromatograms of the engine exhaust emissions sampled onto PDMS traps and analysed in solvent vent mode where a) shows a 2D chromatogram whilst b) is a contour plot view of the analytes. 94
Figure 4.7 Extracted ion 2D chromatogram (m/z = 105) of propylbenzene isomers identified in the DHA aromatic standard (1 µL injection from the 10^6 x dilution solution thermally desorbed from a PDMS trap). 97
Figure 4.8 Mass spectra of propylbenzene isomers identified in the DHA aromatic standard (1 µL injection from the 10^6 x dilution solution onto a PDMS trap) with differences in retention times highlighted. 99
Figure 4.9 n-Alkane HC emission factors for each fuel at different speed phases of the WLTC cycle. 104
Figure 4.10 Relative abundance of the alkylbenzene emissions from each fuel during the low speed phase of the WLTC cycle. 108
Figure 4.11 Relative abundance of the alkylbenzene emissions from each fuel during the medium speed phase of the WLTC cycle. 109
Figure 4.12 Relative abundance of the alkylbenzene emissions from each fuel during the high speed phase of the WLTC cycle. 110
Figure 4.13 Relative abundance of the alkylbenzene emissions from each fuel during the extra high speed phase of the WLTC cycle. 111
Figure 4.14 Sum of n-alkane hydrocarbon emissions for each fuel at different speed phases of the WLTC cycle. 119

Figure 4.15 Sum of alkylbenzene hydrocarbon emissions between the different phases of the WLTC cycle for different fuels. 119
Figure 4.16 Changes in THC, CO, CO_2, and NO_X emissions between the different phases of the WLTC cycle (1 = low phase, 2 = medium phase, 3 = high phase, 4 = extra-high phase) for all three test fuels. 121
Figure 4.17 A comparison of the total n-alkane HC emissions (determined by TD-GC x GC-TofMS) and THC emissions (determined by a FID gas analyzer) for each fuel at different speed phases of the WLTC cycle emissions. 122
Figure 4.18 Comparison of n-alkane cold start and hot start emissions for the SAM10 and EUR10 fuel. 124
Figure 4.19 a-d Comparison of alkylbenzene cold start and hot start emissions for the SAM10 and EUR10 fuel. 126
Figure 4.20 Concentrations of n-alkane associated with particulates from the cold and warm start NEDC emission. 127
Figure 4.21 n-Alkane hydrocarbon emissions with the DOC and DOC+DPF exhaust aftertreatment system configuration. 129
Figure 4.22 a-d Alkylbenzene emissions with the DOC and DOC+DPF exhaust aftertreatment system configuration sampled onto PDMS traps. 131
Figure 4.23 Quartz fibre filter used to collect particulate emissions with (A) and without (B) a diesel particulate filter in line. 132
Figure 4.24 Percentage ozone formation potential of each fuel as calculated from the n-alkane emission factors at each speed phase. 133
Figure A1 Extracted ion 3D chromatogram (m/z = 57 and 91) showing the n-alkane (red) and alkylbenzene (green) hydrocarbon region from analysis of exhaust emissions from the test engine fueled with PAR10 diesel sampled onto a PDMS trap. 142
Figure A2 Extracted ion 2D chromatogram (m/z = 57 and 91) showing the n-alkane (red) and alkylbenzene (green) hydrocarbon region from analysis of exhaust emissions from the test engine fueled with PAR10 diesel sampled onto a PDMS trap. 143
Figure A3 Extracted ion 3D chromatogram (m/z = 57 and 91) showing the n-alkane (red) and alkylbenzene (green) hydrocarbon region from analysis of exhaust emissions from the test engine fueled with SAM10 diesel sampled onto a PDMS trap. 144

Figure A4 Extracted ion 2D chromatogram (m/z = 57 and 91) showing the n-alkane (red) and alkylbenzene (green) hydrocarbon region from analysis of exhaust emissions from the test engine fueled with SAM10 diesel sampled onto a PDMS trap. 145
Figure A5 Extracted ion 3D chromatogram (m/z = 57 and 91) showing the n-alkane (red) and alkylbenzene(green) hydrocarbon region from analysis of exhaust emissions from the test engine fueled with EUR10 diesel sampled onto a PDMS trap. 146
Figure A6 Extracted ion 2D chromatogram (m/z = 57 and 91) showing the n-alkane (red) and alkylbenzene (green) hydrocarbon region from analysis of exhaust emissions from the test engine fueled with EUR10 diesel sampled onto a PDMS trap. 147
Figure B1 Extracted 1D ion chromatogram (m/z = 57) showing the unresolved complex mixture (UCM) that has been sampled onto a PDMS trap and speciated using 2D chromatography. 148
Figure B2 Extracted 2D ion chromatogram (m/z = 57) showing the unresolved complex mixture (UCM) that has been sampled onto a PDMS trap and speciated using 2D chromatography. 149

List of tables

Table 2.2 Hydrocarbon emission factors reported from diesel exhaust characterisation studies. 32
Table 4.1 Target compounds sorted by boiling point (°C) with their physical, reactivity and retention properties. 80
Table 4.1 Continued 81
Table 4.2 Method validation data and limits of detection and quantitation for the n-alkanes present in diesel exhaust emissions sampled onto PDMS traps. 84
Table 4.3 n-Alkane detection limits when sampled onto PDMS traps during the low, medium, high and extra high speed phases. 85
Table 4.4 n-Alkane quantitation limits when sampled onto PDMS traps during the low, medium, high and extra high speed phases. 86
Table 4.5: Calculated n-alkane emission factors of each test fuel during different speed phases of the WLTC cycle. 105
Table 4.6 Aromatic hydrocarbon emission factors expressed as the peak area per km for each of the test fuels during the different speed phases of the WLTC cycle. 112
Table 4.7 Total ozone formation potential of the n-alkane emissions for each fuel during each phase of the WLTC cycle 133

Abbreviations

AA	Automobile Association
ARTEMIS	Assessment and Reliability of Transport Emission Models and Inventory Systems
CARB	California Air Resources Board
CIS	Cooled injection system
CRDPF	Continuously regenerating diesel particulate filter
CVS	Constant volume sampling
DCM	Dichloromethane
DOC	Diesel oxidation catalyst
DPF	Diesel particulate filter
DF	Dilution factor
DTD-GC x GC-TofMS	Direct thermal desorption- two dimensional gas chromatography-time of flight mass spectrometry
EBIR	Equal benefit incremental reactivity
EF	Emission factor
EGR	Exhaust gas recirculation
EIC	Extracted ion chromatogram
EPA	Environmental Protection Agency
FTP	Federal test procedure
GC-FID	Gas chromatography-flame ionisation detection
GC-MS	Gas chromatography-mass spectrometry
HC	Hydrocarbon
HPLC	High performance liquid chromatography
GC x GC-FID	Comprehensive two-dimensional gas chromatography-flame ionisation detection
IR	Incremental reactivity
IS	Internal standard
IVOC	Intermediate volatile organic compound
LOD	Limit of detection
LOD_{exh}	Limit of detection exhaust
LOD_{oc}	Limit of detection on column
LOQ	Limit of quantitation
LOQ_{exh}	Limit of quantitation exhaust
LOQ_{oc}	Limit of quantitation on column
MDLT	Mini dilution tunnel
MIR	Maximum incremental reactivity
MOIR	Maximum ozone incremental reactivity
NAAMSA	National Association of Automobile Manufacturers of South Africa
NAAQS	National Ambient Air Quality Standards
NRC	National Research Council
NEMAQA	National Environmental Management Air Quality Act
NMHC	Non-methane hydrocarbon
NOx	Nitrogen oxides
OFP	Ozone formation potential
PASE	Plunger assisted solvent extraction
PAH	Polycyclic aromatic hydrocarbon
PDMS	Polydimethylsiloxane

PF	Partial sampling factor
PM	Particulate matter
POCP	Potential ozone creation potential
PTR-MS	Proton transfer reaction- mass spectrometry
PUF	Polyurethane foam
SAPRC	Statewide Air Pollution Research Centre
SCR	Selective catalytic reduction
SFAC	Sasol Fuels Application Centre
SOA	Secondary organic aerosol
SR	Split ratio
SVOC	Semi-volatile organic compound
THC	Total hydrocarbon
UCM	Unspeciated complex mixture
ULS	Ultra-low sulphur
UNECE	United Nations Economic Commission for Europe
VOC	Volatile organic compound
WHO	World Health Organization
WLTC	World harmonized light vehicle test cycle

Chapter 1: Introduction

To date, ambient air pollution remains a major environmental and public health concern worldwide (Amegah and Agyei-Mensah, 2017, Anderson, 2009, Babatola, 2018, Jiang et al., 2016). Household, vehicular and industrial emissions may persist in the atmosphere or form potentially harmful secondary pollutants which can accumulate over extended periods. Exposure to these pollutants, can induce respiratory and cardiovascular diseases, aggravate bronchitis, asthma, and emphysema, and have been linked to high mortality or morbidity rates (WHO, 2000). Pollutants such as nitrogen oxides (NOx), sulphur dioxides (SOx), ozone (O_3), carbon monoxide (CO_2) and particulate matter (PM) are routinely monitored. Particles of a diameter < 10 µm (PM_{10}) and ultrafine particles with a diameter < 2.5 µm ($PM_{2.5}$) are the most commonly studied air pollutants, and are used as an indicator of pollutant exposure (WHO, 2006).

Increasingly stringent legislative standards continue to be developed in efforts to minimise the potential negative environmental impacts of these pollutants (Latha et al., 2019, Roberts et al., 2014). The World Health Organization (WHO) provides guidance on the limits of various pollutants that are known to have negative effects on human health; however, they do not factor in the socio-economic status of a particular country, thus each country sets national limits for criteria pollutants. In South Africa, National Ambient Air Quality Standards (NAAQS) were set for seven criteria pollutants under the National Environmental Management: Air Quality Act (NEMAQA), Act no. 39 of 2004. Monitoring of these pollutants is achieved using air quality monitoring stations situated in various areas, including those which are densely populated and highly impacted, to assess compliance to the air quality standards and assess human exposure (Figure 1.1). Exceedances of set standards are often recorded for certain pollutants including O_3 (Laban et al., 2018), which is the main focus of this study.

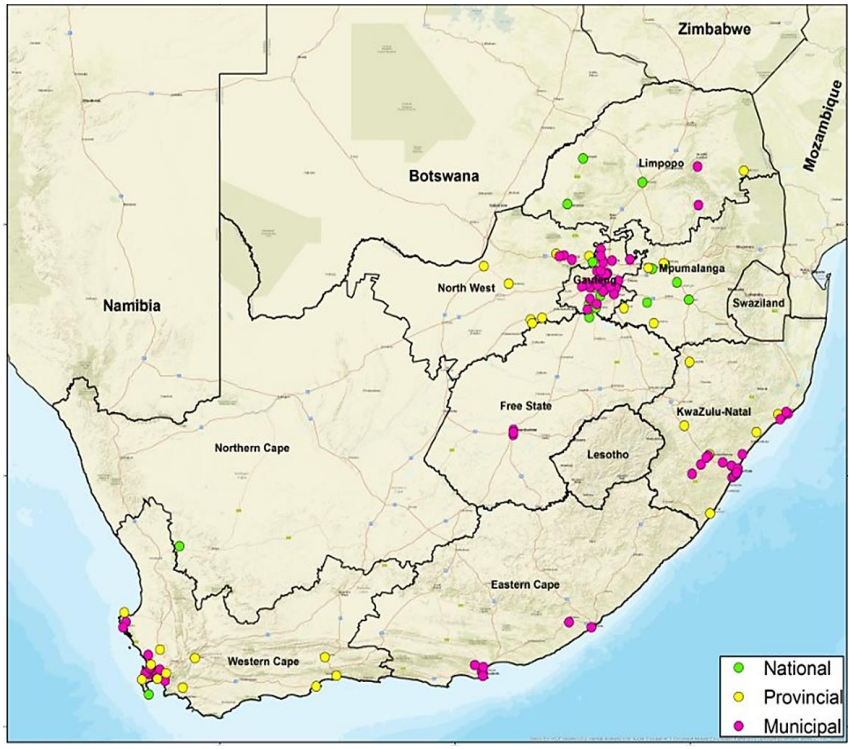

Figure 1.1. National Ambient Air Quality monitoring network consisting of 136 national, provincial and municipal monitoring stations *(Gwaze and Mashele, 2018)*.

1.1 Photochemical smog

Photochemical smog pollution is produced from the photochemical oxidation of ambient organic compounds and nitrogen oxides in the presence of ultraviolet sunlight. Often dubbed 'summer smog' it is typically seen as a brown-grey haze over highly populated (high traffic) cities with relatively warm climates. Photochemical ozone and secondary organic aerosols (SOAs) are the main constituents of photochemical smog (Gentner et al., 2017, Laban et al., 2018, Whitten, 1983).

1.1.1 Photochemical ozone

Photochemical ozone is produced in the lower atmosphere (troposphere) from the reaction of nitrogen oxides (NOx) and volatile organic compounds (VOCs), in the presence of ultraviolet sunlight (Haagen-Smit and Fox, 1954). During a smog chamber irradiation study, it was found that at any given NOx concentration or irradiation time, decreasing the VOC concentration reduced O_3 formation (Glasson, 1981). The effect of NOx concentration on ozone formation however, was more complex as it was seen that reducing the NOx levels may either increase or decrease O_3 formation depending on the irradiation time and hydrocarbon (HC) concentration. Reducing the HC and NOx concentrations simultaneously lead to a decrease in O_3, however this decrease

was less than the reduction observed from VOC reduction alone. These results demonstrate the importance of controlling VOC levels in the atmosphere for potential O_3 reduction in urban areas.

The detrimental health and environmental impacts of photochemical O_3 include reduced visibility, eye irritation, a decline in respiratory function, aggravation of heart disease, reduced resistance pulmonary function, pneumonia and damage to rubber, fabrics, crops and vegetation which is a major setback in industry (Field et al., 1992, Laban et al., 2018, Zunckel et al., 2004).

1.1.2 Secondary organic aerosols

SOAs are formed when low volatility organic species partition into the condensed phase and react with oxidising species, such as hydroxyl radicals, nitrate radicals and ozone (Kroll and Seinfeld, 2008, Robinson et al., 2007). The formation of SOAs from anthropogenic emissions has been estimated to be small, however measurements of ambient levels illustrate that SOAs are higher than what is predicted by emission models, and that anthropogenic emissions might be major contributors to the levels observed.

Exposure to these fine aerosols has negative implications on human health owing to the small size of these particulates (Gentner et al., 2017). There are very few studies that report on the health effects of SOAs, due to the lack of suitable particle exposure techniques required to perform *in vitro* toxicity studies. An epidemiological study by Nawrot et al. (2007), revealed an association between daily mortality and fine particle atmospheric pollution in summer. This suggested that SOAs contributed to the observed mortality, as high PM levels in summer are characterised by high SOA production. Potential toxicological characteristics of PM_{10} and $PM_{2.5}$ are bronchial irritation, inflammation, reduced mucociliary clearance, reduced macrophage response, increased cardiovascular mortality, oxidative stress and inflammation (Naeher et al., 2007, Smith et al., 2013) . Several studies have also referenced the negative effects of SOAs with respect to climate change (Cross et al., 2015, Gentner et al., 2012, Samy and Zielinska, 2010).

1.2 The role played by vehicular engine emissions

Exhaust fumes from vehicular emissions are important contributors to pollution in the ambient atmosphere (Reşitoğlu et al., 2015). Both petrol and diesel engines are sources of NOx and organic compounds that act as precursor molecules for smog formation. The common belief until recently has been that the organic compound contribution in this regard was primarily from petrol engines, as HCs from diesel engines were not considered to be volatile enough to persist in the atmosphere. Recent measurements and characterisation of airborne organic compounds however, show that there is a significant contribution of semi-volatile organic compounds (SVOCs) emanating from diesel exhaust to the atmospheric organic gas load, and that these emissions have not been accounted for by emission inventories (Gentner et al., 2017, Dunmore et al., 2015).

During engine operation, fuel and air combine within the engine. Compression of the air inside the cylinder generates pressure and heat and causes ignition of the diesel fuel, followed by expansion of the burned gases, thereby allowing conversion of the chemical energy to mechanical force. Even very small degrees of incomplete combustion result in the formation of harmful by-products, including SVOCs, which are released into the atmosphere and as a result of their semi-volatile nature, persist in the air where they take part in oxidative conversion reactions forming photochemical O_3 and SOAs (Gentner et al., 2017).

Vehicular emissions have been shown by several studies to be major contributors to photochemical O_3 and SOA production (Cross et al., 2015, Deng et al., 2017, Gentner et al., 2012, Gentner et al., 2013, Weitkamp et al., 2007). However, conflicting data between studies highlights the need for novel approaches to identify and quantify SVOC emissions that may have a substantial contribution to the formation of these pollutants, as they may be important contributors to the observed ambient levels. In addition, Southern Africa has numerous sources of O_3 and SOA forming compounds and presents ideal environmental conditions for formation of these pollutants, hence the relevance of the study in this region.

1.3 Problem statement

The impact of SVOC emissions, released by combustion engines operating on hydrocarbon fuels, on air quality is not clearly understood, due to the difficulty in quantitative collection and chemical analysis of these species, resulting in a potentially severe under-estimation and hence under reporting of these emissions.

1.4 Justification for study

The negative effects of exhaust emissions on ambient air quality have been extensively highlighted in literature. It is thus important to determine the effect of fuel composition and engine operating conditions on the chemical class and concentration of emissions released, particularly in vehicles with advanced exhaust aftertreatment systems that function to reduce harmful engine exhaust emissions. This understanding is vital to better contextualise the contribution of diesel engines and various fuel types to photochemical smog formation.

1.5 Aim and objectives of study

1.5.1 Aim

The aim of the project was to characterise the semi-volatile hydrocarbon emissions from a diesel engine upon combustion of different fuels in such a way that the photochemical smog formation potential of the fuels could be compared.

1.5.2 Objectives

- Experimental work
    - Design of an appropriate experimental procedure and test matrix, and preparation of sampling materials.
    - Development and optimization of a thermal desorption-two dimensional gas chromatography-time of flight mass spectrometry (TD-GC x GC-ToFMS) analytical method for the identification and quantification of SVOCs, specifically aliphatic hydrocarbons sampled onto denuder sampling devices.
    - Execution of diesel engine emission tests (emission testing with three different fuels, collection of engine emissions under hot start and cold start operating conditions, steady state tests, transient cycle tests and

emission testing using two exhaust after treatment systems) at the Sasol Fuels Application Centre (Cape Town).
    - Analysis of collected samples with respect to aliphatic and aromatic semi-volatile organic hydrocarbons by TD-GC x GC-ToFMS.
- Analysis
    - Determination of SVOC hydrocarbon emissions for each test condition and fuel type.
    - Analysis of the significance of differences noted between the calculated hydrocarbon emissions.
    - Calculation of appropriate photochemical smog reactivity factors.
    - Critical analysis of experimental methods and uncertainties thereof.

1.6 Dissertation outline

In this study, a method to collect and characterise semi-volatile organic compounds from diesel exhaust emissions was developed, and it was successfully illustrated how the emission factors of these compounds can be used to characterise their ozone formation potential. Chapter 2 provides a review of techniques reported in the literature to characterise SVOCs from both the ambient atmosphere and vehicular exhaust emissions, and the environmental and health effects of these emissions are highlighted. Chapter 3 details the experimental methods regarding sample collection and analysis used in this study, as well as the methods followed to calculate hydrocarbon emission factors. The results of the study are presented and subsequently discussed in Chapter 4. A summary of the findings of the study and conclusion are provided in Chapter 5. The limitations of the study and future recommendations are also outlined in this chapter. Supporting information (chromatograms, calibration curves, sampling sheet, etc.) including poster presentations and/or publications are presented in the Appendices.

1.7 References

Amegah, A. K. & Agyei-Mensah, S. 2017. Urban air pollution in Sub-Saharan Africa: Time for action. *Environmental Pollution,* 220**,** 738-743.

Anderson, H. R. 2009. Air pollution and mortality: A history. *Atmospheric Environment,* 43**,** 142-152.

Babatola, S. S. 2018. Global burden of diseases attributable to air pollution. *Journal of Public Health in Africa,* 9 (3), 162-166.

Cross, E. S., Sappok, A. G., Wong, V. W. & Kroll, J. H. 2015. Load-dependent emission factors and chemical characteristics of IVOCs from a medium-duty diesel engine. *Environmental Science & Technology,* 49**,** 13483-13491.

Deng, W., Hu, Q., Liu, T., Wang, X., Zhang, Y., Song, W., Sun, Y., Bi, X., Yu, J. & Yang, W. 2017. Primary particulate emissions and secondary organic aerosol (SOA) formation from idling diesel vehicle exhaust in China. *Science of the Total Environment,* 593**,** 462-469.

Dunmore, R., Hopkins, J., Lidster, R., Lee, J., Evans, M., Rickard, A., Lewis, A. & Hamilton, J. 2015. Diesel-related hydrocarbons can dominate gas phase reactive carbon in megacities. *Atmospheric Chemistry and Physics,* 15**,** 9983-9996.

Gentner, D. R., Isaacman, G., Worton, D. R., Chan, A. W., Dallmann, T. R., Davis, L., Liu, S., Day, D. A., Russell, L. M. & Wilson, K. R. 2012. Elucidating secondary organic aerosol from diesel and gasoline vehicles through detailed characterization of organic carbon emissions. *Proceedings of the National Academy of Sciences,* 109**,** 18318-18323.

Gentner, D. R., Worton, D. R., Isaacman, G., Davis, L. C., Dallmann, T. R., Wood, E. C., Herndon, S. C., Goldstein, A. H. & Harley, R. A. 2013. Chemical composition of gas-phase organic carbon emissions from motor vehicles and implications for ozone production. *Environmental Science & Technology,* 47**,** 11837-11848.

Gentner, D. R., Jathar, S. H., Gordon, T. D., Bahreini, R., Day, D. A., El Haddad, I., Hayes, P. L., Pieber, S. M., Platt, S. M. & De Gouw, J. 2017. Review of urban secondary organic aerosol formation from gasoline and diesel motor vehicle emissions. *Environmental Science & Technology,* 51**,** 1074-1093.

Glasson, W. A. 1981. Effect of hydrocarbon and NOx on photochemical smog formation under simulated transport conditions. *Journal of the Air Pollution Control Association,* 31**,** 1169-1172.

Gwaze, P. & Mashele, S. H. 2018. South African Air Quality Information System (SAAQIS) mobile application tool: bringing real time state of air quality to South Africans. *Clean Air Journal,* 28**,** 3-4

Haagen-Smit, A. J. & Fox, M. 1954. Photochemical ozone formation with hydrocarbons and automobile exhaust. *Air Repair,* 4**,** 105-136.

Jiang, X.-Q., Mei, X.-D. & Feng, D. 2016. Air pollution and chronic airway diseases: what should people know and do? *Journal of Thoracic Disease,* 8**,** E31.

Kroll, J. H. & Seinfeld, J. H. 2008. Chemistry of secondary organic aerosol: Formation and evolution of low-volatility organics in the atmosphere. *Atmospheric Environment,* 42**,** 3593-3624.

Laban, T. L., Van Zyl, P. G., Beukes, J. P., Vakkari, V., Jaars, K., Borduas-Dedekind, N., Josipovic, M., Thompson, A. M., Kulmala, M. & Laakso, L. 2018. Seasonal influences on surface ozone variability in continental South Africa and implications for air quality. *Atmospheric Chemistry and Physics,* 18**,** 15491–15514.

Latha, H., Prakash, K., Veerangouda, M., Maski, D. & Ramappa, K. 2019. A review on SCR system for NOx reduction in diesel engine. *Internation Journal of Current Microbiology and Applied Sciences,* 8**,** 1553-1559.

Naeher, L. P., Brauer, M., Lipsett, M., Zelikoff, J. T., Simpson, C. D., Koenig, J. Q. & Smith, K. R. 2007. Woodsmoke health effects: a review. *Inhalation Toxicology,* 19**,** 67-106.

Nawrot, T., Torfs, R., Fierens, F., De Henauw, S., Hoet, P., Van Kersschaever, G., De Backer, G. & Nemery, B. 2007. Stronger associations between daily mortality and fine particulate air pollution in summer than in winter: evidence from a heavily polluted region in western Europe. *Journal of Epidemiology & Community Health,* 61**,** 146-149.

Reşitoğlu, İ. A., Altinişik, K. & Keskin, A. 2015. The pollutant emissions from diesel-engine vehicles and exhaust aftertreatment systems. *Clean Technologies and Environmental Policy,* 17**,** 15-27.

Roberts, A., Brooks, R. & Shipway, P. 2014. Internal combustion engine cold-start efficiency: A review of the problem, causes and potential solutions. *Energy Conversion and Management,* 82**,** 327-350.

Robinson, A. L., Donahue, N. M., Shrivastava, M. K., Weitkamp, E. A., Sage, A. M., Grieshop, A. P., Lane, T. E., Pierce, J. R. & Pandis, S. N. 2007. Rethinking organic aerosols: Semivolatile emissions and photochemical aging. *Science,* 315**,** 1259-1262.

Samy, S. & Zielinska, B. 2010. Secondary organic aerosol production from modern diesel engine emissions. *Atmospheric Chemistry & Physics,* 10**,** 609-625.
Smith, K. R., Frumkin, H., Balakrishnan, K., Butler, C. D., Chafe, Z. A., Fairlie, I., Kinney, P., Kjellstrom, T., Mauzerall, D. L. & Mckone, T. E. 2013. Energy and human health. *Annual Review of Public Health,* 34**,** 159-188.
Weitkamp, E. A., Sage, A. M., Pierce, J. R., Donahue, N. M. & Robinson, A. L. 2007. Organic aerosol formation from photochemical oxidation of diesel exhaust in a smog chamber. *Environmental Science & Technology,* 41**,** 6969-6975.
Whitten, G. 1983. The chemistry of smog formation: A review of current knowledge. *Environment International,* 9**,** 447-463.
WHO, 2000. Air quality guidelines for Europe. Copenhagen: WHO Regional Office for Europe, World Health Organization.
WHO 2006. Air quality guidelines: global update 2005: particulate matter, ozone, nitrogen dioxide, and sulfur dioxide, World Health Organization.

Chapter 2: Literature Review

2.1 Introduction

Exhaust fumes from vehicles are a major contributor to pollution in the urban ambient atmosphere (Reşitoğlu et al., 2015). Pollutants emitted by this source include carbon monoxide (CO), particulate matter (PM), nitrogen oxides (NOx) and hydrocarbons (HCs). Whilst both diesel and petrol engines contribute to NOx emissions, there has been much scientific debate concerning their contribution to the HC load in the atmosphere. Historically, petrol was believed to be the major contributor to atmospheric HC emissions (De Nevers, 2010, Mcdonald et al., 2013, Mcdonald et al., 2015, Warneke et al., 2012), hence many studies focused on characterising volatile organic compounds (VOCs) emitted by petrol engines. As a result, these HCs have been successfully reduced in many cities (Dunmore et al., 2015). Characterisation studies of anthropogenic sources of ambient HCs however, show that there is a significant contribution from semi-volatile HC emissions emanating from diesel exhaust. In addition, the most probable source of intermediate volatile organic compounds (IVOCs) in the atmosphere are diesel engines (Dunmore et al., 2015).

Although several studies have investigated the emission of IVOC species, only a few have measured the total IVOC emissions due to the difficulty in quantitative collection and chemical analysis of these species. Traditional gas chromatography techniques are used extensively to perform qualitative and quantitative analysis of VOCs and organic aerosols (OAs). However, such techniques cannot achieve complete speciation of IVOCs, consequently these compounds are grouped as an unresolved complex mixture (UCM) of co-eluting compounds (Illustrated in Appendix B), and their contribution to quantitative results is often estimated (Zhao et al., 2015). Zielinska et al. (1996), stated that the difficulty in identifying and quantifying IVOCs associated with diesel engine emissions in urban air is due to their low volatility, low concentration and difficulty in resolving such a large number of compounds by gas chromatographic methods. Goldstein and Galbally (2007) stated that the number of possible structural isomers increases exponentially with the number of carbon atoms, and that beyond ~C_9, it becomes nearly impossible to determine the structure of every HC present in air. Hence, a common technique used during quantitative characterisation studies is ‘binning’ of compounds where HCs are grouped into ‘bins’ of chemical classes and/or

volatility ranges, based on their retention behaviour on chromatographic columns (Zhao et al., 2015). Although the results yielded remain an estimation, this is by far a better approach than grouping all the compounds beyond a particular carbon number under a large group of unspeciated compounds.

The organic composition of petrol and diesel fuel differs; petrol consists of low molecular weight volatile HCs in the C_4-C_{10} range, whilst diesel consists of longer chain HCs in the C_9-C_{25} range (Gentner et al., 2017). Based on their partitioning properties at atmospheric pressure, these SVOCs are described as compounds with an effective saturation concentration of 0.1-1000 µg/m^3 (Robinson et al., 2007). They tend to partition between the particulate and gaseous phase at high atmospheric dilution and despite being present at very low concentrations in diesel exhaust, these HCs may act as important precursors for secondary organic aerosol (SOA) and photochemical ozone formation (Gentner et al., 2012).

In 2015, Dunmore et al. (2015) used high resolution gas chromatography to investigate the abundance and trends of diesel-related HCs in the atmosphere at a background site in London, and the results were compared to those reported in emission inventories. The study reported a 38% increase in the contribution of diesel related HCs to VOC hydroxyl reactivity (photochemical conversion of organic compounds by reacting with hydroxyl radicals) in winter and a 26% increase in summer. The seasonal average unmeasured gas phase non-methane HC (NMHC) mass concentration from diesel sources was estimated to be 76.1-97.8 µg/m^3 in winter and 26.8-34.3 µg/m^3 in summer. Comparing these results to typical primary organic aerosol measurements showed that an overwhelming amount of diesel related HCs exist in ambient air. The study concluded that there was an underestimation, hence under-reporting of organic compounds from diesel sources, particularly, the higher carbon number species. Consequently, these species were not included in emission inventories and model chemical mechanisms.

2.2 The diesel combustion engine

Diesel engines function as auto-ignition engines in which fuel and air (oxygen) combine, and compression of the air inside metal cylinders within the engine

generates heat and causes ignition of the diesel fuel, allowing conversion of the chemical energy stored by HCs in the fuel to mechanical force.

The first diesel engines were large and unwieldly. As a result, they were only used for stationary or industrial applications. In the 1920s, compact fuel injection pumps were developed by Robert Bosch, allowing the use of small diesel engines to power commercial transport and automobiles (Wright, 2015). Today, diesel engines are utilised extensively for heavy duty, commercial transport such as buses, heavy duty trucks, trains, ships and off-road industrial machinery such as mining equipment and excavation machines. Diesel engines are also used widely by light-duty vehicles although the relative use varies in different regions. Their extensive use is due to their low operating costs, high durability, energy efficiency and reliability (Reşitoğlu et al., 2015).

A study on diesel-related HCs stated that there is a shift towards diesel-powered vehicles in many developed cities as a response to energy efficiency drivers, and that this trend is likely to be followed by developing countries (Dunmore et al., 2015). Contrary to this however, in February 2018, Germany became the first country to introduce diesel bans following a ruling by The Federal Administrative Court in Leipzig (Leggett, 2018). The ruling banned older diesel vehicles from highly polluted cities, including Hamburg, Stuttgart and Frankfurt, in response to these vehicles failing to meet EU emissions standards. The ruling set a precedent for all German cities and it was predicted that it could lead to similar action by cities across Europe, as diesel vehicles struggle to comply with EU emission limits.

Nonetheless, diesel use remains popular amongst vehicle owners, particularly in South Africa. This beckons the need to assess the potential change in the atmosphere that this may bring about.

2.3 Diesel exhaust emissions

Like most fossil fuels, diesel consists of a mixture of HCs obtained from the distillation of petroleum crude oil (Majewski and Jääskeläinen, 2016). Under ideal thermodynamic conditions, complete combustion of diesel fuel should produce only carbon dioxide

and water in the combustion chamber, however in reality this does not occur and a range of harmful by-products form simultaneously.

Formation of these compounds can be as a result of a number of variables. A major contributing factor is the heterogeneous nature of the combustion process (with respect to species concentrations and temperature zones). Figure 2.1 illustrates the different zones where pollutants form within the combustion chamber. CO and PM are formed in the air-deficient spray core. The components of diesel PM are soot, ash, an adsorbed organic fraction (long chain HCs derived from lubricating oil or unburnt fuel), inorganic sulphates, water and other trace elements (Mollenhauer and Tschoeke, 2010, Wichmann, 2007). Unburned HCs are produced in the lean outer flame zone where the temperatures are too low for complete oxidation of the fuel. These emissions are the result of the heterogenous nature of the combustion process where fuel evaporation, fuel-air mixing, burned-unburned fuel mixing and combustion occur simultaneously. There are two ways that fuel can escape the combustion process, i.e. when the fuel-air mixture becomes too lean to allow ignition or propagation of a flame, or when the mixture becomes too rich to support a flame. In ideal situations, rapid oxidation occurs as the fuel mixes with the air, allowing complete combustion of the fuel, however in reality slow mixing causes over-rich and/or over-lean zones. For the over-rich mixtures, complete combustion requires additional mixing with air before expansion and cooling of the combustion products, whilst the over-lean mixtures will never support the propagation of a flame, resulting in products of incomplete combustion, pyrolysis products and unburned fuel. The HC species formed then exit the engine either as gaseous emissions or are adsorbed onto soot particles (Chehroudi, 2015).

According to Ris (2007), the HCs present in diesel exhaust include a wide variety of compounds which originate from unburnt diesel fuel, lubrication oil, partial combustion products and pyrolysis products. The characteristic HC emissions vary based on fuel composition, engine design and engine load (Shah et al., 2004). Diesel engines are typically characterised by low levels of HC emissions. This is because they operate under highly oxidising conditions which make catalytic removal of HCs and CO relatively simple (Ansell et al., 1996, Nakatsuji et al., 1998). However, because diesel

exhaust HC emissions are typically measured as total hydrocarbons (THC), little information on the removal of individual HCs is available.

NOx species (nitrogen monoxide and nitrogen dioxide) are formed in the excess air-high temperature (> 1600 °C) zone in the combustion chamber, from the reaction of molecular nitrogen and oxygen. The amount of NOx emissions produced is a function of the maximum temperature, O_2 concentration and residence time in the cylinder (Reşitoğlu et al., 2015). As previously stated, diesel engines operate under highly oxidising conditions, and although this makes removal of HCs and CO fairly simple, reducing NOx emissions under these conditions is difficult (Ansell et al., 1996, Nakatsuji et al., 1998). Thus, although petrol and diesel engines produce roughly the same amount of NOx species, larger amounts are emitted by the diesel engine. The effective removal of NOx emissions in petrol engines is a result of a three-way catalytic system which makes use of a reductant to reduce the NOx emissions over the catalyst active site. The system cannot be used for diesel engines as the reductant is quickly ‘burned out’ under the oxidising atmosphere (Nakatsuji et al., 1998). Fortunately, the development of NOx reducing systems such as selective catalytic reduction (SCR) and exhaust gas recirculation (EGR) systems has introduced great prospects to improve diesel engine catalytic systems (Latha et al., 2019), and since the recent introduction of Euro 6 legislation, these systems have become a standard for passenger vehicles.

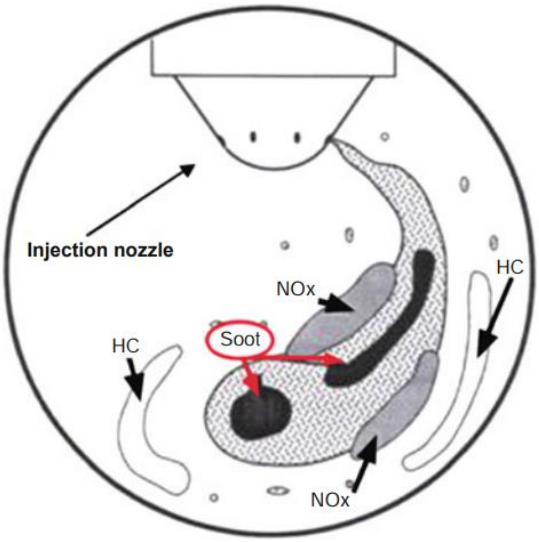

Figure 2.1 Regions of pollutant production in a combustion chamber with a heterogeneous air/fuel mixture *(Mollenhauer and Tschoeke, 2010)*.

2.4 Diesel exhaust aftertreatment systems

Due to increasingly stringent limitations on harmful vehicular exhaust emissions, greater control over the treatment of post combustion emissions is required. As previously discussed, harmful emissions from diesel engines include CO, PM, HCs and NOx species. These are reduced by various control systems: a diesel oxidation catalyst (DOC), diesel particulate filter (DPF) and/or SCR systems.

The function of the DOC is catalytic oxidation of CO, HCs and much of the soluble organic fraction, including HCs that are adsorbed onto the surface of PM. It is usually a ceramic or metallic honeycomb structure consisting of an oxide mixture (Al_2O_3, CeO_2, and ZrO_2) and catalytic precious metals such as Pt, Pd and Rh, with the former two being the most commonly used. The SCR catalyst works in conjunction with the DOC to reduce NOx emissions. This catalyst uses NH_3 (produced from urea) as a reducing agent, to convert NOx emissions to N_2 and H_2O. SCR catalysts are typically vanadium- or zeolite-based such as V_2O_5-WO_3/TiO_2, Fe-ZSM_5, Cu-ZSM_5 (where ZSM is a synthetic zeolite containing a mixture of Si and Al), however, various other catalyst types are also used (Reşitoğlu et al., 2015, Van Setten et al., 2001). The DPF is an exhaust filter which traps PM and soot from the exhaust by means of filtration. Similar to the DOC, DPFs are usually honeycomb structures made of cordierite ($2MgO–2Al_2O_3–5SiO_2$) or silicon carbide (SiC) channels plugged at alternate ends. The plugged channels force PM emissions through the substrate's porous walls, which act

as a mechanical filter. In time, the DPF accumulates PM, which results in an increase in back pressure and hence collected PM must be removed by 'burning' them off the filter through active regeneration at high temperatures, or passive regeneration where oxidation of PM occurs at normal exhaust gas temperatures aided by catalysts deposited within the DPF (Reşitoğlu et al., 2015, Rounce et al., 2012).

Modern day diesel engines have both a DOC and DPF as part of their exhaust aftertreatment system. Liu et al. (2008) used the same fuel and test engine to study the reduction in emissions achieved by different aftertreatment components (SCR and DPF). The study showed that both the DPF and SCR systems resulted in a reduction in the emission rates of organic species including n-alkanes, PAHs, branched alkanes, and aromatics. The DPF performed better in reducing PM, whilst the SCR system was better at removing NOx and lower molecular weight organic emissions. Tang et al. (2007) evaluated the effect of the following emission control systems: a DOC, continuously regenerating diesel particulate filter (CRDPF), as well as a CRDPF coupled with a low pressure EGR system, for the combined reduction of NOx and PM as described by Frank et al. (2004). The study concluded that emission reduction can be achieved with the use of a DOC, however, much higher reductions can be achieved with the use of a CRDPF or a EGR system than by a DOC alone (Tang et al., 2007).

Effective emissions control by such exhaust aftertreatment systems allow diesel engines to meet all current emission standards, albeit with higher cost and significant complexity. The issue remains however, that optimum functioning of the catalysts utilized by the DOC and SCR systems and regeneration of the DPF requires high exhaust gas temperatures which are seldom reached during everyday low-speed urban driving conditions.

2.5 Consequences of diesel exhaust emissions

2.5.1 Health effects

Adverse human health effects arise from environmental exposure to both petrol and diesel exhaust, as particulate and gaseous exhaust emissions contain many carcinogenic, mutagenic and toxic substances (Lloyd and Cackette, 2001). The contribution of these substances to lung cancer, airway inflammations, allergies and

the development of asthma and chronic bronchitis has been highlighted in literature (Kagawa, 2002, US EPA, 2002, Wichmann, 2007).

Diesel PM consists of fine particles with a diameter < 10 µm (PM_{10}) and ultrafine particles with a diameter < 2.5 µm ($PM_{2.5}$). As aggregates, these particles have a large surface area, ideal for adsorption of toxic gaseous HCs, namely PAHs and their nitrated, methylated and oxygenated derivatives, as well as aliphatic HCs (Geldenhuys et al., 2015, Ono-Ogasawara and Smith, 2004). Among the gaseous HC components of diesel exhaust, aldehydes, PAHs, nitro-PAHs, benzene, as well as 1,3-butadiene are notable due to their toxicologic effects, whilst alkanes, alkenes and aldehydes are known to cause respiratory tract infections at elevated levels (US EPA, 2002). Long chain HCs (C_{14}-C_{35}), nitro-PAHs and PAHs with ≥ 4 rings are known mutagens (US EPA 2002). Furthermore, the small size of PM emitted from diesel engines makes it highly respirable, hence long-term exposure could lead to a decline in respiratory function, lung cancer development, airway inflammations, allergies and the development of asthma and chronic bronchitis. The World Health Organisation (WHO) reported that studies on railroad workers and truck drivers showed that they have a 20-40% higher incidence of lung cancer (WHO, 1996). Kagawa (2002) performed studies on diesel exhaust using rat models and showed that carcinogenic effects occur with long term exposure at a particle concentration of 2 mg/m^3 or more.

2.5.2 Environmental effects

Diesel emissions have a detrimental effect on the environment, both directly and indirectly. PM emissions contribute to air, water and soil pollution; resulting in reduced visibility; and impact agricultural production as well as climate change (Englert, 2004, Marchal et al., 2011, Michaels and Kleinman, 2000). NOx species contribute to the formation of acid rain, which affects aquatic and terrestrial organisms, nutrient enrichment, pollutant haze formation and photochemical smog formation, due to their reaction with HCs in the atmosphere. Gaseous HC emissions are a concern as they participate in ambient oxidation reactions which result in the formation of secondary pollutants such as SOAs and photochemical ozone, the principal components of photochemical smog pollution (Gentner et al., 2013).

Photochemical smog was originally identified in Los Angeles, USA, during the 1940s (NRC, 1999). It is typically observed as a brown haze over large cities and was characterised by an irritation of the eyes and a characteristic odour. The term 'smog' was coined by combining the terms 'smoke' and 'fog', which may be misleading as neither smoke nor fog are the constituents of photochemical smog. In one of the earliest smog chamber experiments (1952), Haagen-Smit was able to generate the "smell" of Los Angeles air at low concentrations (ppm level) of heptane and nitrogen oxides, demonstrating that the key elements of photochemical smog are HCs, nitrogen oxides and UV sunlight (Whitten, 1983). Peroxyacetyl nitrates (PANs), aldehydes, acrolein, nitric acid (HNO_3) and PM (including aerosols) are also constituents of photochemical smog. Together these compounds form the brown haze observed over city areas during 'smog' episodes (Figure 2.2). In this study we focus on SOAs and photochemical ozone.

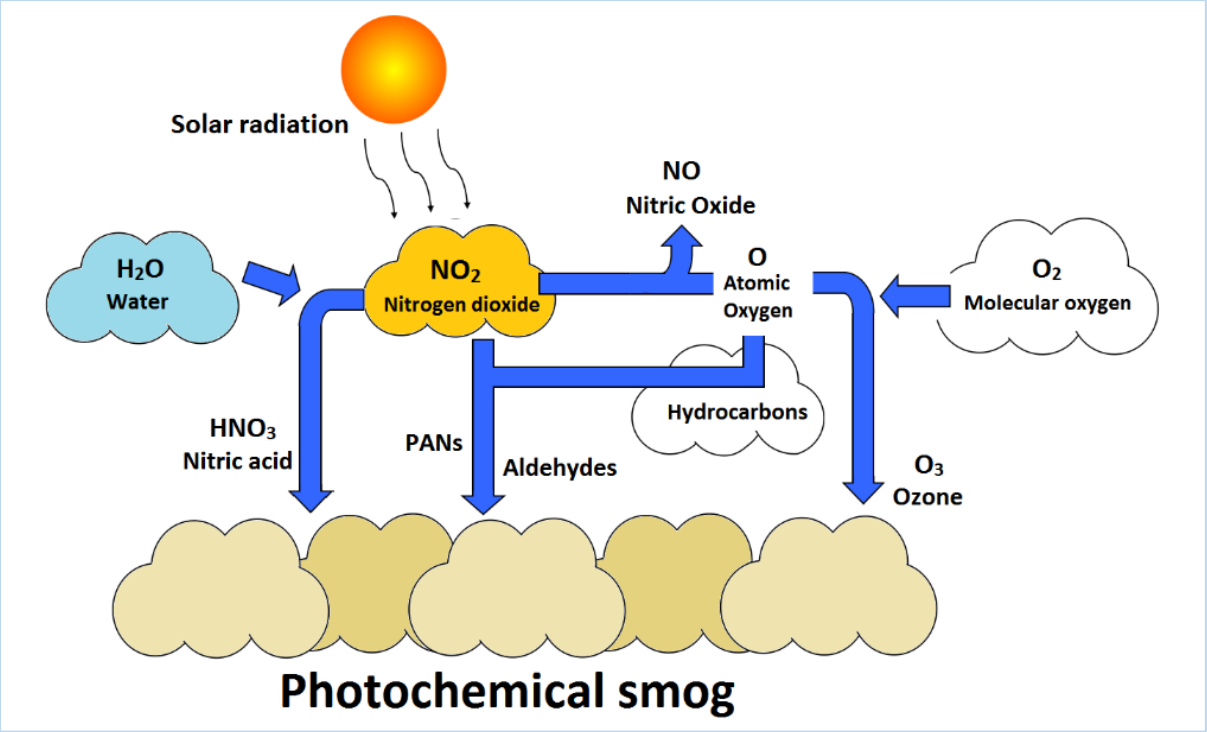

Figure 2.2 Products of atmospheric oxidation reactions that are constituents of photochemical smog *(Miller et al., 2011)*.

2.5.2.1 Secondary organic aerosols

Organic aerosols are a major constituent of $PM_{2.5}$. There are two types of organic aerosols, i.e. primary organic aerosols which are emitted directly from biomass

burning, cooking devices or internal combustion engines fuelled by petrol or diesel, and SOAs formed from the oxidation of gas-phase precursors such as VOCs and SVOCs in the atmosphere. $PM_{2.5}$ is predominantly comprised of elemental carbon, sulphates, nitrates, ammonium, inorganic metals and an organic aerosol fraction, which can be anything between 20-90% of the particle (Gentner et al., 2017).

The source of the organic aerosol fraction of $PM_{2.5}$ is under constant debate among researchers. Whilst some studies state that it is predominantly from biogenic emissions (Griffin et al., 1999, Szidat et al., 2004), most studies argue that both biogenic and anthropogenic sources are important for SOA formation (Gentner et al., 2017, Hallquist et al., 2009, Samy and Zielinska, 2010). Among the anthropogenic sources, both petrol- and diesel-powered vehicles are important sources of SOA precursors, however due to conflicting data from different studies, a debate still exists over the relative importance of each vehicle type.

Jathar et al. (2014) studied the influence of unspeciated organic emissions on the SOA budget in the United States and found that speciated SOA precursors such as isoprene, terpenes, single-ring aromatics and large alkanes that are usually included in atmospheric models are only a fraction of the measured SOA mass. In the study, they estimated that in the US, 90% of SOA was from biomass burning and gasoline (petrol) sources, with 85% of the SOA arising from unspeciated organic emissions. It is speculated that the unexplained SOA comes from the oxidation of heavy organic vapours ($>C_{12}$) that are difficult to speciate using traditional one-dimensional gas chromatography (Robinson et al., 2007). Tkacik et al. (2014) conducted a study to determine the role played by vehicular emissions on ambient SOA formation. In the study, a potential aerosol mass flow reactor (a flow reactor which stimulates atmospheric oxidation reactions in a highly oxidative environment) was deployed at a highway tunnel in Pittsburgh, Pennsylvania, and the SOA formation resulting from the exhaust-dominated tunnel air was assessed. The study found that the contribution of mobile sources to SOAs was six times greater than what was reported by the National Emissions Inventory. Jathar et al. (2013) successfully illustrated SOA formation from dilute exhaust emissions of petrol medium duty and heavy duty diesel vehicles through smog chamber experiments. Robinson et al. (2007) also irradiated dilute diesel exhaust using UV light in a chamber and observed a burst of SOA production, followed

by a steady production throughout the experiment. In order to investigate the contribution of traditional SOA precursors, the chamber was spiked with additional aromatics, roughly enough to double SOA production. The addition, however, only caused a slight inflection on the aerosol-mass time series, leading to the conclusion that the oxidation of traditional precursors only accounts for a small fraction of the SOA formed in the chamber.

Deng et al. (2017) conducted a study to estimate SOA formation from idling diesel vehicle exhaust and similarly observed that the predicted SOA concentrations from NMHCs accounted for less than 3% of the SOA production. The study concluded that primary VOC precursors do not explain the amount of diesel-related SOA formation and that the unexplained portion is most likely due to the photo-oxidation of IVOCs. Zhao et al. (2015) came up with a similar conclusion, during a study on SOA production from speciated, unspeciated and single-ringed aromatic species. The results showed only ~7% of the predicted SOA was from speciated IVOCs and that the majority came from unspeciated cyclic compounds. More than 90% of the IVOCs could not be speciated by GC-MS. Their average mass spectrum was characteristic of C_nH_{2n+1}, C_nH_{2n-1} and C_nH_{2n-3} species, with an abundant m/z = 57 fragment. This led to the assumption that the unspeciated IVOCs were likely branched and cyclic alkanes.

2.5.2.2 Photochemical ozone

Photochemical ozone is formed in the lower atmosphere (troposphere) by a complex process involving the reaction of primary precursors in the presence of ultraviolet sunlight. An early experiment by Haagen-Smit and Fox (1954) demonstrated that HCs, nitrogen oxides and ultraviolet sunlight are the main elements of smog formation.

The mechanism of photochemical ozone formation is fairly complex, however, the key elements can be explained using basic chemistry (Whitten, 1983). The initial reaction is the photolysis of nitrogen dioxide (NO_2) to form nitrogen monoxide (NO) and atomic oxygen (O) (Reaction 1). The formation of O_3 in the troposphere stems from the combination of the oxygen atoms with molecular oxygen (O_2) in the presence of a third body (Reaction 2) which then reacts with O_3 to reform NO_2 and O_2 (Reaction 3). This cycle is called the nitrogen cycle and results in no net ozone formation due to the

formation and destruction of ozone from reactions 2 and 3, respectively. For ozone to accumulate, an additional reaction for the conversion of NO to NO_2 (that will not use O_3) is required. This alternative conversion pathway is made available through the photochemical oxidation of reactive organic molecules such as HCs.

$$NO_2 + h\nu \rightarrow NO + O\bullet \quad (1)$$

$$O\bullet + O_2 + M \rightarrow O_3 + M\bullet \quad (2)$$

$$O_3 + NO \rightarrow NO_2 + O_2\bullet \quad (3)$$

One of the most important reactions for NO conversion via HC oxidation is the fast-radical transfer reaction where NO reacts with peroxy radicals ($RO_2^{\bullet}$) to form NO_2. During this reaction, HCs (RH) react with hydroxyl radicals (OH•), followed by a subsequent reaction with O_2 in the presence of a neutral third body to form alkyl peroxy radicals which become available to convert NO to NO_2 without consuming an O_3 molecule.

$$RH + OH\bullet \rightarrow R\bullet + H_2O \quad (4)$$

$$R\bullet + O_2 + M \rightarrow RO_2\bullet + M \quad (5)$$

$$RO_2\bullet + NO \rightarrow NO_2 + RO\bullet \quad (6)$$

The final reaction pathway is the NOx plus radical sink reaction which forms nitric acid (HNO_3), removing NO_2 from the system.

$$OH\bullet + NO_2 \rightarrow HNO_3 \quad (7)$$

According to Whitten (1983), methyl ethylene, paraffins, olefins and aromatics are the most significant HC species in photochemical smog formation. In this study, we focus on n-alkanes (paraffins) and alkylbenzenes (aromatic) HCs. The initial pathway for n-alkanes is hydroxyl radical attack. This initial attack results in a series of chemical reactions that lead to the formation of key intermediate species including alkoxyl radicals (RO•), alkyl peroxy radicals (RO_2•), aldehydes and ketones, which partake in a series of chemical reactions leading to ozone formation (Whitten, 1983).

The two most important aromatic molecules for smog formation are toluene and m-xylene. Whilst explicit mechanisms have not been published for m-xylene oxidation,

the photo-oxidation of toluene has been studied extensively. There are three descriptions for toluene oxidation at present (Figure 2.3), and all three are in agreement with the ring opening mechanism originally proposed by Atkinson et al. (1979) and Darnall et al. (1979).

More recently this mechanism was described by Ji et al. (2017). Oxidation of toluene is initiated by a reaction with the OH• radical, which results in hydrogen abstraction (minor reaction) and OH• addition (major reaction). The OH• addition reaction leads to the formation of methylhydroxycyclohexadienyl radicals (OH•-toluene adducts) which can react with O_2 via three pathways: hydrogen abstraction to yield hydroperoxyl radicals and phenolic compounds (Pathway I), O_2 addition to form primary peroxy radicals or RO_2• (Pathway II), and hydrogen abstraction followed by O-bridge formation to form oxepin/aromatic oxides (Pathway III). The third pathway remains highly speculative as quantum chemical calculations show a high energy barrier for this reaction pathway. From an atmospheric modelling approach, ozone formation from toluene oxidation is presumed to be predominantly from the production of RO_2• (Pathway II) and a minor contribution from the HO_2• produced during cresol formation (Pathway I). Both the RO_2• and HO_2• react with NO to produce NO_2, which then undergoes photodissociation to form ozone. In addition, aromatic ring cleavage from Pathway I and II results in the formation of glyoxal, methylglyoxal and other low-volatility compounds that are likely to contribute to SOA formation as well.

The detrimental health and environmental impacts of photochemical O_3 include reduced visibility, eye irritation, a decline in respiratory function, aggravation of heart disease, reduced resistance pulmonary function, pneumonia and damage to rubber, fabrics, crops and vegetation which is a major setback in industry (Field et al., 1992, Laban et al., 2018, Zunckel et al., 2004).

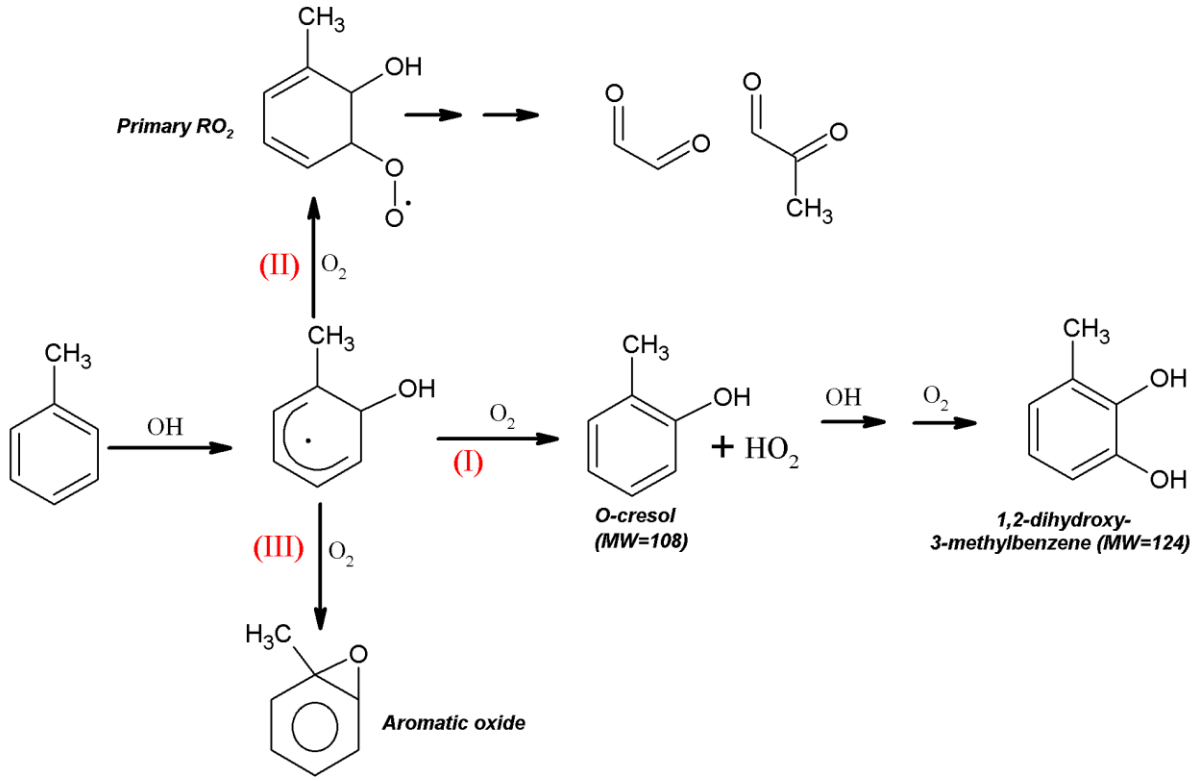

Figure 2.3 Competing atmospheric oxidative pathways for the toluene-OH adduct *(Ji et al., 2017).*

2.6 Statistics on diesel use in South Africa

While petrol engines are still dominantly used in South African passenger cars and light commercial vehicles, new data suggests a shift towards the use of diesel engines. The National Association of Automobile Manufacturers of South Africa (NAAMSA) noted a steady increase in the popularity of diesel engines over recent years. In 2016, diesel passenger car and light commercial vehicle sales accounted for 33.5% of the total light vehicle sales, which was a 1.7% increase from 2015. The Automobile Association (AA) stated that one of the main reasons for purchasing a diesel vehicle is its fuel efficiency, i.e. diesel engines consume less fuel than their petrol counterparts. A report by the Department of Energy studied the petrol and diesel market between the years 2007 and 2016. They too reported a similar decline in the market share of petrol-fuelled car sales, from 73% in 2007 to 63% in 2016, whilst diesel-fuelled car sales increased by 10 percentage points to 37% in 2016 (Figure 2.4). Another analysis made by the Department of Energy is South Africa's consumption by product type, i.e. consumption of petrol fuel in comparison to diesel fuel. They noted a steady decline in petrol consumption over the years, whilst diesel consumption increased by an annual average of 3% during the period studied (2007-

2016). The global economic crisis in 2009 saw a 10% decrease in diesel consumption, however, consumption recovered in the following years reaching a high of 13.7 billion litres in 2015 (Figure 2.5).

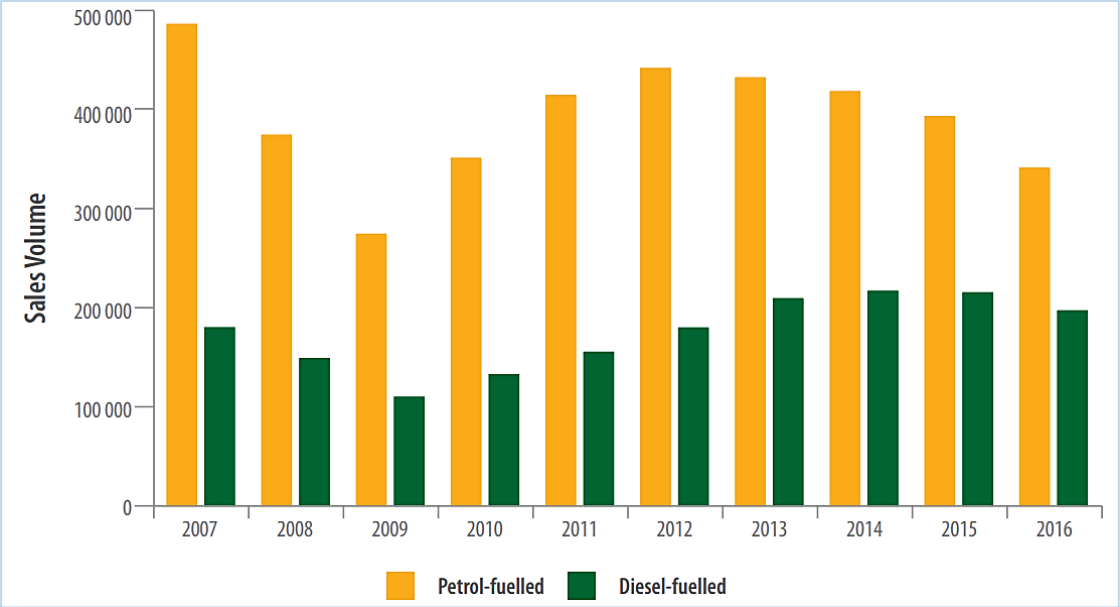

Figure 2.4 Total number of new vehicle sales in South Africa from 2007-2016.
Source: http://www.energy.gov.za/

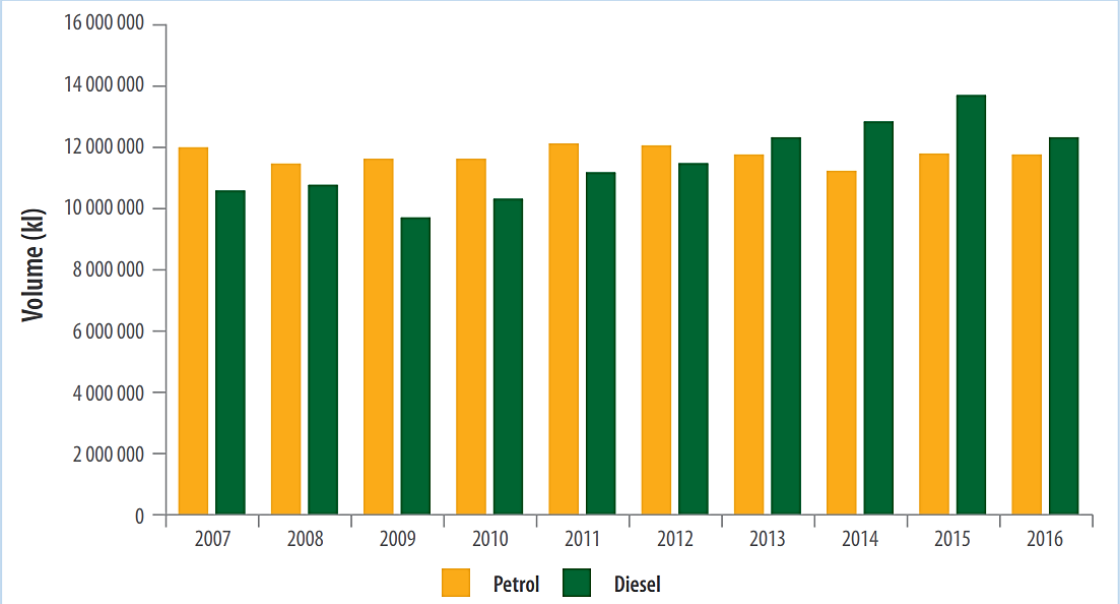

Figure 2.5 Petrol and diesel consumption in South Africa from 2007-2016.
Source: http://www.energy.gov.za/

In 2018, the Department of Energy released annual reports of the fuel sales by volume in South Africa. Figure 2.6 shows the fuel sales for the year 2018, classified by fuel type. It is clear that petrol and diesel were the dominant fuels used, where in this particular year, diesel sales (12,538,744,326 L) were 5% higher than petrol sales (11,141,630,546 L). It is important to note, however, that diesel fuel also has a wide range of non-road applications, including equipment used in the agriculture, forestry, mining, power generation, marine and rail sectors.

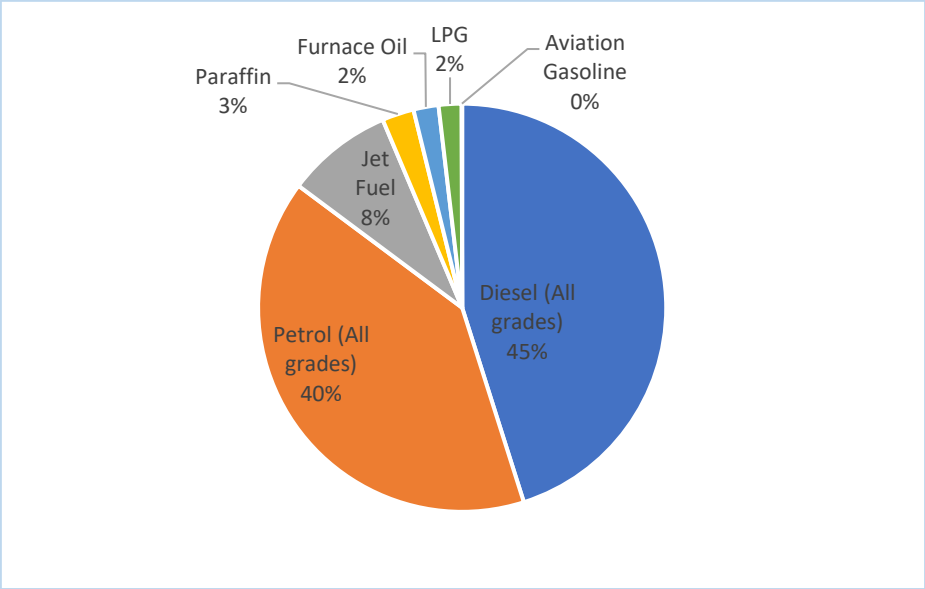

Figure 2.6 Total fuel sales in South Africa for the year 2018.
Source: http://www.energy.gov.za/

2.7 Regulation of air pollutants in South Africa

Air quality limits for pollutants are important for air quality management. They serve to indicate what ambient level of pollutant exposure is generally safe for people, including vulnerable groups (children and the elderly), over their entire lifetime. The WHO provides guidance on the limits of various pollutants that are known to have adverse effects on human health, however, they do not factor in the socio-economic status of a particular country, thus each country uses these limits to inform the development of its own standards. Suspended particulate matter, nitrogen dioxide (NO_2), sulphur dioxide (SO_2), lead (Pb), carbon monoxide (CO) and ozone (O_3) are classified as 'criteria pollutants' and most countries have set air quality limits for all of them (Department of Environmental Affairs, 2009). In South Africa, the National Environmental Management: Air Quality Act (NEMAQA), Act no. 39 of 2004, set out

measures to prevent pollution and set national standards for pollutants to regulate the air quality in the country. In 2009, the ambient air quality standards for seven pollutants, including O_3 and particulate matter (PM_{10}) were issued, and in 2012, the National Ambient Air Quality Standard for $PM_{2.5}$ was established. The National Ambient Air Quality Standards (NAAQS) for the criteria pollutants are shown in Table 2.1. The standard for O_3 is 120 µg/m^3 (61 ppb) and is reported as an 8-hourly running average. Different averaging periods are used to report the $PM_{2.5}$ average, however the one most commonly used is the maximum 24-hour concentration which as from the year 2016 is 40 µg/m^3. As can be seen from Table 2.1, a certain number of exceedances (per year) of the pollutant limit is permissible for certain pollutants.

The state of the air quality across several regions in South Africa is monitored at government level by means of automated continuous air quality monitoring stations. These stations monitor a range of pollutants (including the criteria pollutants mentioned previously) and metrological conditions, e.g. wind direction and speed, ambient pressure and temperature, relative humidity, etc. There is a total of 130 stations which form part of the National Ambient Air Quality Monitoring Network, mostly located in areas with the highest density of people and industries. The data collected by the monitoring stations are used to assess compliance with air quality standards and to monitor the impact of intervention strategies put in place to address air pollution (Gwaze and Mashele, 2018). In South Africa, there are three areas which have been classified as national priority areas: the Vaal Triangle, Highveld, and Waterberg Bojanala regions. A priority area is one where ambient air quality standards may be or are often exceeded. Herein, we will use the Vaal Triangle Priority Area as a case study.

The Vaal Triangle is a highly industrial urban area located approximately 60 km from Johannesburg, South Africa. It is known as South Africa's industrial hub. Industrial, agricultural and domestic emissions, biomass burning, and transport emissions have led to poor air quality over the area, which has had a negative impact on the wellbeing of residents. There are six ambient air monitoring stations in the Vaal Triangle, located in Kliprivier, Diepkloof, Sebokeng, Three Rivers, Sharpeville, and Zamdela (Sasolburg).

Table 2.1 National Ambient Air Quality Standards (NAAQS) for criteria pollutants.
Source: http://saaqis.environment.gov.za/

Pollutant	Averaging time	Concentration	Frequency of exceedance per year	Compliance date
Sulphur dioxide (SO_2)	10 min	500 µg/m^3 (191 ppb)	526	immediately
	1 hour	300 µg/m^3 (134 ppb)	88	immediately
	24 hour	125 µg/m^3 (48 ppb)	4	immediately
	1 year	50 µg/m^3 (19 ppb)	0	immediately
Nitrogen dioxide (NO_2)	1 hour	200 µg/m^3 (106 ppb)	88	immediately
	1 year	40 µg/m^3 (21 ppb)	0	immediately
Ozone (O_3)	8-hour (rha)	120 µg/m^3 (60 ppb)	11	immediately
Carbon monoxide (CO)	1 hour	30 mg/m^3 (26 ppm)	88	immediately
	8-hour (rha)	10 mg/m^3 (8.7 ppm)	11	immediately
Lead (Pb)	1 year	0.5 µg/m^3 (19 ppb)	0	immediately
Benzene	1 year	10 µg/m^3 (3.2 ppb)	0	immediately
		5 µg/m^3 (1.6 ppb)	_	01-Jan-15
Particulate matter (PM_{10})	24 hour	120 µg/m^3	4	immediately
		75 µg/m^3	4	01-Jan-15
	1 year	10 µg/m^3	0	immediately
		5 µg/m^3	0	01-Jan-15
Particulate matter ($PM_{2.5}$)	24 hour	65 µg/m^3	4	immediately
		40 µg/m^3	4	01-Jan-16
		25 µg/m^3	4	01-Jan-30
	1 year	25 µg/m^3	0	immediately
		20 µg/m^3	0	01-Jan-16
		15 µg/m^3	0	01-Jan-30

*rha = running hourly average

Pollutant data measured at the stations is compiled and published as monthly reports. Pollutant levels are compared with the standards (limits) and exceedances of the limits

are noted. The $PM_{2.5}$ concentration measured from the year 2007 to 2016 is shown in Figure 2.7 and the 8-hour average concentration for O_3 from December 2016 to May 2018 is shown in Figure 2.8, for the Vaal Triangle Priority Area. Exceedances of the $PM_{2.5}$ standard are observed in all six monitoring stations for the ten-year period. The O_3 levels measured in the Vaal Triangle were relatively low, however a few exceedances of the standard were also noted and the mean O_3 level throughout the studied period is relatively close to the limit.

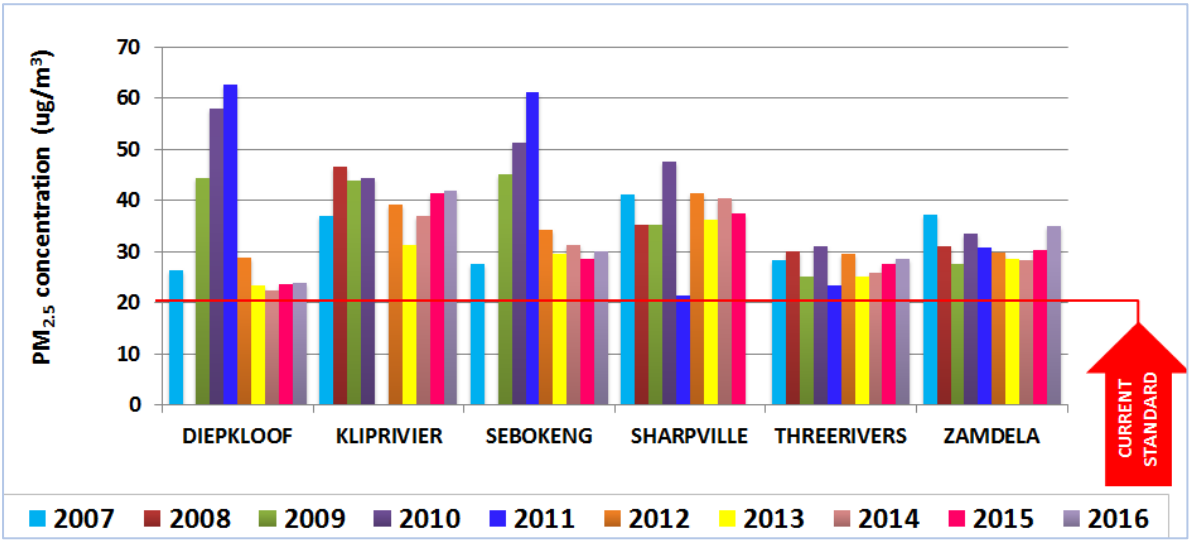

Figure 2.7 Change in $PM_{2.5}$ levels from the year 2007 to 2016 in the Vaal Triangle Priority Area.
Source: https://cer.org.za/

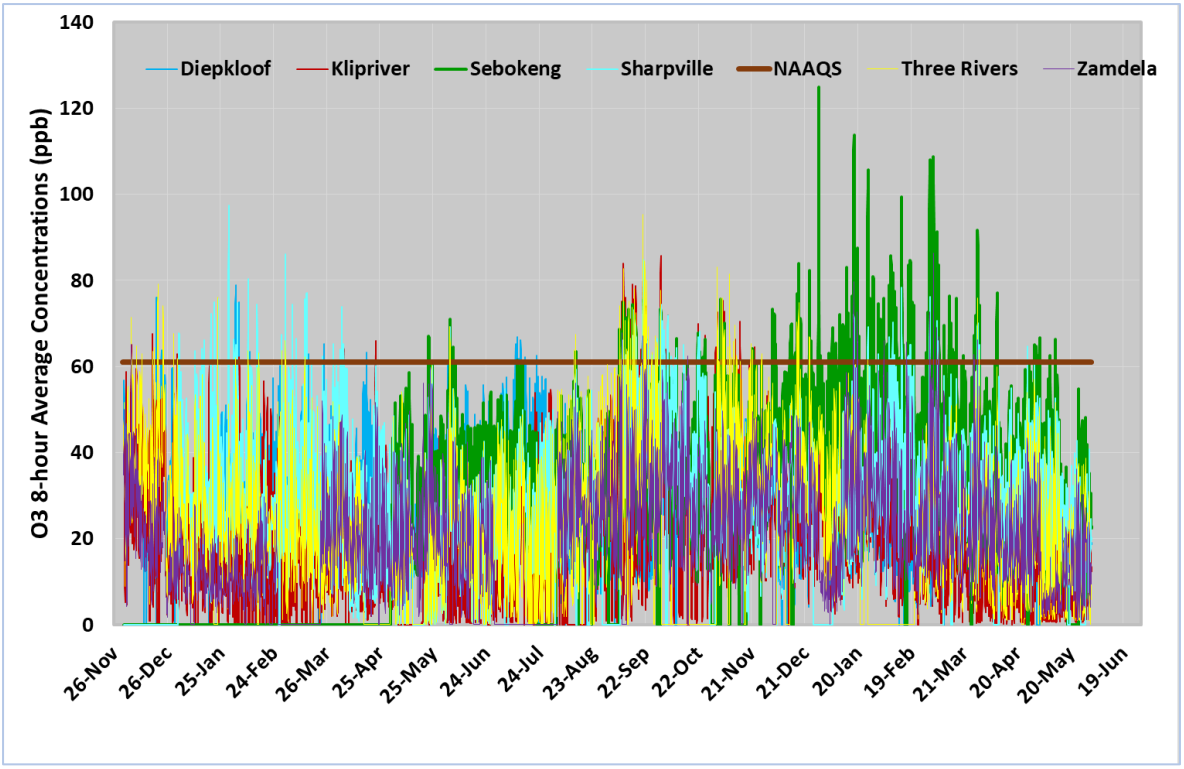

Figure 2.8 Change in O_3 levels monitored from December 2016 to May 2018 in the Vaal Triangle Priority Area.
Source: https://cer.org.za/

The high levels of O_3 and $PM_{2.5}$ observed, illustrate the need to study the emission of precursor compounds that lead to the formation of these pollutants, as they may be important contributors to observed ambient levels. In addition, the region of Southern Africa contains numerous sources of ozone and SOA forming compounds while presenting ideal environmental conditions for formation of these pollutants.

2.8 Hydrocarbon classes relevant to this study

2.8.1 Review of previous work on sampling and analysis of SVOCs

Several researchers have conducted diesel exhaust emission characterisation studies using a variety of sampling devices and analysis techniques. The emission factors reported by quantitative studies vary depending on the method used to collect the exhaust emissions, instrumental analysis techniques, fuel composition, engine design and engine operation, among other factors. The HCs identified in diesel exhaust span a wide range of chemical classes. Gaseous diesel exhaust HCs are composed predominantly of straight, branched and cycloalkanes, alkylbenzenes, 2-5 ring polycyclic aromatic hydrocarbons, and alkenes (Gentner et al., 2012, Storey et al.,

1999). Different studies focus on different classes of HCs, and report their emission factors using various formats, e.g. mass per distance travelled, mass per volume of fuel consumed, etc.

In this study, we focus on two HC classes: n-alkanes and alkylbenzenes, which are abundant in diesel exhaust emissions (Islam et al., 2011). Table 2.2 highlights the n-alkane and alkylbenzene HCs reported by four diesel exhaust characterisation studies, which have been used as an example. Gautam et al. (1996) attempted to speciate heavy duty diesel exhaust emissions under steady state conditions. In the study, dilute exhaust emissions were collected onto Teflon-coated glass fibre filters (particulates), XAD-2 resin cartridges (semi-volatiles) and Tedlar bags (volatiles) and were analysed using GC-FID (gas chromatography-flame ionisation detection). The emission rates of individual volatiles in the C_1-C_9 range, semi-volatiles in the C_8-C_{24} range and particulate bound organics in the C_9-C_{23} range were found. A total ozone formation potential (OFP) of 402.89 mg O_3/bhp-hr (ozone per brake horsepower-hour) was reported at 50% load conditions.

In 1999, Schauer et al. measured gaseous and particulate tailpipe organic emissions (C_1-C_{30}) from medium duty diesel trucks using a two-stage dilution source sampling system. Hot-start tests were conducted using the Federal Test Procedure (FTP) urban driving cycle and the study was able to determine the emission factors of 52 volatile HCs, 67 semi-volatile HCs and 28 particle phase HCs. Gentner et al. (2013) estimated the emission factors of unburned HCs from gasoline (petrol) and diesel engines using a fuel composition-based approach, which uses the weight fraction of each compound in the fuel and the total gas-phase organic carbon emission factor for uncombusted fuels. The study found that per mass of gas-phase compounds emitted, the organics in gasoline exhaust have the highest potential impact on ozone production (followed by gasoline non-tailpipe emissions and diesel exhaust respectively) due to products of incomplete combustion like alkenes and oxygenated VOCs.

Recently Alves et al. (2015) measured emissions from in-use light duty diesel and gasoline vehicles (Euro 4 – Euro 5) using the European driving cycle and the Assessment and Reliability of Transport Emission Models and Inventory Systems (ARTEMIS) real-world driving cycle. PM was collected onto pre-baked quartz fibre

filters and VOCs were sampled using steel tubes filled with Carbopack B and Carbopack C solid adsorbents. The study found that not all regulated emissions decreased between Euro 4 and Euro 5 vehicles and in general, cold-start driving conditions yielded higher emission factors.

2.8.2 Estimating the ozone formation potential of diesel exhaust hydrocarbons

In 1999 the National Research Council (NRC) of the United States stated that in order to use the OFP in mitigation programmes, it is necessary to develop an appropriate definition, and a protocol to quantify this potential.

One such definition, developed by Derwent et al. (1996) is the potential ozone creation potential (POCP) scale, calculated using a five day photochemical trajectory model that runs over Europe. The POCP index for each VOC is calculated from the change in mid-afternoon O_3 concentrations that result from removing the test VOC from the emissions. The model assesses the chemical development of an 'air parcel' as it travels across Europe. An additional 4.7 kg/km^2 is added for each HC, and the additional ozone formation is studied over a base case (highest O_3 concentration produced). HC POCPs are reported relative to a reference HC taken to be ethene. In general, when compared to the incremental reactivity scales (discussed below), the POCP approach produces qualitatively similar results (NRC, 1999).

The incremental reactivity (IR) scale, initially proposed by Atkinson and Carter (Carter, 1994, Carter and Atkinson, 1989) is defined as the additional mass (g) of O_3 formed per mass (g) of VOC added to a base mixture, i.e. the IR of a particular organic compound is the change in the O_3 generated upon introducing a small amount of the compound into an organic/NOx species mixture undergoing photo-oxidation. The IR value of each organic compound is highly dependent on organic/NOx mixture (concentration ratio) as well as the environmental conditions in the system, hence chemical mechanisms that model these variables are used to assign IR values to each species (Bowman and Seinfeld, 1994). Carter (1993, 1994) went on to develop 18 reactivity scales to calculate the reactivity of VOCs under varying conditions, using the Statewide Air Pollution Research Centre 1990 (SAPRC-90) chemical mechanism in a single-cell trajectory model. Three of these reactivity scales: the equal benefit incremental reactivity (EBIR) scale, the maximum ozone incremental reactivity (MOIR)

scale, and the maximum incremental reactivity (MIR) scale, have been used widely among researchers.

The MIR scale gives the impact of each compound on the peak ozone concentration in a system where the VOC-to-NOx ratio is low, hence ozone is being formed under high NOx concentrations, and is most sensitive to hydrocarbon emissions (Dunmore et al., 2015, NRC, 1999). The MOIR reactivity scale is computed for conditions that maximise the O_3 concentration, hence during conditions where the VOC-to-NOx ratio is moderate. The EBIR scale is used during conditions where O_3 is equally sensitive to the VOC and NOx concentration.

Although the MIOR and EBIR scales have their advantages, the California Air Resources Board (CARB, 1990) proposed use of the MIR scale for regulatory applications, as it yields reactivities under conditions that are most sensitive to VOC control. It was also found to correlate well with integrated O_3 yields, even at lower NOx conditions. For this reason, this scale is used extensively in the United States for policy-making as well as during VOC characterisation studies (Clark et al., 1996, Newkirk and Bass, 1995, Ou et al., 2015). The specific reactivity (MIR index) is normalised to the change in the mass of the VOC emissions and is expressed as the mass of O_3 formed per mass VOC emitted. The OFP (mass of O_3 formed per distance travelled) is obtained by multiplying the specific reactivity by the emission factor (EF) expressed as the mass of VOC emitted per distance driven (Equation 1).

$$MIR\ [gO_3/gVOC] \times EF\ [gVOC/km] = OFP\ [gO_3/km] \qquad (1)$$

Numerous diesel exhaust speciation studies that estimate the OFP of HC emissions report that alkylbenzene emissions have the highest OFP. This is most likely as a result of the high MIR indices of alkylbenzenes. For the same reason, n-alkanes, which have low MIR indices (<1), are reported to have the lowest OFP (Duffy et al., 1999, Gentner et al., 2013, Olumayede, 2014, Ou et al., 2015). It is important to note, however, that although n-alkanes have low MIR indices, their presence in large quantities (high emission rates) can make a significant contribution to the overall OFP of the fuel.

Table 2.2 Hydrocarbon emission factors reported from diesel exhaust characterisation studies.

Hydrocarbon	Emission factors				
	Schauer et al. 1999	Gentner et al. 2013	Gautam et al. 1996	Alves et al. 2015	
	Isuzu, four cylinder diesel engine (1995) & GMC Vandura 3500 eight-cylinder diesel engine	Tunnel study	MWM D916-6 diesel engine	Euro 4, Diesel, Citroen Xsara Picasso (2006)	Euro 5, Diesel DPF, Opel Astra (2011)
		n-alkanes			
propane		–			
n-butane	3.83 mg/km	–			
n-pentane	1.86 mg/km	–			
n-hexane		–			
n-heptane	0.47 mg/km	–		39.5 mg/km	110 mg/km
n-octane	0.26 mg/km	490 ± 412 µg C/L		128 mg/km	153 mg/km
n-nonane	0.16 mg/km	1070 ± 870 µg C/L	0.328 µg/Bhp-hr	102 mg/km	112 mg/km
n-decane		2710 ± 2110 µg C/L	0.349 µg/Bhp-hr	52.5 mg/km	53 mg/km
n-undecane		4930 ± 3040 µg C/L	0.55 µg/Bhp-hr	47mg/km	13.5 mg/km
n-dodecane	0.503 mg/km	4470 ± 1940 µg C/L	0.516 µg/Bhp-hr		
n-tridecane	0.477 mg/km	4030 ± 1470 µg C/L			
n-tetradecane	0.629 mg/km	4330 ± 1270 µg C/L	0.418 µg/Bhp-hr		
n-pentadecane	0.398 mg/km	4810 ± 1540 µg C/L	0.371 µg/Bhp-hr		
n-hexadecane	0.711 mg/km		1.007 µg/Bhp-hr		
n-heptadecane	0.614 mg/km		0.63 µg/Bhp-hr		
n-octadecane	0.601 mg/km		1.078 µg/Bhp-hr		
n-nonadecane	0.411 mg/km		0.7 µg/Bhp-hr		
n-eicosane	0.206 mg/km		0.604 µg/Bhp-hr		
n-heneicosane	0.0658 mg/km		0.541 µg/Bhp-hr		
n-docosane			0.744 µg/Bhp-hr		
n-tricosane			0.591 µg/Bhp-hr		
n-tetracosane			0.313 µg/Bhp-hr		
		alkylbenzenes			
benzene	2.74 mg/km	–		275 mg/km	521 mg/km
toluene	3.98 mg/km	911 ± 688 µg C/L		61.1 mg/km	63.3 mg/km
ethylbenzene	0.47 mg/km	529 ± 324 µg C/L		6.95 mg/km	4.11 mg/km
m- and p-xylene	2.33 mg/km	2760 ± 1580 µg C/L		28.6 mg/km	64.6 mg/km
o-xylene	0.83 mg/km	918 ± 438 µg C/L		20.6 mg/km	23.7 mg/km
styrene		–		11.1 mg/km	–
n-propylbenzene	0.1 mg/km	592 ± 251 µg C/L	0.564 µg/Bhp-hr	5.33 mg/km	1.68 mg/km
isopropylbenzene		187 ± 153 µg C/L	2.326 µg/Bhp-hr		
m- and p-ethyltoluene	0.73 mg/km	2920 ± 1250 µg C/L			
o-ethyltoluene		1100 ± 440 µg C/L			
isopropyltoluene			0.169 µg/Bhp-hr		
1,2,3-**trimethylbenzene**		1630 ± 910 µg C/L	0.199 µg/Bhp-hr		

Table 2.2 continued.

Hydrocarbon	Emission factors				
	Schauer et al. 1999	Gentner et al. 2013	Gautam et al. 1996	Alves et al. 2015	
	Isuzu, four cylinder diesel engine (1995) & GMC Vandura 3500 eight-cylinder diesel engine	Tunnel study	MWM D916-6 diesel engine	Euro 4, Diesel, Citroen Xsara Picasso (2006)	Euro 5, Diesel DPF, Opel Astra (2011)
1,3,5-trimethylbenzene	0.26 mg/km	982 ± 567 µg C/L	0.441 µg/Bhp-hr	28 mg/km	10.7 mg/km
1,2,4-trimethylbenzene	0.88 mg/km	5070 ± 2640 µg C/L	0.737 µg/Bhp-hr		
indan		1290 ± 970 µg C/L			
indene		–			
alpha-methylstyrene		–			
o- or m-methylstyrene		176 ± 136 µg C/L			
p-cymene		247 ± 232 µg C/L			
m-cymene		298 ± 253 µg C/L			
n-butylbenzene		1260 ± 880 µg C/L	0.231 µg/Bhp-hr	–	–
isobutylbenzene		69.6 ± 34.1 µg C/L			
sec-butylbenzene		–			
m-diethylbenzene		5960 ± 4670 µg C/L			
p-diethylbenzene		4180 ± 3300 µg C/L			
o-diethylbenzene		317 ± 121 µg C/L			
1-methyl-2-n-propylbenzene		717 ± 330 µg C/L			
1-methyl-3-n-propylbenzene		2470 ± 1430 µg C/L			
1-methyl-4-propylbenzene		–			
1,4-dimethyl-2-ethylbenzene		1750 ± 840 µg C/L			
1,3-dimethyl-4-ethylbenzene		1560 ± 760 µg C/L			
1,2-dimethyl-4-ethylbenzene		1120 ± 760 µg C/L			
1,3-dimethyl-2-ethylbenzene		642 ± 521 µg C/L			
1,2-dimethyl-3-ethylbenzene		498 ± 240 µg C/L			
1,2,4,5-tetramethylbenzene		736 ± 633 µg C/L			
1,2,3,5-tetramethylbenzene		1080 ± 650 µg C/L			
1,2,3,4-tetramethylbenzene		1630 ± 790 µg C/L			
1-methylindan		1470 ± 1200 µg C/L			
2-methylindan		2490 ± 1620 µg C/L			
trans-2-butenylbenzene		81 ± 44.6 µg C/L			
pentylbenzene			1.945 µg/Bhp-hr		
hexylbenzene			0.716 µg/Bhp-hr		

2.9 Characterising engine exhaust emissions

2.9.1 Engine emission test procedures

Dynamometer studies, remote sensing, on-road measurements, and tunnel air quality measurements are commonly utilized procedures for exhaust emissions testing (El-Fadel and Hashisho, 2001, Franco et al., 2013). These techniques have been used extensively for air quality and vehicle emission studies (Dong et al., 2014, Frank et al., 2004, Huang et al., 2017, Kerbachi et al., 2006, López-Aparicio and Hak, 2013, May et al., 2013, Mcgaughey et al., 2004, Schauer et al., 1999, Zhao et al., 2015).

On-road measurements, also called ‘chase’ measurements, involve following vehicles using a mobile laboratory which is equipped with on-board gas and/or aerosol measuring analytical instruments to conduct on-line measurements of emissions from the vehicle in motion. Remote sensing is similar to on-road measurements, however in remote sensing the sensor is placed by the side of the road and determines emissions as vehicles pass. Fast instrumentation (usually spectroscopic sensing) measures pollutant concentrations for each exhaust plume, corrected for the background concentrations, and report an average value for each passing vehicle. Both on-road measurements and remote sensing express the concentration ratio of the pollutant to CO_2, and can be normalised to fuel consumption. These techniques are advantageous as they allow for ‘screening’ of a large number of vehicles, under everyday operating conditions using local fuels (El-Fadel and Hashisho, 2001, Franco et al., 2013).

Tunnel studies are often performed to measure vehicular emission factors or to assess the air quality inside a roadway tunnel. The importance of these studies is due to the continuous increase in the size of the vehicle fleet, and because inadequate traffic flow results in saturation of tunnels and frequent congestion episodes, particularly in tunnels located in densely populated urban areas. Like remote sensing, during tunnel studies a large number of vehicles can be studied at their normal operating conditions, using local fuels. In addition, these measurements are able to measure contributions from non-tailpipe emissions, however parameters such as variability in the traffic, flow, speed and tunnel ventilation can introduce non-uniformities across the tunnel, hence affecting emission measurements (El-Fadel and Hashisho, 2001). As a result

emissions are often collected at the entrance and exit of the tunnel (Franco et al., 2013).

Vehicle dynamometer testing, typically used for emission testing from light-duty vehicles, employs a chassis dynamometer, also called a ‘rolling road’, which uses large rollers to simulate the resistance of a road, usually within an enclosed, controlled environment. During testing, the test vehicle’s driving wheels are positioned on the rollers, and the vehicle is driven according to a defined driving cycle. The dynamometer and associated instrumentation also give accurate measurements of the engine’s speed, torque, power and exhaust temperature, among other parameters. Exhaust emissions are diluted in a dilution tunnel located in a Constant Volume Sampler (CVS), and measurement/sampling of exhaust emissions can be made from the dilution tunnel (Alves et al., 2015, El-Fadel and Hashisho, 2001). Due to the practical limitation of testing heavy duty vehicles, their emissions are tested using engine dynamometer tests, where the stand alone engine is coupled to a transient engine dynamometer. The engine is operated using transient or steady-state speed and load schedules which are determined from real-world operating conditions and then adapted for engine dynamometer testing.

Engine dynamometers can also be used to directly simulate transient engine operation as if the engine were mounted in a vehicle, using so-called “road-load simulation”. During testing a continuously varying load is applied to the engine, simulating the frictional, inertial and aerodynamic forces which would be experienced by the vehicle, as well as simulating the transient loads that are generated in the drivetrain during operation of the clutch and gear changing. These loads are calculated using variables such as the vehicle mass, drag coefficient and a model of the vehicle’s drivetrain. Hence the engine is operated in a similar manner to when it is within a vehicle being physically driven through the driving cycle. Emissions can then be sampled directly from the exhaust pipe, or diluted using a full flow or partial flow dilution system as previously discussed, and sampled from the dilution system (El-Fadel and Hashisho, 2001, Schaberg and Wattrus, 2014).

2.9.2 Techniques used for sampling of PM and SVOC exhaust emissions

Diesel exhaust emissions consist of a mixture of gaseous and particulate substances from combustion products, unburned fuel and lubricant oil. A commonly used sampling method is the collection of dilute exhaust emissions into Tedlar® bags from a CVS, followed by direct instrumental analysis of the collected emissions. During analysis, a portion (volume) of the air can be injected directly into the instrument or the gaseous sample may be drawn from the bag and pre-concentrated on a suitable sorbent material prior to analysis. The sampling method is adequate for sampling of low molecular mass VOCs, however, heavier compounds tend to condense onto the walls of the sampling bags, which results in errors during quantitative analysis. As a result, it is used primarily for analysis of low molecular mass volatiles from petrol-powered engines and analysis of the light fraction ($<C_{12}$) of diesel engine exhaust (Bramston-Cook et al., 2000, Gordon et al., 2014, Hammerle et al., 1995, Lev-On et al., 2002).

Traditional partitioning sampling techniques employ high volume samplers that make use of a fibre filter to remove particles from the sample flow, whilst an adsorbent material such as Tenax or polyurethane foam (PUF), removes the gas phase analytes downstream of the filter (Geldenhuys et al., 2015). During their study of IVOC emissions from on-road diesel vehicles, Zhao et al. (2015) passed dilute diesel exhaust from a CVS system and employed a quartz filter followed by two adsorbent Tenax tubes, connected in series, where the second adsorbent tube was used to determine the IVOC breakthrough from the first adsorbent that occurred during sampling. In another study, diesel vehicles were operated on a chassis dynamometer. The exhaust emissions were diluted with filtered air using a CVS system, and then sampled onto quartz filters and preconditioned PUF (Kim et al., 2016). Corrêa and Arbilla (2006) successfully characterised aromatic emissions from diesel and biodiesel exhaust by pumping exhaust air through Teflon filters to retain PAHs associated with particulate matter, and XAD-2 cartridges that were in series with the filters, to retain vapour phase PAHs.

Although such high-volume samplers are robust and easy to use in the field, they exhibit inherent limitations due to the sampling configuration, high volumetric flow

rates, as well as high blank values, due to the presence of the pollutants in some sorbents. These sampling artifacts may be addressed by using denuders.

Denuder sampling devices have been used extensively for air monitoring applications (Forbes and Rohwer, 2015). During sampling, the gas phase analytes are stripped from the air sample onto a sorbent surface usually on the walls of the denuder, whilst particulates together with the particle-associated analytes remain in the airstream and are collected onto a filter downstream of the sorbent. A second sorbent is incorporated downstream of the filter to collect any breakthrough analytes from the first sorbent bed or any analyte volatilised from the particulate matter. The process is known as denudation and is a result of movement of analytes in the direction of the air stream due to active pumping, and movement perpendicular to the air stream due to radial diffusion. The retention of gaseous analytes by the sorbent during radial diffusion is a result of their high diffusion coefficients (Forbes and Rohwer, 2015).

In 1996, Ortner and Rohwer developed a multi-channel PDMS trap for analysis of SVOCs, and subsequently used these to successfully sample organic compounds that spanned a wide boiling point range from aqueous samples (Ortner and Rohwer, 1996). Since then the use of multi-channel PDMS traps as denuders for the partitioning of gas-particulate phase analytes has been illustrated in a number of studies; Forbes et al. (2012) demonstrated the suitability of multi-channel PDMS denuders for gas-particle partitioning of aerosols containing SVOCs, specifically PAHs. These denuders consist of two multi-channel PDMS traps for the collection of gas phase analytes and a quartz fibre filter sandwiched between the two traps for collection of particulates. The study also highlighted other applications where these denuder devices have been used successfully including collection of emissions from sugar cane burning and sampling of vehicular exhaust emissions (Forbes et al., 2012). Schauer et al. (1999) used a denuder/filter/PUF sampler and a traditional filter sampler during an early study on organic compounds from medium duty diesel trucks. It was observed that both the samplers yielded the same elemental carbon emission rate, however the particulate organic carbon emission rate determined by the denuder based sampler was 35% lower than the organic carbon mass collected by the traditional filter, and this was attributed to a positive vapour-phase sorption artefact affecting the traditional filter sampling technique. A study by Naudé and Rohwer (2012) used the PDMS denuder

for determination of vapour and particulate phase DDT in indoor air. Geldenhuys et al. (2015) successfully made use of denuder sampling devices for the simultaneous determination of gas and particle phase PAHs from diesel emissions in underground platinum mines in South Africa (the same sampling technique is employed in this study).

There are two major limitations suffered by high volume samplers. The first is adsorption of the target gas phase analyte onto the particulate matter collected on the filter or onto the filter medium itself. In a denuder setup, this is avoided by removal of the gas phase analytes prior to collection of the particulate matter downstream. The second artefact relates to volatilisation of the particle phase analyte from the filter. This is commonly referred to as "blow off." With a denuder device, this sampling artefact is addressed by placing a second gas phase sampling device downstream of the filter, which collects any blow off from the filter (Forbes and Rohwer, 2015).

2.10 Techniques for the compositional analysis of organic compounds in diesel exhaust emissions

2.10.1 Sample introduction methods

During analysis, organic compounds that have been sampled are extracted from the sorbent materials and/or filter substrates either by chemical extraction into solvents or by thermal extraction (Ballesteros et al., 2008), followed by instrumental analysis. After sampling diesel and biodiesel exhaust through SiO_2–C18 cartridges coated with 2,4-dinitrophenylhydrazine, Corrêa and Arbilla (2006) extracted the cartridges with acetonitrile, and quantitation of carbonyls was done by HPLC with UV detection. Brandenberger et al. (2005) determined particle bound paraffins from the exhaust of light duty vehicles. The filters used to collect the particulate emissions were extracted with dichloromethane (DCM) using a Soxhlet extraction apparatus and analysed by 2D-HPLC followed by GC-FID analysis.

Although used extensively, solvent extraction is time consuming, labour intensive and may introduce impurities that are present in the solvent. In addition, the use of large quantities of solvent makes this an environmentally unfriendly and economically wasteful method. To address this, alternative approaches have been developed. An

example is the plunger assisted solvent extraction (PASE) method developed by Munyeza et al. (2018), which uses a small volume of solvent (2 mL) for extraction. In the study, the PASE method was used to extract PAHs collected onto multi-channel PDMS traps with analysis by GC-MS. Fifteen priority PAHs (as determined by the U.S. Environmental Protection Agency) were successfully extracted with good recoveries. They compared the recovery and repeatability of the PASE method to that of thermal desorption of these samplers and found a recovery range of 76-99% for PASE and 66-93% for thermal desorption, showing that PASE was superior to thermal desorption in this regard. The efficiency of the PASE approach for more volatile analytes has not been established, however.

An alternative to solvent based extraction techniques is thermal desorption of the analytes from the sampler/filter substrates directly into the analytical systems. Thermal desorption is commonly used with gas chromatography yielding numerous advantages including the reduction of time and solvent consuming sample-preparation steps, reduction of analyte loss and memory effects (contamination by previous samples) by desorption of the sample within the GC-injector, and the low limit of quantitation (LOQ) achieved. To introduce the sample into the GC, elevated temperatures are used to release the analytes from the sorbent material and a Cooled Injection System (CIS) is used to concentrate them onto the stationary phase at the GC column head. A gradual temperature ramp is then applied to aid separation between compounds of different volatility (Ho and Yu, 2004). Limitations of the method include the loss of thermally degradable compounds and heavy compounds which may not completely desorb.

Schnelle-Kreis et al. (2005) demonstrated the use of direct thermal desorption-two dimensional gas chromatography-time of flight mass spectrometry (DTD-GC x GC-TOF-MS) to quantify SVOCs from ambient aerosol particles. Successful quantification of n-alkanes (C_{16}-C_{40}), n-alkan-2-ones (C_{13}-C_{35}), n-alkanoic acid methylesters (C_{12}-C_{27}), acetic acid esters (C_{20}-C_{34}), n-alkanoic acid amides (C_{12}-C_{20}), nitriles (C_{14}-C_{32}), linear alkylbenzenes and 2-alkyl-toluenes (chain length C_{13}-C_{29}), hopanes, as well as alkylated- and oxidised PAHs was achieved. Ho and Yu (2004) demonstrated the feasibility of using in-injection port thermal desorption to analyse n-alkanes (n-C_{13} to n-C_{36}) and PAHs from atmospheric aerosol samples collected on filter paper. They

found that TD provides LODs that were 12-120 times lower for n-alkanes and 9-500 times lower for PAHs than solvent extraction. Comparing the total ion chromatograms obtained from the use of both techniques showed fewer contamination peaks from the samples that were thermally desorbed. They did however find a good agreement in the concentrations determined by both techniques. The extent of agreement between the two methods was investigated by a linear fit model, and a strong correlation (R^2 = 0.94 for the n-alkanes and R^2 = 0.95 for the PAHs) was found (Ho and Yu, 2004).

2.10.2 Separation and detection methods

Comprehensive two dimensional gas chromatography is a relatively novel technique, especially useful for analysing analytes in complex samples, with a large number of compounds belonging to various chemical classes (Dallüge et al., 2003, Mondello et al., 2008). The key lies in the use of two capillary columns either positioned together in a single oven or in two separate ovens, connected in series. The primary column is usually apolar, and analyte separation is typically (but not entirely) related to the boiling points/volatility. The secondary column is usually polar and separates analytes according to their polarity (Mondello et al., 2008).

A transfer device called the modulator is located at the head of the secondary column and functions to isolate, reconcentrate and introduce portions of the effluent from the primary column into the secondary column. Modulation today is often achieved using either flow modulation or thermal modulation. The latter technique is used herein, where a cryogen (liquid N_2) is used to achieve the low temperatures required to trap and focus analytes from the primary column. In principle, during modulation, a sharp band (plug) of effluent from the primary column is formed at the head of the modulator which is maintained at a low temperature (cryofocused). Rapid heating allows for mobilization of this plug to cold jet 1. Simultaneously hot jet 2 is turned on to release the cryofocused analytes from the previous modulation into the secondary column. Hot jet 1 then turns on to release the cryofocused analytes from the primary column and simultaneously cold jet 2 is turned on to trap these incoming analytes and later release them onto the secondary column (Savareear and Shellie, 2013). The time required to complete this 3-step process is called the modulation period (3-8 s). Modulation occurs continuously throughout the analysis (Mondello et al., 2008). Depending on the peak width (sec), a peak might be modulated 3-4 times and the

peak area is obtained by summing up the peak areas belonging to the same analyte (Tranchida et al., 2019, Mondello et al., 2008).

It is evident that modulation is the crux of two dimensional gas chromatography, where analytes are not only separated but also grouped into different chemical class and/or structural groups. Coupled with detectors such as flame ionisation, thermal conductivity, electron capture and mass spectrometry detectors, it becomes a very powerful technique for analysis of complex samples. A few drawbacks of the technique include high operational costs, instrumentation complexity and operational expertise requirements.

Diesel engine exhaust is a highly complex mixture containing a vast number of compounds, spanning various chemical classes and phases, hence high-resolution separation techniques coupled to suitable detectors are often employed for sample analysis. Erickson et al. (2014) used thermal desorption with proton transfer reaction mass spectrometry (PTR-MS) to analyse diesel exhaust samples. VOCs and heavier organic compounds were collected on Tenax TA adsorbent traps. During PTR-MS, long chain alkanes undergo proton transfer reactions that form a series of fragment ions (with the formula C_nH_{2n+1}) and from the abundance of these ions, the alkanes can be quantified. Although it is insensitive to n-alkanes smaller than n-C_8, PTR-MS shows increasing sensitivity for longer alkanes.

Gas chromatography with flame ionisation detection (GC-FID) is also a technique commonly used to analyse petroleum emission samples, however according to Mao et al. (2009) the technique does not allow complete resolution of complex samples. In order to characterise HCs in motor oil, Mao et al. (2009) used high-performance liquid chromatography (HPLC) followed by comprehensive two dimensional gas chromatography-flame ionisation detection (GC x GC-FID). HPLC achieved prior fractionation of the samples, followed by further separation by 2D-GC. This method proved to be more applicable and more reliable for accurate, group-type characterisation of oils. In a study of diesel related HCs in mega cities, Dunmore et al. (2015) used comprehensive two dimensional gas chromatography-flame ionisation detection (GC x GC-FID) to analyse air samples acquired at an urban background site.

They successfully characterised HCs from n-C_6 to n-C_{13} and a large group of oxygenated VOCs.

Multi-dimensional gas chromatography is evidently a powerful technique that has been used extensively to characterise complex samples from different sources (Cortes et al., 2009, Marriott et al., 2012, Seeley and Seeley, 2013), and is commonly used for fuel analysis (Adam et al., 2008, Van Der Westhuizen et al., 2011). The resolving power of 2D chromatography lies in the use of two independent gas chromatographic columns to achieve separation along two dimensions.

For this study, engine dynamometer tests were used for emissions testing. This test procedure proved to be useful to simulate on-road transient vehicle operation. Emissions could also be sampled directly from the exhaust pipe and diluted using an MDLT dilution system, making it suitable for analysis by TD-GC×GC-TofMS. Portable PDMS sampling devices were employed for collection of emissions, as this sampling technique has been successfully utilised for collection of SVOCs particularly from vehicle exhaust, in addition to being an efficient and convenient sampling method considering that samples had to be stored and transported post sampling. Thermal desorption-two dimensional gas chromatography-time of flight mass spectrometry was chosen for sample analysis. The resolving power of 2D chromatography was especially useful to separate emissions from a complex sample like diesel exhaust, containing a large number of compounds from different chemical classes. The use of temperature programmed analysis also allowed for improved resolution between peaks, particularly high molecular mass HCs which dominate the UCM.

2.11 References

Adam, F., Bertoncini, F., Coupard, V., Charon, N., Thiébaut, D., Espinat, D. & Hennion, M. 2008. Using comprehensive two-dimensional gas chromatography for the analysis of oxygenates in middle distillates: I. Determination of the nature of biodiesels blend in diesel fuel. *Journal of Chromatography A,* 1186**,** 236-244.

Alves, C. A., Lopes, D. J., Calvo, A. I., Evtyugina, M., Rocha, S. & Nunes, T. 2015. Emissions from light-duty diesel and gasoline in-use vehicles measured on chassis dynamometer test cycles. *Aerosol and Air Quality Research,* 15**,** 99-116.

Ansell, G., Bennett, P., Cox, J., Frost, J., Gray, P., Jones, A.-M., Rajaram, R., Walker, A., Litorell, M. & Smedler, G. 1996. The development of a model capable of predicting diesel lean NOx catalyst performance under transient conditions. *Applied Catalysis B: Environmental,* 10**,** 183-201.

Atkinson, R., Darnall, K. R., Lloyd, A. C., Winer, A. M. & Pitts Jr, J. N. 1979. Kinetics and mechanisms of the reactions of the hydroxyl radical with organic compounds in the gas phase. *Advances In Photochemistry,* 11**,** 375-488.

Ballesteros, R., Hernandez, J., Lyons, L., Cabanas, B. & Tapia, A. 2008. Speciation of the semivolatile hydrocarbon engine emissions from sunflower biodiesel. *Fuel,* 87**,** 1835-1843.

Bowman, F. M. & Seinfeld, J. H. 1994. Fundamental basis of incremental reactivities of organics in ozone formation in VOC/NOx mixtures. *Atmospheric Environment,* 28**,** 3359-3368.

Bramston-Cook, R., Scesny, M. & Brittain, R. D. 2000. Determination of Hydrocarbons in diesel exhaust. *Proc. of International Symposium on the Measurement of Toxic and Related Air Pollutants*. North Carolina, USA.

Brandenberger, S., Mohr, M., Grob, K. & Neukom, H. P. 2005. Contribution of unburned lubricating oil and diesel fuel to particulate emission from passenger cars. *Atmospheric Environment,* 39**,** 6985-6994.

Carter, W. P. & Atkinson, R. 1989. Computer modeling study of incremental hydrocarbon reactivity. *Environmental Science & Technology,* 23**,** 864-880.

Carter, W.P. 1993. Development and Application of an Up-to-Date Photo-chemical Mechanism for Airshed Modeling and Reactivity Assessment, Draft Final Report for California Air Resources Board, Contract No. A934-094 Research Division, Sacramento, CA. April 26.

Carter, W. P. 1994. Development of ozone reactivity scales for volatile organic compounds. *Air & Waste*, 44, 881-899.

Chehroudi, B. 2015. Diesel engine emissions: Hydrocarbons (HC). [Online] Available at https://www.researchgate.net/pblication/277303525_Diesel_Engine_Hydrocarbons_HC/stat [Accessed 22-03-2020].

Clark, N. N., Atkinson, C. M., Mckain, D. L., Nine, R. D. & El-Gazzar, L. 1996. Speciation of Hydrocarbon Emissions from a Medium Duty Diesel Engine. *SAE Technical Paper* 960322. https://doi.org/10.4271/960322

Correa, S. M. & Arbilla, G. 2006. Aromatic hydrocarbons emissions in diesel and biodiesel exhaust. *Atmospheric Environment,* 40**,** 6821-6826.

Cortes, H. J., Winniford, B., Luong, J. & Pursch, M. 2009. Comprehensive two dimensional gas chromatography review. *Journal of Separation Science,* 32**,** 883-904.

Cross, E. S., Sappok, A. G., Wong, V. W. & Kroll, J. H. 2015. Load-dependent emission factors and chemical characteristics of IVOCs from a medium-duty diesel engine. *Environmental Science & Technology,* 49**,** 13483-13491.

Dallüge, J., Beens, J. and Udo, A., 2003. Comprehensive two-dimensional gas chromatography: a powerful and versatile analytical tool. *Journal of Chromatography A*, 1000(1-2), pp.69-108.

Darnall, K. R., Atkinson, R. & Pitts, J. N. 1979. Observation of biacetyl from the reaction of OH radicals with o-xylene. Evidence for ring cleavage. *Journal of Physical Chemistry,* 83**,** 1943-1946.

De Nevers, N. 2010, Chapter 13: The Motor Vehicle Problem in Air Pollution Control Engineering, 2nd ed., pp. 471-506, *Waveland Press*, USA.

Deng, W., Hu, Q., Liu, T., Wang, X., Zhang, Y., Song, W., Sun, Y., Bi, X., Yu, J. & Yang, W. 2017. Primary particulate emissions and secondary organic aerosol (SOA) formation from idling diesel vehicle exhaust in China. *Science of the Total Environment,* 593**,** 462-469.

Department of Environmental Affairs. 2009. State of Air Report 2005 [Online]. Available: www.environment.gov.za [Accessed 28 February 2020].

Derwent, R., Jenkin, M. & Saunders, S. 1996. Photochemical ozone creation potentials for a large number of reactive hydrocarbons under European conditions. *Atmospheric Environment,* 30**,** 181-199.

Dong, D., Shao, M., Li, Y., Lu, S., Wang, Y., Ji, Z. & Tang, D. 2014. Carbonyl emissions from heavy-duty diesel vehicle exhaust in China and the contribution to ozone formation potential. *Journal of Environmental Sciences,* 26**,** 122-128.

Duffy, B., Nelson, P., Ye, Y. & Weeks, I. 1999. Speciated hydrocarbon profiles and calculated reactivities of exhaust and evaporative emissions from 82 in-use light-duty Australian vehicles. *Atmospheric Environment,* 33**,** 291-307.

Dunmore, R., Hopkins, J., Lidster, R., Lee, J., Evans, M., Rickard, A., Lewis, A. & Hamilton, J. 2015. Diesel-related hydrocarbons can dominate gas phase reactive carbon in megacities. *Atmospheric Chemistry and Physics,* 15**,** 9983-9996.

El-Fadel, M. & Hashisho, Z. 2001. Vehicular emissions in roadway tunnels: a critical review. *Critical Reviews in Environmental Science and Technology,* 31**,** 125-174.

Englert, N. 2004. Fine particles and human health—a review of epidemiological studies. *Toxicology Letters,* 149**,** 235-242.

Erickson, M., Gueneron, M. & Jobson, B. 2014. Measuring long chain alkanes in diesel engine exhaust by thermal desorption PTR-MS. *Atmospheric Measurement Techniques,* 7**,** 225-239.

Field, R., Goldstone, M., Lester, J. & Perry, R. 1992. The sources and behaviour of tropospheric anthropogenic volatile hydrocarbons. *Atmospheric Environment. Part A. General Topics,* 26**,** 2983-2996.

Forbes, P. B., Karg, E. W., Zimmermann, R. & Rohwer, E. R. 2012. The use of multi-channel silicone rubber traps as denuders for polycyclic aromatic hydrocarbons. *Analytica Chimica Acta,* 730**,** 71-79.

Forbes, P. B. & Rohwer, E. R. 2015, Chapter 5: Denuders in Comprehensive Analytical Chemistry, vol. 70: Monitoring of Air Pollutants: Sampling, Sample Preparation and Analytical Techniques, Patricia Forbes (ed.). pp. 153-181, *Elsevier*, Netherlands.

Franco, V., Kousoulidou, M., Muntean, M., Ntziachristos, L., Hausberger, S. & Dilara, P. 2013. Road vehicle emission factors development: A review. *Atmospheric Environment,* 70**,** 84-97.

Frank, B. P., Tang, S., Lanni, T., Rideout, G., Beregszaszy, C., Meyer, N., Chatterjee, S., Conway, R., Lowell, D. & Bush, C. 2004. A study of the effects of fuel type and emission control systems on regulated gaseous emissions from heavy-duty diesel engines. *SAE Technical Paper 2004-01-1085* https://doi.org/10.4271/2004-01-1085.

Gautam, M., Gupta, D., El-Gazzar, L., Lyons, D. W. & Popuri, S. 1996. Speciation of heavy duty diesel exhaust emissions under steady state operating conditions. *SAE Technical Paper* 962159. https://doi.org/10.4271/962159.

Geldenhuys, G., Rohwer, E. R., Naudé, Y. & Forbes, P. B. 2015. Monitoring of atmospheric gaseous and particulate polycyclic aromatic hydrocarbons in South African platinum mines utilising portable denuder sampling with analysis by thermal desorption–comprehensive gas chromatography–mass spectrometry. *Journal of Chromatography A,* 1380**,** 17-28.

Gentner, D. R., Isaacman, G., Worton, D. R., Chan, A. W., Dallmann, T. R., Davis, L., Liu, S., Day, D. A., Russell, L. M. & Wilson, K. R. 2012. Elucidating secondary organic aerosol from diesel and gasoline vehicles through detailed characterization of organic carbon emissions. *Proceedings of the National Academy of Sciences,* 109**,** 18318-18323.

Gentner, D. R., Worton, D. R., Isaacman, G., Davis, L. C., Dallmann, T. R., Wood, E. C., Herndon, S. C., Goldstein, A. H. & Harley, R. A. 2013. Chemical composition of gas-phase organic carbon emissions from motor vehicles and implications for ozone production. *Environmental Science & Technology,* 47**,** 11837-11848.

Gentner, D. R., Jathar, S. H., Gordon, T. D., Bahreini, R., Day, D. A., El Haddad, I., Hayes, P. L., Pieber, S. M., Platt, S. M. & De Gouw, J. 2017. Review of urban secondary organic aerosol formation from gasoline and diesel motor vehicle emissions. *Environmental Science & Technology,* 51**,** 1074-1093.

Gordon, T., Presto, A., May, A., Nguyen, N., Lipsky, E., Donahue, N., Gutierrez, A., Zhang, M., Maddox, C. & Rieger, P. 2014. Secondary organic aerosol formation exceeds primary particulate matter emissions for light-duty gasoline vehicles. *Atmospheric Chemistry & Physics,* 14**,** 4661–4678.

Griffin, R. J., Cocker Iii, D. R., Seinfeld, J. H. & Dabdub, D. 1999. Estimate of global atmospheric organic aerosol from oxidation of biogenic hydrocarbons. *Geophysical Research Letters,* 26**,** 2721-2724.

Gwaze, P. & Mashele, S. H. 2018. South African Air Quality Information System (SAAQIS) mobile application tool: bringing real time state of air quality to South Africans. *Clean Air Journal,* 28**,** 3-4.

Haagen-Smit, A. J. & Fox, M. 1954. Photochemical ozone formation with hydrocarbons and automobile exhaust. *Air Repair,* 4**,** 105-136.

Hallquist, M., Wenger, J. C., Baltensperger, U., Rudich, Y., Simpson, D., Claeys, M., Dommen, J., Donahue, N., George, C. & Goldstein, A. 2009. The formation, properties and impact of secondary organic aerosol: current and emerging issues. *Atmospheric Chemistry and Physics,* 9**,** 5155-5236.

Hammerle, R. H., Siegl, W. O., Herrmann, H. M. & Wenclawiak, B. W. 1995. A method for the speciation of diesel fuel and the semi-volatile hydrocarbon fraction of diesel-fueled vehicle exhaust emissions. *SAE Technical Paper* 952353. https://doi.org/10.4271/952353

Ho, S. S. H. & Yu, J. Z. 2004. In-injection port thermal desorption and subsequent gas chromatography–mass spectrometric analysis of polycyclic aromatic hydrocarbons and n-alkanes in atmospheric aerosol samples. *Journal of Chromatography A,* 1059**,** 121-129.

Huang, C., Tao, S., Lou, S., Hu, Q., Wang, H., Wang, Q., Li, L., Wang, H., Quan, Y. & Zhou, L. 2017. Evaluation of emission factors for light-duty gasoline vehicles based on chassis dynamometer and tunnel studies in Shanghai, China. *Atmospheric Environment*, 169, 193-203.

Islam, M. R., Joardder, M. U. H., Kader, M. & Sarker, M. 2011. Valorization of solid tire wastes available in Bangladesh by thermal treatment. *Proceedings of the Waste Safe 2011 – 2nd International Conference on Solid Waste Management in the Developing Countries*, 13-15 February 2011, Khulna, Bangladesh.

Jathar, S. H., Miracolo, M. A., Tkacik, D. S., Donahue, N. M., Adams, P. J. & Robinson, A. L. 2013. Secondary organic aerosol formation from photo-oxidation of unburned fuel: Experimental results and implications for aerosol formation from combustion emissions. *Environmental Science & Technology*, 47, 12886-12893.

Jathar, S. H., Gordon, T. D., Hennigan, C. J., Pye, H. O., Pouliot, G., Adams, P. J., Donahue, N. M. & Robinson, A. L. 2014. Unspeciated organic emissions from combustion sources and their influence on the secondary organic aerosol budget in the United States. *Proceedings of the National Academy of Sciences*, 111, 10473-10478.

Ji, Y., Zhao, J., Terazono, H., Misawa, K., Levitt, N. P., Li, Y., Lin, Y., Peng, J., Wang, Y. & Duan, L. 2017. Reassessing the atmospheric oxidation mechanism of toluene. *Proceedings of the National Academy of Sciences,* 114**,** 8169-8174.

Kagawa, J. 2002. Health effects of diesel exhaust emissions—a mixture of air pollutants of worldwide concern. *Toxicology,* 181**,** 349-353.

Kerbachi, R., Boughedaoui, M., Bounoua, L. & Keddam, M. 2006. Ambient air pollution by aromatic hydrocarbons in Algiers. *Atmospheric Environment,* 40**,** 3995-4003.

Kim, Y., Sartelet, K., Seigneur, C., Charron, A., Besombes, J.-L., Jaffrezo, J.-L., Marchand, N. & Polo, L. 2016. Effect of measurement protocol on organic aerosol measurements of exhaust emissions from gasoline and diesel vehicles. *Atmospheric Environment,* 140**,** 176-187.

Laban, T. L., Van Zyl, P. G., Beukes, J. P., Vakkari, V., Jaars, K., Borduas-Dedekind, N., Josipovic, M., Thompson, A. M., Kulmala, M. & Laakso, L. 2018. Seasonal influences on surface ozone variability in continental South Africa and implications for air quality. *Atmospheric Chemistry and Physics,* 18**,** 15491–15514.

Latha, H., Prakash, K., Veerangouda, M., Maski, D. & Ramappa, K. 2019. A Review on SCR System for NOx Reduction in Diesel Engine. *International Journal of Current Microbiology and Applied Sciences,* 8**,** 1553-1559.

Lee, T., Park, J., Kwon, S., Lee, J. & Kim, J. 2013. Variability in operation-based NOx emission factors with different test routes, and its effects on the real-driving emissions of light diesel vehicles. *Science of the Total Environment,* 461**,** 377-385.

Leggett, T. 2018. Diesel ban approved for German cities to cut pollution [Online]. Available: https://www.bbc.com/news/business-43211946 [Accessed 27 February 2018].

Lev-On, M., Letavec, C., Uihlein, J., Kimura, K., Alleman, T. L., Lawson, D. R., Vertin, K., Gautam, M., Thompson, G. J. & Wayne, W. S. 2002. Speciation of organic compounds from the exhaust of trucks and buses: Effect of fuel and after-treatment on vehicle emission profiles. *SAE Technical Paper* 2002-01-2873. https://doi.org/10.4271/2002-01-2873

Liu, Z. G., Berg, D. R., Swor, T. A. & Schauer, J. J. 2008. Comparative analysis on the effects of diesel particulate filter and selective catalytic reduction systems on a wide spectrum of chemical species emissions. *Environmental Science & Technology,* 42**,** 6080-6085.

Lloyd, A. C. & Cackette, T. A. 2001. Diesel engines: environmental impact and control. *Journal of the Air & Waste Management Association,* 51**,** 809-847.

López-Aparicio, S. & Hak, C. 2013. Evaluation of the use of bioethanol fuelled buses based on ambient air pollution screening and on-road measurements. *Science of the Total Environment,* 452**,** 40-49.

Majewski, W. & Jääskeläinen, H. 2016. What is Diesel Fuel [Online]. Available: https://dieselnet.com/tech/fuel_diesel.php [Accessed 2019-01-24].
Mao, D., Van De Weghe, H., Lookman, R., Vanermen, G., De Brucker, N. & Diels, L. 2009. Resolving the unresolved complex mixture in motor oils using high-performance liquid chromatography followed by comprehensive two-dimensional gas chromatography. *Fuel,* 88**,** 312-318.
Marchal, V., Dellink, R., Van Vuuren, D., Clapp, C., Chateau, J., Magné, B. & Van Vliet, J. 2011. OECD environmental outlook to 2050. *Organization for Economic Co-operation and Development,* 8**,** 397-413.
Marriott, P. J., Chin, S.-T., Maikhunthod, B., Schmarr, H.-G. & Bieri, S. 2012. Multidimensional gas chromatography. *TrAC Trends in Analytical Chemistry,* 34**,** 1-21.
May, A. A., Presto, A. A., Hennigan, C. J., Nguyen, N. T., Gordon, T. D. & Robinson, A. L. 2013. Gas-particle partitioning of primary organic aerosol emissions:(2) Diesel vehicles. *Environmental Science & Technology,* 47**,** 8288-8296.
Mcdonald, B. C., Gentner, D. R., Goldstein, A. H. & Harley, R. A. 2013. Long-term trends in motor vehicle emissions in US urban areas. *Environmental Science & Technology,* 47**,** 10022-10031.
Mcdonald, B. C., Goldstein, A. H. & Harley, R. A. 2015. Long-term trends in California mobile source emissions and ambient concentrations of black carbon and organic aerosol. *Environmental Science & Technology,* 49**,** 5178-5188.
Mcgaughey, G. R., Desai, N. R., Allen, D. T., Seila, R. L., Lonneman, W. A., Fraser, M. P., Harley, R. A., Pollack, A. K., Ivy, J. M. & Price, J. H. 2004. Analysis of motor vehicle emissions in a Houston tunnel during the Texas Air Quality Study 2000. *Atmospheric Environment,* 38**,** 3363-3372.
Michaels, R. A. & Kleinman, M. T. 2000. Incidence and apparent health significance of brief airborne particle excursions. *Aerosol Science & Technology,* 32**,** 93-105.
Miller, G. T., Hackett, J. & Hackett, D. 2011, Chapter 20: Photochemical and Industrial Smog in Living in the Environment, 2nd ed., 465-471, *Nelson*, USA.
Mollenhauer, K. & Tschoeke, H. 2010, Chapter 3: Diesel Engine Combustion in Handbook of Diesel Engines, Klaus Mollenhauer & Helmut, Tschoeke (eds.). pp. 61-75, *Springer*, Berlin.
Mondello, L., Tranchida, P.Q., Dugo, P. and Dugo, G., 2008. Comprehensive two-dimensional gas chromatography-mass spectrometry: A review. *Mass spectrometry reviews*, 27(2), pp.101-124.
Munyeza, C. F., Dikale, O., Rohwer, E. R. & Forbes, P. B. 2018. Development and optimization of a plunger assisted solvent extraction method for polycyclic aromatic hydrocarbons sampled onto multi-channel silicone rubber traps. *Journal of Chromatography A,* 1555**,** 20-29.
Naeher, L. P., Brauer, M., Lipsett, M., Zelikoff, J. T., Simpson, C. D., Koenig, J. Q. & Smith, K. R. 2007. Woodsmoke health effects: a review. *Inhalation Toxicology,* 19**,** 67-106.
Nakatsuji, T., Yasukawa, R., Tabata, K., Ueda, K. & Niwa, M. 1998. Catalytic reduction system of NOx in exhaust gases from diesel engines with secondary fuel injection. *Applied Catalysis B: Environmental,* 17**,** 333-345.
Naudé, Y. & Rohwer, E. R. 2012. Novel method for determining DDT in vapour and particulate phases within contaminated indoor air in a malaria area of South Africa. *Analytica Chimica Acta,* 730**,** 112-119.
Nawrot, T., Torfs, R., Fierens, F., De Henauw, S., Hoet, P., Van Kersschaever, G., De Backer, G. & Nemery, B. 2007. Stronger associations between daily mortality and fine particulate air pollution in summer than in winter: evidence from a heavily polluted region in western Europe. *Journal of Epidemiology & Community Health,* 61**,** 146-149.
Newkirk, M. S. & Bass, E. A. 1995. Reactivity comparison of exhaust emissions from heavy-duty engines operating on gasoline, diesel, and alternative fuels. *SAE Transactions* 952442*,* 104**,** 1339-1348.
NRC 1999, Chapter 3: The Concept of Ozone-Forming Potential and Its Quantification in Ozone-Forming Potential of Reformulated Gasoline, RJ Crossgrove (ed.). 33-69, *National Academies Press*, Washington D.C.
Olumayede, E. G. 2014. Atmospheric volatile organic compounds and ozone creation potential in an urban center of southern Nigeria. *International Journal of Atmospheric Sciences,* Article ID 764948 https://doi.org/10.1155/2014/764948.
Ono-Ogasawara, M. & Smith, T. J. 2004. Diesel exhaust particles in the work environment and their analysis. *Industrial Health,* 42**,** 389-399.
Ortner, E. K. & Rohwer, E. R. 1996. Trace analysis of semi-volatile organic air pollutants using thick film silicone rubber traps with capillary gas chromatography. *Journal of High Resolution Chromatography,* 19**,** 339-344.

Ou, J., Zheng, J., Li, R., Huang, X., Zhong, Z., Zhong, L. & Lin, H. 2015. Speciated OVOC and VOC emission inventories and their implications for reactivity-based ozone control strategy in the Pearl River Delta region, China. *Science of the Total Environment,* 530**,** 393-402.

Reşitoğlu, İ. A., Altinişik, K. & Keskin, A. 2015. The pollutant emissions from diesel-engine vehicles and exhaust aftertreatment systems. *Clean Technologies and Environmental Policy,* 17**,** 15-27.

Ris, C. 2007. US EPA health assessment for diesel engine exhaust: a review. *Inhalation Toxicology,* 19**,** 229-239.

Robinson, A. L., Donahue, N. M., Shrivastava, M. K., Weitkamp, E. A., Sage, A. M., Grieshop, A. P., Lane, T. E., Pierce, J. R. & Pandis, S. N. 2007. Rethinking organic aerosols: Semivolatile emissions and photochemical aging. *Science,* 315**,** 1259-1262.

Rounce, P., Tsolakis, A. & York, A. 2012. Speciation of particulate matter and hydrocarbon emissions from biodiesel combustion and its reduction by aftertreatment. *Fuel,* 96**,** 90-99.

Samy, S. & Zielinska, B. 2010. Secondary organic aerosol production from modern diesel engine emissions. *Atmospheric Chemistry & Physics,* 10**,** 609-625.

Savareear, B. and Shellie, R.A., 2013. Multiplexed dual second-dimension column comprehensive two-dimensional gas chromatography (GC× 2GC) using thermal modulation and contra-directional second-dimension columns. *Analytica Chimica Acta*, 803, pp.160-165.

Schaberg, P. & Wattrus, M. 2014. Comparative Emissions Performance of Blends of GTL Diesel and FAME. *SAE Technical Paper* 2014-01-2769 https://doi.org/10.4271/2014-01-2769.

Schauer, J. J., Kleeman, M. J., Cass, G. R. & Simoneit, B. R. 1999. Measurement of emissions from air pollution sources. 2. C1 through C30 organic compounds from medium duty diesel trucks. *Environmental Science & Technology,* 33**,** 1578-1587.

Schnelle-Kreis, J., Welthagen, W., Sklorz, M. & Zimmermann, R. 2005. Application of direct thermal desorption gas chromatography and comprehensive two-dimensional gas chromatography coupled to time of flight mass spectrometry for analysis of organic compounds in ambient aerosol particles. *Journal of Separation Science,* 28**,** 1648-1657.

Seeley, J. V. & Seeley, S. K. 2013. Multidimensional gas chromatography: fundamental advances and new applications. *Analytical Chemistry,* 85**,** 557-578.

Shah, S. D., Cocker, D. R., Miller, J. W. & Norbeck, J. M. 2004. Emission rates of particulate matter and elemental and organic carbon from in-use diesel engines. *Environmental Science & Technology,* 38**,** 2544-2550.

Smith, K. R., Frumkin, H., Balakrishnan, K., Butler, C. D., Chafe, Z. A., Fairlie, I., Kinney, P., Kjellstrom, T., Mauzerall, D. L. & Mckone, T. E. 2013. Energy and human health. *Annual Review of Public Health,* 34**,** 159-188.

Storey, J. M., Domingo, N., Lewis, S. A. & Irick, D. K. 1999. Analysis of semivolatile organic compounds in diesel exhaust using a novel sorption and extraction method. *SAE Technical Paper* 1999-01-3534 https://doi.org/10.4271/1999-01-3534.

Szidat, S., Jenk, T. M., Gäggeler, H. W., Synal, H.-A., Fisseha, R., Baltensperger, U., Kalberer, M., Samburova, V., Reimann, S. & Kasper-Giebl, A. 2004. Radiocarbon (14C)-deduced biogenic and anthropogenic contributions to organic carbon (OC) of urban aerosols from Zürich, Switzerland. *Atmospheric Environment,* 38**,** 4035-4044.

Tang, S., Frank, B. P., Lanni, T., Rideout, G., Meyer, N. & Beregszaszy, C. 2007. Unregulated emissions from a heavy-duty diesel engine with various fuels and emission control systems. *Environmental Science & Technology,* 41**,** 5037-5043.

Tkacik, D. S., Lambe, A. T., Jathar, S., Li, X., Presto, A. A., Zhao, Y., Blake, D., Meinardi, S., Jayne, J. T. & Croteau, P. L. 2014. Secondary organic aerosol formation from in-use motor vehicle emissions using a potential aerosol mass reactor. *Environmental Science & Technology,* 48**,** 11235-11242.

Tranchida, P.Q. & Mondello, L. 2019, Chapter 2: Two dimensional capillary gas chromatography based processes combined with mass spectrometry in Hyphenations of Capillary Chromatography with Mass Spectrometry, pp 135-267, *Elsevier*, Netherlands.

US EPA 2002. Health assessment document for diesel engine exhaust. Environmental Protection Agency, Office of Research and Development, National Center for Environmental Assessment, EPA 600/8-90/057F. Washington, DC*,* U.S. [Online]. Available: https://cfpub.epa.gov/ncea/risk/recordisplay.cfm?deid=29060 [Accessed 2019-08-21]

Van Der Westhuizen, R., Ajam, M., De Coning, P., Beens, J., De Villiers, A. & Sandra, P. 2011. Comprehensive two-dimensional gas chromatography for the analysis of synthetic and crude-derived jet fuels. *Journal of Chromatography A,* 1218**,** 4478-4486.

Van Setten, B. A., Makkee, M. & Moulijn, J. A. 2001. Science and technology of catalytic diesel particulate filters. *Catalysis Reviews,* 43**,** 489-564.

Wang, X., Westerdahl, D., Hu, J., Wu, Y., Yin, H., Pan, X. & Zhang, K. M. 2012. On-road diesel vehicle emission factors for nitrogen oxides and black carbon in two Chinese cities. *Atmospheric Environment,* 46**,** 45-55.

Warneke, C., De Gouw, J. A., Holloway, J. S., Peischl, J., Ryerson, T. B., Atlas, E., Blake, D., Trainer, M. & Parrish, D. D. 2012. Multiyear trends in volatile organic compounds in Los Angeles, California: Five decades of decreasing emissions. *Journal of Geophysical Research: Atmospheres,* 117**,** 1-10.

Whitten, G. 1983. The chemistry of smog formation: A review of current knowledge. *Environment International,* 9**,** 447-463.

WHO 1996. Investing in health research and development. Report of the ad hoc committee on health research relating to future intervention options. Geneva, Switzerland: World Health Organization [Online]. Available: https://apps.who.int/iris/handle/10665/63024 [Accessed: 14-05-2018].

Wichmann, H.-E. 2007. Diesel exhaust particles. *Inhalation Toxicology,* 19**,** 241-244.

Wright, G. 2015, Chapter 1: Introduction to Diesel Engines in Fundamentals of Medium/Heavy Duty Diesel Engines. pp. 4-17, *Jones & Bartlett Publishers*, Burlington, MA, USA. ISBN 978-1-2840-6705-7, 1378.

Zhao, Y., Nguyen, N. T., Presto, A. A., Hennigan, C. J., May, A. A. & Robinson, A. L. 2015. Intermediate volatility organic compound emissions from on-road diesel vehicles: chemical composition, emission factors, and estimated secondary organic aerosol production. *Environmental Science & Technology,* 49**,** 11516-11526.

Zunckel, M., Venjonoka, K., Pienaar, J., Brunke, E., Pretorius, O., Koosialee, A., Raghunandan, A. & Van Tienhoven, A. 2004. Surface ozone over southern Africa: synthesis of monitoring results during the Cross border Air Pollution Impact Assessment project. *Atmospheric Environment,* 38**,** 6139-6147.

Chapter 3: Experimental methods and materials

In this chapter, the methods followed to identify the target compounds relevant to the study, as well as development and optimization of the appropriate experimental procedures for emissions testing and sample analysis are described. The experiments carried out during emissions testing are described in detail and the methods used for instrumental analysis of collected samples as well as qualitative and quantitative analysis of the data are outlined.

3.1 Identifying semi-volatile hydrocarbons of relevance to the study: hydrocarbons that play a role in photochemical ozone formation

3.1.1 Selecting target hydrocarbons

An extensive review of literature on emission speciation, as well as atmospheric composition studies (related to photochemical smog episodes) was conducted. Six example studies (Ciccioli et al., 1992, Clark et al., 1996, Gentner et al., 2012, Gentner et al., 2013, Liu et al., 2010, Schauer et al., 1999) were used to compile an initial potential target list which consisted of 620 compounds. The list was narrowed down based on several criteria including: importance for photochemical ozone formation (MIR index assignment), volatility (as the study focus was on long-chain, semi-volatile HCs), known presence in diesel engine emissions (based on a preliminary study discussed in Section 3.1.2), as well as the availability of analytical standards. The full process for selecting the target compounds is outlined in Figure 3.1.

3.1.2 Preliminary study: Identifying hydrocarbons in diesel exhaust samples

Figure 3.1 outlines the process followed to determine the target HCs for the study. After assigning MIR indices, sorting the HCs by volatility and grouping the compounds according to their chemical classes, a preliminary study was conducted to determine the presence of these HCs in diesel exhaust samples that had been collected during a previous study conducted in 2015 at the Sasol Fuels Application Centre (SFAC) in Cape Town, South Africa. During the study, tests were done in a controlled test cell environment. The test engine was a Euro 2 compliant, 1.6 L passenger car engine, fuelled with an ultra-low sulphur (ULS) diesel fuel. Emission samples were collected using the same portable denuder samplers used in this study. An electronic control unit was used to simulate diesel engine operation in underground mining

environments, as this was the focus of the study. The test engine was operated at five different modes: idle, high idle, as well as 25, 50 and 100% torque at 4000 rpm (M1-M5). Thermal desorption coupled with comprehensive gas chromatography–time of flight mass spectrometry (TD–GC × GC–TofMS) was used for sample analysis, targeting polycyclic aromatic hydrocarbons (PAHs). The analytical conditions employed were therefore not optimised for the potential target analytes of this study, nor had they been quantified, however, the data generated could be mined for these analytes, in order to assess their presence and relative abundance in the emission samples.

Mass spectral matching was utilised to identify HCs present in the emission samples. The NIST 16 mass spectral library was employed, with a match quality criterion of ≥ 80% where compounds with a match quality < 80% were removed from the potential target list. Gaseous and particulate associated hydrocarbons were successfully identified in primary PDMS traps and filters, respectively, which had been used to collect emissions during each operating mode (M1-M5). The HC peak areas showed that alkylbenzene, n-alkane and cycloalkane emissions were higher in abundance than branched alkane and alkene emissions for this particular fuel. This aided in deciding which chemical classes to focus on for this study. From this a final list of 43 HCs in the n-alkane and alkylbenzene compound classes was compiled (Table 4.1).

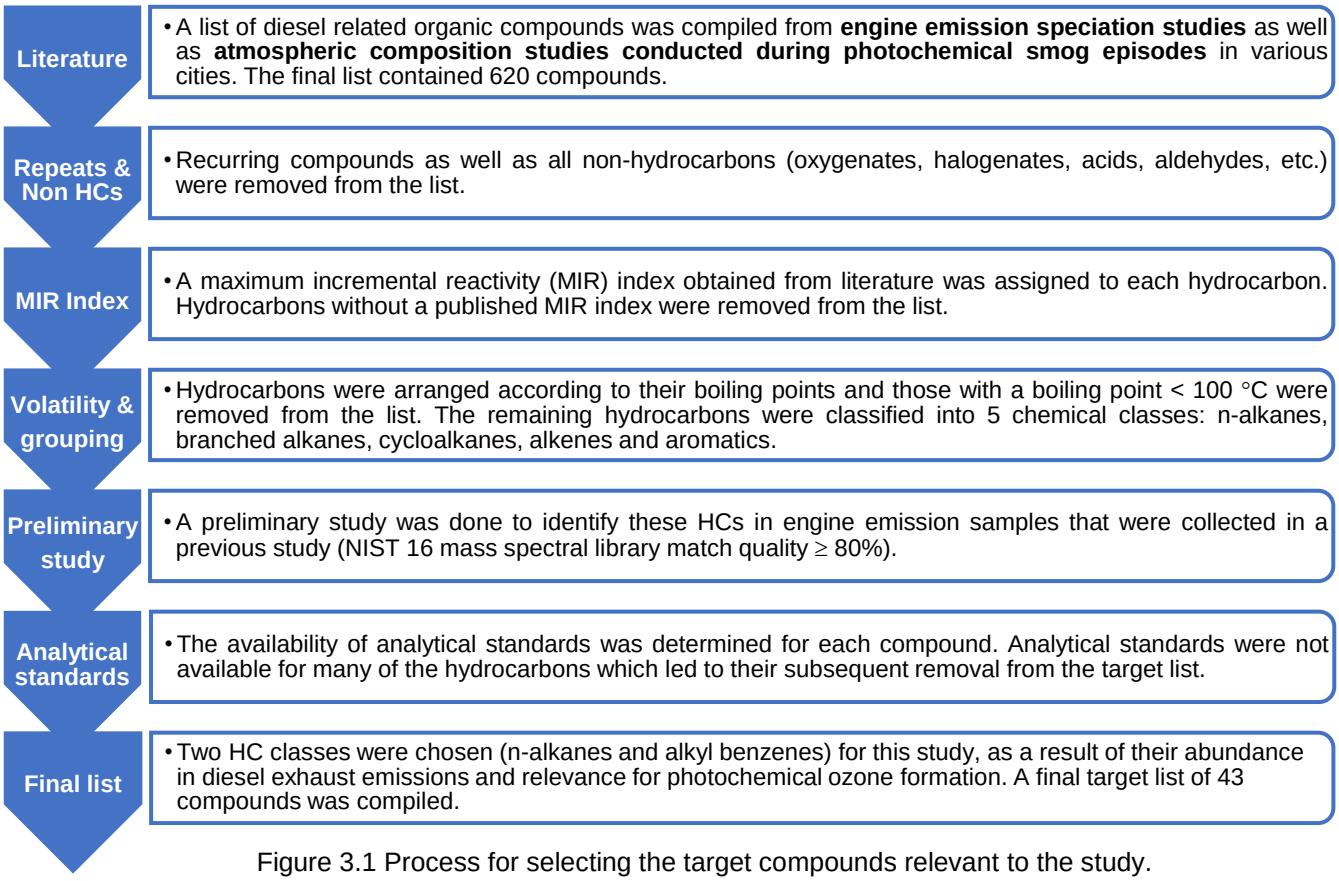

Figure 3.1 Process for selecting the target compounds relevant to the study.

3.2 Emissions testing

3.2.1 Test cell setup

Emissions sampling was conducted over two sampling campaigns, held at the SFAC (Cape Town, South Africa). Sampling campaign 1 was from 21-31 August 2018 and sampling campaign 2 from 21 January-1 February 2019. Tests were performed in a controlled engine test cell, equipped with a Euro 3 certified 1.6 L test engine. The chosen vehicle model was a popular passenger car that is representative of the vehicle fleet on South African roads. The test engine was coupled to an electrical (AC) engine dynamometer, used to simulate engine operation during emissions testing. The dynamometer was controlled by a dynamometer controller, located outside the test cell. The dynamometer controller uses a mathematical model based on the characteristic specifications of the vehicle (mass, aerodynamic drag coefficient, gear ratios, wheel diameter, etc.) to simulate the load a vehicle would experience as it travels on the road. The engine was thus operated in a similar manner to when it is

within a vehicle being driven through the test cycle on a chassis dynamometer, which produces results that are more repeatable than on-road measurements.

The engine was equipped with an electronically controlled, common rail, direct fuel injection system using piezo injectors. The fuel was stored in fuel barrels located outside the test cell. The fuel was supplied to the engine via a fuel mass flow meter (AVL 735, AVL, Graz, Austria) and fuel temperature conditioning system (AVL 753C, AVL, Graz, Austria). During engine operation, the exhaust fumes produced by the engine entered the exhaust piping system, flowed through a DOC and/or a DPF, passed through a muffler and then exited at the end of the exhaust pipe, where they were extracted into an air duct and vented outside the test cell.

During sampling, a portion (split ratio of 1:110) of the exhaust was drawn directly from the exhaust pipe and fed into a partial flow dilution system (Horiba MDLT-1304 Mini Dilution Tunnel, Horiba, Kyoto, Japan) where it was diluted with compressed air, and then passed downstream at a flow rate of 100 L/min. The required flow rate for the raw exhaust sample was calculated and controlled in real time by the MDLT flow control unit, using the measured air mass flow to the engine and the measured relative air/fuel ratio as inputs. The air mass flow rate was measured using a thermal mass flow sensor (Sensyflow FMT-700P, ABB Automation Products, Goettingen, Germany). The relative air/fuel ratio (or lambda) was measured using a wide band lambda sensor (LA4 Lambda Meter, ETAS, Stuttgart, Germany).

The sampling point was located downstream of the partial dilution system. Polydimethylsiloxane (PDMS) denuders were used for the collection of exhaust emissions. Each denuder consisted of two multi-channel rubber traps. Each trap consisted of 22 PDMS tubes (70 mm length, 0.30 mm i.d., 0.64 mm o.d., Sil-Tec Technical Products, Inc., Georgia, USA) within a glass tube (178 mm long, 4 mm i.d., 6 mm o.d., Listco Glassblowers (Pty) Ltd, South Africa), and a quartz fibre filter (6 mm diameter, punched from Qm-A quartz filters (Whatman, GE Healthcare, UK) sandwiched between the two traps. Teflon connectors were used to hold all three components in place and insulation tape was used to secure the connection and improve the ruggedness of the sampler (Figure 3.2). Both ends of the denuder were end capped with glass stoppers when not in use to prevent premature collection of

emissions and/or volatilisation of collected emissions. Gaseous HC emissions were collected on the PDMS traps whilst particulate emissions were captured on the quartz fibre filter.

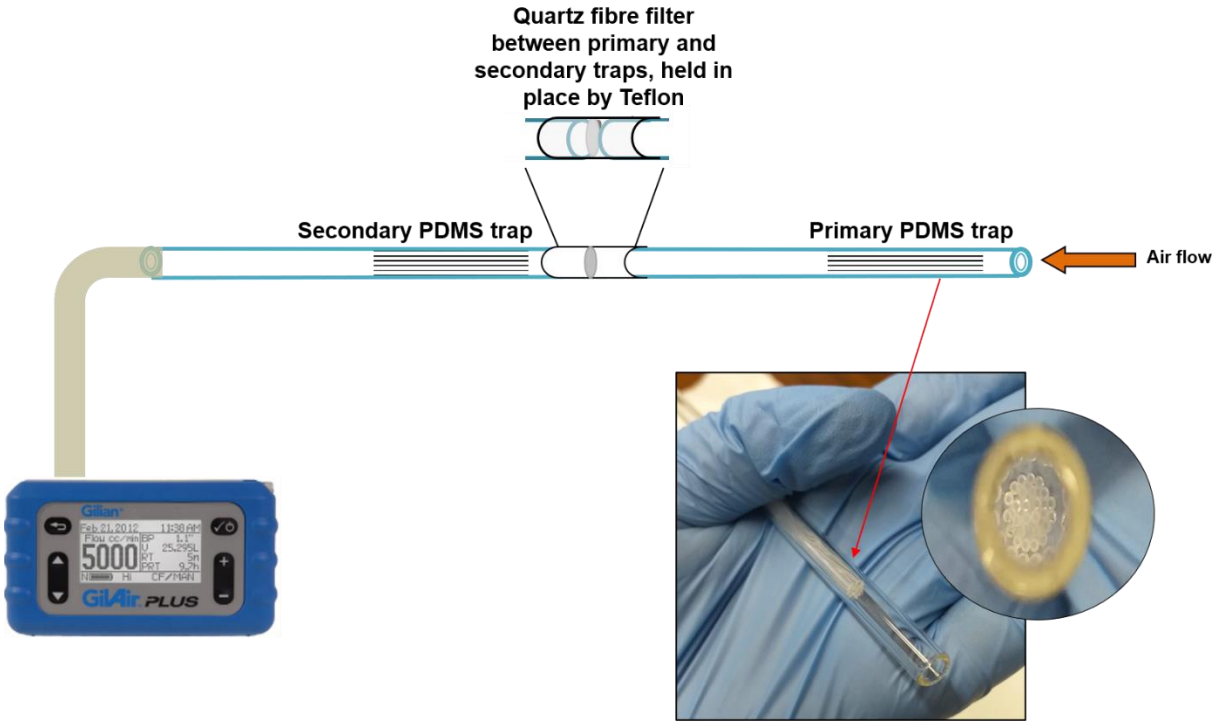

Figure 3.2 Schematic diagram showing the denuder setup employed during exhaust emission sampling.
Adapted from Geldenhuys et al., 2015.

The PDMS traps were made in-house (Chemistry Department, University of Pretoria) and the denuders were assembled as described by Forbes et al. and Geldenhuys et al. (Forbes et al., 2012 and Geldenhuys et al., 2015), at the SFAC shortly before sampling. During sampling, one end of the denuder was connected to a single port on the four-port flow splitter located at the exit of the mini dilution tunnel (MDLT) using Teflon tubing, while the other end was connected to a battery powered portable sampling pump (Sensidyne GilAir Plus, Envirocon, South Africa). Emissions were collected at a sampling flow rate of 500 mL/min. Constant monitoring of the flow rate was achieved using a thermal mass flow meter (TSI Series 4100, TSI Inc, Minneapolis, USA) located outside the test cell.

In addition to the collection of diluted exhaust emissions, samples of the undiluted exhaust gas were sampled directly from the exhaust stream and analysed in real time,

before and after the exhaust aftertreatment system (pre-catalyst and post catalyst) to measure the concentrations of CO, CO_2, NOx and THC emissions (Horiba MEXA Series 7000, Horiba, Kyoto, Japan). The instrument operated at 10 Hz hence 10 measurements were taken each second. Real-time measurements of the soot concentration in the undiluted exhaust were also performed (AVL483 Micro Soot Sensor, AVL, Graz, Austria). The instantaneous data was integrated over each phase to yield an average emission factor. Figure 3.3 shows the test cell setup while Figure 3.4 illustrates the main components employed in the test cell.

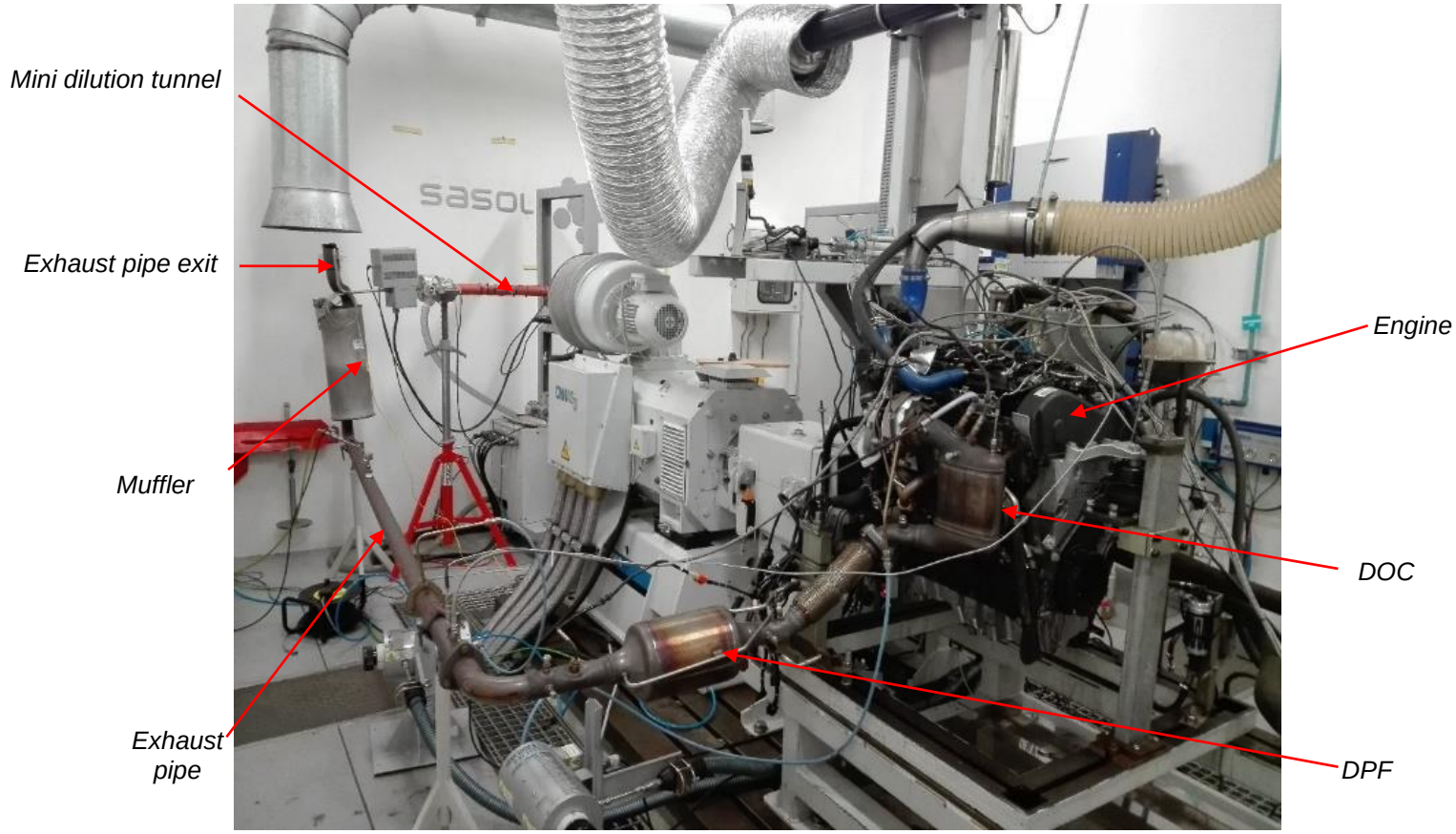

Figure 3.3 Test cell setup.

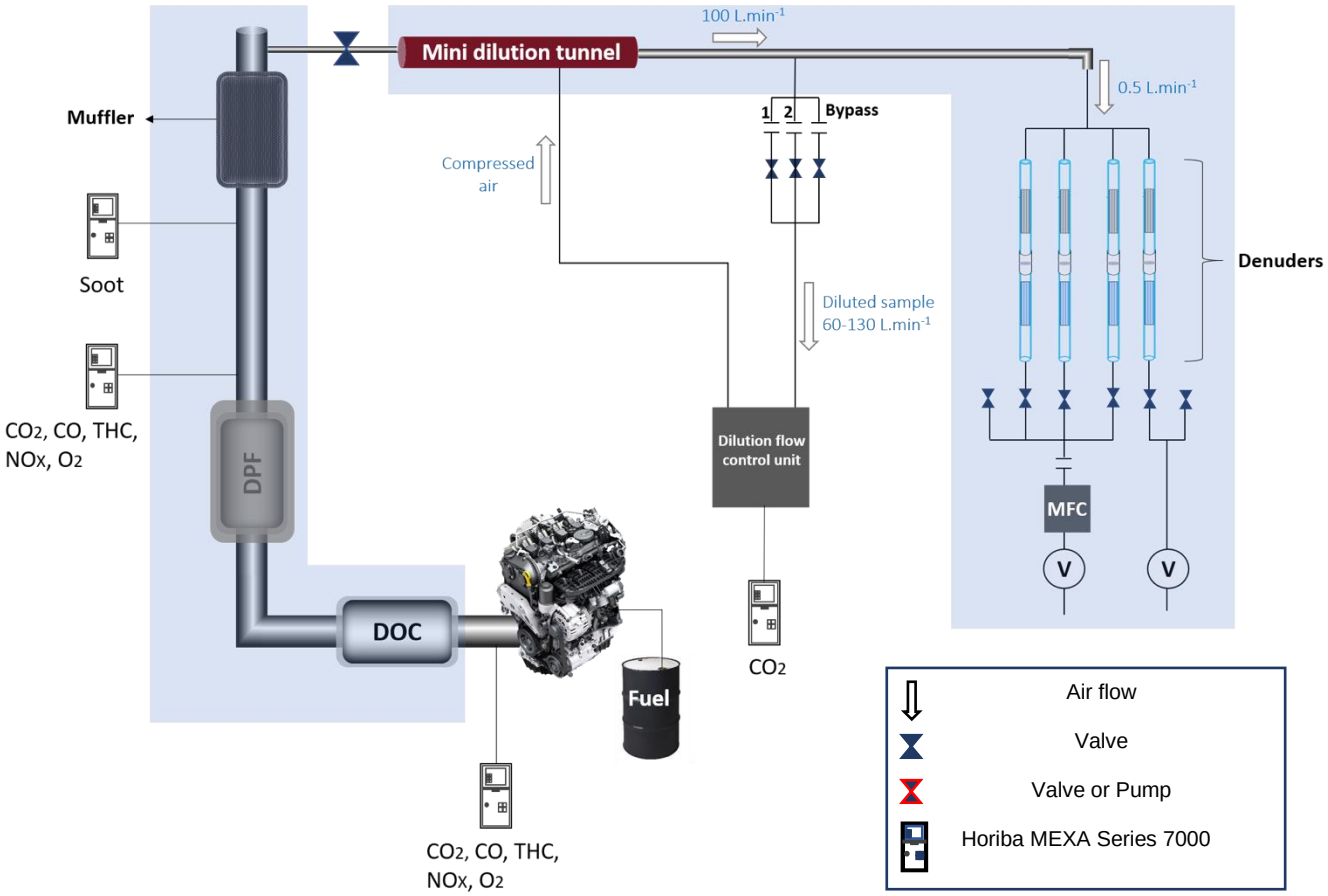

Figure 3.4 Schematic diagram of the test cell setup *(*not drawn to scale)*.
DOC = diesel oxidation catalyst, DPF = diesel particulate filter, MFC = mass flow controller, 1 = first sample filter, 2 = second sample filter.

3.2.2 Driving cycle and test fuels

The World harmonized Light vehicle Test Cycle (WLTC) was used for emissions testing of the Euro 3 certified test engine. The WLTC test cycles are chassis dynamometer tests used to determine the fuel consumption and emissions from light-duty vehicles under repeatable and standardised conditions. They were developed by the United Nations Economic Commission for Europe (UNECE) Working Party on Pollution and Energy (GRPE) group, and are part of the World harmonized Light Vehicle Test Procedures (WLTP); a number of procedures that are needed for type approval of a vehicle. The WLTCs are subdivided into different classes according to

the vehicle's power-to-mass ratio (PMR), as well as the maximum speed of the vehicle as stated by the manufacturer. The PMR is a measure of the performance of an engine or power source, and is calculated as the engine's power output divided by the mass of the vehicle (W/kg). There are different classes of test cycles, depending on the maximum speed of the vehicle as stated by the manufacturer. Class 3 of the WLTC cycle was used in this study, which is representative of vehicles that are driven in Europe and Japan, and it is further divided into two subclasses based on the vehicle's maximum speed (class 3a with a maximum speed < 120 km/h and class 3b with a maximum speed ≥ 120 km/h). The test engine used in this study falls under vehicle class 3b. Figure 3.5 illustrates the speed profile of the driving cycle employed, which consisted of four characteristic speed phases; low, medium, high and extra high.

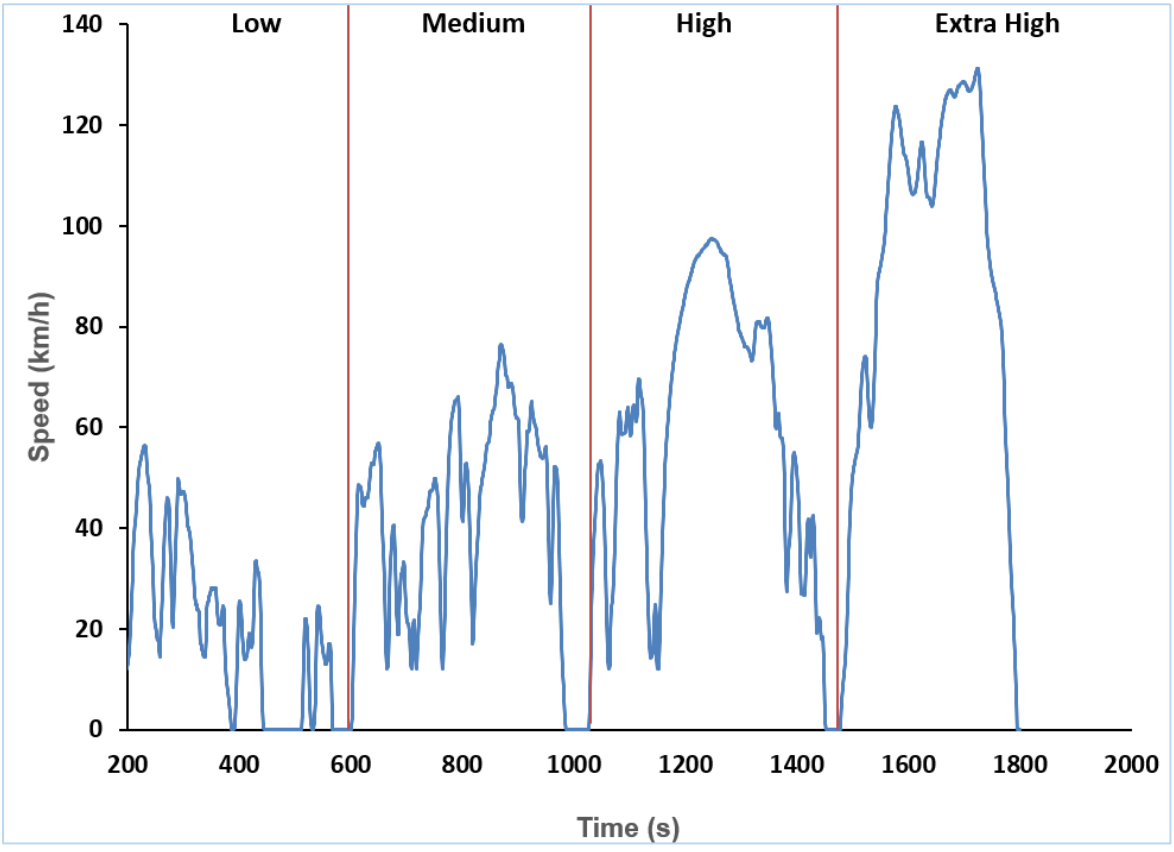

Figure 3.5 Speed profile of the WLTC driving cycle used during emissions testing.

Emissions testing was conducted using three diesel fuels: a highly paraffinic diesel fuel (PAR10), a fully synthetic South African market fuel (SAM10), complying with the South African SANS 342 specification, and a standard Carcal RF-06-03 crude oil derived European reference diesel (EUR10). All of the fuels contained less than 10

ppm sulphur, and were chosen because of their distinct compositional characteristics (Figure 3.6 shows an illustration of each fuel's chemical composition). PAR10 diesel is a high performance, low emission fuel which is a major air quality advantage. SAM10 is a synthetic fuel obtained from the Sasol Synfuels refinery in Secunda, South Africa. It is representative of the Sasol turbodiesel™ ULS 10 ppm fuel, which contains the lowest sulphur content of any diesel available in the country. EUR10 diesel is a crude oil derived reference fuel that meets the European EN590:2013 standard, with a sulphur level of 10 ppm. The GC x GC-MS fuel analysis data and fuel specifications for these fuels (as provided by Sasol) are listed in Table 3.1.

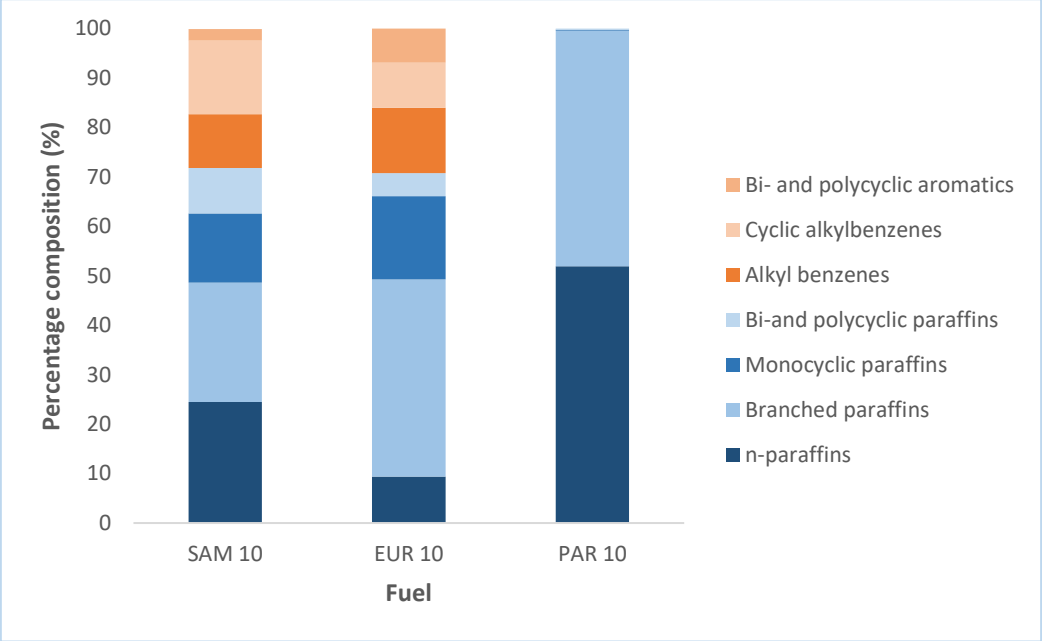

Figure 3.6 Chemical composition of the test fuels. The paraffinic (blue) and aromatic (orange) fractions of each fuel have been illustrated (data provided by Sasol).

Table 3.1 Properties and percentage composition of test fuels employed in this study.
* cSt = centistokes (data provided by Sasol)

Analysis	Method	SAM10	EUR10	PAR10
Sulfur, mg/kg	ASTM D5453	**5**	**<1**	**<1**
Density, kg/l @ 20 °C	ASTM D4052	**0.8163**	**0.8328**	**0.7650**
Flash Point, °C	ASTM D93	**63.9**	**83.0**	**57.0**
Distillation, °C				
Initial Boiling Point	ASTM D86	**176.8**	**193.1**	**150.6**
5%		**187.0**	**207.1**	**173.9**
10%		**192.4**	**218.1**	**184.3**
50%		**232.8**	**277.0**	**262.8**
90%		**333.5**	**333.0**	**338.6**
95%		**368.2**	**347.9**	**352.4**
Final Boiling Point		**389.1**	**355.6**	**356.7**
Cetane number	ASTM D6890	**49.7**	**53.8**	**80.0**
Viscosity, cSt @ 40°C	ASTM D445/D7042	**2.06**	**2.79**	**2.20**
n-paraffins	GC X GC-MS (mass %)	**24.5**	**9.4**	**51.9**
Branched paraffins		**24.1**	**39.9**	**47.7**
Monocyclic paraffins		**14.0**	**16.8**	**0.2**
Bi-and polycyclic paraffins		**9.2**	**4.7**	**0.2**
Alkylbenzenes		**10.9**	**13.2**	**0.0**
Cyclic alkylbenzenes		**14.9**	**9.1**	**0.0**
Bi- and polycyclic aromatics		**2.3**	**6.9**	**0.0**
Sum		**99.9**	**100.0**	**100.0**

3.2.3 Sampling campaign one

3.2.3.1 Preparation of PDMS traps and quartz fibre filters

Multichannel PDMS traps that had been made shortly before the sampling campaign were conditioned at a temperature of 280 °C for 12 hr using a hydrogen flow of ca, 100 cm^3 min^{-1} TC2 tube conditioner (Gerstel Inc., USA). Additional traps that had been made some time prior to the sampling campaign had originally been conditioned for 12 hr when they were made, however, to desorb any analytes that might have collected during storage, these traps were re-conditioned for an additional 2 hr. The traps were then cooled down to room temperature, removed from the conditioner and end-capped with tight-fitting glass stoppers which were previously rinsed with 1:1 hexane-toluene (Sigma-Aldrich, ACE Chemicals, South Africa). The traps were stored in sealed polyethylene ziplock bags prior to sampling.

To prepare the filters, a sheet of quartz fibre filter paper (Whatman, GE Healthcare, UK) was punched using a 6 mm diameter punch (Groz Engineering Tools (Pty) Ltd., India). Punched filters were placed in a 250 mL beaker and rinsed with methanol (Sigma-Aldrich, South Africa). The beaker was swirled gently to rinse the filters after which the methanol was decanted and DCM (ACE Chemicals, South Africa) was added to the beaker. The filters were similarly rinsed with the DCM (ACE Chemicals, South Africa) after which the solvent was discarded. The process was repeated twice, after which the wet filters were gently placed in a porcelain dish and oven dried at 100 °C. After 30 min the dry filters were removed and placed in a 5 mL amber vial, which was stored in a sealed ziplock bag.

3.2.3.2 Collection of background air samples

Duplicate samples of the background air were collected. Two PDMS traps were positioned at the outlet of the duct used to supply the inlet air to the engine. One end of each trap was connected to a portable sampling pump (Sensidyne GilAir Plus, Envirocon, South Africa), and the samples were collected for 10 min at a sampling flow rate of 500 mL/min. It was later determined however, that a true background sample should consist of both the exhaust inlet air as well as the compressed air used to dilute the exhaust emissions in the partial dilution system. The background air sampling point was thus changed for the second sampling campaign, where the new background sample was taken at the same location as the exhaust emissions sampling point (i.e. at the four-way flow splitter located after the dilution tunnel). The method for the collection of the second set of background samples is further detailed in Section 3.2.4.

After sampling, each PDMS trap was end capped on both ends and wrapped in Al foil, and each quartz fibre filter was placed in a tightly sealed 1 mL amber vial. Samples were placed in sealed ziplock bags and were refrigerated at -18 °C prior to analysis.

3.2.3.3 Steady state tests: optimization studies

The SAM10 diesel was used for these emissions tests which were done at steady state operating conditions (40 km/h at 50% of full load). These tests were used to determine the optimal sampling time (breakthrough studies), sampler configuration and sample split ratio for instrumental analysis.

For the breakthrough study, three sampling times were investigated: 5, 10 and 30 min. Two sampler configurations were also investigated: a denuder configuration consisting of two PDMS traps connected by a Teflon connector containing a quartz fibre filter, and a trap-trap configuration consisting of two PDMS traps connected by a Teflon connector without a quartz fibre filter. During sampling, four samplers (two in a denuder configuration and two in a trap-trap configuration) were connected to the ports on the 4-way flow splitter at the exit of the MDLT. The other end of each sampler was connected to a portable sampling pump (Sensidyne GilAir Plus, Envirocon, South Africa) using Teflon tubing (Figure 3.7).

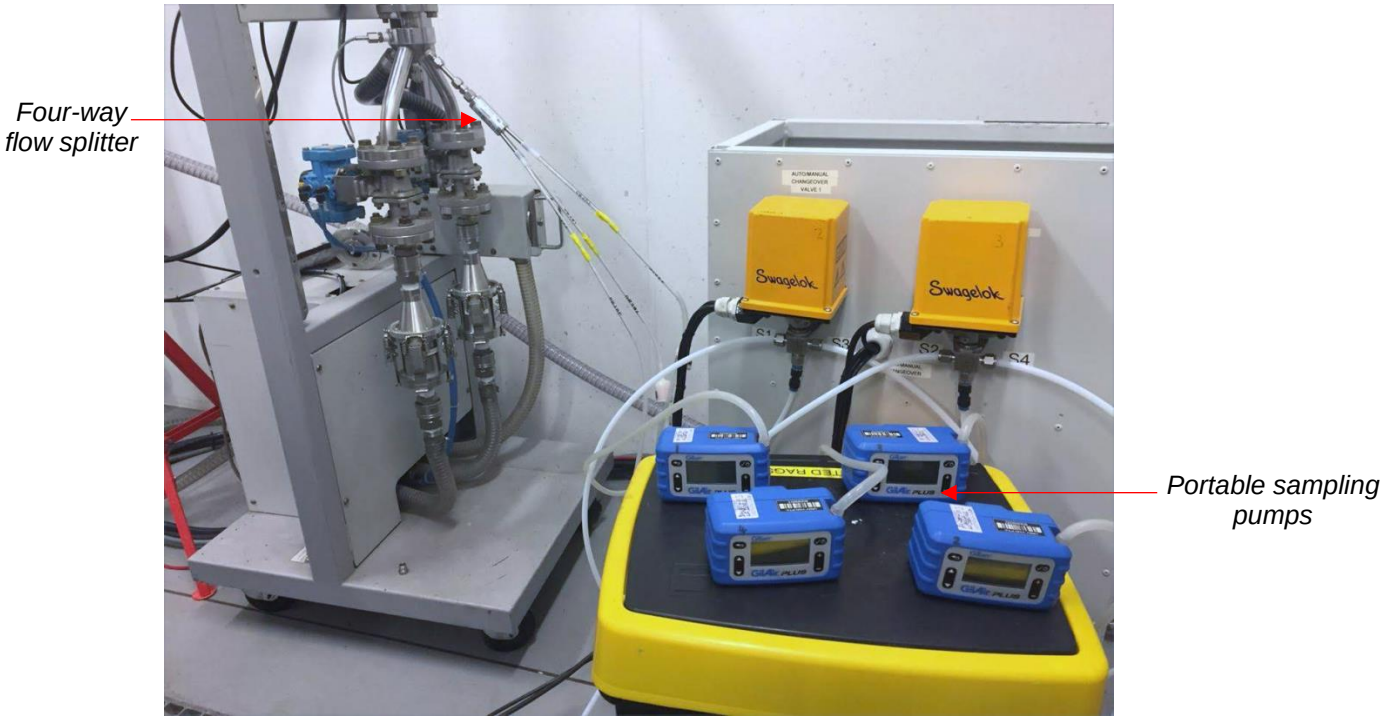

Figure 3.7 Sampler setup during the steady state emissions tests.

The engine was allowed to run for approximately 10 min until it reached stable conditions, at which point the pumps were switched on. The engine emissions were collected simultaneously on all four samplers, at a flow rate of 500 mL/min, for 5 min, after which the pumps were switched off and the exact sampling volume on each pump was recorded. The engine was placed on standby and the samplers were removed. A new set of samplers (two in a denuder configuration and two in a trap-trap configuration) was connected to the four-way flow splitter and the test was repeated, however during this test, engine emissions were collected at a flow rate of 500 mL/min

for a duration of 10 min, after which the pumps were switched off and the final sampling volume recorded. The last test was the 30 min steady state test. During this test a new set of samplers (one in a denuder and one in a trap-trap configuration) was connected to two ports on the four-way flow splitter, whilst air flow through the other two ports was blocked off. Emissions were collected at a flow rate of 500 mL/min for 30 min, after which the pumps were switched off and the final sampling volumes were noted.

During the split ratio optimization tests three primary traps, obtained from the 10 min steady state sampling were employed. The samples were analysed on the TD-GC x GC-ToFMS in solvent vent mode (splitless), and at a split ratio of 50:1 and 100:1 respectively.

3.2.3.4 Transient cycle tests

Transient cycle testing involved the engine being operated over a sequence of test points, each with a defined speed/torque. During emissions testing, the WLTC cycle, or part thereof (a particular speed phase), was run on the test engine. Cold start transient cycle tests were performed, where the engine had been left unoperated overnight to cool down to ambient temperature (20-25 °C) prior to testing. Hot start tests were also performed, where the engine had been operating before testing.

For the cold start transient cycle test, four samplers (in a trap-trap configuration) were used to collect exhaust emissions. Emissions from each phase of the WLTC cycle were collected onto a different sampler. A four-port valve system (Swagelok South Africa (Pty) Ltd) was used to control air flow through each sampler (Figure 3.8). During sampling, one end of each sampler was connected to a port on the 4-way flow splitter at the exit of the MDLT, while the other end was connected to a port on the four-port valve system using Teflon tubing. The valve system was then connected to a single portable pump (Sensidyne GilAir Plus, Envirocon, South Africa) which was placed outside the test cell.

Figure 3.8 Sampler setup during the transient cycle emissions tests.

Emissions were collected at a flow rate of 500 mL/min over the entire duration of the test cycle (1800 s). The sampling volumes (L) were recorded from the sampling pump at the end of each phase and after all phases were complete, and the samplers were removed from the flow splitter. Four new samplers were then connected in the same configuration and the test procedure was repeated. At this point however, the engine was fully warmed up, hence the second test was a hot-start transient cycle test.

After sampling, each sampler was disassembled into its individual components outside the test cell and stored as previously described.

3.2.3.5 Low phase emissions tests

A number of low phase cold start and hot start tests were performed, where exhaust emissions from only the low phase of the WLTC cycle were sampled. These tests were done using the SAM10 and EUR10 diesel. For these tests, four samplers (two in a denuder configuration and two in a trap-trap configuration) were employed. Each sampler was connected to a single port on the 4-way flow splitter at the exit of the dilution tunnel and the other end of each sampler was connected to a portable sampling pump using Teflon tubing. The first phase of the WLTC cycle was run on the

test engine and emissions were collected at a flow rate of 500 mL/min for a duration of 590 s (duration of the low phase). At the end of the test, the pumps were switched off manually and the final sampling volume (L) was noted, after which a new set of samplers was loaded. The engine was kept running during repeat measurements.

A summary of the samples collected during sampling campaign 1 is shown in Table 3.2. Details of each experiment (sample name, sample volume, flow rate, sampling duration, fuel type, etc.) were recorded on a sampling information sheet (Appendix C).

Table 3.2 Summary of samples taken during sampling campaign one.

SAMPLING CAMPAIGN 1					
Fuel	**Sample name**	**Sampling configuration**	**No. of replicates**	**Sampling duration**	**Volume sampled (L)**
SAM10	SAM SS5	TT	2	5 min	2.694 ± 0.067
	SAM SS5	D	2	5 min	2.674 ± 0.017
	SAM SS10	TT	2	10 min	5.115 ± 0.032
	SAM SS10	D	2	10 min	5.048 ± 0.008
	SAM SS30	TT	1	30 min	15. 061
	SAM SS30	D	1	30 min	14.791
	SAM PH1CS	TT	2	590 s	5.198 ± 0.039
	SAM PH1CS	D	2	590 s	5.123 ± 0.004
	SAM PH1HS	TT	2	590 s	5.247 ± 0.021
	SAM PH1HS	D	2	590 s	5.173 ± 0.010
	SAM TCCS PH1	TT	1	590 s	4.920
	SAM TCCS PH2	TT	1	433 s	3.410
	SAM TCCS PH3	TT	1	455 s	3.784
	SAM TCCS PH4	TT	1	322 s	2.693
	SAM TCHS PH1	TT	1	590 s	4.902
	SAM TCHS PH2	TT	1	433 s	3.600
	SAM TCHS PH3	TT	1	455 s	3.793
	SAM TCHS PH4	TT	1	322 s	2.676
EUR10	EUR PH1CS	TT	1	590 s	4.940
	EUR PH1HS	TT	1	590 s	4.926

SAM = SAM10 diesel, EUR = EUR10 diesel, SS = steady state, PH = phase, TCCS = transient cycle cold start, TCHS = transient cycle hot start, TT = trap-trap, D = denuder, ± = plus, minus the standard deviation for replicate samples (n = 2).

3.2.4 Sampling campaign two

3.2.4.1 Background air samples

As previously discussed, a new set of background air samples, which accounted for both the inlet air as well as the compressed air used to dilute the exhaust emissions, was collected during the second sampling campaign. These samples were taken at the four-way flow splitter (the same location where the exhaust emissions were collected). This sampling location was also ideal as it accounted for the flow path that the exhaust emissions were exposed to prior to collection. Duplicate measurements were conducted using two denuder samplers. Each denuder was connected to a port on the four-way flow splitter, while the other two ports were blocked off using nylon plugs (Festo, South Africa) The other end of each denuder was connected to a portable sampling pump. The engine remained off during sampling and the samples were collected at a flow rate of 500 mL/min for 10 min.

3.2.4.2 Cold start transient tests

Cold start transient cycle tests were conducted in duplicate for each fuel in the following order: PAR10 diesel, SAM10 diesel and EUR10 diesel. During these tests, the WLTC cycle was run on the test engine from a cold start up, where the engine had been left un-operated overnight, allowing it to equilibrate to ambient temperature. Four denuder samplers were used to collect exhaust emissions, with emissions from each of the four phases of the WLTC cycle (low, medium, high and extra-high) collected onto a different sampler. Each denuder was connected to a single port on the four-way flow splitter, at the exit of the MDLT, while the other end of each denuder was connected to a single port on the four-port valve system used to channel the exhaust flow through one denuder at a time. The valve system was connected to a single portable sampling pump (Sensidyne GilAir Plus, Envirocon, South Africa), positioned outside the test cell and a TSI mass flowmeter was used to monitor the instantaneous flow rate.

The engine emissions were collected at a flow rate of 500 mL/min for the entire duration of the test cycle (1800 s). The sampling volume was recorded at the end of each phase. The engine was then switched off and a repeat of this test was performed

the following day (two repeat cold start measurements), after which the fuel was changed.

The fuel was obtained from 200 L storage barrels located outside the test cell. A pump was used to draw the fuel from the barrels into the test cell. During fuel change over, the fuel supply pipe was changed over from one barrel to another. The fuel supply system was then flushed with approximately 10 L (2 L for the stall fuel circuit and 8 L for the engine test cell fuel circuit) of the new fuel to flush out the remaining old fuel from the system. Fuel change-over was then followed by a 60 min run where the engine was operated at mid-load conditions (50% of full load), at 2500 rpm, consuming approximately 6-7 litres of fuel. The engine was then pre-conditioned with the new fuel by running the WLTC cycle once, followed by a 20 min run at mid-load conditions (50% of full load) at 2500 rpm once again. The engine was then shut down, and left un-operated overnight.

3.2.4.3 Investigating the effect of exhaust aftertreatment systems

To investigate the effect of the exhaust aftertreatment systems on HC emissions, cold start transient cycle tests were conducted with a DPF in line (in addition to the DOC) i.e. exhaust emissions entering the exhaust system flowed through the DOC, followed by the DPF, passed through the muffler and exited at the end of the exhaust pipe. For these tests the EUR10 diesel was used. During testing the WLTC cycle was run on the test engine. Four denuder samplers were setup as previously described for the cold start transient cycle tests (Section 3.2.4.2) and the engine emissions were collected at a flow rate of 500 mL/min over the duration of the test cycle, where emissions from each phase of the test cycle were collected onto a different denuder.

After sampling, the denuders were disassembled and each PDMS trap was end capped on both ends and wrapped in Al foil, while each quartz fibre filter was stored in a sealed 1 mL clean amber vial. Samples were placed in sealed ziplock bags and refrigerated at -18 °C prior to analysis.

A summary of the samples collected during sampling campaign 2 is shown in Table 3.3.

Table 3.3 Summary of samples taken during sampling campaign two.

SAMPLING CAMPAIGN 2				
Fuel	**Sample name**	**No. of repeats**	**Sampling duration (s)**	**Volume sampled (L)**
PAR10	PAR TCCS PH1	2	591.90	5.066 ± 0.034
	PAR TCCS PH2	2	431.50	3.400 ± 0.003
	PAR TCCS PH3	2	453.35	3.782 ± 0.004
	PAR TCCS PH4	2	321.35	2.679 ± 0.002
SAM10	SAM TCCS PH1	2	591.70	5.067 ± 0.014
	SAM TCCS PH2	2	431.30	3.394 ± 0.002
	SAM TCCS PH3	2	453.25	3.785 ± 0.006
	SAMTCCS PH4	2	321.50	2.687± 0.001
EUR10	EUR TCCS PH1	2	591.50	5.072 ± 0.011
	EUR TCCS PH2	2	431.30	3.393 ± 0.001
	EUR TCCS PH3	2	453.45	3.791 ± 0.001
	EUR TCCS PH4	2	321.45	2.681 ± 0.008
	EUR DPF TCCS PH1	1	591.80	5.046
	EUR DPF TCCS PH2	1	431.50	3.389
	EUR DPF TCCS PH3	1	453.40	3.790
	EUR DPF TCCS PH4	1	321.40	2.689
	EUR PH1HS TT	1	592.80	5.116
	EUR PH1HS D	1	592.80	5.153

PAR10 = paraffinic diesel, SAM = SAM10 diesel, EUR = EUR10 diesel, PH = phase, TCCS = transient cycle cold start, PH1HS = phase1 hot start, TT = trap-trap, D = denuder, DPF = diesel particulate filter, ± = plus, minus the standard deviation for replicate samples (n = 2).

3.3 Instrumental analysis

All samples were transported in a cooler box to the University of Pretoria, where they were stored at -18 °C upon arrival. Sample analysis was conducted using a LECO Pegasus 4D TD-GC x GC-TofMS system which consisted of an Agilent© 7890A GC (LECO Africa (Pty) Ltd., Kempton Park, South Africa) equipped with a dual stage modulator and secondary oven. The primary and secondary traps were desorbed directly in the thermal desorber (TDS), while each quartz fibre filter was placed into a clean glass tube and inserted into the TDS such that the end containing the filter was within the heated zone. Data acquisition and processing were carried out using the ChromaTOF software (Version 4.50.8.0 optimised for Pegasus, LECO Africa (Pty) Ltd.). The column set consisted of a Rxi-1 MS, 30 m × 0.25 mm ID × 0.25 µm film thickness in the first dimension and Rxi-17Sil MS 0.790 m × 0.25 mm ID × 0.25 µm

film thickness in the second dimension (Restek, Bellefonte, PA, USA). The primary oven had an initial temperature of 40 ºC (held for 1.50 min) and was ramped at 5 ºC/min to 315 ºC (held for 15 min). The secondary oven temperature had an offset of 5 ºC relative to the primary oven and the modulator temperature had an offset of 30 ºC relative to the secondary oven temperature. The modulation period was 3 s and the total run time was 71.50 min. Sample introduction was achieved using a Gerstel 3 thermal desorption system (TDS) in solvent vent mode.

A 1 ng/µL internal standard mix was prepared containing 99% hexadecane-d34 (Sigma-Aldrich, South Africa), 99 atom % D naphthalene-d8 (Isotec™, Sigma-Aldrich, South Africa) and 98 atom % D phenanthrene-d10 (Isotec™, Sigma-Aldrich, South Africa) in 99% n-hexane (Sigma-Aldrich. South Africa). Samples were spiked with 1 µL of the internal standard mix prior to analysis (i.e. 1 ng on column) and were placed directly into the heating zone of the TDS. Samplers were thermally desorbed from 30 ºC (held for 3 min) at 60 ºC/min to 280 ºC (held for 5 min). The thermal desorption flow rate was 100 mL/min at a vent pressure of 0.5 psi (helium 5.0, Afrox, South Africa) and the TDS transfer line temperature was 350 ºC. Cryogenic focusing of the desorbed analytes at -50 ºC was achieved using liquid nitrogen (Afrox, South Africa) in a cooled injection system (Gerstel CIS 4) with a baffled, deactivated glass liner (Agilent, Chemetrix, South Africa). After thermal desorption, introduction of the analytes onto the column was achieved by rapidly ramping the temperature of the CIS from -50 ºC at 12 ºC/s to 280 ºC. The MS transfer line temperature was 300 ºC. The acquisition mass range was 50 - 300 Da at a rate of 100 spectra/s. The electron energy was -70 eV and the ion source temperature was set at 230 ºC. A summary of the instrumental parameters used is given in Table 3.4.

Table 3.4 Summary of the instrumental parameters used during analysis of the emission samples.

Sample introduction	
Thermal desorption method	
Flow mode	Splitless
Initial temperature	30 °C (3 min hold time)
Final temperature	280 °C (5 min hold time)
Desorption flow rate	100 mL/min
Ramp rate	60 °C/min
Transfer line temperature	350 °C
Cooled Injection System (CIS) method	
Initial temperature	-50 °C
Final temperature	280 °C
Ramp rate	12 °C/s

Sample analysis	
Gas chromatography (GC) method	
Carrier gas	Helium
Back inlet flow rate	1.0 mL/min
Back inlet mode	Solvent vent
Primary column	Rxi-1MS (30 m, 0.25 mm i.d., 0.25 µm df)
Secondary column	Rxi 17 Sil MS (0.790 m, 0.25 mm i.d., 0.25 µm df)
Primary oven initial temperature	40 °C (1.50 min hold time)
Primary oven final temperature	315 °C (15 min hold time)
Ramp rate	5 °C/min
Secondary oven temperature offset	5 °C
Modulation period	3 s
Modulator offset	30 °C
Total run time	71.50 min
Mass spectrometry (MS) method	
Start mass	50 Da
End mass	300 Da
Electron energy	70 eV
Ion source temperature	230 °C
Data processing (DP) method	
Minimum S/N	50

3.4 Characterisation of target hydrocarbons

3.4.1 n-Alkane hydrocarbons

3.4.1.1 Preparation of n-alkane calibration solutions and internal standards

A C_8-C_{20} n-alkane standard mix (Sigma-Aldrich, South Africa: COA in Appendix D was used to prepare five calibration solutions with concentrations of 1, 5, 10, 20, and 30 ppm (Figure 3.9). The n-alkane standard mix had a concentration 40 ppm, and the calibration solutions were prepared directly from the standard using 99% n-hexane (Sigma-Aldrich, South Africa) as a diluent, e.g. to prepare a 1 ppm solution, 25 µL of the n-alkane standard was injected into a clean 1 mL amber vial, followed by 10 µL of the 100 ppm internal standard (IS) solution, and 965 µL n-hexane to achieve a final volume of 1 mL. Deuterated hexadecane (99% d34-hexadecane, Sigma-Aldrich, South Africa: COA in Appendix D) was used as an IS for quantitative analysis of the n-alkanes. The standard was purchased as a neat liquid (100 mg) and diluted to 10 mL with 99% n-hexane (Sigma-Aldrich, South Africa) to yield a 10 g/L solution. This solution was then sequentially diluted to a 100 ppm working solution (Figure 3.9).

3.4.1.2 Linear regression analysis and determination of detection and quantification limits.

For calibration, 1 µL of each of the 1, 5, 10, 20 and 30 ppm standard solutions were spiked onto pre-conditioned traps, while 2 µL of the 30 ppm standard was spiked onto a trap to yield 60 ng of analyte on the trap; which yields the same mass equivalent as injecting 1 µL of a 60 ppm standard. Analysis was done in duplicate by TD-GC x GC-TofMS. During linear regression analysis, the concentration of each analyte was plotted against the average peak area to generate a calibration curve for each n-alkane.

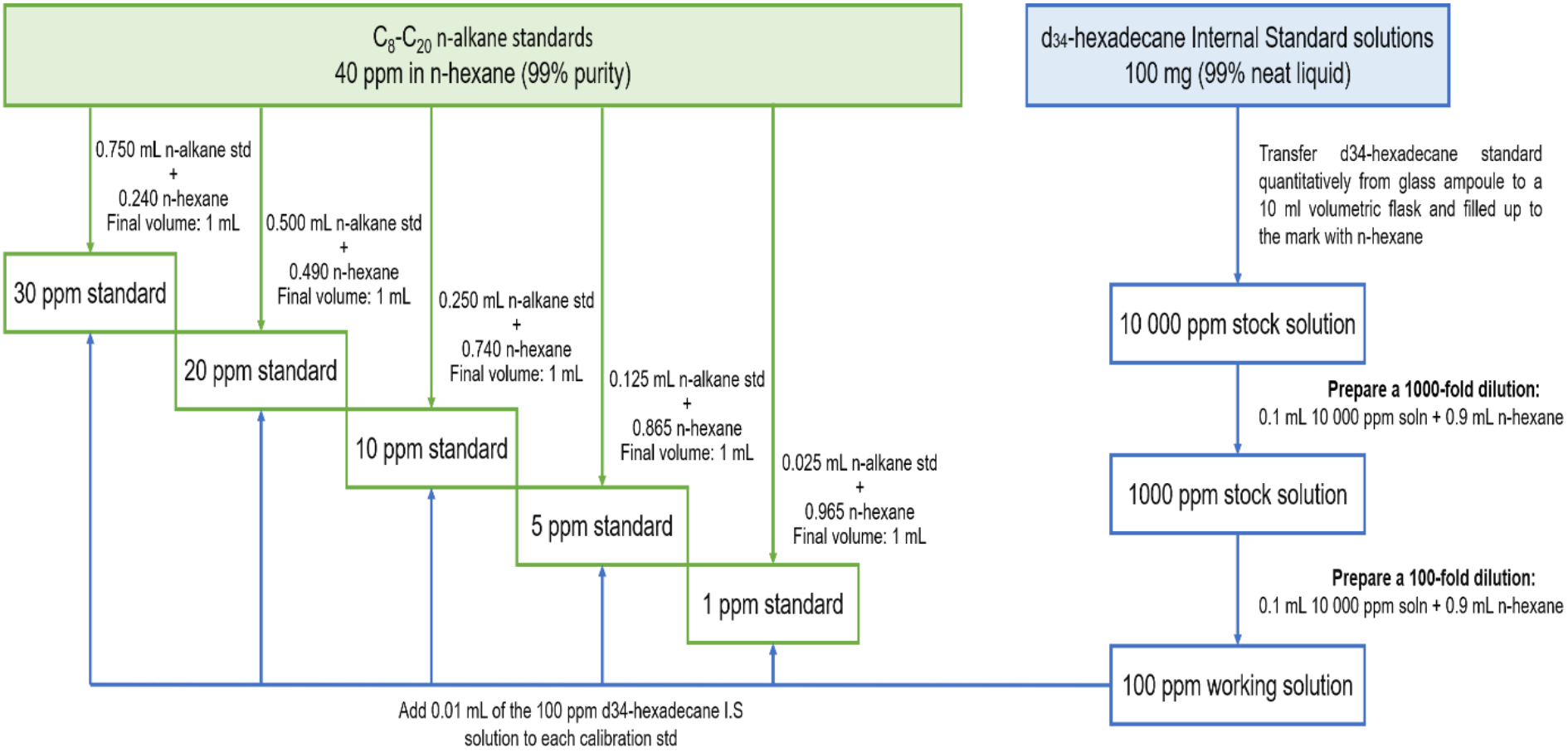

Figure 3.9 Outline of methods used to prepare calibration standards and internal standard solutions.

Determination of the limit of detection (LOD) and limit of quantitation (LOQ) are important method validation parameters which delineate the limitations of an analytical method. The LOD is defined as the lowest concentration of the analyte that can be reliably detected in a sample under a defined method or conditions (Armbruster et al., 1994), while the LOQ is the lowest concentration of the analyte that can be quantified in a sample with acceptable accuracy and precision by a given method (Uhrovčík, 2014). There are various methods that can be used to determine these parameters. In this study the signal-to-noise (S/N) method was used, where a S/N ratio of 3 and 10 is accepted to estimate the LOD and LOQ of each n-alkane respectively (Equation 3.1 and Equation 3.2). The LOD and LOQ on column (ng) was determined for each n-alkane using the lowest standard concentration (except for octane where the 10 ppm standard was used as octane could not be detected at lower concentrations). The instrument has a LOD of 1 pg and thus a LOQ of 3.3 pg, hence these values were assigned for analytes with an estimated calculated LOD and LOQ less than the instrumental limit (Table 4.2).

$$LOD\ (n\text{-}alkane) = (standard\ concentration/SN) \times 3 \qquad 3.1$$

$$LOQ\ (n\text{-}alkane) = (standard\ concentration/SN) \times 10 \qquad 3.2$$

The LOD and LOQ were also estimated per volume of air sampled (Equation 3.3 and 3.4) as well as distance travelled as a result of diesel engine operation (Equation 3.5 and 3.6). These LOD and LOQ values were termed the LOD_{exh} (Table 4.3) and LOQ_{exh} (Table 4.4) and were determined for each phase of the WLTC cycle, as each phase was associated with a different distance travelled and volume of air sampled.

To determine these values, the LOD/LOQ (pg) was multiplied by the split ratio (SR), dilution factor (DF) and partial sampling factor (PF) (explained in detail in Section 3.5). The values obtained were then divided either by the volume sampled (m^3) or distance travelled (km) during that particular phase.

$$LOD\ corrected = LOD\ (n\text{-}alkane) \times SR \times DF\ x \times PF$$

$$LOD\ (ng/m^3) = LOD\ corrected/volume\ sampled\ during\ phase \quad (3.3)$$

$$LOQ\ corrected = LOQ\ (n\text{-}alkane) \times SR \times DF \times PF$$

$$LOQ\ (ng/m^3) = LOQ\ corrected/volume\ sampled\ during\ phase \quad (3.4)$$

$$LOD\ corrected = LOD\ (n\text{-}alkane) \times SR \times DF \times PF$$

$$LOD\ (ng/km) = LOD\ corrected/distance\ travelled\ during\ phase \quad (3.5)$$

$$LOQ\ corrected = LOQ\ (n\text{-}alkane) \times SR \times DF \times PF$$

$$LOQ\ (ng/km) = LOQ\ corrected/distance\ travelled\ during\ phase \quad (3.6)$$

3.4.2 Alkylbenzene hydrocarbons

Qualitative analysis was performed to determine the presence of the alkylbenzenes in the fuel emissions, as certified reference standards could not be obtained for every target alkylbenzene. A Detailed Hydrocarbon Analysis (DHA) aromatic standard mix (Restek, USA: COA in Appendix D) was used for tentative identification of the alkylbenzenes. The standard was purchased as a neat standard (0.15 mL) containing varying concentrations (wt/wt%) of each compound (concentration range of 0.118% to 12.342% for 2-methylbutylbenzene and toluene, respectively). The neat standard was diluted to 10 mL using 99% toluene (Sigma-Aldrich, South Africa). A 10^6 x dilution of this solution was then made to obtain a final working solution. During analysis 1 µL of the working solution was spiked onto a pre-conditioned trap and analysed in duplicate by TD-GC x GC-TofMS.

Identification of the target compounds in the emission samples was achieved by matching their retention times to those of the compounds in the reference standard, as well as mass spectral matching, with a match quality criterion of ≥ 80% (similarity of 800), using the NIST 16 mass spectral library. The primary column (Rxi-1 MS) retention indices (RIs) were also calculated and used to differentiate between alkylbenzene isomers having similar retention times and mass spectra. To determine the RI of each alkylbenzene, 1 µL of the C_8-C_{20} n-alkane and 1 µL DHA-aromatic standard mix were spiked onto a clean trap and analysed by TD-GC x GC-TofMS. The Kovatz retention index system, which uses the n-alkane eluting directly before and after the compound of interest as a reference point, was used to calculate the RI of each alkylbenzene. The RI of each alkylbenzene was calculated using Equation 3.7

which uses the retention time of the alkylbenzene (t_x) as well as the retention time of the n-alkane eluting directly before (t_n) and after (t_{n+1}) the alkylbenzene of interest.

The calculated RIs; under temperature programmed conditions (White et al., 1992) were then used to confirm the presence of the alkylbenzenes in each sample.

$$RI_x = 100 \frac{t_x - t_n}{t_{(n+1)} - t_n} + 100n \quad (3.7)$$

3.5 Identification of target analytes

As exhaust emissions are such a complex sample, the total ion chromatogram (TIC) of a diesel exhaust sample contains a large number of compounds in different chemical classes. With mass spectrometry as a detection technique, however, an extracted ion chromatogram (EIC) may be obtained, where an ion of a particular mass to charge ratio (m/z) may be used to isolate and easily identify a particular compound. An EIC may also be used to identify a class of compounds using a common ion amongst the compounds. In this study m/z = 57 was used for the n-alkanes and m/z = 91 was used for the alkylbenzenes.

During mass spectrometric analysis, analytes are energised by an ion source, which may lead to subsequent ionization and fragmentation of the compound. Due to their stability, certain compounds undergo minimum fragmentation, while the opposite is true for low stability compounds such as aliphatic HCs. These compounds readily fragment into smaller ions with m/z = 57 and m/z = 43 being the dominant ion fragments. With alkyl benzenes, during fragmentation, cleavage will commonly occur at the beta position. The fragment formed then undergoes subsequent rearrangement into a highly stable tropylium ion with m/z = 91 (Maccoll, 1999 and Pretsch et al., 2009)

3.6 Calculation of hydrocarbon emission factors and ozone-formation potentials

To calculate the EF of each n-alkane, the mass (ng) obtained from the linear regression analysis (combined mass of primary and secondary trap) was corrected to account for the dilution of emissions in the sampling line. The dilution factors had been measured continuously during emissions testing: a split ratio (SR) of 110 was employed to sample a portion of the raw exhaust, i.e. 1 out of 110 parts of the engine

exhaust emissions were transferred into the partial dilution system while the remainder was allowed to exit at the end of the exhaust pipe extraction system. Within the dilution tunnel, the exhaust emissions were diluted using compressed air. The dilution factor (DF) varied between different phases of the WLTC cycle in order to account for expected variations in emission concentrations. After dilution in the MDLT, the diluted exhaust emissions were passed downstream at a flow rate of 100 L/min. Samples of the diluted exhaust were collected at a flow rate of 500 mL/min onto the samplers, resulting in a partial sampling factor (PF) of 200. Hence to calculate the HC mass emitted by the engine, the HC mass obtained from linear regression analysis (ng on GC column) was multiplied by the SR, DF and PF. To calculate the HC emission factor (gSVOC/km) this mass was divided by the distance travelled (Equation 3.8) for the particular speed phase (s) tested.

$$EF[gSVOC/km] = (SVOC\ mass[ng] \times SR \times DF \times PF)/distance\ travelled[km] \quad (3.8)$$

Ozone formation potentials (OFPs) were then calculated for the n-alkane emissions. As previously discussed, the OFP of each HC can be estimated using Carter's MIR index, which gives the impact of each compound on the peak ozone concentration in a system where ozone is being formed under high NOx concentrations, and is most sensitive to HC emissions. The MIR index of each compound is given as the mass of additional ozone formed per mass of compound added to the emissions (gO_3/gSVOC). Thus using the calculated EF (gSVOC/km) of each n-alkane, the OFP (gO_3/km) of each hydrocarbon was determined from the product of the emission factor EFn and MIRn where n refers to the n-alkane with n number of carbons (Equation 3.9).

$$OFPn[gO_3/km] = EFn\ [gSVOC/km] \times MIRn\ [gO_3/gSVOC] \quad (3.9)$$

For the alkylbenzene emissions, emission factors were determined by multiplying the peak area by the SR, DF and PF to obtain a corrected peak area. The emission factor of each compound was then determined by dividing the corrected peak area of each compound by the distance travelled. This provided semi-quantitative information about the emission of these hydrocarbons, which was useful for comparative analysis of the emissions between fuels, and different engine operating conditions.

3.7 References

Armbruster, D. A., Tillman, M. D. & Hubbs, L. M. 1994. Limit of detection (LQD)/limit of quantitation (LOQ): comparison of the empirical and the statistical methods exemplified with GC-MS assays of abused drugs. *Clinical Chemistry,* 40**,** 1233-1238.

Carter, W. Updated Maximum Incremental Reactivity Scale and Hydrocarbon Bin Reactivities for Regulatory Applications. 2010. *California Air Resources Board Contract*. 07e339.

Ciccioli, P., Cecinato, A., Brancaleoni, E., Frattoni, M. & Liberti, A. 1992. Use of carbon adsorption traps combined with high resolution gas chromatography–mass spectrometry for the analysis of polar and non-polar C4-C14 hydrocarbons involved in photochemical smog formation. *Journal of High Resolution Chromatography,* 15**,** 75-84.

Clark, N. N., Atkinson, C. M., Mckain, D. L., Nine, R. D. & El-Gazzar, L. 1996. Speciation of hydrocarbon emissions from a medium duty diesel engine. *SAE Technical Paper* 960322. https://doi.org/10.4271/960322

Dunmore, R., Hopkins, J., Lidster, R., Lee, J., Evans, M., Rickard, A., Lewis, A. & Hamilton, J. 2015. Diesel-related hydrocarbons can dominate gas phase reactive carbon in megacities. *Atmospheric Chemistry and Physics,* 15**,** 9983-9996.

Forbes, P. B., Karg, E. W., Zimmermann, R. & Rohwer, E. R. 2012. The use of multi-channel silicone rubber traps as denuders for polycyclic aromatic hydrocarbons. *Analytica Chimica Acta,* 730**,** 71-79.

Geldenhuys, G., Rohwer, E. R., Naudé, Y. & Forbes, P. B. 2015. Monitoring of atmospheric gaseous and particulate polycyclic aromatic hydrocarbons in South African platinum mines utilising portable denuder sampling with analysis by thermal desorption–comprehensive gas chromatography–mass spectrometry. *Journal of Chromatography A,* 1380**,** 17-28.

Gentner, D. R., Isaacman, G., Worton, D. R., Chan, A. W., Dallmann, T. R., Davis, L., Liu, S., Day, D. A., Russell, L. M. & Wilson, K. R. 2012. Elucidating secondary organic aerosol from diesel and gasoline vehicles through detailed characterization of organic carbon emissions. *Proceedings of the National Academy of Sciences,* 109**,** 18318-18323.

Gentner, D. R., Worton, D. R., Isaacman, G., Davis, L. C., Dallmann, T. R., Wood, E. C., Herndon, S. C., Goldstein, A. H. & Harley, R. A. 2013. Chemical composition of gas-phase organic carbon emissions from motor vehicles and implications for ozone production. *Environmental Science & Technology,* 47**,** 11837-11848.

Liu, Z. G., Berg, D. R., Vasys, V. N., Dettmann, M. E., Zielinska, B. & Schauer, J. J. 2010. Analysis of C1, C2, and C10 through C33 particle-phase and semi-volatile organic compound emissions from heavy-duty diesel engines. *Atmospheric Environment,* 44**,** 1108-1115.

Macák, J., Nabivach, V., Buryan, P. & Šindler, S. 1982. Dependence of retention indices of alkylbenzenes on their molecular structure. *Journal of Chromatography A,* 234**,** 285-302.

Maccol, A., 1999, Encyclopedia of Spectroscopy and Spectrometry: Mass Spectrometry, Historical Perspective, Lindon, J.C., (e.d). pp 1241-1248, *Elsevier*, Netherlands.

Pretsch, E., Bühlmann, P., Badertscher, M. 2009. Chapter 8: Mass Spectrometry in Structure Determination of Organic Commpounds pp 1-64, *Springer*, Berlin, Heidelberg.

Schauer, J. J., Kleeman, M. J., Cass, G. R. & Simoneit, B. R. 1999. Measurement of emissions from air pollution sources. 2. C1 through C30 organic compounds from medium duty diesel trucks. *Environmental Science & Technology,* 33**,** 1578-1587.

Uhrovčík, J. 2014. Strategy for determination of LOD and LOQ values–Some basic aspects. *Talanta,* 119**,** 178-180.

White, C.M., Hackett, J., Anderson, R.R., Kail, S. and Spock, P.S., 1992. Linear temperature programmed retention indices of gasoline range hydrocarbons and chlorinated hydrocarbons on cross-linked polydimethylsiloxane. *Journal of High Resolution Chromatography*, 15(2), pp.105-120.

Yaws, C. 2008. Yaws' Handbook of Physical Properties for Hydrocarbons and Chemicals, *Knovel*, New York.

Chapter 4: Results and Discussion

4.1 Preliminary study: Identifying target hydrocarbons in diesel exhaust samples

As part of the preliminary study, exhaust samples (traps and filters) from a 1.6 L engine fuelled with ultra-low sulphur (ULS) diesel (collected and analysed during an earlier study) were examined for the presence of the target analytes. Mass spectral matching (NIST 16 mass spectral library, match quality ≥ 80%) was used for tentative identification of HC emissions. A large number of HCs spanning a wide range of chemical classes (n-alkanes, branched alkanes, cycloalkanes, alkylbenzenes and alkenes) were found in these samples. The abundance of each chemical class varied as indicated by the peak areas. To obtain a rough estimate of the abundance of each chemical class in the exhaust emissions, peak areas of the identified HCs were plotted (Figure 4.1). n-Alkanes (aliphatics) and alkylbenzenes (aromatics) were found in higher concentrations than the branched- and cyclo- alkanes, as well as the alkenes.

Various emission studies state that alkenes and aromatic compounds are more important for photochemical O_3 and SOA production (Gautam et al., 1996, Volkamer et al., 2006, Weitkamp et al., 2007). Gautam et al. (1996) stated that aromatic compounds contribute more than 80% of the OFP from the semi-volatile phase of diesel exhaust emissions. This was followed by alkenes (10%) as well as n-alkanes and cyclic compounds which together made up the remainder. Weitkamp et al. (2007) concluded that 9 out of the 58 species in their study (benzene, toluene, xylene isomers, 1,2,4- and 1,3,5-trimethylbenzene, ethylbenzene and naphthalene) accounted for more than 90% of the SOA production predicted by their model. These compounds are also highly reactive, hence chamber studies and/or models assign higher reactivity indices to these compounds. A good example is Carter's reactivity scale where alkenes and aromatics have some of the higher MIR indices, however, as relatively low levels of these compounds (particularly alkenes) are found in vehicular emissions, it was important to investigate the ozone formation potential of compounds such as n-alkanes which have relatively low reactivity indices, but are emitted at higher concentrations.

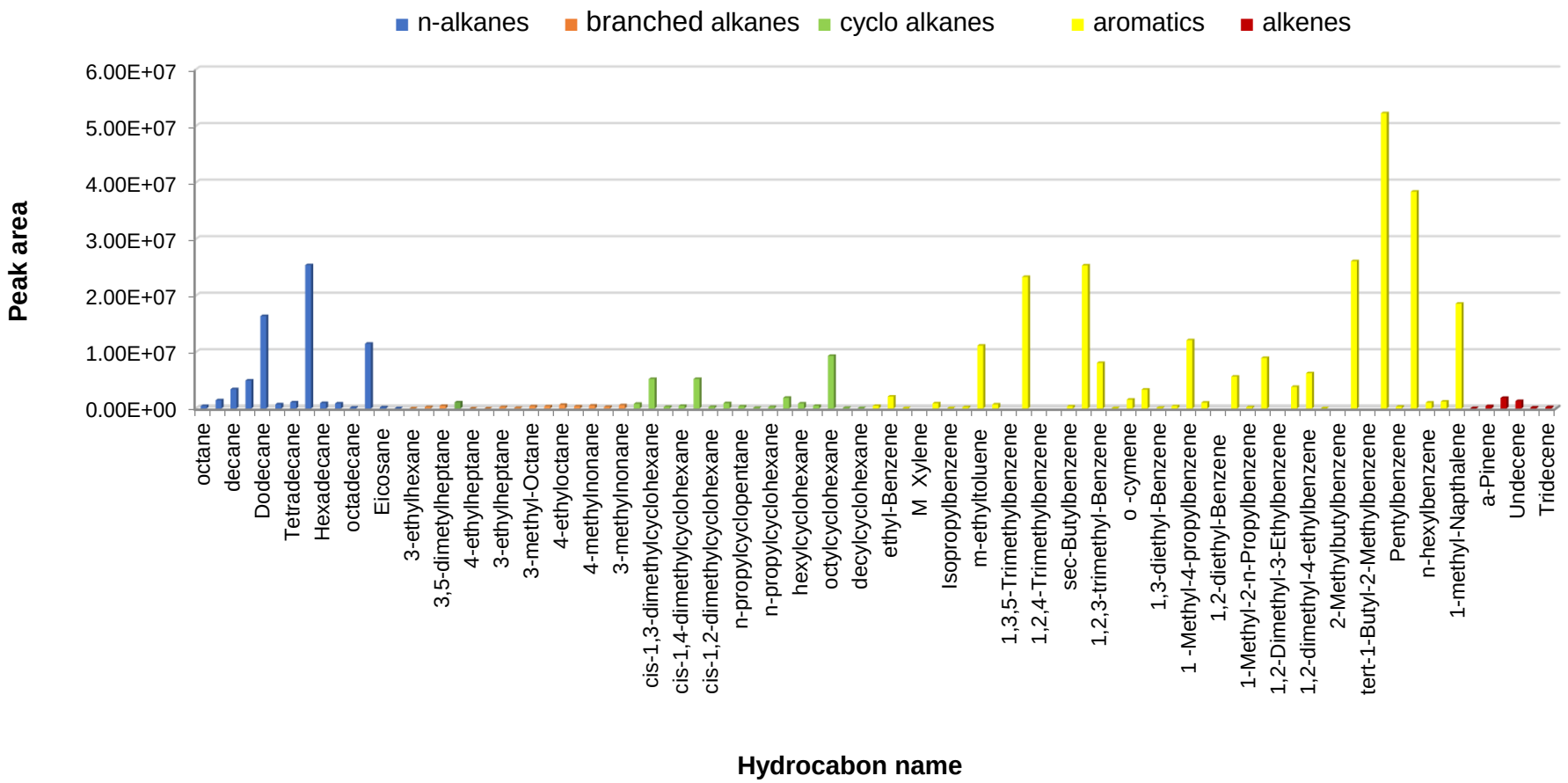

Figure 4.1 A comparison of the tentatively identified HC peak areas from the exhaust engine emissions of a 1.6 L test engine, fuelled with ultra-low sulphur (ULS) diesel.

Interestingly, qualitative analysis of the chromatograms from the primary traps used to sample the exhaust emissions showed two distinct regions of n-alkane emissions (Figure 4.2). These were dubbed ‘butterfly wings’ where a Gaussian like distribution in intensities was observed for the C_8 - C_{20} n-alkanes and again for C_{21} to ~ C_{40} n-alkanes. Figure 4.2 a shows the target HC peaks found on the primary traps used to sample diesel engine exhaust emissions during operating mode M1. Lower HC intensities were observed for C_8 - C_{20}, while higher intensities were seen beyond eicosane (‘right side of the wing’ highlighted in red). The ‘butterfly wings’ were observed in most of the samples on both the traps and filters, however it was found at greater intensities on the filter samples. The greatest n-alkane intensities were observed during the third operating mode M3 (Figure 4.2 c). The compounds in this region were a series of straight and branched alkanes that were speculated to originate from the lubricant oil, due to their high carbon numbers. As seen later in this section, butterfly wings were not observed in the diesel exhaust samples collected during this study.

Based on the results from this preliminary study, it was decided that focus would be placed on the n-alkane and alkylbenzenes (Table 4.1) as these compounds were found at relatively high levels in the diesel engine exhaust.

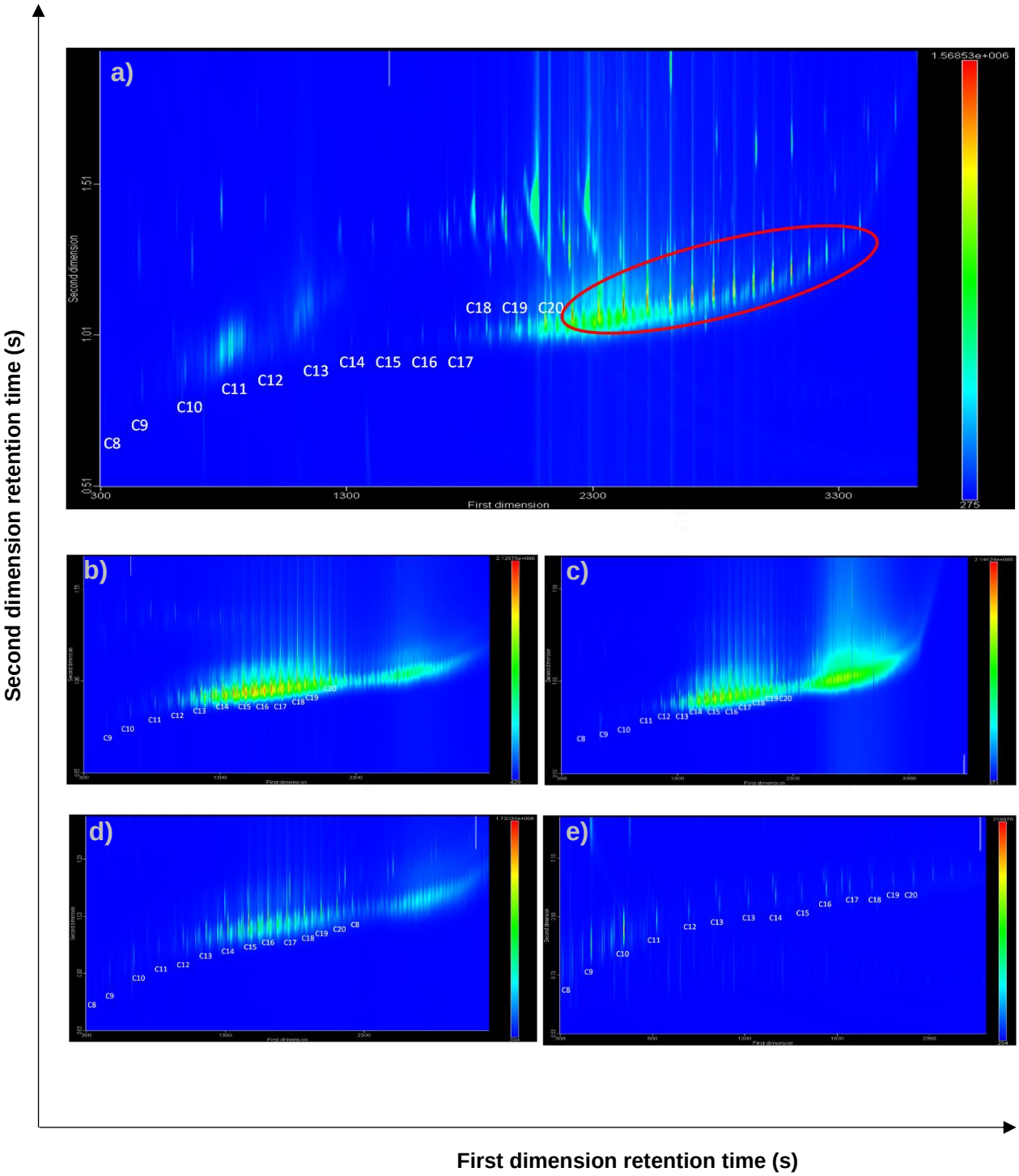

Figure 4.2 Extracted ion 2D chromatogram (m/z = 57) showing the aliphatic hydrocarbon region observed from the analysis of primary traps used to sample diesel engine exhaust emissions during operating modes M1-M5 (a-e).

Table 4.1 Target compounds sorted by boiling point (°C) with their physical, reactivity and retention properties.

Compound Number	Hydrocarbon	MW (g/mol)†	Bp (°C)†	MIR index (Carter, 2010)	1D RT (s)	2D RT (s)	RI calc	RI lit (Macak et al., 1983)
			n-alkanes					
	octane	114	125.7	0.9	315	0.65	*	
	nonane	128	150.8	0.78	489	0.82	*	
	decane	142	174.1	0.68	669	0.87	*	
	undecane	156	195.9	0.61	840	0.93	*	
	dodecane	170	216.3	0.55	1017	0.97	*	
	tridecane	184	235.4	0.53	1182	0.98	*	
	tetradecane	198	253.7	0.51	1341	0.99	*	
	pentadecane	212	270.6	0.5	1494	0.98	*	
	hexadecane	226	287.0	0.45	1635	1	*	
	heptadecane	240	302.0	0.42	1770	1.01	*	
	octadecane	254	316.3	0.4	1899	1.01	*	
	nonadecane	268	329.9	0.38	2019	1.02	*	
	eicosane	282	343.0	0.42	2136	1.03	*	
			alkylbenzenes					
1	**ethylbenzene**	106	136.5	3.04	381	1.09	842.6	847.7
2	**m-xylene**	106	139.0	9.75	393	1.09	851.1	863.2
3	**p-xylene**	106	137.7	5.84	393	1.09	851.1	861.2
4	**o-xylene**	106	144.0	7.64	426	1.16	874.5	883
5	**isopropylbenzene**	120	153.4	2.52	477	1.13	908.8	906.7
6	**1-methyl-3-ethylbenzene**	120	162.5	7.39	540	1.22	945.6	947.4
7	**1-methyl-4-ethylbenzene**	120	162.0	4.44	552	1.18	952.6	950.4
8	**1,3,5-trimethylbenzene**	120	164.6	11.76	567	1.27	961.4	967.1
9	**1-methyl-2-ethylbenzene**	120	162.0	5.59	594	1.28	977.2	963.4
10	**1,2,4-trimethylbenzene**	120	169.8	8.87	642	1.35	1005.1	985.3
11	**propylbenzene**	120	157.5	2.3	525	1.19	936.8	935.1
12	**tert-butylbenzene**	134	168.7	1.95	591	1.22	975.4	972.5
13	**sec-butylbenzene**	134	180.0	2.36	624	1.22	994.7	989.1
14	**m-cymene**	134	175.0	4.44	648	1.24	1008.5	1001.8
15	**p-cymene**	134	176.0	4.44	648	1.24	1008.5	1009.9
16	**o-cymene**	134	157.0	5.49	672	1.29	1022	1015.8
17	**1-methyl-3n-propylbenzene**	134	176.9	7.1	696	1.26	1035.6	1032.8
18	**butylbenzene**	134	180.0	2.36	705	1.28	1040.7	1034.9
19	**1,3-dimethyl-5-ethylbenzene**	134	185.0	10.08	708	1.3	1042.4	–
20	**1-methyl-4-n-propylbenzene**	134	182.8	4.43	717	1.22	1047.5	1038.8
21	**1-methyl-2n-propylbenzene**	134	184.9	5.49	723	1.31	1050.8	1045.4
22	**1,4-dimethyl-2-ethylbenzene**	134	185.9	7.55	741	1.33	1061	–
23	**1,2-dimethyl-4-ethylbenzene**	134	189.8	7.55	756	1.34	1069.5	–

Table 4.1 Continued

	Hydrocarbon	MW (g/mol)	Bp (°C)	MIR index (Carter, 2010)	1D RT (s)	2D RT (s)	RI calc	RI lit (Macak et al., 1983)
24	**1,2-dimethyl-3-ethylbenzene**	134	193.9	10.15	786	1.43	1086.4	–
25	**1,3-dimethyl-2-ethylbenzene**	134	190.0	10.15	786	1.43	1086.4	–
26	**1,2,4,5-tetramethylbenzene**	134	195.0	9.26	810	1.38	1100	1105.9
27	**2-methylbutylbenzene**	148	189.5	4.73	816	1.25	1103.4	
28	**tert-1-butyl-2-methyl-benzene**	148	200.5	4.73	834	1.4	1113.8	1090.9
29	**pentylbenzene**	148	202.1	2.12	882	1.3	1141.4	1136.2
30	**hexylbenzene**	162	226.1	4.39	1059	1.29	1245.5	–

* RI of a reference n-alkane (100n) where n is the number of carbon atoms in the n-alkane.
MIR = Maximum incremental reactivity, MW = molecular weight, Bp = boiling point 1D RT = 1st dimension retention time, 2D RT = 2nd dimension retention time, RI = Retention index.
†(Bingham and Cohrssen, 2012, Gilman and Beaber, 1925, Schlatter and Clark, 1953, Washburn, Yaws, 2012, Yaws and Gabbula, 2003)

4.2 Method validation

Validation of an analytical method is crucial during an experimental study. Various parameters including the linearity, repeatability, LOD and LOQ are investigated as part of the validation process.

To investigate the linearity, five calibration solutions with concentrations of 1, 5, 10, 20 and 30 ppm were prepared from a 40 ppm C_8–C_{20} n-alkane standard. To each solution 10 µL of 1 ppm hexadecane-d34 IS was added. During instrumental analysis 1 µL of each of the standard solutions (except in the case of 60 ppm where 2 µL of the 30 ppm standard was used) were spiked onto pre-conditioned traps and analysed in duplicate by TD-GC x GC-TofMS using the same method used to analyse the emissions samples. Six-point calibration curves were drawn for each target n-alkane and the error was calculated as the relative standard deviation between the two replicates. Figure 4.3 shows example calibration curves obtained for octane, nonane, hexadecane and eicosane (the rest are available in Appendix E). Low mass, volatile n-alkanes, such as octane, had lower linearity (as indicated by the correlation coefficient, R^2) than the heavier n-alkanes. This could be due to volatile/zation of these compounds during standard preparation and/or injection, or possible loss of the analyte during solvent delay: a short period of time after injection where the solvent is allowed to evaporate off, to protect the MS filament from damage that would result if

large amounts of the solvent vapour reached the source. Overall good linearity was observed with the R^2 value ranging from 0.9469 (octane) to 0.9999 (eicosane). Table 4.2 shows the target list of n-alkanes with their respective linear equation and R^2 values.

Good precision between duplicate calibration points was observed, however, at certain concentration levels, large error bars indicated poor repeatability (%RSD range of 0.21 – 101.61%). This might be due to gross errors during preparation and/or analysis mainly resulting from the volatility of the analytes, particularly octane which was undetected at low concentrations. Another contributing factor could be the pre-existence of certain ubiquitous HCs on 'clean' traps. Although the PDMS traps are conditioned prior to use, this might not have been sufficient enough to remove all the HCs that may have been introduced during storage. When clean unused traps were analysed on the TD-GC x GC-TofMS, HC peaks were observed in detectable amounts. Although they were not found in significantly high enough concentrations to affect quantitative results (hence a blank correction was not performed), they may have affected the repeatability between duplicate samples measured using two different samplers. In general, calibration curve standards are run in triplicate to improve precision. More so, ideally the standards are analysed in one day to prevent inter-day variability, however, the long analysis time of the TD-GC x GC-TofMS method (71 min) meant that the linear aggression analysis was conducted over a number of days. In addition, less variation is observed with direct analysis of liquid samples (as opposed to injection onto traps followed by thermal desorption) where a repeatable amount of standard is aliquoted directly into the instrument, reducing the chances of gross errors.

The detection and quantitation limits of the n-alkanes (Table 4.2) were calculated using the S/N ratio method where the lowest standard concentration was divided by the instrumental S/N ratio and multiplied by 3 and 10 for the LOD and LOQ respectively (detailed in Section 3.4.1.2). These were termed the on column LOD and LOQ (LOD_{OC} and LOQ_{OC}, pg). The instrument employed has a detection limit (sensitivity) of 1 pg, thus the LOD cannot be less than 1 pg (LOQ of 3.3 pg), hence these values were assigned for analytes with an estimated LOD and LOQ less than the instrumental limit. Because each engine speed phase was associated with a different distance travelled

and volume of air sampled (including dilution ratios), the detection and quantitation limits were also were also estimated per volume of air sampled (µg/m^3) as well as per kilometre travelled (µg/km). These were termed the LOD exhaust (LOD_{exh}), Table 4.3 and LOQ exhaust (LOQ_{exh}), Table 4.4. Higher detection and quantitation limits are observed for the more volatile n-alkanes (particularly octane, nonane and decane), while the heavier n-alkanes had calculated limits lower than the instrumental LOD and LOQ, thus the instrumental detection limits were employed.

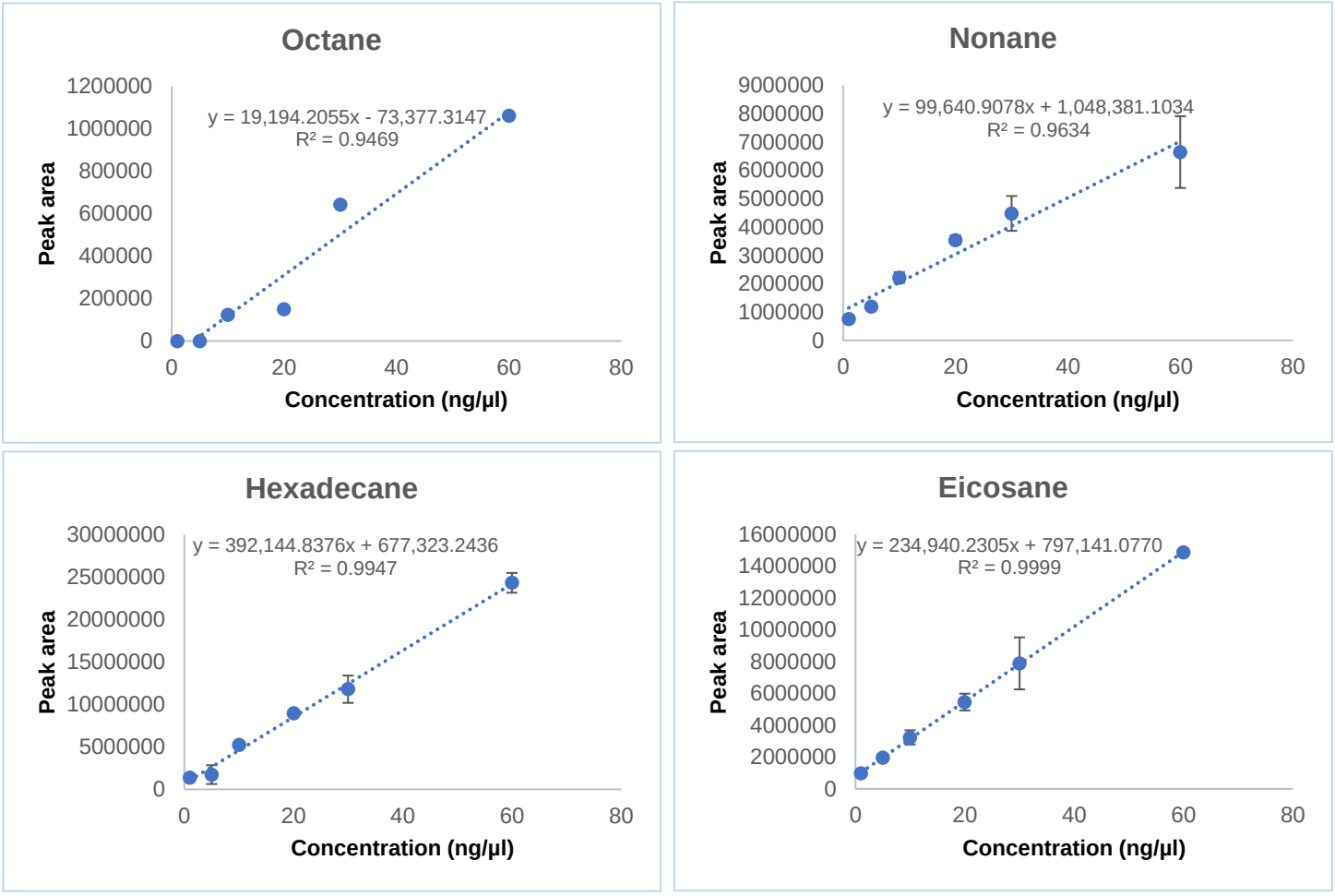

Figure 4.3 Six point calibration curves obtained for octane, nonane, hexadecane and eicosane (injected onto PDMS traps) with the respective linear equation and correlation coefficient indicated as well as the error bars calculated as the standard deviation between the two replicate standard solutions.

Table 4.2 Method validation data and limits of detection and quantitation for the n-alkanes present in diesel exhaust emissions sampled onto PDMS traps.

Hydrocarbon	MW (g/mol)†	Bp (°C)†	MIR (g O_3/g VOC) (Carter, 2010)	Linear equation	R^2	LOD_{OC} (pg)	LOQ_{OC} (pg)
octane	114	125	0.9	y = 19,194x - 73,377	0.947	125	416.6
nonane	128	151	0.78	y = 99,640x + 1,048,381	0.963	41.7	138.9
decane	142	174	0.68	y = 382,468x + 1,784,021	0.988	42.9	143.1
undecane	156	196	0.61	y = 551,731x + 1,627,543	0.996	3.4	11.2
dodecane	170	216	0.55	y = 540,633x + 1,927,710	0.991	1	3.3
tridecane	184	234	0.53	y = 503,498x + 1,006,625	0.994	1	3.3
tetradecane	198	254	0.51	y = 491,120x + 528,321	0.993	14.3	47.6
pentadecane	212	271	0.5	y = 373,306x + 1,266,347	0.998	1	3.3
hexadecane	226	287	0.45	y = 392,144x + 677,323	0.995	1	3.3
heptadecane	240	303	0.42	y = 305,187x + 3,015,643	0.962	1	3.3
octadecane	254	316	0.4	y = 273,940x + 1,627,580	0.994	1	3.3
nonadecane	268	330	0.38	y = 250,657x + 1,255,882	0.996	1	3.3
eicosane	282	344	0.42	y = 234,940x + 797,141	1.000	1	3.3

MIR = Maximum incremental reactivity, LOD_{OC} = limit of detection on column, LOQ_{OC} = limit of quantitation on column

†(Bingham and Cohrssen, 2012, Gilman and Beaber, 1925, Schlatter and Clark, 1953, Washburn, Yaws, 2012, Yaws and Gabbula, 2003)

Table 4.3 n-Alkane detection limits when sampled onto PDMS traps during the low, medium, high and extra high speed phases.

	Low			Medium			High			Extra-high		
Hydrocarbon	**LOD_{exh} (µg)**	**LOD_{exh} (µg/km)**	**LOD_{exh} (µg/m³)**	**LOD_{exh} (µg)**	**LOD_{exh} (µg/km)**	**LOD_{exh} (µg/m³)**	**LOD_{exh} (µg)**	**LOD_{exh} (µg/km)**	**LOD_{exh} (µg/m³)**	**LOD_{exh} (µg)**	**LOD_{exh} (µg/km)**	**LOD_{exh} (µg/m³)**
Octane	44.67	14.36	9056.98	35.18	7.38	9785.82	31.77	4.43	8406.90	19.02	2.31	7099.96
Nonane	14.90	4.79	3020.33	11.73	2.46	3263.39	10.59	1.48	2803.55	6.34	0.77	2367.70
Decane	15.34	4.93	3110.25	12.08	2.54	3360.54	10.91	1.52	2887.01	6.53	0.79	2438.19
Undecane	1.20	0.39	244.18	0.95	0.20	263.83	0.86	0.12	226.66	0.51	0.06	191.42
Dodecane	0.36	0.12	72.47	0.28	0.06	78.30	0.25	0.04	67.27	0.15	0.02	56.81
Tridecane	0.36	0.12	72.47	0.28	0.06	78.30	0.25	0.04	67.27	0.15	0.02	56.81
Tetradecane	5.10	1.64	1034.66	4.02	0.84	1117.92	3.63	0.51	960.39	2.17	0.26	811.09
Pentadecane	0.36	0.12	72.47	0.28	0.06	78.30	0.25	0.04	67.27	0.15	0.02	56.81
Hexadecane	0.36	0.12	72.47	0.28	0.06	78.30	0.25	0.04	67.27	0.15	0.02	56.81
Heptadecane	0.36	0.12	72.47	0.28	0.06	78.30	0.25	0.04	67.27	0.15	0.02	56.81
Octadecane	0.36	0.12	72.47	0.28	0.06	78.30	0.25	0.04	67.27	0.15	0.02	56.81
Nonadecane	0.36	0.12	72.47	0.28	0.06	78.30	0.25	0.04	67.27	0.15	0.02	56.81
Eicosane	0.36	0.12	72.47	0.28	0.06	78.30	0.25	0.04	67.27	0.15	0.02	56.81

Table 4.4 n-Alkane quantitation limits when sampled onto PDMS traps during the low, medium, high and extra high speed phases.

	Low			Medium			High			Extra-high		
Hydrocarbon	**LOQ_{exh} (µg)**	**LOQ_{exh} (µg/km)**	**LOQ_{exh} (µg/m³)**	**LOQ_{exh} (µg)**	**LOQ_{exh} (µg/km)**	**LOQ_{exh} (µg/m³)**	**LOQ_{exh} (µg)**	**LOQ_{exh} (µg/km)**	**LOQ_{exh} (µg/m³)**	**LOQ_{exh} (µg)**	**LOQ_{exh} (µg/km)**	**LOQ_{exh} (µg/m³)**
Octane	148.90	47.86	30189.92	117.26	24.61	32619.39	105.88	14.78	28023.01	63.39	7.69	23666.52
Nonane	49.66	15.96	10067.78	39.10	8.21	10877.96	35.31	4.93	9345.16	21.14	2.57	7892.35
Decane	51.13	16.44	10367.50	40.27	8.45	11201.80	36.36	5.07	9623.36	21.77	2.64	8127.31
Undecane	4.01	1.29	813.94	3.16	0.66	879.44	2.85	0.40	755.52	1.71	0.21	638.07
Dodecane	1.18	0.38	239.15	0.93	0.19	258.40	0.84	0.12	221.99	0.50	0.06	187.48
Tridecane	1.18	0.38	239.15	0.93	0.19	258.40	0.84	0.12	221.99	0.50	0.06	187.48
Tetradecane	17.01	5.47	3448.86	13.40	2.81	3726.40	12.10	1.69	3201.32	7.24	0.88	2703.64
Pentadecane	1.18	0.38	239.15	0.93	0.19	258.40	0.84	0.12	221.99	0.50	0.06	187.48
Hexadecane	1.18	0.38	239.15	0.93	0.19	258.40	0.84	0.12	221.99	0.50	0.06	187.48
Heptadecane	1.18	0.38	239.15	0.93	0.19	258.40	0.84	0.12	221.99	0.50	0.06	187.48
Octadecane	1.18	0.38	239.15	0.93	0.19	258.40	0.84	0.12	221.99	0.50	0.06	187.48
Nonadecane	1.18	0.38	239.15	0.93	0.19	258.40	0.84	0.12	221.99	0.50	0.06	187.48
Eicosane	1.18	0.38	239.15	0.93	0.19	258.40	0.84	0.12	221.99	0.50	0.06	187.48

4.3 Comparison of engine exhaust hydrocarbon emissions

4.3.1 Optimization studies: Steady state tests

Steady state tests were conducted to determine the optimal sampling time, sampler configuration and instrumental conditions for analysis by TD-GC x GC-TofMS. These studies were performed using samples from the repeat measurements taken using the SAM10 diesel during sampling campaign one (Section 3.2.3.3).

4.3.1.1 Breakthrough studies and selection of sampler configuration

Breakthrough studies were performed by collecting emissions over three different sampling durations: 5, 10 and 30 min at 500 mL/min (corresponding to ~2.5, 5 and 15 L of air sampled, respectively).

The collection efficiency of a sampler is affected by various factors including the sorbent bed length, type of sorbent, sampling flow rate and analyte concentration. A review by Pauláthomas (1989) highlighted that with increasing sampling volume and/or sampling time, at a constant sampling rate the collection efficiency of the sampler decreases due to a depletion of active sites on the adsorbent or due to breakthrough of the analyte when absorbents (such as PDMS) are used. Consequently, under certain conditions the analyte may leave the denuder unretained, and the sampler is said to have reached breakthrough conditions when 10% of the total concentration of the analyte entering the sampler, leaves the sampler at the outlet (Kohlmeier et al. 2015). Because analytes are collected at a particular sampling rate, a longer sampling time results in a larger volume of air sampled. During trace analysis or analysis of less concentrated samples this is beneficial, as it allows for pre-concentration of the analytes if the breakthrough volume is not exceeded, enabling them to be more easily detected. In a denuder setup, any analytes which breakthrough the primary trap are collected by a secondary trap located downstream of the filter. Hence, to investigate the breakthrough of the HC engine emissions from the primary PDMS trap, the HC concentration on the secondary trap of each sampler was compared to that found on the primary trap.

Ideally a significantly lower amount of analyte should be found on the secondary trap as compared to the respective primary trap. It is important to note however, that another source of analytes found on the secondary trap may be from blow-off effects where particle associated analytes may be volatilised from the particles collected on the filter. Overall, to reduce sampling artefacts, sampling times must be minimized, thus preventing concentration and temperature fluctuations that may perturb the partitioning equilibrium, hence the importance of breakthrough studies.

Figure 4.4 shows a comparison of the HC levels found on the primary and secondary traps for all three sampling durations. These samples were collected using both trap-trap and denuder (trap-filter-trap) sampler configurations.

Lower amounts of HCs were found on the secondary traps when 2.5 and 5 L of air was sampled, as expected. More breakthrough occurred for the lower mass hydrocarbons (C_8 - C_{11}), as a consequence of their higher volatility. In certain incidences higher amounts of HCs were observed on the secondary trap than on the primary trap. This was observed predominantly when the trap-trap sampler was used. Theoretically speaking, as both the primary and secondary traps have the same dimensions, they should have the same retention capacity; hence the worst case scenario would be if they both contained the same amount of analyte (under complete breakthrough or equilibrium sampling conditions). The higher amounts of HCs found on the secondary traps might be as a result of lack of retention of low mass HCs by the primary trap due to the elevated sampling temperature, whilst retention was possible in the secondary trap as some degree of cooling of the exhaust gases would occur through the sampling device. When 15 L of air was sampled a large amount of breakthrough was observed, as expected. The secondary traps contained ≥ 50% of the amount of analyte on the primary trap for all the n-alkanes and this was observed for both the denuders and trap-trap samplers. This indicated that 5 and 10 min were ideal sampling durations at the sampling flow rate of 500 mL/min, however 30 min sampling should be avoided, as breakthrough would make interpretation of the results difficult. It was noted that there was a major difference in the analyte

concentration between the trap-trap and denuder samples during the 10 min steady state test. Further investigation into these results would be needed to determine the cause.

This informed the decision that emissions from each phase of the driving cycle would be sampled onto different samplers. The shortest phase was 322 s (5.33 min) long while the longest phase was long 590s (9.83 min). This also meant that sampling emissions from the entire driving cycle onto one sampler was not feasible as the total test cycle was 1800 s (30 min) long. Furthermore, the portable sampling pumps employed cannot be operated in a stable manner at flow rates less than 500 mL/min, consequently running at a lower flow rate was not an option.

It was also concluded that the denuder sampling configuration was superior to the trap-trap configuration, as it allows for collection of gaseous and particle associated SVOCs. In addition, fluctuations in the flow rate during sampling were observed when samplers in the trap-trap configurations were employed, which is problematic as it introduces errors in the quantitative analysis and could result in elevated breakthrough. Upon further investigation, it was found that placing an external filter downstream of the trap-trap sampler stabilised the pump operation and minimized changes in the flow rate caused by fluctuations in back pressure. In the denuder sampler this would be achieved by the quartz fibre filter nestled in between the primary and secondary trap. When the denuder samplers were employed, no back pressure fluctuations were observed and the flow rate remained at a steady 500 mL/min. This effect was likely due to the fact that the portable sampling pumps employed are designed primarily for occupational hygiene air sampling onto filters, and thus function optimally with sampling systems of a similar back pressure. Thus overall the denuder samplers proved to be superior to the trap-trap samplers and therefore only these samplers were used during the second sampling campaign where emissions were collected for different test fuels (Section 3.2.4).

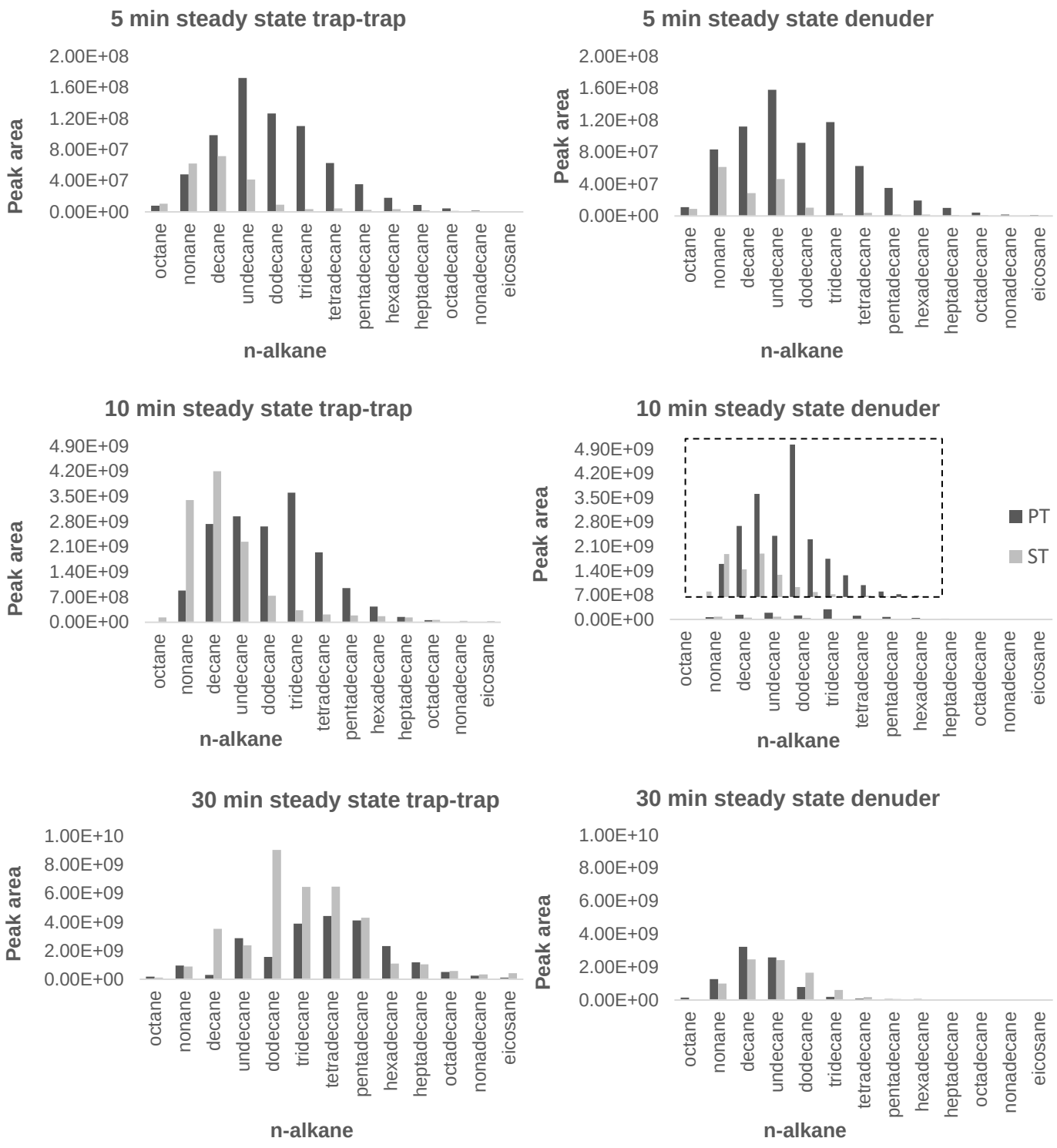

Figure 4.4 A comparison of the hydrocarbon levels found on the primary and secondary traps during the 5, 10 and 30 min breakthrough studies for both the denuder and trap-trap sampler configurations where exhaust emissions were sampled with the test engine being operated under steady state conditions.
PT = primary trap ST = secondary trap

4.3.1.2 Optimization of the instrumental analysis method

The initial phase of this study involved an extensive review of emission speciation and atmospheric composition studies to identify semi-volatile HCs of relevance. A preliminary study was then conducted to determine the presence of these HCs in diesel exhaust samples that had been collected during a previous study conducted at the SFAC by Geldenhuys et al. (2015), which had focussed on polycyclic aromatic hydrocarbons (PAHs) in diesel emissions. From the preliminary study, it was decided that a similar method which had been used to analyse the load haul dump (LHD) mine samples would be used for analysis in this study, as both aliphatic and aromatic HCs had been successfully detected and resolved in these samples.

Because engine exhaust samples contain high levels of HCs, emission samples often require split injection. This is to prevent overloading of the column, which would result in peak broadening and shape distortion, leading to inaccurate quantitative results. To determine whether to use split or splitless injection for this study, the 10 min steady state samples (Table 3.2) were analysed at a split ratio of 50:1 (Figure 4.5 a), 100:1 (Figure 4.5 b) and in solvent vent (splitless) mode (Figure 4.6 a). From qualitative analysis of the 2D chromatograms obtained, the n-alkanes were observed at high intensities during both split and splitless modes. For the 100:1 split ratio however, the alkylbenzene peaks were seen at a fairly low intensity. Improved intensities were found using a split ratio of 50:1, and in splitless mode both the alkylbenzene and n-alkane HC peaks were clearly observed. It was thus decided that samples would be analysed in solvent vent mode to ensure that the analytes present at lower concentrations could also be detected.

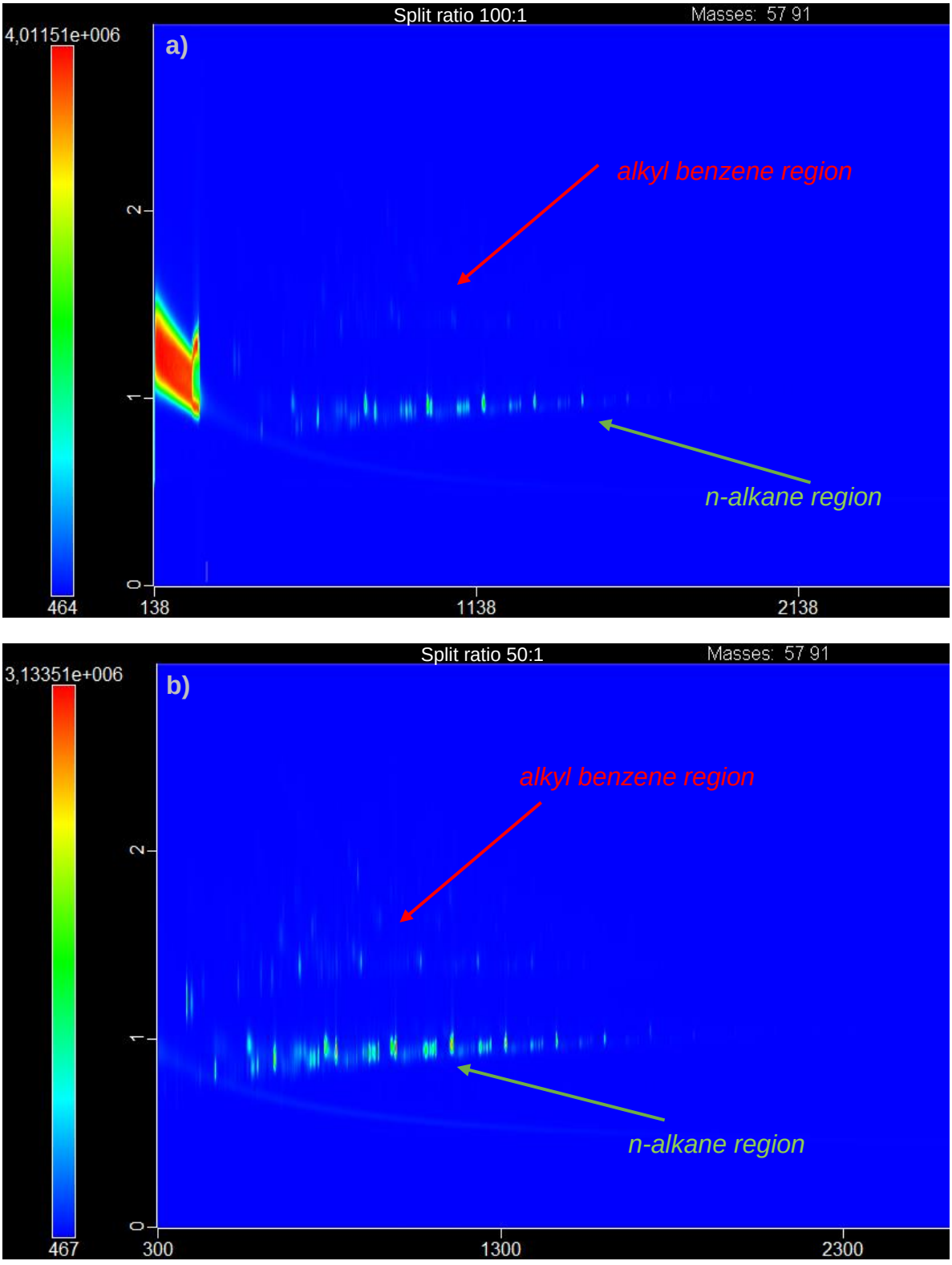

Figure 4.5 Extracted ion (m/z = 57, 91) 2D chromatograms of exhaust emissions collected onto PDMS traps from the steady state tests, analysed at a split ratio of 100:1 (a), and 50:1 (b).

Typical chromatograms of the exhaust emission samples analysed using solvent vent mode are shown in Figure 4.6, with the n-alkane and alkylbenzene regions indicated. Two dimensional gas chromatography proved to be a useful technique for chromatographic separation of the two compound classes. A non-polar column was used in the first dimension and a mid-polar column in the second dimension. As a consequence, the analytes were separated by volatility in the first dimension and polarity in the second dimension. The alkylbenzenes thus also elute later in the second dimension relative to the n-alkanes, and complete elution of the alkylbenzenes is achieved relatively early in the first dimension. Good separation of both the n-alkane and alkylbenzene peaks was achieved however, better resolution was observed for the n-alkanes. This reflects the difficulty of separating isomers with very similar volatilities compared to the relative ease of separating homologs of different molecular masses and boiling points. Fortunately, by nature diesel fuel contains a lot more n-alkanes than other isomers. This also applies to its exhaust emissions. Hence overlap with minor isomers are hardly noticed.

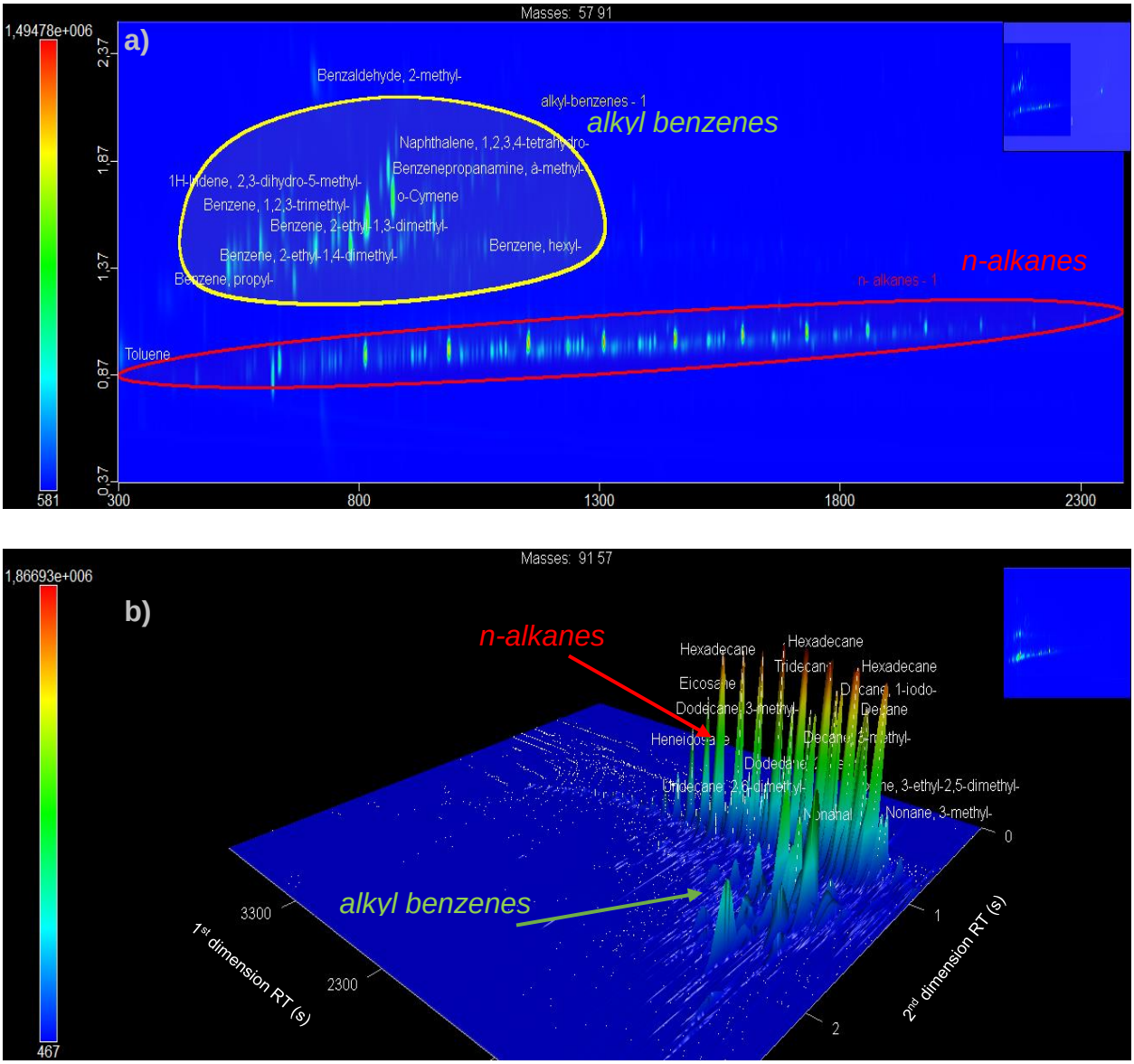

Figure 4.6 Typical extracted ion (m/z = 57, 91) 2D chromatograms of the engine exhaust emissions sampled onto PDMS traps and analysed in solvent vent mode where a) shows a 2D chromatogram whilst b) is a contour plot view of the analytes.

4.4 The role of two dimensional gas chromatography and mass spectrometry for engine exhaust emission speciation

Diesel exhaust is made up of a complex array of a large number of chemical species. The composition and concentration of emissions depends on various factors including, but not limited to, engine design, fuel and lubricant composition, vehicle model, age etc. thus making quantitative collection and chemical analysis of the exhaust emissions

challenging. A large number of compounds were detected in the exhaust samples. Qualitative analysis of the chromatograms obtained showed that the compounds spanned various chemical classes: predominantly straight, branched and cyclo-alkanes, alkylbenzenes and PAHs. To analyse such a complex sample, targeted analysis is useful during which a selected target list of compounds is analysed. However, even with a narrowed down target list of compounds it might not be financially practical to quantify all the compounds, hence tentative identification is often used to confirm the presence of compounds in a sample. Tentative identification involves matching the mass spectrum of the sample analyte to that found in a commercial library or compound database using a match threshold.

In this study, obtaining analytical standards for each alkylbenzene would not have been viable from a cost perspective. In addition, analytical standards are not commercially available for all the isomers of certain alkylbenzenes, hence tentative identification was a useful method to identify alkylbenzenes present in the diesel exhaust emissions.

A standard containing a mix of 37 aromatic compounds (Appendix D), originally designed for the qualitative determination of individual hydrocarbons in spark ignition engine fuels, was injected onto a trap and analysed using the TD-GC x GC-TofMS. As a consequence of the intended use of this standard, quantitative analysis of the alkylbenzenes could not be performed, however using the retention times, tentative identification was possible, where the retention times of the alkylbenzenes found in the samples were matched to those of the reference standard. In addition, mass spectral matching using the NIST 16 mass spectral library (with a match quality $\geq$ 80%) aided in positive identification of the alkylbenzenes present in the emission samples.

Separation of individual compounds occurs along the 1st chromatographic dimension where a Rxi-1 MS column was used. It was observed that all the alkylbenzenes eluted roughly between C_8 and C_{11} n-alkanes, as expected from their boiling points (see order in Figure 4.6) and the isomer peaks eluted fairly close to each other (lower resolution) than the n-alkanes. Lowering the carrier gas flow rate and or initial primary oven

temperature might have aided in improving the chromatographic resolution; however, this would result in a significant increase in the analysis time which is not feasible due to the presence of late-eluting heavier n-alkanes. This compromise in resolution resulted in certain alkylbenzene isomers remaining unresolved, i.e. the following pairs of isomers co-eluted and were thus identified as a single peak; m/p – xylene, m/p – cymene and 1,2-dimethyl-3-ethylbenzene/1,3-dimethyl-2-ethylbenzene. The majority of the target HCs were identified, hence the method was deemed fit for purpose for the analysis of both classes of compounds.

As discussed earlier in this section, mass spectral matching was a powerful technique for tentative identification of the target compounds; however, for detailed differentiation between structurally similar compounds (having similar mass spectra), retention time played a key role. An example is shown in Figure 4.7. The chromatogram (1 µl of a 10^6 dilution of the DHA aromatic standards injected into a trap and analysed) shows six structural isomers of propylbenzene. Although some peak tailing is observed, good separation was obtained between each of these compounds. The MS spectra are shown in Figure 4.8. Their fragmentation patterns are strikingly similar with a base peak at m/z = 105. Extensive fragmentation is observed, a direct consequence of the ion-source used during analysis. The instrument uses an electron ionization (EI) ion source, where the compounds are bombarded with high energy electrons resulting in extensive fragmentation of the compound. Thus, although as intact compounds the isomers differ structurally, they generate similar fragments resulting in similar mass spectra. Thus the elution order along the first dimension and differences in retention times proved to be crucial to differentiate between these isomers. An alternative could have also been the use of a soft ionization technique, which would allow for less fragmentation, e.g. chemical ionization.

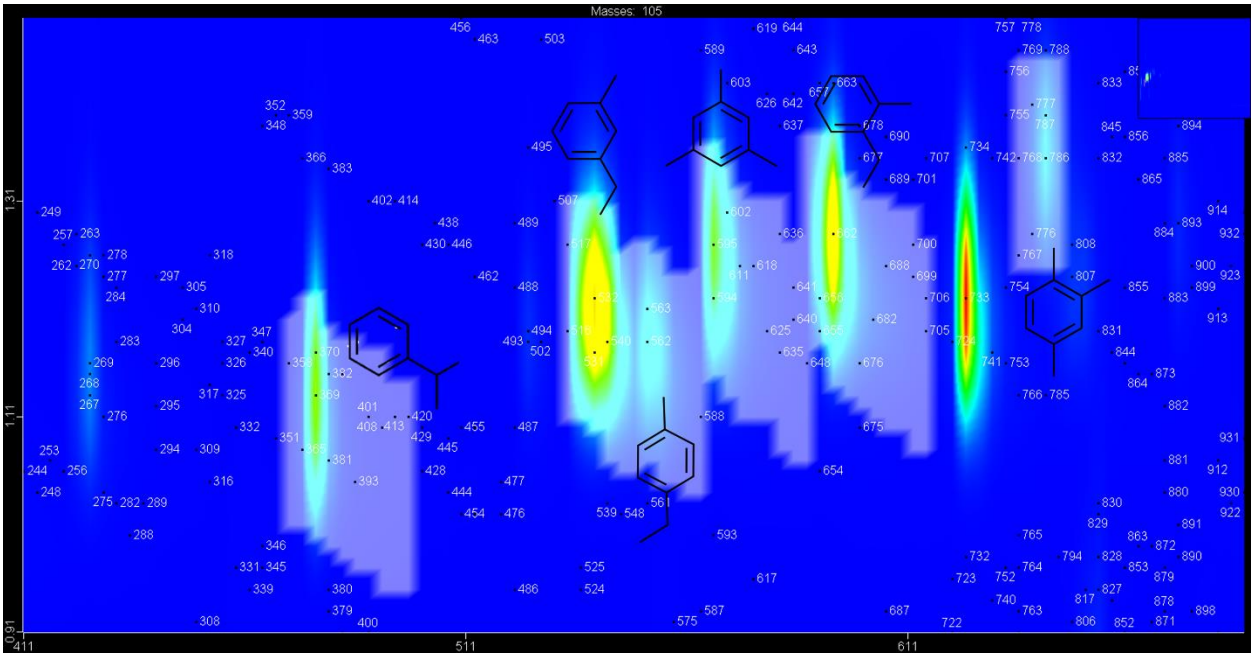

Figure 4.7 Extracted ion 2D chromatogram (m/z = 105) of propylbenzene isomers identified in the DHA aromatic standard (1 µL injection from the 10^6 x dilution solution thermally desorbed from a PDMS trap).

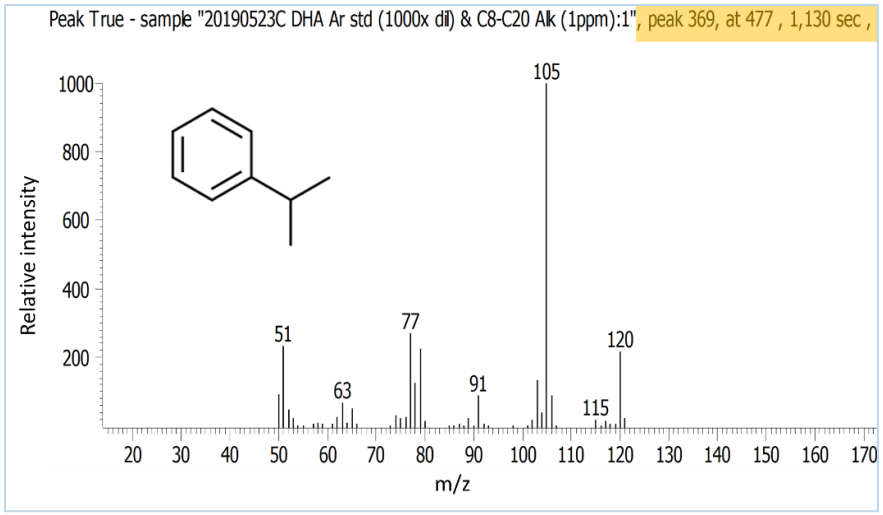
Peak True - sample "20190523C DHA Ar std (1000x dil) & C8-C20 Alk (1ppm):1", peak 369, at 477 , 1,130 sec ,
Relative intensity
m/z
105
77
51
120
91
63
115

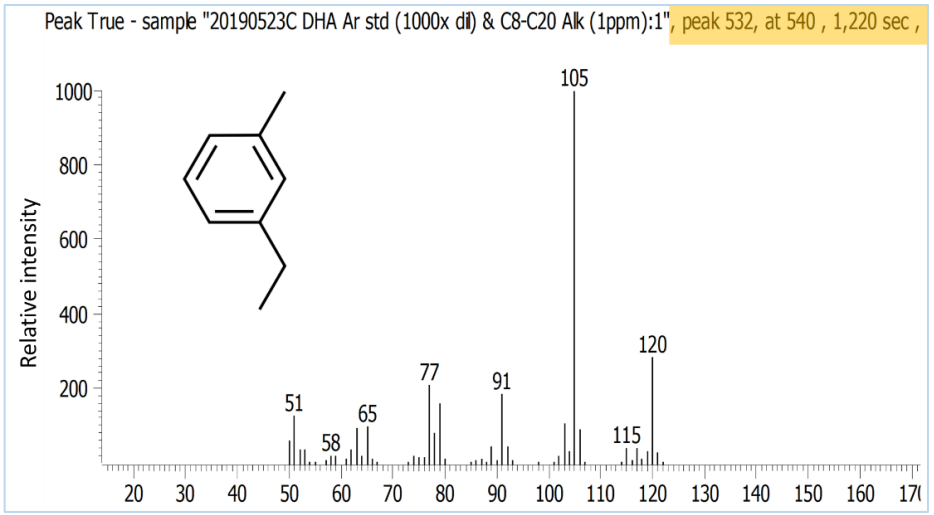
Peak True - sample "20190523C DHA Ar std (1000x dil) & C8-C20 Alk (1ppm):1", peak 532, at 540 , 1,220 sec ,
Relative intensity
105
120
77
91
51
65
58
115

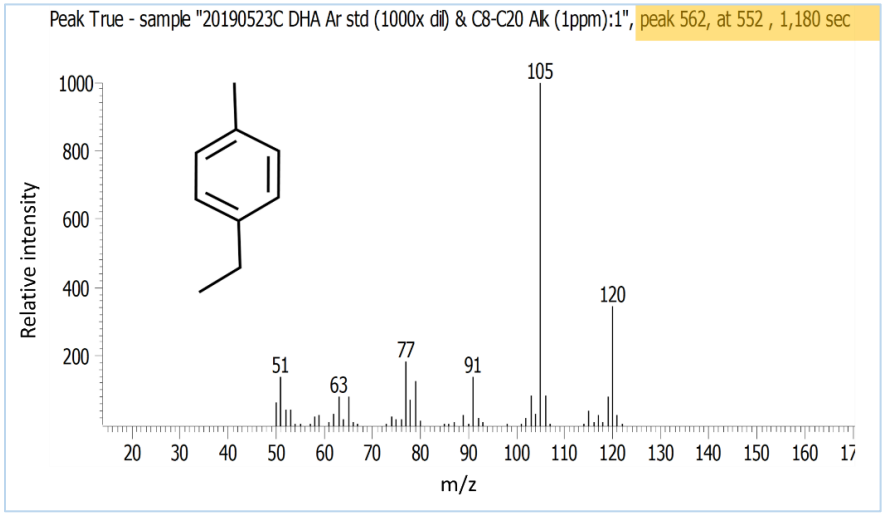
Peak True - sample "20190523C DHA Ar std (1000x dil) & C8-C20 Alk (1ppm):1", peak 562, at 552 , 1,180 sec
Relative intensity
m/z
105
120
77
91
51
63

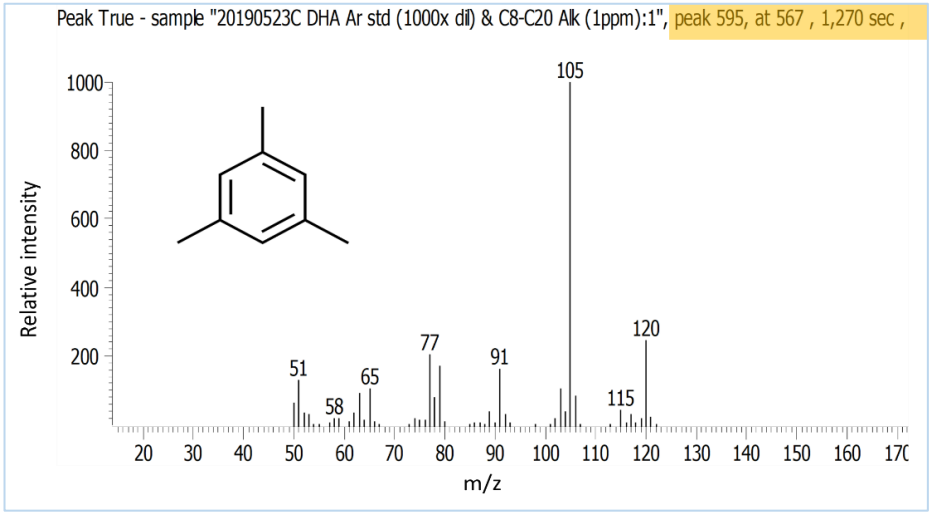
Peak True - sample "20190523C DHA Ar std (1000x dil) & C8-C20 Alk (1ppm):1", peak 595, at 567 , 1,270 sec ,
Relative intensity
m/z
105
120
77
91
51
65
58
115

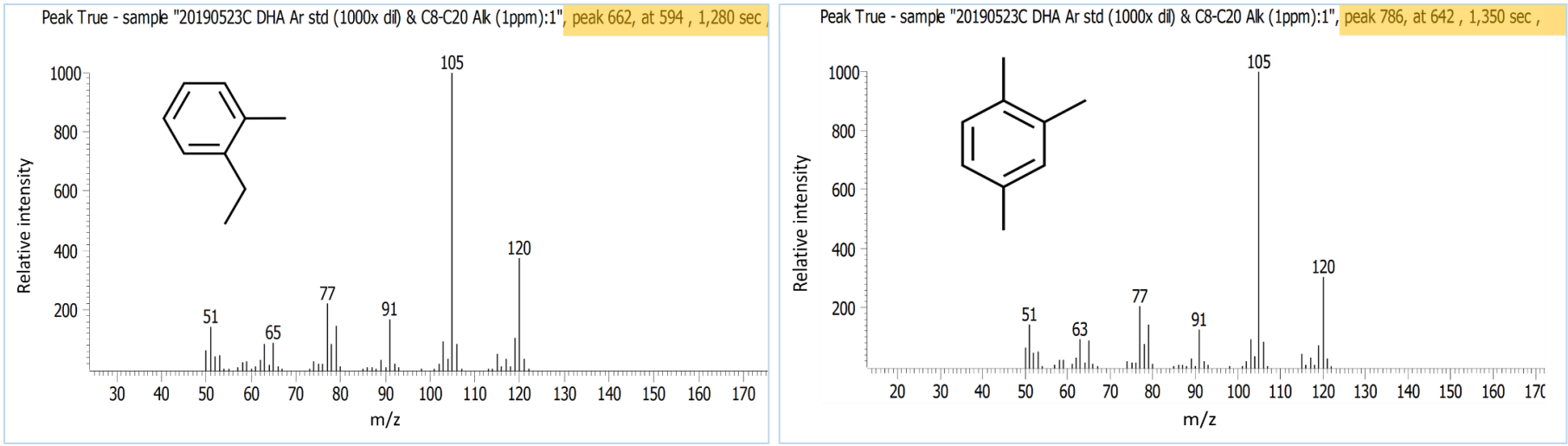

Figure 4.8 Mass spectra of propylbenzene isomers identified in the DHA aromatic standard (1 µL injection from the 10^6 x dilution solution onto a PDMS trap) with differences in retention times highlighted.

n-Alkanes usually elute closer to the baseline in order of increasing carbon number (C_n), where the peaks are spaced equidistant from each other as a result of the linear column temperature ramp. Although, like the alkylbenzenes, their mass spectra are also similar (typically with abundant peaks at m/z = 57, 71 and 85), they are more easily identified by their retention times and molecular ion (M^+).

It is clearly evident that comprehensive 2D-chromatography is a powerful technique for the analysis of complex samples such as diesel exhaust emissions, particularly in resolving peaks that remained unresolved (overlap) when 1D-chromatography is employed. Figure A6 (Appendix) shows how the aromatic fraction is readily separated from n-alkanes of the same volatility via the additional retention on the mid-polar secondary column.

4.5 Comparison of exhaust emissions from different fuels

In this section, changes in the exhaust emissions from the combustion of the three test fuels under varying test conditions are presented. It should be noted that the results presented are from gaseous emissions sampled on PDMS traps only. The results obtained from analysing the filter samples showed no aromatic hydrocarbons and only the heavier aliphatic hydrocarbons, hence it was decided that these samples would not be further characterised. In addition, particle phase analytes would not be relevant to the study, which focused on photochemical smog formation from gas phase SVOCs.

The calculated emission factors for both n-alkane and alkylbenzene emissions during cold start engine operation are presented initially. This is followed by the changes in the HC emission factors during engine operation at different speed phases of the WLTC test cycle in Section 4.5.2. A comparison of the HC emissions to the THC, CO, CO_2 and NOx engine emissions is performed in Section 4.5.3. Hot start emission testing was also conducted for the SAM10 and EUR10 fuel. A comparison of the hot start and cold start HC emissions was done and these results are presented in Section 4.5.4. To investigate the effect of the exhaust aftertreatment system, emissions testing was conducted for the EUR10 fuel

with a DOC and DPF in line, and the results of these tests are presented in the final subsection.

4.5.1 Cold start emissions testing using different fuels

The term cold-start is used to describe the phase when the engine is being operated below its optimum operational temperature. It is also referred to as the engine warm-up period, due to the term cold-'start' being misinterpreted as the brief moment when the engine starts running, when in fact it refers to the extended period of time where the engine operates below optimal temperature conditions. The study of cold-start emissions is important because any exhaust gas aftertreatment systems present will not have reached their optimal operating temperature and are likely to be less effective in removing the generated exhaust emissions.

In this study, during cold-start emissions testing the engine had been left unoperated overnight, allowing for the components of the engine to cool down to ambient temperature. Cold-start, transient cycle tests were performed for all three fuels, and for each phase of the WLTC test cycle. Emissions from each of the four phases were collected using portable denuder samplers and analysed by comprehensive TD-GC x GC-TofMS.

4.5.1.1 n-Alkane emissions

Quantitative analysis of gas phase n-alkane HC emissions was performed. Figure 4.9 shows the n-alkane emission factors for each fuel and for each phase of the test cycle. EFs (Table 4.5) were obtained by initially correcting the HC mass obtained from the linear regression analysis (ng) to account for the dilution of emissions during sampling, then to obtain the EF (ng/km) the quantified mass of each n-alkane was divided by the distance travelled in that particular speed phase as outlined in Section 3.5.

The SAM10 diesel was found to have the highest total (sum of C_8 - C_{20}) n-alkane emissions (26.91 – 255.31 mg/km from the extra high to the low phase) compared to the other fuels, with greater emissions observed in the earlier phases (low and medium

phase) of the test cycle. The PAR10 diesel had the second highest n-alkane emissions (34.77 – 162.05 mg/km from the extra high to the low phase) and the EUR10 diesel had the lowest n-alkane emissions (21.63 – 63.97 mg/km from the extra high to the low phase) amongst the three test fuels. The relative abundance in n-alkane emissions was compared to the n-paraffin content of each fuel (Table 3.1) and no direct correlation was observed in this regard. The PAR10 fuel had the highest paraffin content (51.9%), however it generated the second highest n-alkane emissions, while the SAM10 fuel, which had the second highest n-paraffin content (24.5%) was seen to have the highest n-alkane emissions. This suggested that the level of HC emissions depends on additional properties and parameters other than the fuel chemical composition, i.e. the n-paraffin content alone does not predict its concentration in the exhaust gas.

Another property associated with the fuel composition; the cetane (CN) number was investigated. The cetane number is a unitless parameter associated with the diesel fuel ignition delay; the period of time between fuel injection and the beginning of the oxidation reaction. Fuels with a higher CN have a shorter ignition delay period, i.e. autoignition occurs relatively soon after fuel injection, while the opposite is true for fuels with a lower CN. Simply put, a higher CN means the fuel ignites easily which results in better fuel combustion and thus reduction of harmful emissions from unburnt HCs (Ladommatos et al., 1996). Various studies have reported the effect of the CN on exhaust emissions as well as engine performance. These studies report a reduction in emissions with an increase in CN, however the effect does plateau at a particular value specific to the fuel, beyond which a further increase in CN has no effect on exhaust emissions (Bartlett et al., 1992). In general, fuels with a higher n-paraffin content have a higher CN number (lower ignition delay) because a lower activation energy is required to form free radicals that initiate the oxidation process from n-paraffins than from iso-paraffins or aromatic compounds (due to the high stability of these compounds). This was indeed observed in the test fuels, where the PAR10 diesel had the highest CN (80), followed by the EUR10 (53.8) and SAM10 (49.7) diesel, respectively. Thus, although PAR10 diesel had a high n-paraffin fuel content, low n-alkane emissions may be a result of its high CN as compared

to the SAM10 diesel. The EUR10 diesel had the lowest n-alkane emissions and this may be due jointly to its low n-paraffin content (9.4%) and relatively high CN (53.8).

Although a relationship between the HC emissions, fuel content and CN was clearly demonstrated, it is important to note that combustion efficiency and diesel exhaust emissions are dependent on various parameters, including but not limited to, engine design, operating parameters, and other fuel properties such as the viscosity and volatility.

4.5.1.2 Aromatic hydrocarbon emissions

Semi-quantitative analysis of the test fuel emissions was conducted to identify target alkylbenzene HCs. The target list contained 30 (3 pairs of isomers were co-eluting hence they were given the same peak number) alkylbenzenes and most of the target aromatic compounds were successfully identified in the emissions of all three fuels. The relative abundance of the alkylbenzenes was expressed as the peak area per distance driven in kilometres for the particular speed phase being tested. This method of semi-quantifying the emissions was illustrated by Ruiz-Hernández (2018), and although a physical emission factor is not obtained, the relative abundance of exhaust SVOCs determined in exactly the same way can be compared (Ruiz-Hernández et al., 2018).

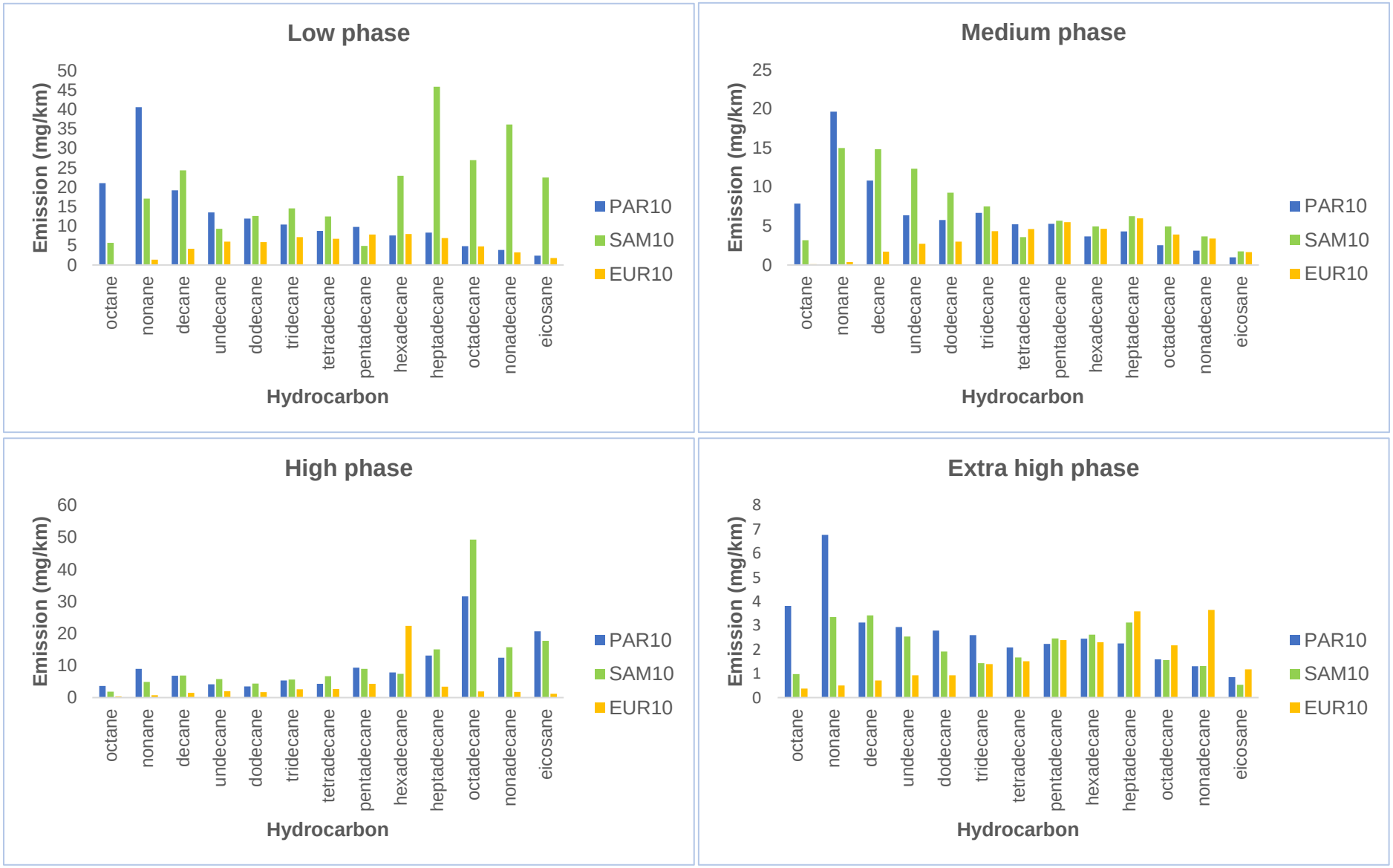

Figure 4.9 n-Alkane HC emission factors for each fuel at different speed phases of the WLTC cycle.

Table 4.5: Calculated n-alkane emission factors of each test fuel during different speed phases of the WLTC cycle.

		PAR10		SAM10		EUR10	
Speed phase	**n-Alkane**	**EF (mg/km)**	**OFP (mgO_3/ gVOC)**	**EF (mg/km)**	**OFP (mgO_3/ gVOC)**	**EF (mg/km)**	**OFP (mgO_3/ gVOC)**
Low	octane	21.00	18.90	5.72	5.15	0.03	0.03
	nonane	40.56	31.63	17.05	13.30	1.38	1.08
	decane	19.20	13.06	24.36	16.56	4.20	2.85
	undecane	13.49	8.23	9.32	5.68	6.02	3.67
	dodecane	11.91	6.55	12.59	6.92	5.85	3.22
	tridecane	10.39	5.51	14.57	7.72	7.19	3.81
	tetradecane	8.74	4.46	12.50	6.38	6.75	3.44
	pentadecane	9.79	4.90	4.91	2.46	7.84	3.92
	hexadecane	7.58	3.41	22.92	10.31	7.97	3.59
	heptadecane	8.34	3.50	45.83	19.25	6.94	2.92
	octadecane	4.83	1.93	26.94	10.78	4.78	1.91
	nonadecane	3.85	1.46	36.09	13.72	3.25	1.24
	eicosane	2.37	1.00	22.50	9.45	1.76	0.74
	Sum	*162.05*		*255.31*		*63.97*	
Medium	octane	7.87	7.08	3.16	2.84	0.10	0.09
	nonane	19.64	15.32	14.99	11.70	0.37	0.29
	decane	10.81	7.35	14.84	10.09	1.71	1.16
	undecane	6.37	3.89	12.34	7.53	2.70	1.65
	dodecane	5.76	3.17	9.25	5.09	2.98	1.64
	tridecane	6.67	3.53	7.49	3.97	4.34	2.30
	tetradecane	5.22	2.66	3.57	1.82	4.60	2.35
	pentadecane	5.26	2.63	5.66	2.83	5.50	2.75
	hexadecane	3.66	1.65	4.93	2.22	4.64	2.09
	heptadecane	4.31	1.81	6.26	2.63	5.97	2.51
	octadecane	2.54	1.02	4.93	1.97	3.90	1.56
	nonadecane	1.83	0.69	3.67	1.39	3.39	1.29
	eicosane	0.98	0.41	1.73	0.73	1.66	0.70
	Sum	*80.91*		*92.82*		*41.87*	

Table 4.5 continued.

		PAR10		SAM10		EUR10	
Speed phase	**n-Alkane**	**EF (mg/km)**	**OFP (mgO_3/ gVOC)**	**EF (mg/km)**	**OFP (mgO_3/ gVOC)**	**EF (mg/km)**	**OFP (mgO_3/ gVOC)**
High	octane	3.64	3.27	1.87	1.68	0.38	0.34
	nonane	8.94	6.97	4.91	3.83	0.76	0.60
	decane	6.80	4.62	6.89	4.68	1.51	1.02
	undecane	4.17	2.54	5.81	3.54	1.99	1.21
	dodecane	3.48	1.91	4.36	2.40	1.73	0.95
	tridecane	5.32	2.82	5.60	2.97	2.61	1.38
	tetradecane	4.26	2.17	6.64	3.39	2.70	1.38
	pentadecane	9.35	4.67	8.97	4.48	4.28	2.14
	hexadecane	7.84	3.53	7.40	3.33	22.36	10.06
	heptadecane	13.09	5.50	15.06	6.32	3.41	1.43
	octadecane	31.59	12.64	49.28	19.71	1.92	0.77
	nonadecane	12.44	4.73	15.70	5.97	1.78	0.68
	eicosane	20.67	8.68	17.74	7.45	1.19	0.50
	Sum	*131.59*		*150.22*		*46.61*	
Extra high	octane	3.81	3.43	0.98	0.88	0.38	0.34
	nonane	6.77	5.28	3.35	2.61	0.51	0.39
	decane	3.12	2.12	3.42	2.32	0.71	0.48
	undecane	2.93	1.79	2.53	1.55	0.93	0.57
	dodecane	2.79	1.53	1.91	1.05	0.93	0.51
	tridecane	2.59	1.37	1.43	0.76	1.40	0.74
	tetradecane	2.08	1.06	1.67	0.85	1.51	0.77
	pentadecane	2.23	1.12	2.46	1.23	2.39	1.19
	hexadecane	2.46	1.10	2.62	1.18	2.30	1.03
	heptadecane	2.25	0.95	3.12	1.31	3.58	1.51
	octadecane	1.59	0.64	1.56	0.62	2.17	0.87
	nonadecane	1.30	0.49	1.31	0.50	3.65	1.39
	eicosane	0.85	0.36	0.54	0.23	1.18	0.49
	Sum	*34.77*		*26.91*		*21.63*	

Figures 4.10 - 4.13 show the relative abundance of the alkylbenzenes identified in the maccollemissions of all three fuels. Emission factors (Table 4.6) were determined by multiplying the peak area of each alkylbenzene by the SR, DF and PF to obtain a corrected peak area, then dividing the corrected peak area of each compound by the distance travelled.

It is apparent that the EUR10 fuel has the highest alkylbenzene emissions, followed by the SAM10 diesel, while minute amounts are observed for the PAR10 fuel. The PAR10 diesel has an alkylbenzene content of 0%, thus aromatic emissions observed for this fuel were suspected to be from residual traces of aromatic emissions in the exhaust system from the previous combustion of other fuels. Between the two alkylbenzene containing fuels, the EUR10 fuel was seen to have higher alkylbenzene emissions. From Table 3.1, however, it can be seen that the alkylbenzene content of these fuels is quite similar, hence the observed differences in the alkylbenzene emission factors might be the effect of another fuel and/or engine property. This would require further investigation.

Plots of the relative abundance of the alkylbenzenes (Figures 4.10 - 4.13) showed that the same HCs were typically found to have higher abundances than others at each speed phase. For the EUR10 fuel, 1-methyl-3-ethylbenzene, 1-methyl-4-ethylbenzene, 1,3,5-trimethylbenzene, 1-methyl-2-ethylbenzene, 1,2,4-trimethylbenzene and 1,2,4,5-tetramethylbenzene were seen at higher levels, while for the SAM10 fuel sec-butylbenzene, 1-methyl-3n-propylbenzene and n-butylbenzene were found at higher levels. Upon evaluation of the GC x GC-MS analysis data of both fuels (as provided by Sasol), it was noted that C_9 and C_{10} compounds make up 6% and 4% of the fuels respectively, which is strongly reflected in the engine exhaust emissions.

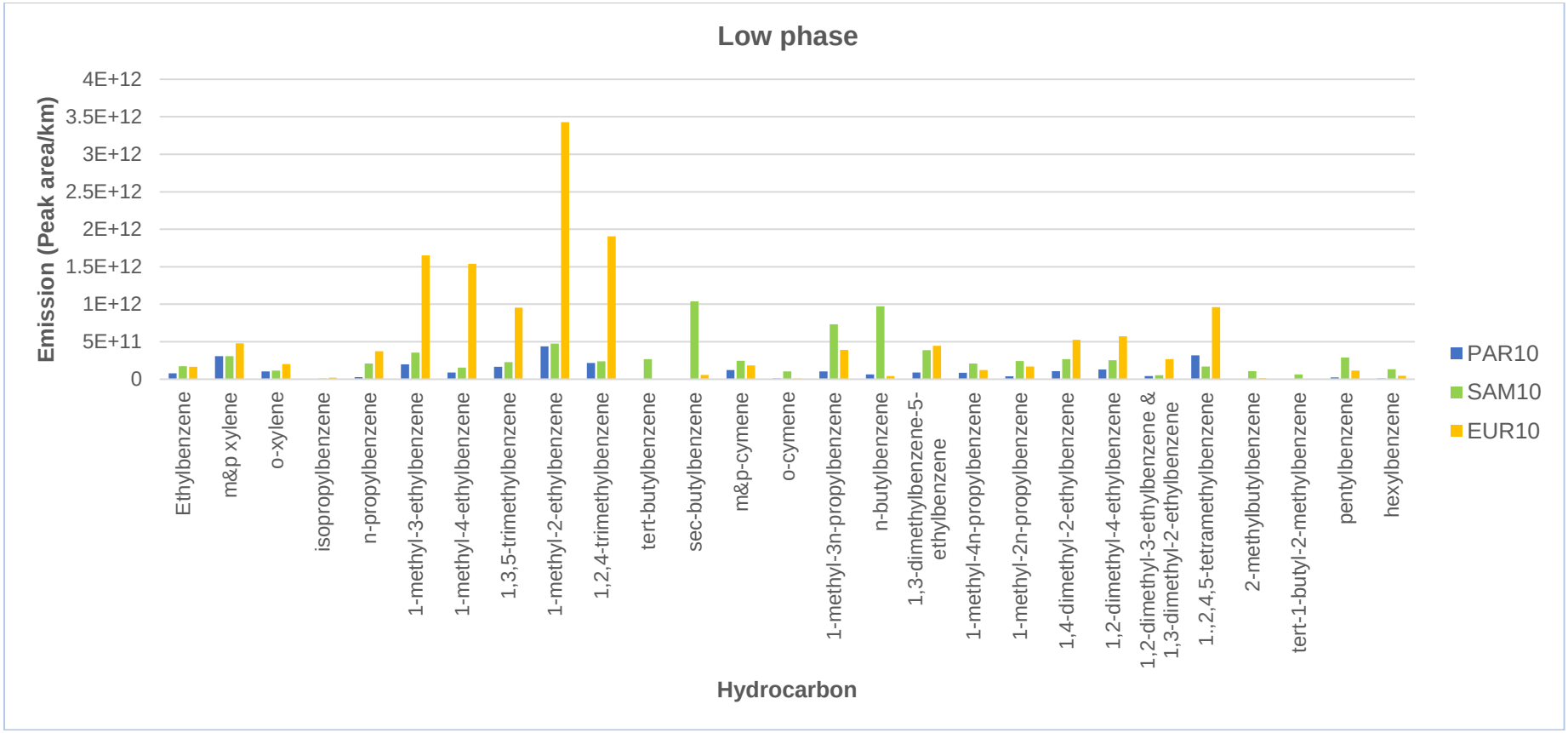

Figure 4.10 Relative abundance of the alkylbenzene emissions from each fuel during the low speed phase of the WLTC cycle.

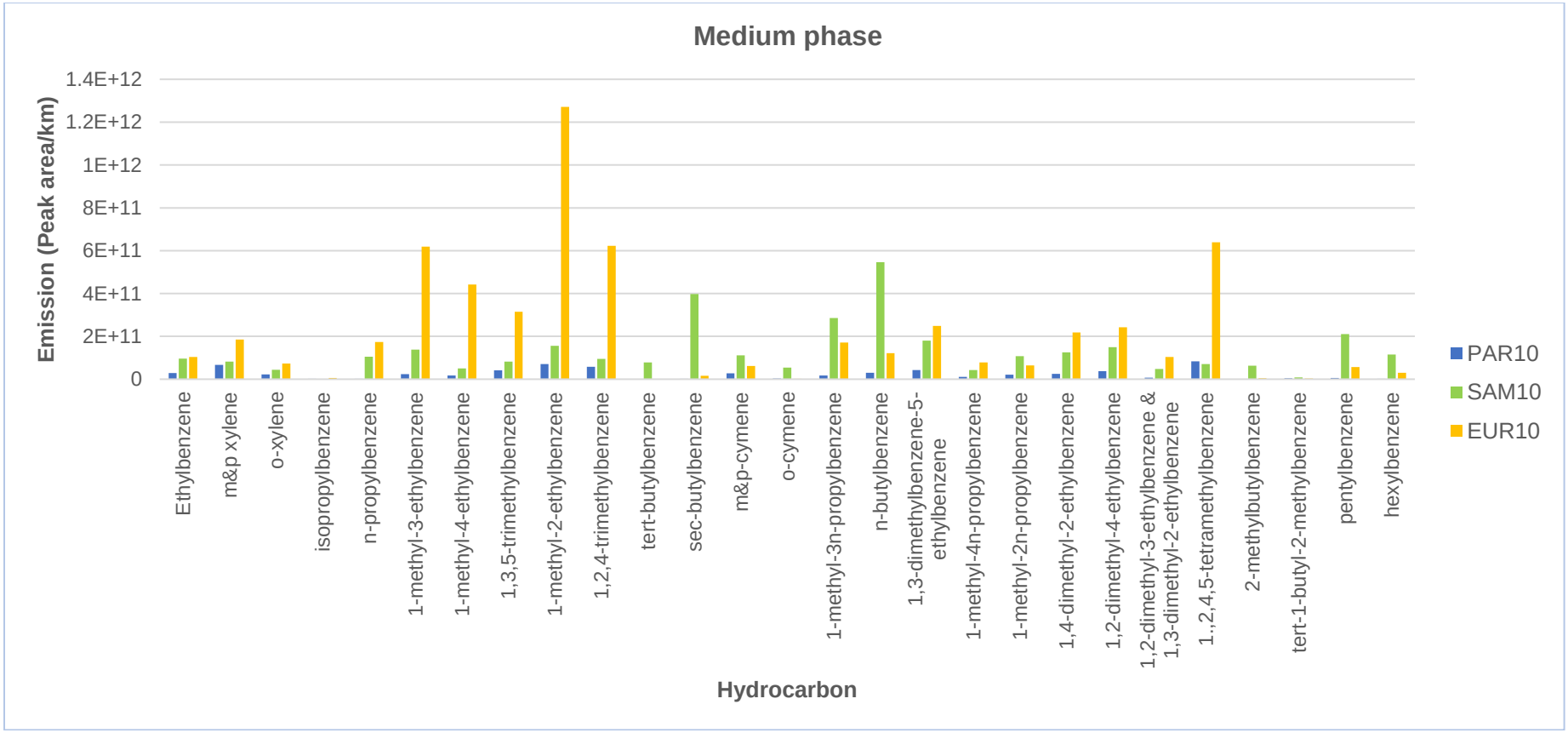

Figure 4.11 Relative abundance of the alkylbenzene emissions from each fuel during the medium speed phase of the WLTC cycle.

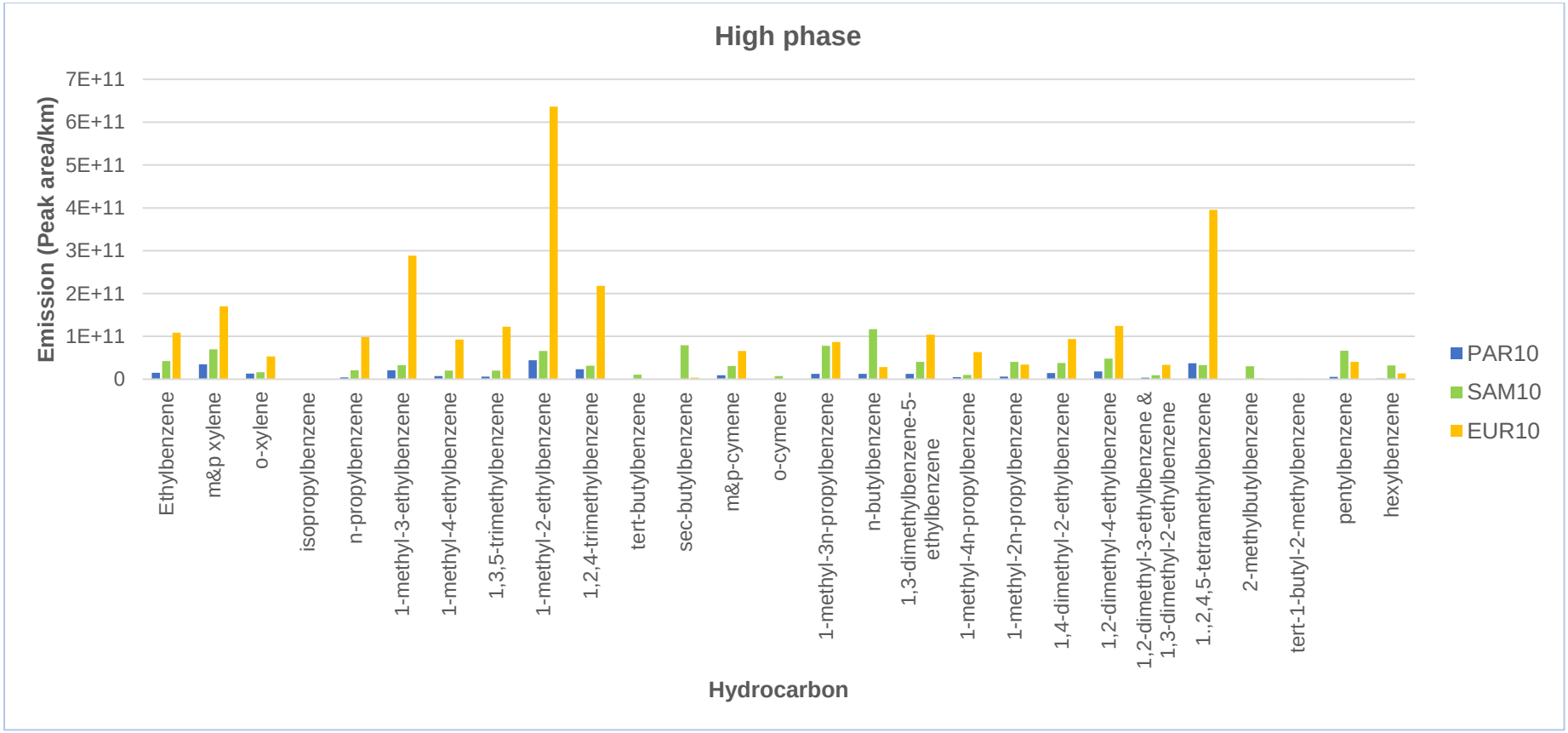

Figure 4.12 Relative abundance of the alkylbenzene emissions from each fuel during the high speed phase of the WLTC cycle.

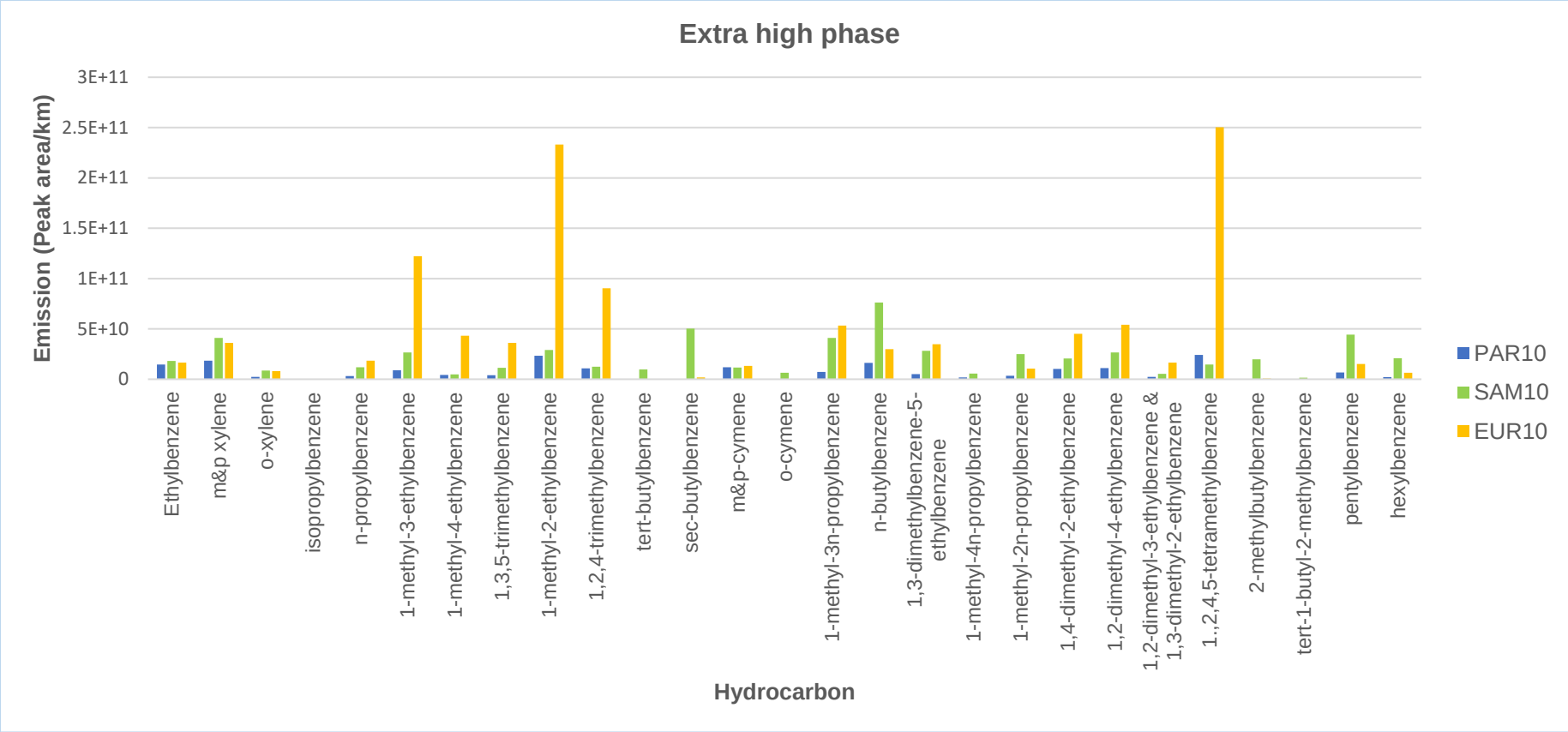

Figure 4.13 Relative abundance of the alkylbenzene emissions from each fuel during the extra high speed phase of the WLTC cycle.

Table 4.6 Aromatic hydrocarbon emission factors expressed as the peak area per km for each of the test fuels during the different speed phases of the WLTC cycle.

	Emission factor (Peak area/km)				
Hydrocarbon	**PAR10 CS**	**SAM10 CS**	**EUR10 CS**	**EUR10 DPF**	**EUR10 HS**
ethylbenzene	7.98×10^{10}	1.71×10^{11}	1.66×10^{11}	3.65×10^{10}	7.03×10^{10}
m&p xylene	3.08×10^{11}	3.08×10^{11}	4.79×10^{11}	2.35×10^{11}	3.08×10^{11}
o-xylene	1.04×10^{11}	1.17×10^{11}	2.02×10^{11}	8.36×10^{10}	1.02×10^{11}
isopropylbenzene	5.66×10^{08}	1.10×10^{10}	2.01×10^{10}	-	1.03×10^{09}
n-propylbenzene	2.79×10^{10}	2.08×10^{11}	3.73×10^{11}	6.66×10^{10}	1.32×10^{11}
1-methyl-3-ethylbenzene	1.98×10^{11}	3.56×10^{11}	1.65×10^{12}	1.98×10^{11}	7.72×10^{11}
1-methyl-4-ethylbenzene	9.04×10^{10}	1.54×10^{11}	1.54×10^{12}	2.84×10^{11}	4.02×10^{11}
1,3,5-trimethylbenzene	1.65×10^{11}	2.27×10^{11}	9.53×10^{11}	1.53×10^{11}	3.24×10^{11}
1-methyl-2-ethylbenzene	4.37×10^{11}	4.75×10^{11}	3.43×10^{12}	5.24×10^{11}	1.77×10^{12}
1,2,4-trimethylbenzene	2.16×10^{11}	2.38×10^{11}	1.91×10^{12}	2.79×10^{11}	6.99×10^{11}
tert-butylbenzene	-	2.67×10^{11}	1.46×10^{09}	-	-
isobutylbenzene	-	1.22×10^{11}	6.14×10^{10}	-	5.79×10^{09}
sec-butylbenzene	-	1.04×10^{11}	5.57×10^{10}	-	4.81×10^{09}
m&p-cymene	1.23×10^{11}	2.45×10^{11}	1.84×10^{11}	4.78×10^{10}	6.35×10^{10}
o-cymene	1.06×10^{10}	1.03×10^{11}	1.04×10^{10}	-	2.95×10^{09}
1-methyl-3n-propylbenzene	1.06×10^{11}	7.32×10^{11}	3.91×10^{11}	4.88×10^{10}	2.07×10^{11}
n-butylbenzene	6.27×10^{10}	9.71×10^{11}	4.35×10^{10}	-	1.83×10^{10}
1,3-dimethylbenzene-5-ethylbenzene	8.86×10^{10}	3.86×10^{11}	4.46×10^{11}	1.04×10^{11}	3.30×10^{10}
1-methyl-4n-propylbenzene	8.49×10^{10}	2.09×10^{11}	1.22×10^{11}	8.24×10^{10}	1.45×10^{11}
1-methyl-2n-propylbenzene	3.93×10^{10}	2.43×10^{11}	1.68×10^{11}	2.77×10^{10}	7.06×10^{10}
1,4-dimethyl-2-ethylbenzene	1.09×10^{11}	2.66×10^{11}	5.25×10^{11}	7.17×10^{10}	2.82×10^{11}
1,2-dimethyl-4-ethylbenzene	1.31×10^{11}	2.53×10^{11}	5.72×10^{11}	7.99×10^{10}	3.15×10^{11}
1,2-dimethyl-3-ethylbenzene & 1,3-dimethyl-2-ethylbenzene	4.35×10^{10}	5.40×10^{10}	2.67×10^{11}	1.88×10^{10}	2.32×10^{11}
1.,2,4,5-tetramethylbenzene	3.19×10^{11}	1.69×10^{11}	9.60×10^{11}	3.23×10^{11}	8.15×10^{11}
2-methylbutylbenzene	7.71×10^{08}	1.08×10^{11}	1.19×10^{10}	-	5.11×10^{09}
tert-1-butyl-2-methylbenzene	-	6.47×10^{10}	3.31×10^{09}	-	1.09×10^{09}
pentylbenzene	2.32×10^{10}	2.88×10^{11}	1.15×10^{11}	2.25×10^{10}	7.01×10^{10}
tert-1-butyl-4-ethylbenzene	-	2.77×10^{10}	-	-	-
hexylbenzene	1.01×10^{10}	1.33×10^{11}	4.50×10^{10}	7.28×10^{09}	2.54×10^{10}

Table 4.6 continued.

	Emission factor (Peak area/km)				
Hydrocarbon	**PAR10 CS**	**SAM10 CS**	**EUR10 CS**	**EUR10 DPF**	**EUR10 HS**
ethylbenzene	2.93×10^{10}	9.56×10^{10}	1.04×10^{11}	3.55×10^{10}	
m&p xylene	6.66×10^{10}	8.20×10^{10}	1.85×10^{11}	1.12×10^{11}	
o-xylene	2.20×10^{10}	4.39×10^{10}	7.29×10^{10}	4.45×10^{10}	
isopropylbenzene	2.41×10^{09}	0.00	6.17×10^{09}	-	
n-propylbenzene	2.63×10^{09}	1.05×10^{11}	1.73×10^{11}	3.30×10^{10}	
1-methyl-3-ethylbenzene	2.38×10^{10}	1.39×10^{11}	6.19×10^{11}	2.11×10^{11}	
1-methyl-4-ethylbenzene	1.75×10^{10}	5.05×10^{10}	4.41×10^{11}	2.73×10^{11}	
1,3,5-trimethylbenzene	4.21×10^{10}	8.19×10^{10}	3.15×10^{11}	1.31×10^{11}	
1-methyl-2-ethylbenzene	7.13×10^{10}	1.56×10^{11}	1.27×10^{12}	6.45×10^{11}	
1,2,4-trimethylbenzene	5.79×10^{10}	9.47×10^{10}	6.23×10^{11}	2.82×10^{11}	
tert-butylbenzene	-	7.89×10^{10}	-	-	
isobutylbenzene	-	1.76×10^{10}	7.73×10^{09}	-	
sec-butylbenzene	1.66×10^{09}	3.97×10^{11}	1.63×10^{10}	-	
m&p-cymene	2.73×10^{10}	1.12×10^{11}	6.14×10^{10}	1.87×10^{10}	
o-cymene	3.43×10^{10}	5.46×10^{10}	2.34×10^{09}	-	
1-methyl-3n-propylbenzene	1.70×10^{10}	2.85×10^{11}	1.72×10^{11}	5.14×10^{10}	
n-butylbenzene	2.96×10^{10}	5.46×10^{11}	1.22×10^{11}	-	
1,3-dimethylbenzene-5-ethylbenzene	4.27×10^{10}	1.80×10^{11}	2.49×10^{11}	1.00×10^{11}	
1-methyl-4n-propylbenzene	1.11×10^{10}	4.31×10^{10}	7.84×10^{10}	5.83×10^{10}	
1-methyl-2n-propylbenzene	2.07×10^{10}	1.07×10^{11}	6.47×10^{10}	2.20×10^{10}	
1,4-dimethyl-2-ethylbenzene	2.43×10^{10}	1.25×10^{11}	2.18×10^{11}	7.27×10^{10}	
1,2-dimethyl-4-ethylbenzene	3.76×10^{10}	1.49×10^{11}	2.42×10^{11}	7.62×10^{10}	
1,2-dimethyl-3-ethylbenzene & 1,3-dimethyl-2-ethylbenzene	6.99×10^{09}	4.74×10^{10}	1.04×10^{11}	2.55×10^{10}	
1.,2,4,5-tetramethylbenzene	8.32×10^{10}	7.07×10^{10}	6.40×10^{11}	6.17×10^{11}	
2-methylbutylbenzene	2.89×10^{08}	6.25×10^{10}	4.65×10^{09}	-	
tert-1-butyl-2-methylbenzene	4.21×10^{09}	8.78×10^{09}	3.00×10^{09}	1.42×10^{10}	
pentylbenzene	6.02×10^{09}	2.10×10^{11}	5.71×10^{10}	3.42×10^{09}	
tert-1-butyl-4-ethylbenzene	-	2.28×10^{10}	-	2.15×10^{09}	
hexylbenzene	1.84×10^{09}	1.16×10^{11}	2.96×10^{10}	1.32×10^{10}	

*Hydrocarbons with an EF of 0.00 mg/km were not detected in the sample.

Table 4.6 continued.

	Emission factor (Peak area/km)				
Hydrocarbon	**PAR10 CS**	**SAM10 CS**	**EUR10 CS**	**EUR10 DPF**	**EUR10 HS**
ethylbenzene	1.51×10^{10}	4.27×10^{10}	1.09×10^{11}	2.87×10^{10}	
m&p xylene	3.45×10^{10}	6.96×10^{10}	1.70×10^{11}	5.19×10^{10}	
o-xylene	1.28×10^{10}	1.64×10^{10}	5.34×10^{10}	1.05×10^{10}	
isopropylbenzene	-	5.47×10^{08}	-	-	
n-propylbenzene	4.20×10^{09}	2.05×10^{10}	9.85×10^{10}	9.35×10^{09}	
1-methyl-3-ethylbenzene	2.09×10^{10}	3.30×10^{10}	2.88×10^{11}	5.85×10^{09}	
1-methyl-4-ethylbenzene	7.46×10^{09}	2.01×10^{10}	9.26×10^{10}	2.03×10^{10}	
1,3,5-trimethylbenzene	6.39×10^{09}	1.99×10^{10}	1.22×10^{11}	1.36×10^{10}	
1-methyl-2-ethylbenzene	4.44×10^{10}	6.57×10^{10}	6.36×10^{11}	1.88×10^{10}	
1,2,4-trimethylbenzene	2.31×10^{10}	3.18×10^{10}	2.18×10^{11}	5.34×10^{10}	
tert-butylbenzene	-	1.05×10^{10}	1.31×10^{09}	-	
isobutylbenzene	-	5.54×10^{09}	1.01×10^{09}	6.13×10^{08}	
sec-butylbenzene	-	7.89×10^{10}	3.28×10^{09}	-	
m&p-cymene	9.32×10^{09}	3.07×10^{10}	6.59×10^{10}	9.66×10^{09}	
o-cymene	-	7.70×10^{09}	3.82×10^{08}	-	
1-methyl-3n-propylbenzene	1.25×10^{10}	7.82×10^{10}	8.66×10^{10}	8.72×10^{09}	
n-butylbenzene	1.22×10^{10}	1.17×10^{11}	2.85×10^{10}	1.65×10^{10}	
1,3-dimethylbenzene-5-ethylbenzene	1.27×10^{10}	4.03×10^{10}	1.04×10^{11}	8.96×10^{09}	
1-methyl-4n-propylbenzene	4.83×10^{09}	9.98×10^{09}	6.36×10^{10}	1.75×10^{09}	
1-methyl-2n-propylbenzene	5.87×10^{09}	4.04×10^{10}	3.40×10^{10}	2.54×10^{09}	
1,4-dimethyl-2-ethylbenzene	1.47×10^{10}	3.79×10^{10}	9.37×10^{10}	1.12×10^{10}	
1,2-dimethyl-4-ethylbenzene	1.80×10^{10}	4.82×10^{10}	1.24×10^{11}	1.17×10^{10}	
1,2-dimethyl-3-ethylbenzene & 1,3-dimethyl-2-ethylbenzene	3.51×10^{09}	9.07×10^{09}	3.32×10^{10}	2.75×10^{09}	
1.,2,4,5-tetramethylbenzene	3.72×10^{10}	3.30×10^{10}	3.95×10^{11}	4.04×10^{10}	
2-methylbutylbenzene	3.15×10^{08}	3.06×10^{10}	1.64×10^{09}	9.13×10^{09}	
tert-1-butyl-2-methylbenzene	-	7.41×10^{08}	1.44×10^{08}	-	
pentylbenzene	5.70×10^{09}	6.63×10^{10}	4.07×10^{10}	6.46×10^{09}	
tert-1-butyl-4-ethylbenzene	-	4.99×10^{09}	-	-	
hexylbenzene	1.85×10^{09}	3.21×10^{10}	1.39×10^{10}	3.21×10^{09}	

Table 4.6 continued.

Hydrocarbon	Emission factor (Peak area/km)				
	PAR10 CS	SAM10 CS	EUR10 CS	EUR10 DPF	EUR10 HS
ethylbenzene	1.46×10^{10}	1.81×10^{10}	1.66×10^{10}	3.48×10^{10}	
m&p xylene	1.83×10^{10}	4.09×10^{10}	3.62×10^{10}	1.21×10^{10}	
o-xylene	2.46×10^{09}	8.59×10^{09}	8.04×10^{09}	9.36×10^{09}	
isopropylbenzene	1.07×10^{08}	-	-	-	
n-propylbenzene	3.18×10^{09}	1.18×10^{10}	1.85×10^{10}	1.70×10^{09}	
1-methyl-3-ethylbenzene	8.78×10^{09}	2.67×10^{10}	1.22×10^{11}	1.12×10^{10}	
1-methyl-4-ethylbenzene	4.25×10^{09}	4.85×10^{09}	4.31×10^{10}	5.88×10^{09}	
1,3,5-trimethylbenzene	3.98×10^{09}	1.14×10^{10}	3.61×10^{10}	5.49×10^{09}	
1-methyl-2-ethylbenzene	2.33×10^{10}	2.92×10^{10}	2.33×10^{11}	2.97×10^{10}	
1,2,4-trimethylbenzene	1.07×10^{10}	1.25×10^{10}	9.04×10^{10}	1.71×10^{10}	
tert-butylbenzene	-	9.82×10^{09}	-	-	
isobutylbenzene	-	5.68×10^{09}	2.05×10^{09}	-	
sec-butylbenzene	1.54×10^{08}	5.02×10^{10}	1.78×10^{09}	-	
m&p-cymene	1.18×10^{10}	1.15×10^{10}	1.33×10^{10}	8.62×10^{09}	
o-cymene	-	6.51×10^{09}	1.43×10^{08}	8.06×10^{08}	
1-methyl-3n-propylbenzene	7.26×10^{09}	4.09×10^{10}	5.34×10^{10}	1.11×10^{10}	
n-butylbenzene	1.63×10^{10}	7.61×10^{10}	2.99×10^{10}	3.85×10^{09}	
1,3-dimethylbenzene-5-ethylbenzene	5.19×10^{09}	2.82×10^{10}	3.49×10^{10}	6.65×10^{09}	
1-methyl-4n-propylbenzene	1.68×10^{09}	5.54×10^{09}	-	-	
1-methyl-2n-propylbenzene	3.51×10^{09}	2.50×10^{10}	1.06×10^{10}	2.88×10^{09}	
1,4-dimethyl-2-ethylbenzene	1.02×10^{10}	2.05×10^{10}	4.51×10^{10}	7.21×10^{09}	
1,2-dimethyl-4-ethylbenzene	1.11×10^{10}	2.65×10^{10}	5.41×10^{10}	7.65×10^{09}	
1,2-dimethyl-3-ethylbenzene & 1,3-dimethyl-2-ethylbenzene	2.44×10^{09}	5.30×10^{09}	1.66×10^{10}	3.40×10^{09}	
1.,2,4,5-tetramethylbenzene	2.41×10^{10}	1.46×10^{10}	2.50×10^{11}	1.68×10^{10}	
2-methylbutylbenzene	1.32×10^{08}	1.98×10^{10}	8.07×10^{08}	-	
tert-1-butyl-2-methylbenzene	-	1.61×10^{09}	1.18×10^{08}	1.03×10^{09}	
pentylbenzene	6.59×10^{09}	4.42×10^{10}	1.51×10^{10}	0.00	
tert-1-butyl-4-ethylbenzene	-	2.72×10^{09}	-	-	
hexylbenzene	2.05×10^{09}	2.10×10^{10}	6.53×10^{09}	4.94×10^{08}	

The (-) symbol indicates that the hydrocarbon was not detected in the sample.

4.5.2 Hydrocarbon emissions at different speed phases of the WLTC test cycle

The change in the total HC emission factors at each speed phase of the WLTC test cycle was studied, for each test fuel (Figure 4.14 and Figure 4.15). Due to the improved

combustion conditions that result from elevated engine temperatures with prolonged engine operation, a decrease in the emissions (from the low speed to the extra high speed phase) was expected. This was indeed observed for the alkylbenzenes, while for the n-alkanes an overall decrease was observed when moving from the low phase to the extra-high phase, however the high phase emissions were higher than expected.

In diesel engines, the major processes that play a role in the production of unburnt HCs during cold start conditions are overleaning, undermixing, flame quenching at the combustion chamber walls and misfires (Heywood, 1988). Overleaning occurs during fuel injection into the cylinder where the fuel is mixed leaner (low proportion of fuel to air mixture) than the lean combustion limit. This fuel will not auto ignite or support fast reaction. At light loads or during idling, undermixing is particularly important. This occurs when the fuel leaves the injection nozzle late during the combustion process or when excess fuel enters during injection. The fuel enters at a slow rate and/or mixes slowly with air thus may escape the combustion process. Quenching, where fuel impinges on the walls of the cylinder, as well as misfires may also lead to unburnt HC emission. Misfires are however unlikely in well designed and controlled engines. Low mass hydrocarbons are not problematic as they are volatile enough for vaporization at these temperatures, rather it is the heavier fractions which reach the cylinder and fail to vaporize easily that undergo partial burning and result in high emissions and poor fuel economy (Chehroudi, 2015).

Beyond improved combustion conditions, another important implication of elevated engine temperatures is the activation of catalytic exhaust aftertreatment systems. These systems need to reach a certain temperature, termed the “light-off” temperature for efficient conversion of HC emissions to less harmful emissions (Raja and Arasu, 2015). Hence at low engine temperatures, insignificant oxidation of HC emissions occurs.

In the real-world, high cold-start emissions are a result of driving when the engine temperature is lower than its optimal value, which has an effect on the engine performance and emissions as discussed. According to Roberts et al. (2014), the lower thermal efficiency of the internal combustion engine during cold-start can be attributed to low temperatures of the lubricant oil and engine components. Increasing the rate of the lubricant oil warm-up is desirable as frictional losses (energy dissipation due to increased friction between engine components) occur when the lubricant oil is at sub-optimal temperatures, resulting in an increase in engine emissions. It was also demonstrated that higher temperatures of the cylinder liner are required for improved combustion conditions during engine operation. The study concluded that improvements need to be made during the cold-start and warm-up engine phases, particularly because average urban car journeys involve short distance trips where the engine does not reach its optimal operating temperature (Roberts et al., 2014).

Diesel engines are highly fuel efficient, however, this characteristic results in low exhaust temperatures, particularly during low speed driving. This together with the presence of SO_2 (a catalyst poison) in the exhaust gas makes achieving and maintaining good catalytic performance at low temperatures challenging. Platinum based catalysts are often used for CO and HC emission oxidation. When the engine is started, the catalyst is not warm enough to oxidize HCs present in the exhaust, however as engine operation continues, an increase in temperature allows the catalyst to reach its light-off temperature, and HC emissions are oxidized over the active sites of the catalyst (Raja and Arasu, 2015). The problem however, is that this temperature is well above ambient conditions and is only reached after some time of engine operation. This is the prime reason for high levels of vehicular emissions found in urban/city areas characterized by short driving trips. The average length of city trips might even be shorter than the driving cycles used during emissions testing, hence the full effect of cold start emissions might not be fully realized in laboratory studies. Even as engine technology improves to meet the increasingly stringent air quality regulations, more focus needs to be applied to reducing emissions

during the cold-start phase of an engine. Otherwise, low-speed city driving will continue to be a major contributor to poor air quality including elevated ozone levels in urban areas.

As previously noted, a deviation from the expected results was observed for the n-alkane emissions during the high speed phase (total emissions higher than those found in low and medium speed phases). Because a strong decreasing trend was observed for the alkylbenzene emissions from the low to extra-high speed phases, it was initially speculated that this might have been due to a sampling error that occurred during the high-phase. This is however unlikely as the effect was consistent across all fuel types. Another possible explanation is the “trap and release” mechanism of the DOC, i.e. HCs are trapped by the DOC at low temperatures and are subsequently released at high temperatures. Further investigation into these results needs to be done.

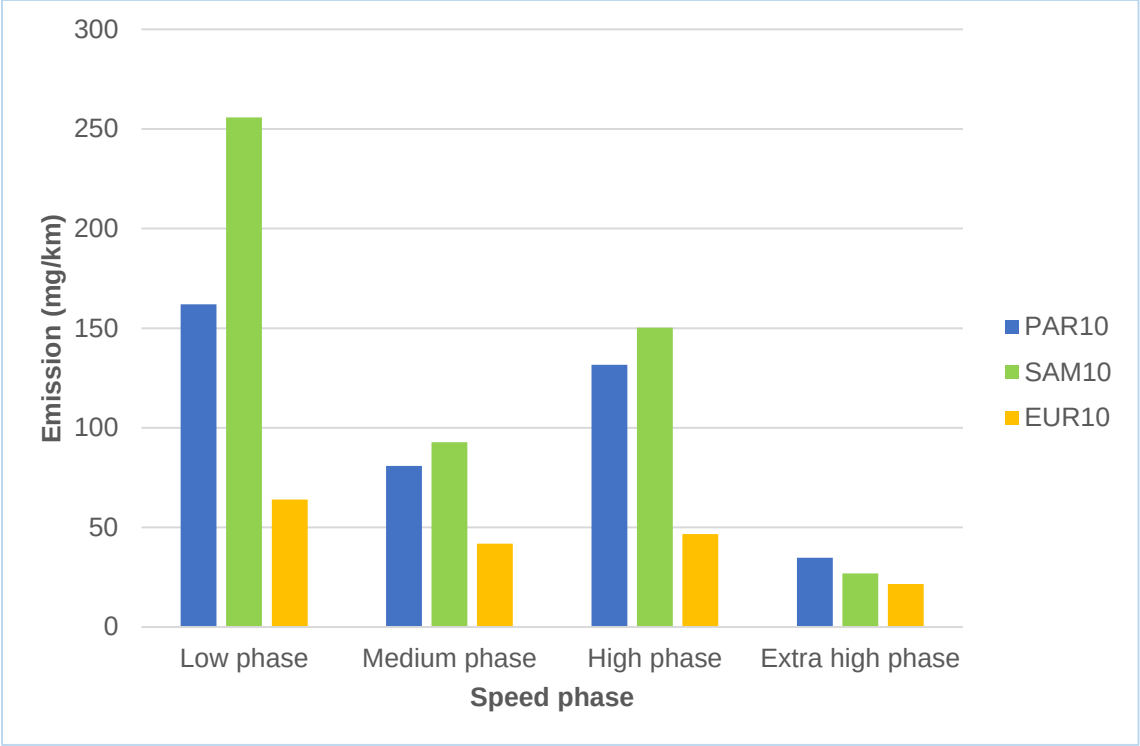

Figure 4.14 Sum of n-alkane hydrocarbon emissions for each fuel at different speed phases of the WLTC cycle.

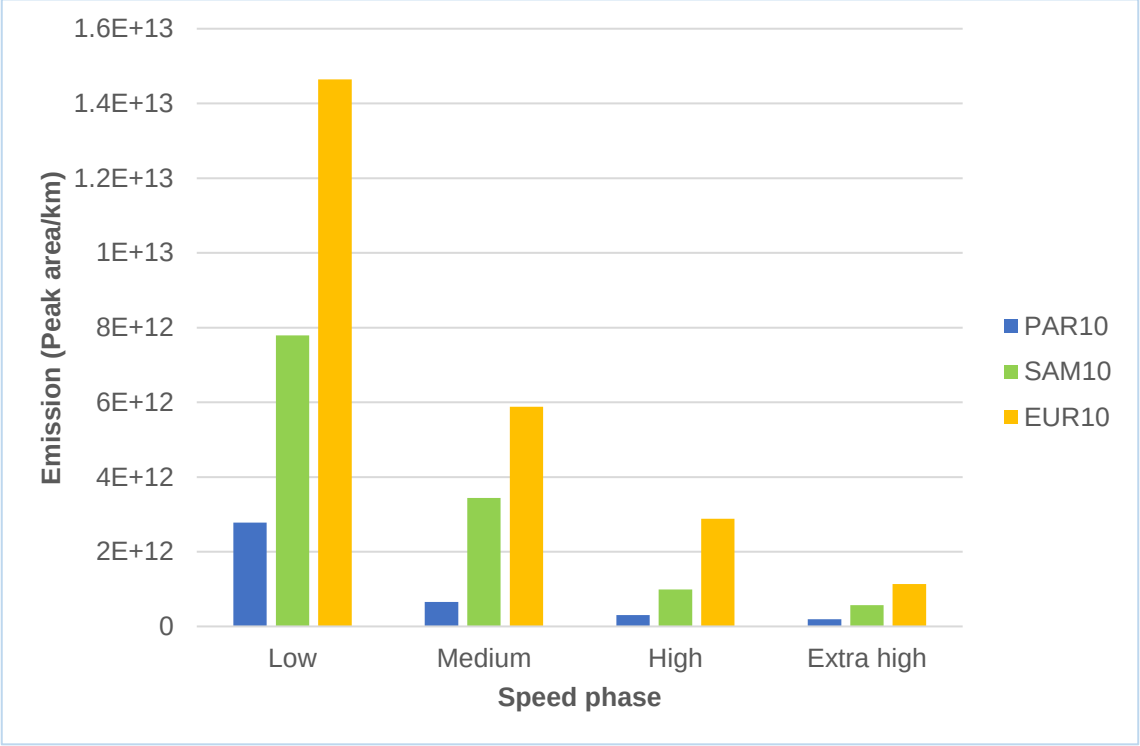

Figure 4.15 Sum of alkylbenzene hydrocarbon emissions between the different phases of the WLTC cycle for different fuels.

4.5.3 Target hydrocarbon emissions compared to other gaseous emissions

The emission results obtained from the denuder samplers were compared to the online measurements of CO, CO_2, NOx and THC gas emissions. Emission factors could not be directly compared as a reading of the 'total' hydrocarbons is obtained from the FID as opposed to emission factors for individual compounds obtained from TD-GC x GC-TofMS analysis. The study also determined the EFs of select HCs as opposed to all HCs in the diesel exhaust. It was of interest however, to compare the trends observed.

From Figure 4.16, a decrease in CO and THC emissions was seen from the low phase to the extra high phase, similar to what was observed for the individual HCs. This decrease in CO and THC demonstrates the impact of a temperature increase on emissions reduction. Further evidence of the effect of increased engine temperatures on emissions is the observed increase in NOx emissions. The rise in NOx emissions as a result of increased engine temperatures has been reported by several studies (Hountalas et al., 2008, Johnson, 2008, Ladommatos et al., 2000). During engine performance, elevated temperatures (1600 °C) result in the formation of NOx species from the reaction of N_2 and O_2. The amount of NOx produced is a function of the O_2 concentration, residence time and maximum cylinder temperature, hence increasing the combustion temperature results in increased NOx formation (Reşitoğlu et al., 2015).

When comparing the calculated emission factors to those obtained from the gas analyzer, a great difference in magnitude is observed. From Figure 4.17 the THC emission factors are much lower than the n-alkane emission factors. According to the United States EPA (2004), HC measurements from mobile sources are measured using a FID calibrated with propane, i.e. the FID uses propane as a proxy in determining the change in concentration of C atoms in a gas sample. Propane (C_3) is a relatively volatile gas thus this assumption might not hold for heavier, less volatile HCs found in diesel engine emissions. In their study on HC measurements by means of flame ionization, Garthe et al. (2003) stated that contrary to gas chromatographic measurements exhaust HC measurements by FID are neither a concentration nor a mass measurement. The signal generated is proportional to the number of C atoms bound in HC molecules (Garthe et al., 2003). This highlights

the importance of analytical techniques that elucidate and quantify individual exhaust species from vehicular emissions in addition to the regular measurements of exhaust gases. This might provide more information regarding the role played by these exhaust emissions in the formation of secondary polluting species in the atmosphere.

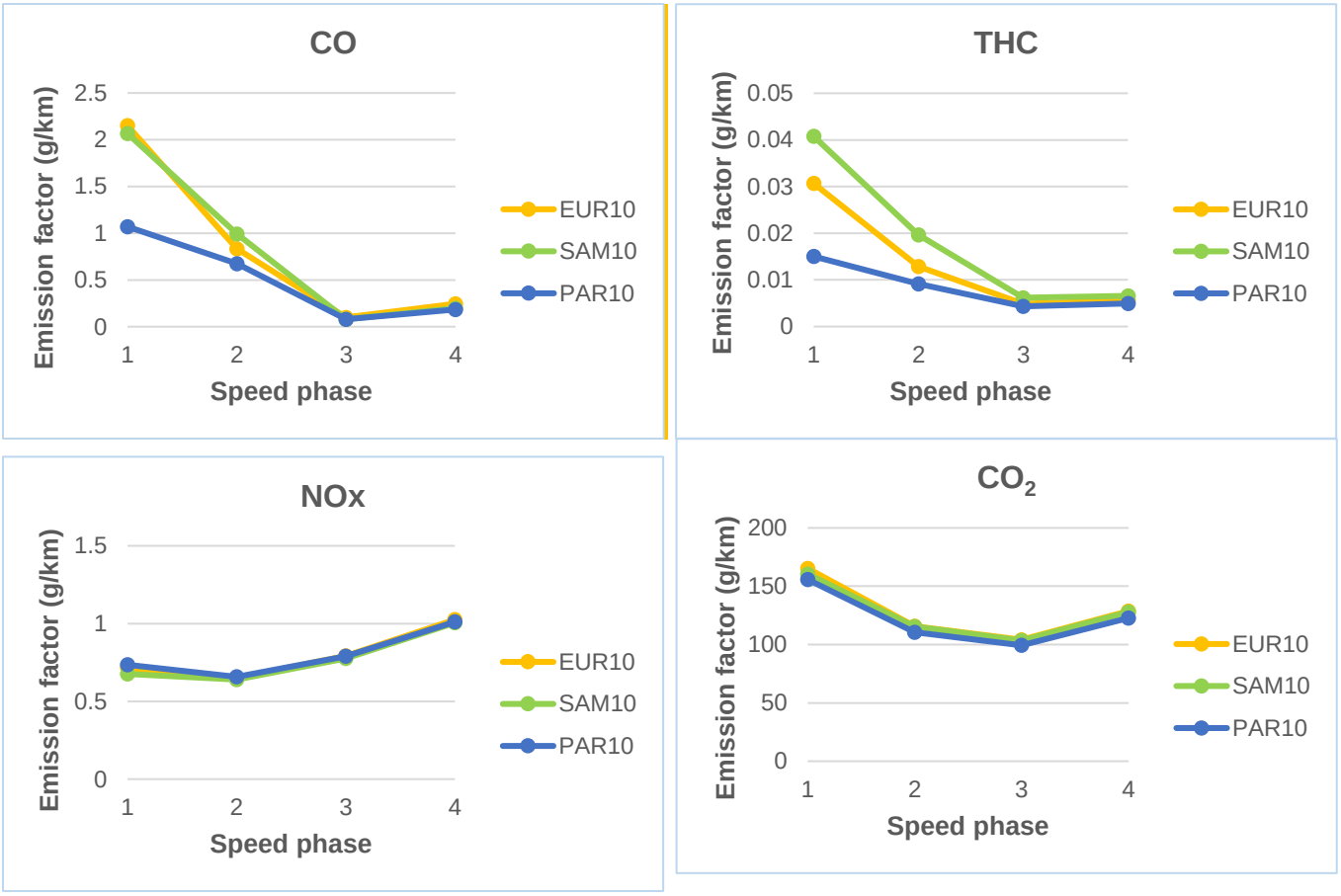

Figure 4.16 Changes in THC, CO, CO_2, and NO_X emissions between the different phases of the WLTC cycle (1 = low phase, 2 = medium phase, 3 = high phase, 4 = extra-high phase) for all three test fuels.

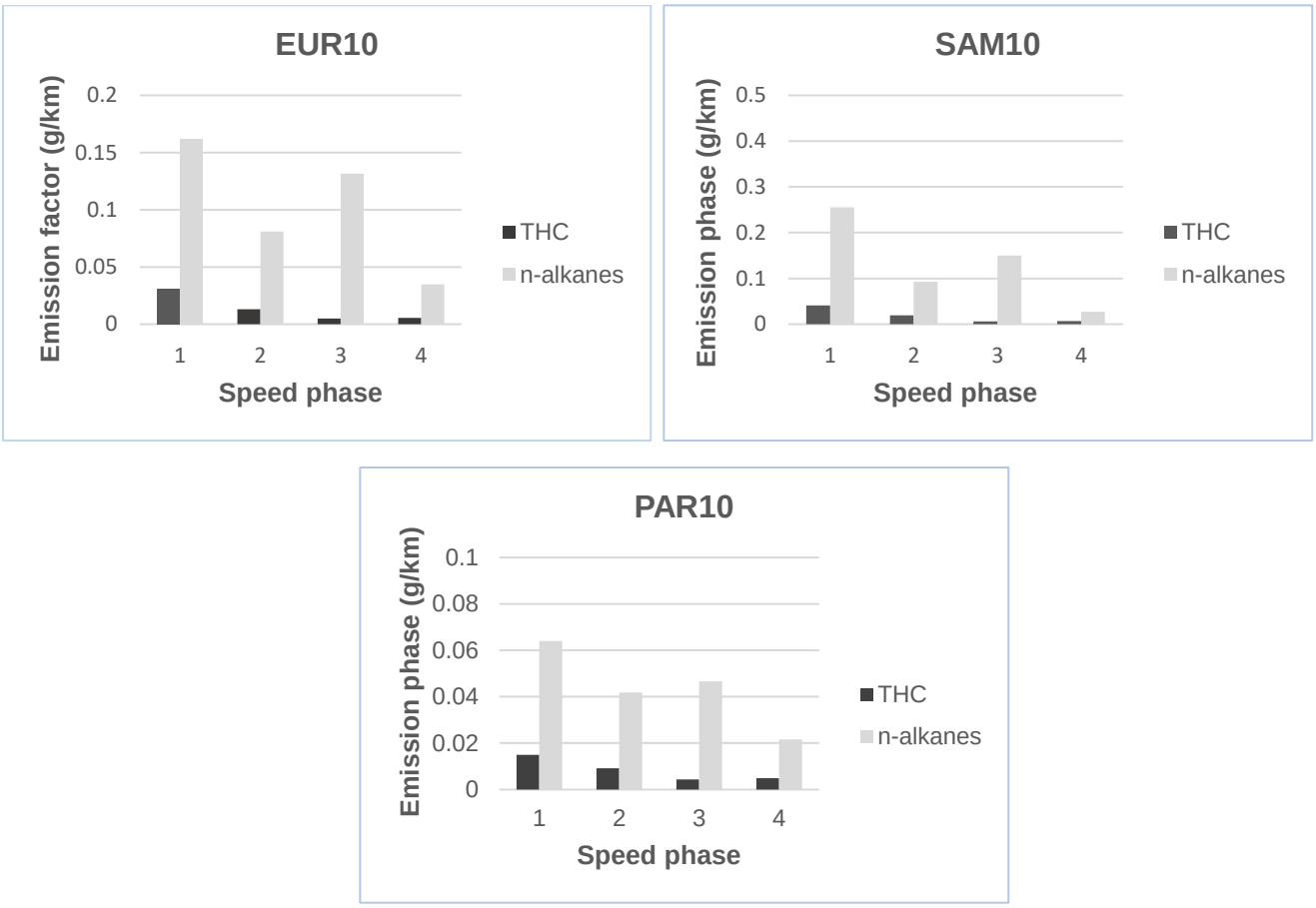

Figure 4.17 A comparison of the total n-alkane HC emissions (determined by TD-GC x GC-TofMS) and THC emissions (determined by a FID gas analyzer) for each fuel at different speed phases of the WLTC cycle emissions.

4.5.4 Comparison of cold start and hot start hydrocarbon emissions

Numerous studies have been conducted on hot-start emissions in comparison to cold-start and/or engine warm-up emissions (Bielaczyc et al., 2001, Weilenmann et al., 2005, Zare et al., 2017). Hot-start emissions are reported to be substantially lower than cold-start emissions primarily as a result of improved combustion conditions and efficient HC conversion by the engine catalytic systems as previously discussed (Section 4.5.2).

During sampling campaign one, multiple hot-start emissions tests were conducted for the SAM10 and EUR10 diesels, and were compared to the cold-start emissions for each fuel.

Typically, a hot-start test was conducted directly after a transient cycle cold-start test was performed, hence the engine would have been running continuously for the duration of the preceding test cycle (30 min), at which point it was assumed that the engine had reached its normal operating temperature. Figures 4.18 and 4.19 show a comparison of the cold-start and hot-start n-alkane and alkylbenzene emissions, respectively. A clear trend in the emissions was not observed and contrary to expectation, hot-start emissions were higher than cold start emissions, especially for the n-alkanes.

Tian (2015) investigated the effects of engine temperature on exhaust emissions from an engine operated on the New European Driving Cycle (NEDC) at two temperatures; ambient (20 °C) and warm up conditions (85 °C). The study (Figure 4.20) reported finding higher C_{11}-C_{18} n-alkanes when the engine was started from ambient conditions and lower emissions of these species during warm start, however in contrast, n-alkanes >C_{20} were four times higher during the warm start (Tian, 2015). Pereira et al. (2018) also stated that increased engine temperatures and/or combustion conditions resulted in larger proportions of high mass n-alkane emissions in the exhaust (Pereira et al., 2018). In this study, however, this phenomenon was observed for some of the more volatile HCs.

It is important to note that studying HCs at the individual level may yield different results than when they are analysed as a group, which is the case in most emission speciation studies. In terms of photochemical reactions of emitted HCs, studying individual HCs is useful as these species react individually to form photochemical pollutants. However, making a direct comparison between the emission of individual species and grouped compounds might not be feasible, as the emission characteristics of a group of compounds is a result of the sum. Further testing, perhaps targeting a wider range of compounds or a repeat of the experiments, will need to be conducted to verify these results.

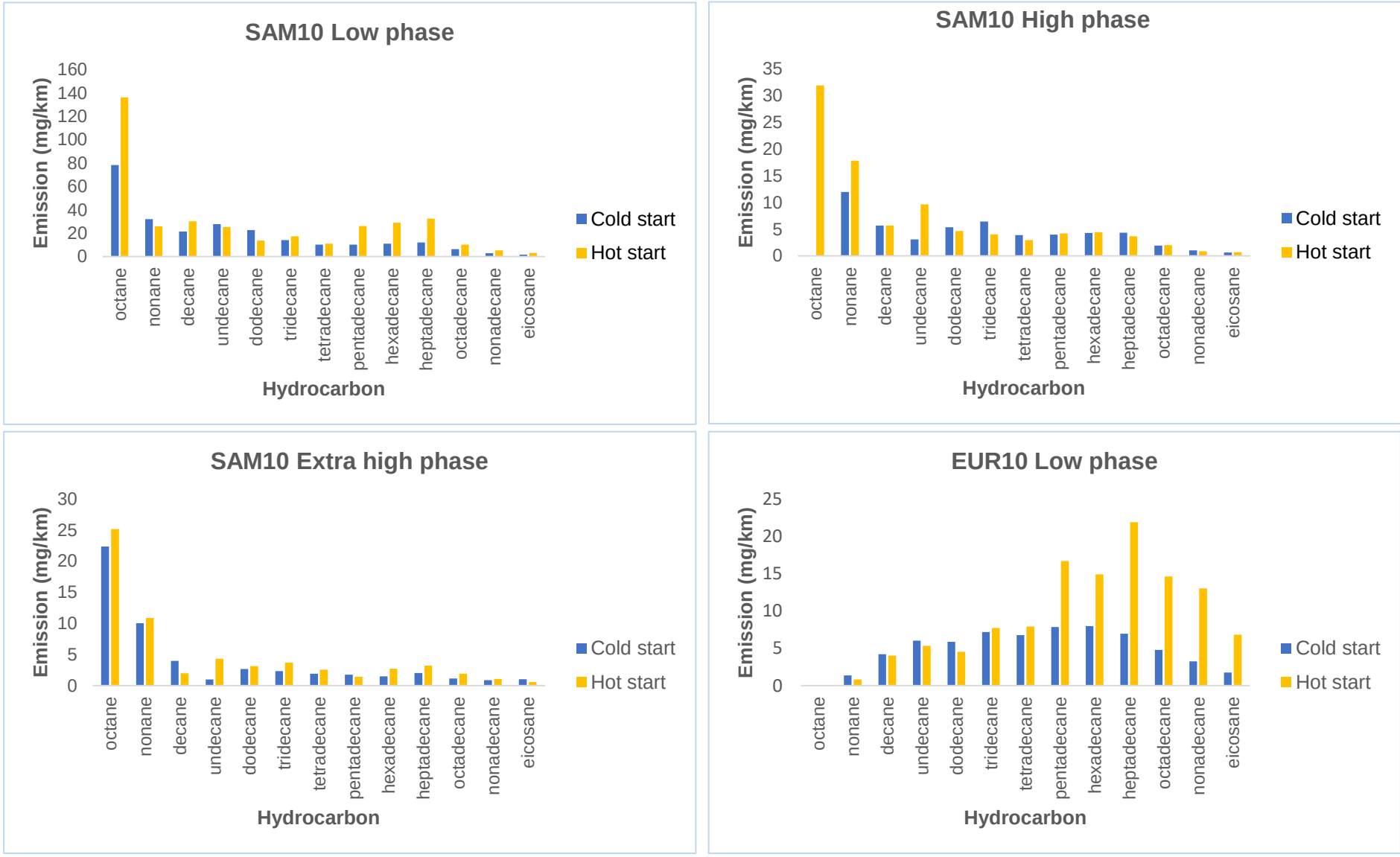

Figure 4.18 Comparison of n-alkane cold start and hot start emissions for the SAM10 and EUR10 fuels.
**SAM10 medium phase results excluded due to instrumental error during testing. Test only conducted at the low phase for EUR10 fuel.*

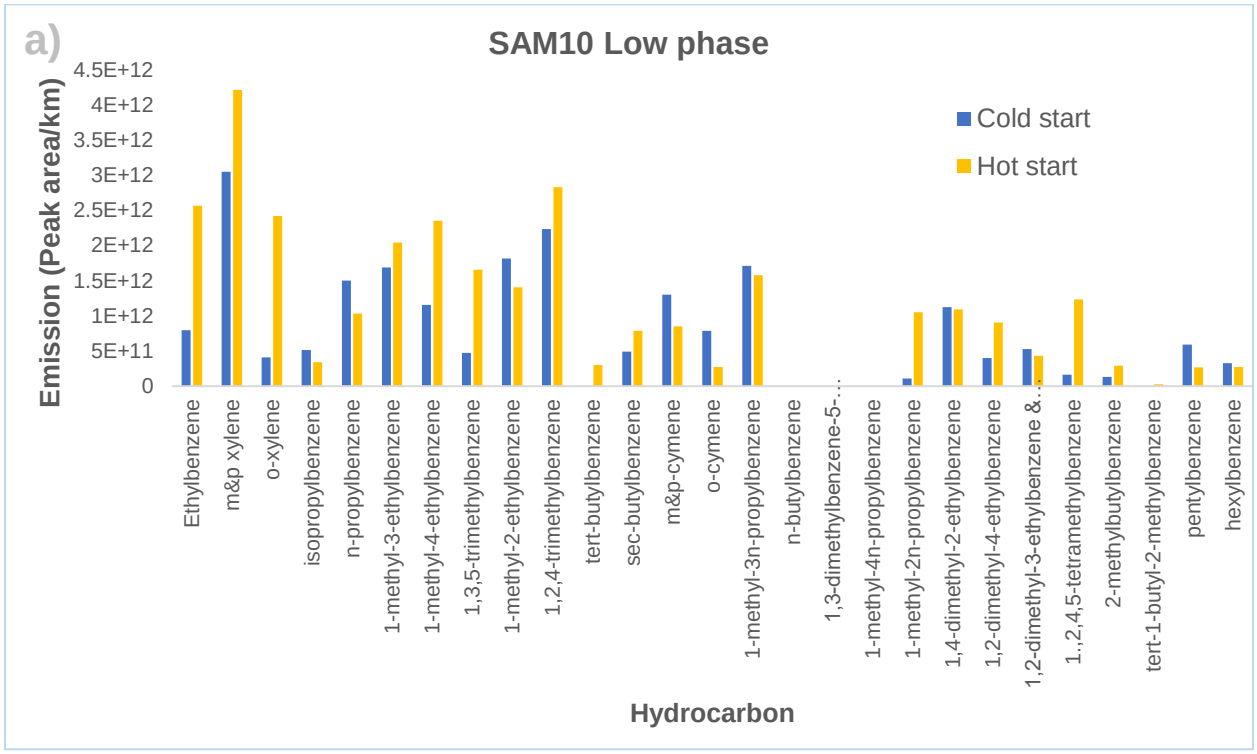
a)
SAM10 Low phase
Emission (Peak area/km)
4.5E+12
4E+12
3.5E+12
3E+12
2.5E+12
2E+12
1.5E+12
1E+12
5E+11
0
Cold start
Hot start
Ethylbenzene
m&p xylene
o-xylene
isopropylbenzene
n-propylbenzene
1-methyl-3-ethylbenzene
1-methyl-4-ethylbenzene
1,3,5-trimethylbenzene
1-methyl-2-ethylbenzene
1,2,4-trimethylbenzene
tert-butylbenzene
sec-butylbenzene
m&p-cymene
o-cymene
1-methyl-3n-propylbenzene
n-butylbenzene
1,3-dimethylbenzene-5-...
1-methyl-4n-propylbenzene
1-methyl-2n-propylbenzene
1,4-dimethyl-2-ethylbenzene
1,2-dimethyl-4-ethylbenzene
1,2-dimethyl-3-ethylbenzene &...
1.,2,4,5-tetramethylbenzene
2-methylbutylbenzene
tert-1-butyl-2-methylbenzene
pentylbenzene
hexylbenzene
Hydrocarbon

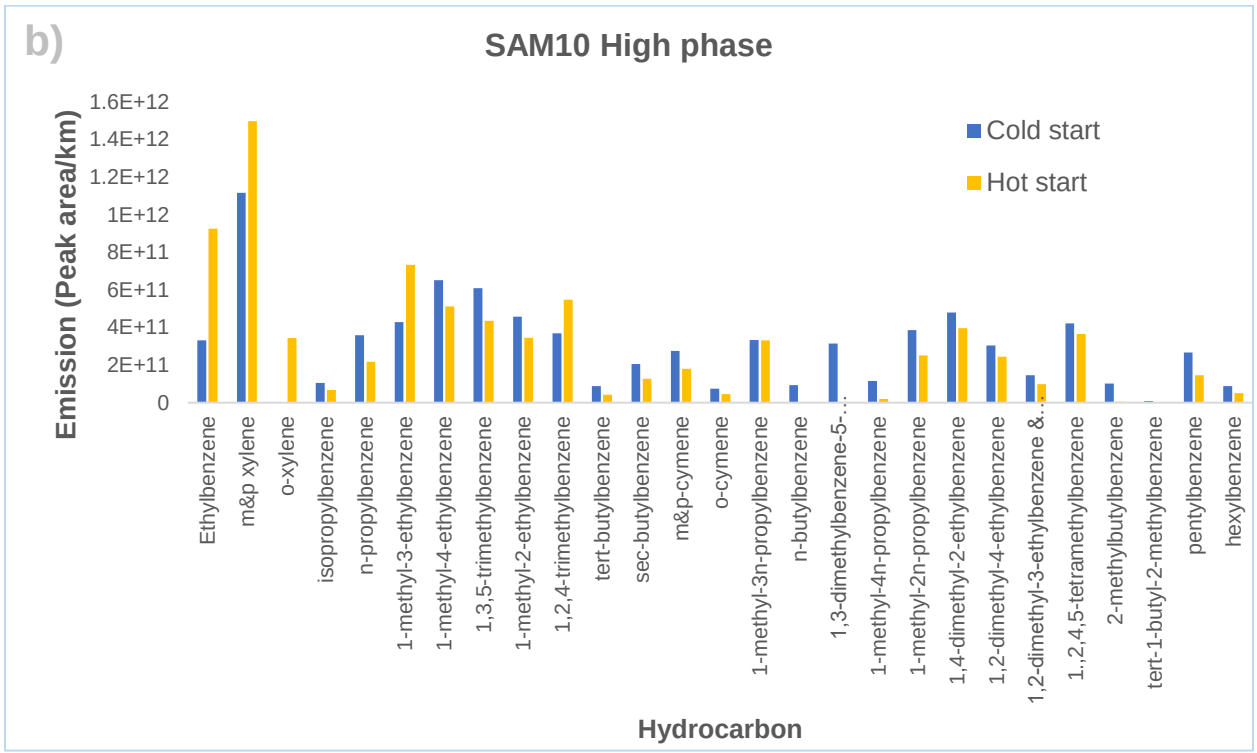
b)
SAM10 High phase
Emission (Peak area/km)
1.6E+12
1.4E+12
1.2E+12
1E+12
8E+11
6E+11
4E+11
2E+11
0
Cold start
Hot start
Ethylbenzene
m&p xylene
o-xylene
isopropylbenzene
n-propylbenzene
1-methyl-3-ethylbenzene
1-methyl-4-ethylbenzene
1,3,5-trimethylbenzene
1-methyl-2-ethylbenzene
1,2,4-trimethylbenzene
tert-butylbenzene
sec-butylbenzene
m&p-cymene
o-cymene
1-methyl-3n-propylbenzene
n-butylbenzene
1,3-dimethylbenzene-5-...
1-methyl-4n-propylbenzene
1-methyl-2n-propylbenzene
1,4-dimethyl-2-ethylbenzene
1,2-dimethyl-4-ethylbenzene
1,2-dimethyl-3-ethylbenzene &...
1.,2,4,5-tetramethylbenzene
2-methylbutylbenzene
tert-1-butyl-2-methylbenzene
pentylbenzene
hexylbenzene
Hydrocarbon

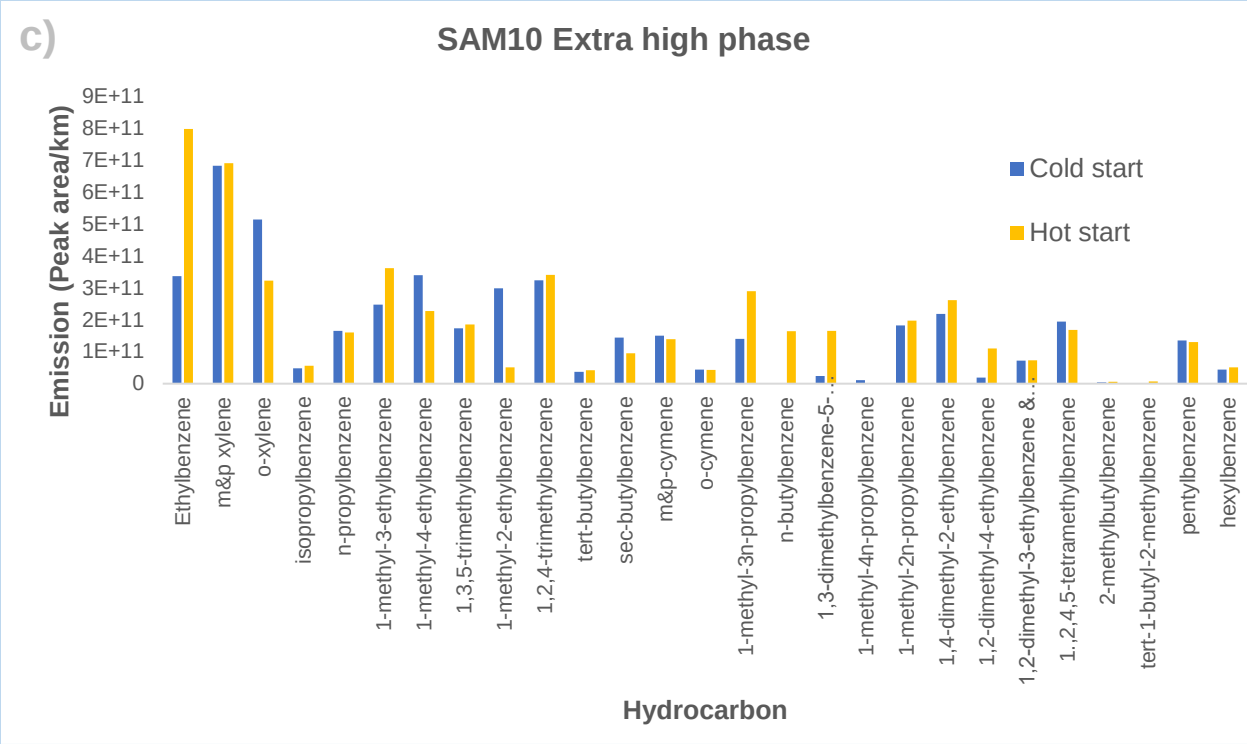

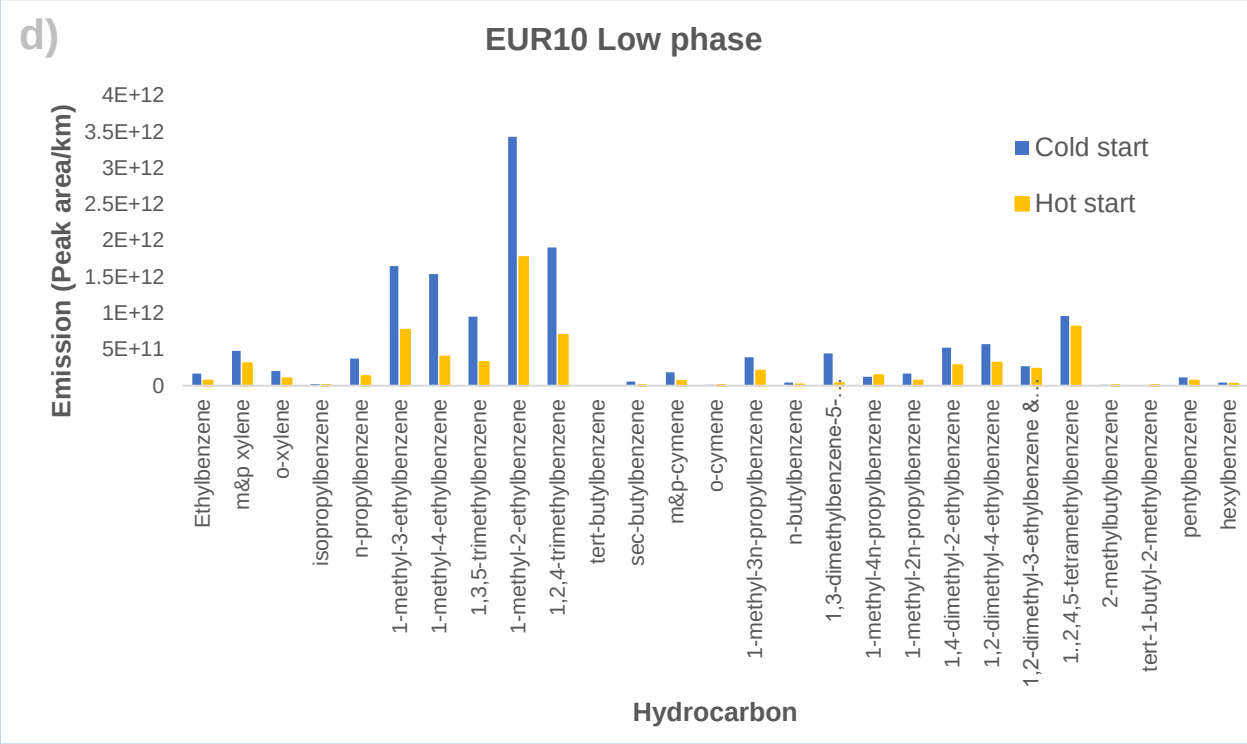

Figure 4.19 Comparison of alkylbenzene cold start and hot start emissions for the SAM10 and EUR10 fuels.

**SAM10 medium phase results excluded due to instrumental error during testing. Test only conducted at the low phase for EUR10 fuel*

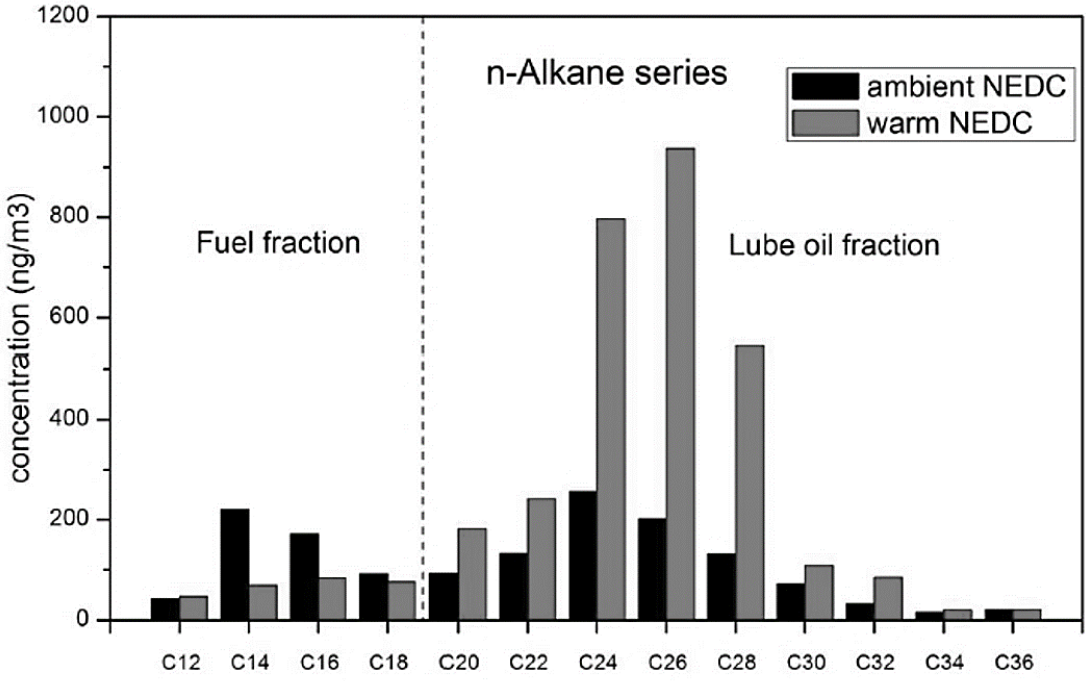

Figure 4.20 Concentrations of n-alkanes associated with particulates from the cold and warm start NEDC emission.
Adapted from Tian (2015).

4.5.5 The effect of exhaust aftertreatment technology

Cold start emissions testing was conducted using the EUR10 diesel to investigate the effect of the exhaust aftertreatment system. A DOC remained fitted throughout testing; hence the emission reduction observed was due to the combined effect of thermal breakdown of HCs and oxidative conversion of these HCs by the DOC. To investigate the role played by a more advanced aftertreatment system in the reduction of emissions, an additional catalyst (DPF) was added in the sampling train. Exhaust emissions produced by the engine now passed through a DOC followed by a DPF before exiting at the exhaust pipe. The DOC+DPF combination is typical of the technology used to meet a more advanced exhaust emission standard, for example Euro 4. A comparison of the emissions before and after installation of the DPF was made.

For both the n-alkanes (Figure 4.21) and alkylbenzenes (Figure 4.22), there were less emissions when both the DOC and DPF were present (deviation observed during the high speed phase was discussed in Section 4.5.2). Far less emissions were found during the later speed phases of the WLTC driving cycle. This was justifiable as the earlier speed phases are during the warm-up stage of the engine, where the catalytic systems may not be functioning as efficiently due to low engine temperatures.

For vehicles equipped with catalytic aftertreatment systems, the implication is that the oxidation catalyst is unable to convert exhaust emissions sufficiently at low engine temperatures as the catalyst has not reached its light-off temperature. Optimum functioning of the DPF is also temperature dependent. The DPF functions like a ‘sieve’, trapping PM emissions within a substrate’s porous walls, much like a mechanical filter. Over time the DPF accumulates PM, which results in an increase in back pressure, hence collected particulates must be removed from the filter. For most catalytic systems this is done by active regeneration where the particulates are ‘burned off’ at high temperatures (Reşitoğlu et al., 2015, Rounce et al., 2012), hence effective regeneration and continued function of the DPF also requires periodic high exhaust temperatures.

Figure 4.21 n-Alkane hydrocarbon emissions with the DOC and DOC+DPF exhaust aftertreatment system configuration.

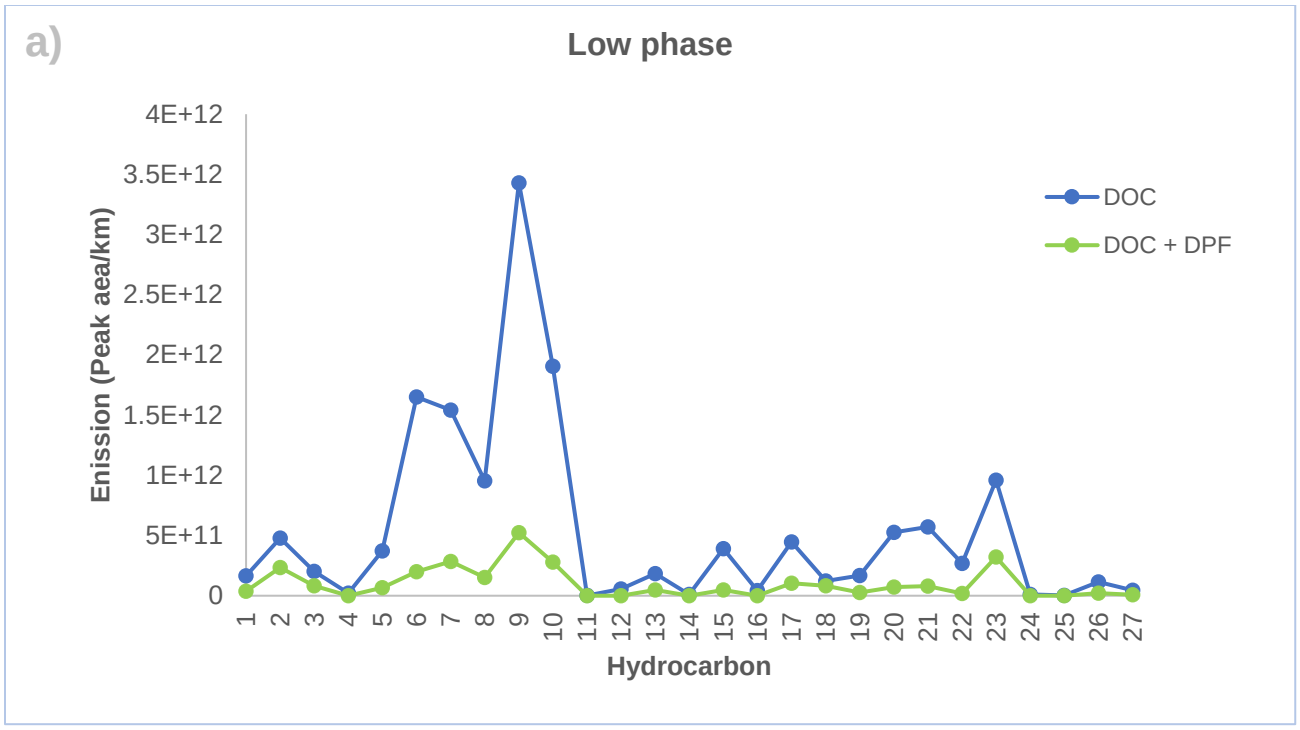
a)
Low phase
Enission (Peak aea/km)
4E+12
3.5E+12
3E+12
2.5E+12
2E+12
1.5E+12
1E+12
5E+11
0
1 2 3 4 5 6 7 8 9 10 11 12 13 14 15 16 17 18 19 20 21 22 23 24 25 26 27
Hydrocarbon
DOC
DOC + DPF

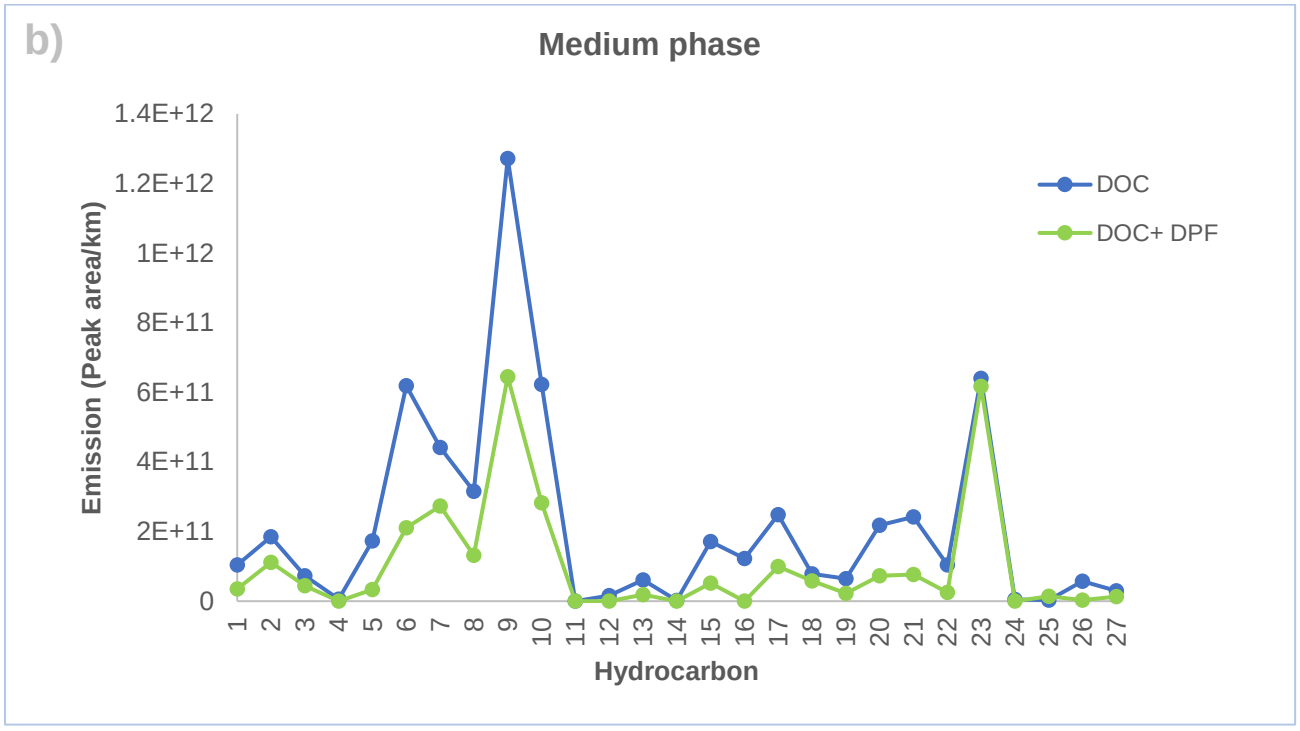
b)
Medium phase
Emission (Peak area/km)
1.4E+12
1.2E+12
1E+12
8E+11
6E+11
4E+11
2E+11
0
1 2 3 4 5 6 7 8 9 10 11 12 13 14 15 16 17 18 19 20 21 22 23 24 25 26 27
Hydrocarbon
DOC
DOC+ DPF

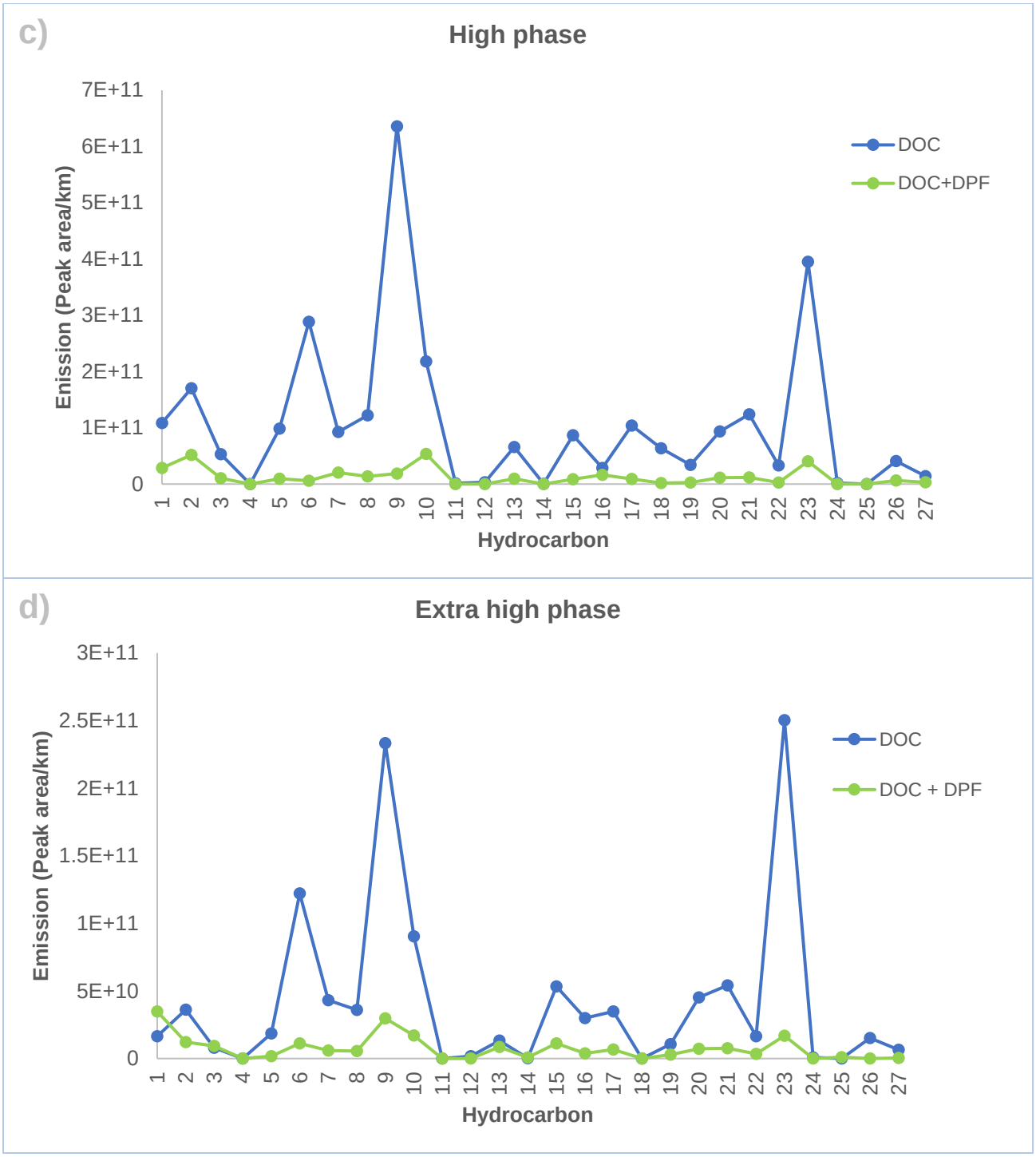

Figure 4.22 Alkylbenzene emissions with the DOC and DOC+DPF exhaust aftertreatment system configuration sampled onto PDMS traps.
NOTE: Numbers 1-27 corresponds to alkylbenzenes as labelled in Table 4-1.

Due to the minimal role played by particulates during the formation of photochemical pollutants, EFs were not calculated for collected particulate emissions. A visual inspection

of the quartz fibre filters used to collect particulate emissions was however performed, and these filters appeared significantly cleaner after the DPF was installed, illustrating efficient removal of exhaust emissions by the DPF (Figure 4.23).

These results also illustrate the suitability of denuders for exhaust characterization studies where both gaseous and particulates are studied, as particulate emissions were collected at detectable amounts.

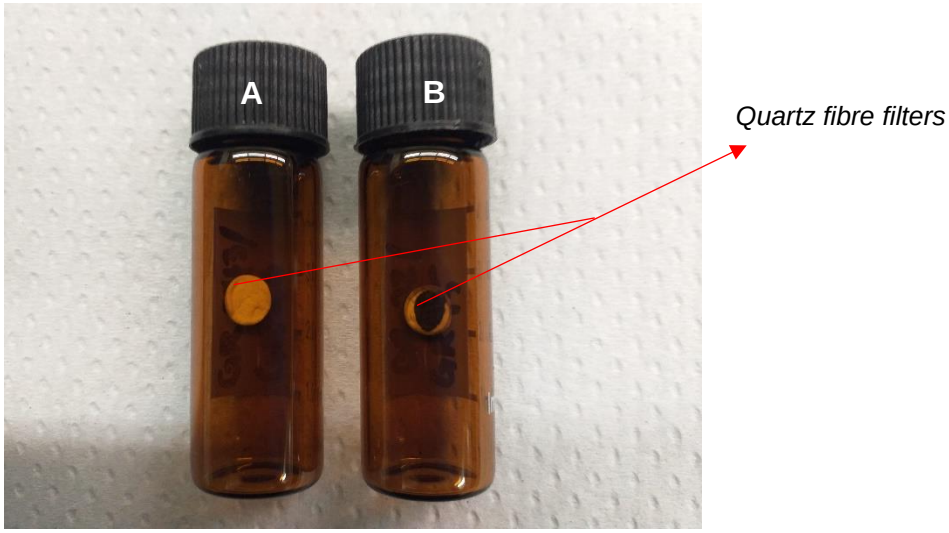

Figure 4.23 Quartz fibre filter used to collect particulate emissions with (A) and without (B) a diesel particulate filter in line.

4.6 Ozone formation potential of different fuels

The OFP of a particular HC depends on its oxidation mechanism and concentration (Wang et al., 2012). Atmospheric oxidation occurs mainly by reaction of HCs with the OH• radical, hence HCs are typically assigned a reactivity index, using a reaction mechanism, that represents the contribution of this species to the OH• radical sink (removal of OH• radicals from the atmosphere).

To determine the total OFP of each fuel, EFs would need to be calculated for all ozone forming compounds in the fuels' emissions. Herein, EFs were calculated for the n-alkanes only. The OFP of the n-alkanes was then estimated from their respective EFs and the total OFP was determined as the sum of the individual n-alkane OFPs. This was used as

a proxy to study the fuel's OFP. Figure 4.24 illustrates the percentage OFP of each fuel for each speed phase of the WLTC cycle and Table 4.7 shows the total (C_8-C_{20}) OFP for the individual fuels. The OFP (summed over the entire driving cycle) was 267.34 mg/km, 241.05 mg/km and 85.53 mg/km for the SAM10, PAR10 and EUR10 fuels respectively.

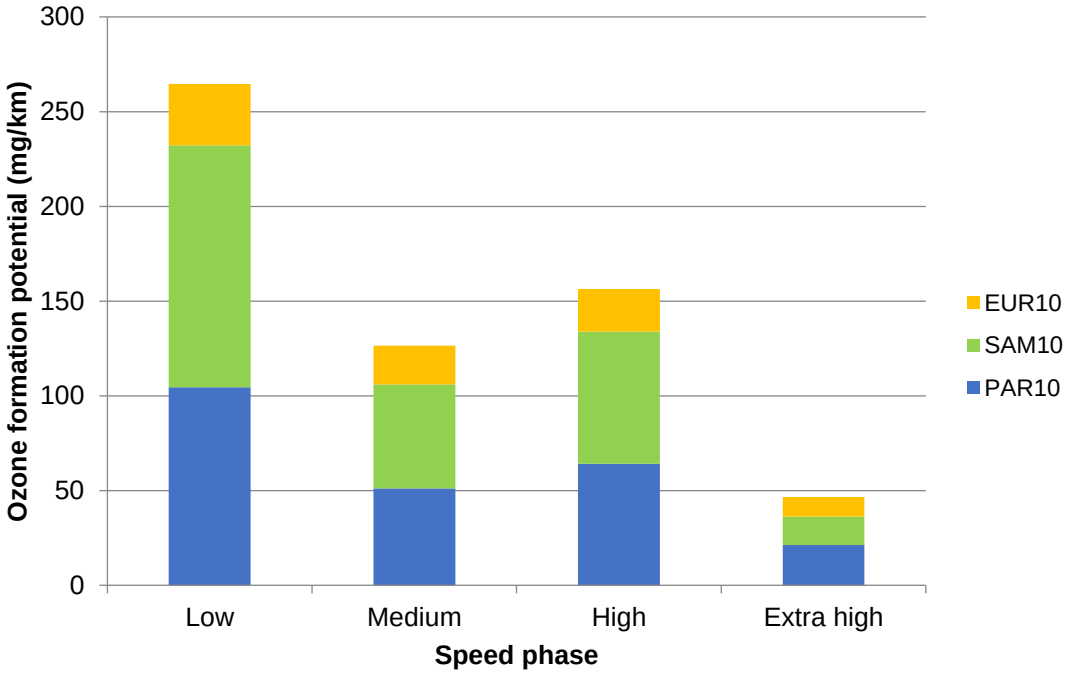

Figure 4.24 Ozone formation potential contribution of each fuel as calculated from the n-alkane emission factors at each speed phase.

Table 4.7 Total ozone formation potential of the n-alkane emissions for each fuel during each phase of the WLTC cycle.

	Ozone formation potential (mg/km)		
	PAR10	**SAM10**	**EUR10**
Low	104.54	127.68	32.41
Medium	51.21	54.81	20.37
High	64.07	69.76	22.46
Extra high	21.24	15.10	10.29

As discussed previously, both the concentration and type of species (due to higher photochemical reactivity of certain compounds) emitted are important to determine the overall OFP. Thus an analysis of the fuel's emission profile revealed that the SAM10 fuel

emitted more ozone-forming n-alkanes and had the second highest alkylbenzene HC emissions. The EUR10 diesel had the least n-alkane emissions (hence the lowest calculated OFP), however, it had relatively high aromatic HC emissions. Interestingly, six aromatic HCs: 1-methyl-3-ethylbenzene, 1-methyl-4-ethylbenzene, 1,3,5-trimethylbenzene, 1-methyl-2-ethylbenzene, 1,2,4-trimethylbenzene and 1,2,4,5-tetramethylbenzene, had higher abundances in the fuel's emissions. The MIR index of these compounds range from 4.44-11.76 gO_3/gVOC, thus they could contribute greatly to the overall OFP of this fuel. The PAR10 fuel is paraffinic, having relatively high n-alkane emissions. Although n-alkanes have low MIR indices, high emission factors would contribute greatly to the OFP of this fuel.

It is important to note that results of the OFP determination of the test fuels are not conclusive, as only a few species were analysed and used as a proxy to study the fuel's OFP. A major aim of the study was, however, to illustrate that the sampling and analysis techniques developed herein were successful in qualitative and quantitative characterisation of ozone forming semi-volatile hydrocarbon emissions, particularly 'missing emissions' from current monitoring approaches, and to illustrate that once these emissions have been speciated, it is possible to calculate their OFPs.

As mentioned previously, the EFs of HC emissions vary based on various factors, thus it is not ideal to perform inter study comparisons of the OFPs subsequently calculated from these EFs. This technique is however useful for comparisons between fuels with varying compositions tested in exactly the same way. The same approach may also be used to investigate the ozone formation potential of varying engines, lubricants, engine model and age, etc.

4.7 References

Bartlett, C., Betts, W., Booth, M., Giavazzi, F., Guttmann, H., Heinze, P. & Mayers, R. 1992. Diesel Fuel Aromatic Content and Its Relationship with Emissions from Diesel Engines, *Congawe*, Brussels.

Bielaczyc, P., Merkisz, J. and Pielecha, J., 2001. Investigation of exhaust emissions from DI diesel engine during cold and warm start. *Sae Technical Paper* 2001-01-1260 https://doi.org/10.4271/2001-01-1260

Bingham, E., Cohrssen, B., & Patty, F. A. 2012,.Patty's Toxicology, *N.J., John Wiley & Sons*, Hoboken.

Carter, W. P. 1994. Development of ozone reactivity scales for volatile organic compounds. *Air & Waste*, 44, 881-899.Chehroudi, B. 2015. Diesel engine emissions: Hydrocarbons (HC). [Online] Available at https://www.researchgate.net/pblication/277303525_Diesel_Engine_Hydrocarbons_HC/stat [Accessed 22-03-2020].

Garthe, C., Ballik, R., Hornreich, C. & Thiel, W. 2003. HC measurements by means of flame ionization: Background and limits of low emission measurement. *SAE Transactions*, 250-264.

Gautam, M., Gupta, D., El-Gazzar, L., Lyons, D. W. & Popuri, S. 1996. Speciation of heavy duty diesel exhaust emissions under steady state operating conditions. *SAE Technical Paper* 962159. https://doi.org/10.4271/962159

Gilman, H. & Beaber, N. J. 1925, The preparation of hydrocarbons by the reaction between alkyl sulfonates and organomagnesium halides, *Journal of the American Chemical Society,* 47, 518-525.

Heywood, J. B. 1988. Internal Combustion Engine Fundamentals, Chapter 11: Pollution Formation and Control, Jack Holman (ed.) pp 567-659, *McGraw-Hill*, New York.

Hountalas, D., Mavropoulos, G. & Binder, K. 2008. Effect of exhaust gas recirculation (EGR) temperature for various EGR rates on heavy duty DI diesel engine performance and emissions. *Energy,* 33, 272-283.

Johnson, B. T. 2008. Diesel engine emissions and their control. *Platinum Metals Review,* 52, 23-37.

Ladommatos, N., Parsi, M. & Knowles, A. 1996. The effect of fuel cetane improver on diesel pollutant emissions. *Fuel,* 75, 8-14.

Ladommatos, N., Abdelhalim, S. & Zhao, H. 2000. The effects of exhaust gas recirculation on diesel combustion and emissions. *International Journal of Engine Research,* 1, 107-126.

Pauláthomas, C. 1989. Denuder tubes for sampling of gaseous species. A review. *Analyst,* 114, 759-769.

Pereira, K. L., Dunmore, R. E., Whitehead, J., Rami Alfarra, M., Allan, J., Alam, M., Harrison, R. M., Mcfiggans, G. & Hamilton, J. F. 2018. Use of an atmospheric simulation chamber to investigate the effect of different engine conditions on unregulated VOC-IVOC diesel exhaust emissions. *Atmospheric Chemistry and Physics*, 11073-11096.

Raja, A. S. & Arasu, A. V. 2015. Exhaust gas treatment for reducing cold start emissions of a motorcycle engine fuelled with gasoline-ethanol blends. *Journal of Energy in Southern Africa,* 26, 84-93.

Reşitoğlu, İ. A., Altinişik, K. & Keskin, A. 2015. The pollutant emissions from diesel-engine vehicles and exhaust aftertreatment systems. *Clean Technologies and Environmental Policy,* 17, 15-27.

Roberts, A., Brooks, R. & Shipway, P. 2014. Internal combustion engine cold-start efficiency: A review of the problem, causes and potential solutions. *Energy Conversion and Management,* 82, 327-350.

Rounce, P., Tsolakis, A. & York, A. 2012. Speciation of particulate matter and hydrocarbon emissions from biodiesel combustion and its reduction by aftertreatment. *Fuel,* 96, 90-99.

Ruiz-Hernández, V., Roca, M. J., Egea-Cortines, M. & Weiss, J. 2018. A comparison of semi-quantitative methods suitable for establishing volatile profiles. *Plant Methods,* 14, 67.

Schlatter, M. J. & Clark, R. D. 1953, T-alkyl groups. I. Orientation of t-alkylation products of toluene and ethylbenzene, *Journal of the American Chemical Society,* 75, 361-369.

Tian, J. 2015. *Particulate emission characteristics of a light duty diesel engine under transient operation conditions.* Unpublished doctoral thesis, University of Birmingham.

Volkamer, R., Jimenez, J. L., San Martini, F., Dzepina, K., Zhang, Q., Salcedo, D., Molina, L. T., Worsnop, D. R. & Molina, M. J. 2006. Secondary organic aerosol formation from anthropogenic air pollution: Rapid and higher than expected. *Geophysical Research Letters,* 33.

Wang, X., Westerdahl, D., Hu, J., Wu, Y., Yin, H., Pan, X. & Zhang, K. M. 2012. On-road diesel vehicle emission factors for nitrogen oxides and black carbon in two Chinese cities. *Atmospheric Environment,* 46, 45-55.

Washburn, E. W. 2003, International Critical Tables of Numerical Data, Physics, Chemistry and Technology, 1st Electronic Edition. pp. 1926–1930, *Knovel*, Norwich, NY.

Weilenmann, M., Soltic, P., Saxer, C., Forss, A.M. and Heeb, N., 2005. Regulated and nonregulated diesel and gasoline cold start emissions at different temperatures. *Atmospheric Environment*, 39(13), pp.2433-2441.

Weitkamp, E. A., Sage, A. M., Pierce, J. R., Donahue, N. M. & Robinson, A. L. 2007. Organic aerosol formation from photochemical oxidation of diesel exhaust in a smog chamber. *Environmental Science & Technology,* 41**,** 6969-6975.

Yaws, C. L. 2003, Yaws' Handbook of Thermodynamic and Physical Properties of Chemical Compounds: Physical, Thermodynamic and Transport Properties For 5,000 Organic Chemical Compounds, *Knovel*, Norwich, N.Y.

Yaws, C. L. 2012, Yaws' Critical Property Data for Chemical Engineers and Chemists, *Knovel*, Norwich, N.Y.

Zare, A., Nabi, M. N., Bodisco, T. A., Hossain, F. M., Rahman, M., Van, T. C., Ristovski, Z. D. & Brown, R. J. 2017. Diesel engine emissions with oxygenated fuels: A comparative study into cold-start and hot-start operation. *Journal of Cleaner Production,* 162**,** 997-1008.

Chapter 5: Conclusions and future work

SVOC emissions from a diesel engine used in a light-duty passenger vehicle were characterized for three different fuels, which differed in chemical composition. The engine was operated over the World Harmonized Light Vehicle Test Cycle consisting of different speed phases: low, medium, high, and extra-high. Sampling of exhaust emissions was performed using denuder samplers (prepared in-house) consisting of PDMS traps for collection of gaseous emissions and quartz fibre filters for particulate emissions. Thermal desorption coupled with comprehensive 2D gas chromatography–time of flight mass spectrometry was used for sample analysis.

Characterization of n-alkane and alkylbenzene gas phase emissions was performed for each test fuel under various engine operating conditions. The three test fuels showed distinctly differing levels of n-alkane and alkylbenzene SVOC emissions. The SAM10 diesel emitted more n-alkanes and had the second highest alkylbenzene HC emissions. The EUR10 diesel had the least n-alkane emissions, however it had the highest alkylbenzene emissions. The PAR10 diesel emissions had relatively high n-alkane HCs, however it had the lowest alkylbenzene emissions. The observed trends in HC emissions were attributed to differences in chemical composition and physical properties (volatility and cetane number) between the fuels, and it can be concluded that fuel composition is an important factor in determining the quantity and composition of SVOC emissions from diesel engines.

Changes in HC emissions at different operating conditions were studied. In general, a decrease in HC emissions was observed for each fuel when moving from the “Low” to the “Extra high” speed phase of the test cycle. This decrease was attributed to a rise in exhaust temperatures which resulted in improved combustion conditions and facilitated catalytic conversion of harmful emissions by the DOC and removal of particulate emissions by the DPF. A deviation from these results was observed for the n-alkane emissions during the high speed phase. Because a strong decreasing trend was observed in the emissions of the alkylbenzenes and n-alkanes during the other speed phases, it was speculated that this deviation might have been due to the “trap and

release” mechanism of the DOC, i.e. hydrocarbons are trapped by the DOC at low temperatures and are subsequently released at high temperatures. Further investigation into these results needs to be done to elucidate the reason.

A comparison between hot-start and cold-start gaseous HC emissions was also made. A decrease in alkylbenzene HC emissions was observed during hot-start engine operation, however the opposite effect was found for the n-alkane emissions. Due to improved combustion conditions brought about by elevated temperatures, lower hot-start emissions were expected. A possible explanation for the results found might be that the oxidation catalyst has a different selectivity for different mass range HCs or that HC deposition might be occurring during cold-start conditions, where analytes condense and are volatilised and emitted during later stages when the engine is warmer.

The test engine’s exhaust aftertreatment system consisted of a close-coupled DOC and a DPF (added later). Cold-start tests were performed for the EUR10 diesel, with and without a DPF fitted in line. A decrease in HC emissions was observed when the DPF was installed. The quartz fibre filters used to collect particulate emissions and soot also appeared significantly cleaner than when the DPF was absent. This illustrates the importance of the presence and optimal functioning of exhaust aftertreatment technology in modern day vehicles for effective removal of exhaust HC and PM emissions.

The OFP of each fuel was investigated and it was found that the emission profile of each fuel contributes differently to its OFP. SAM10 diesel emitted more ozone forming n-alkane and aromatic HC emissions than the other two fuels, while EUR10 diesel had relatively high aromatic HC emissions, which have high MIR indices, thus greatly contributing to the OFP of this fuel. The PAR10 fuel had relatively high n-alkane emissions, which have lower MIR indices, however it was noted that the presence of the n-alkane emissions in high enough concentrations would contribute to the OFP of this fuel. Obtaining the overall OFP of each fuel would require characterising all ozone forming HCs and calculating each of their OFP values as demonstrated in this study. The sum of the OFPs will then give the overall OFP of the fuel. Many studies conclude that the fuel with higher amounts of

aromatic emissions has a higher OFP as a result of the high MIR indices of these compounds, however as illustrated in the study, it is important to consider both the MIR index as well as emission factors of the HCs.

Monitoring of semi-volatile HC emissions may be critical in understanding elevated ozone levels in urban areas, which are often higher than model predictions. This study has illustrated the successful use of denuders and comprehensive 2D gas chromatography with mass spectrometric detection to collect and characterize semi-volatile HC emissions from diesel exhaust. This illustrates the suitability of these analytical techniques for collection and analysis of dilute exhaust emissions. The use of denuder samplers provided an inexpensive, efficient and easy sampling method for use in vehicular exhaust emission applications and allowed for simultaneous sampling of gas and particle phase SVOCs across various chemical classes, while the power of two dimensional gas chromatography enabled identification and quantification of exhaust emission species, particularly semi-volatile emissions that contribute significantly to the formation of atmospheric pollutants. This work may thus contribute significantly towards air quality management and understanding of the photochemical ozone levels both in South Africa and globally.

5.1 Limitations of the study

High error bars indicated poor repeatability for the duplicate measurements of some HCs. Variations may mainly be attributed to volatility of certain HCs. Other contributing factors may include variations in denuder construction, storage conditions, insufficient conditioning periods and/or prolonged storage periods of samplers prior to use.

Technical challenges with the gas chromatography instrumentation may often impact sample analysis. During this study, malfunctioning of the N_2 generator used during cryocooling resulted in pressure build up which caused the piping leading to the second cold jet to disconnect during a run. This resulted in a wrap-around effect where certain peaks were not visible on the chromatogram, hence they could not be characterised. Another technical difficulty occurred with subsequent breaking of the modulator. The modulator, located between the primary and secondary column is key during GC x GC

separation of analytes. It functions by collecting the separated peaks from the primary column where they are trapped, re-focussing (using very low temperatures) and injecting them onto the secondary column as narrow bands which allows for improved chromatographic sensitivity and resolution. Incorrect functioning of the modulator increases likelihood of wrap-around (which was observed), although the structure of the 2D chromatogram is maintained.

Analysis of diesel exhaust filter samples also caused soot entering the chromatographic system, which resulted in a column change being required. This may have been prevented by the use of a different inlet liner (for example one containing deactivated glass wool which would retain any particulates). Even though a significant amount of dilution of diesel exhaust emissions before sampling was performed, these concentrations may still be high for a TD-GC x GC-TofMS, hence split analysis is usually performed for vehicle exhaust emission samples. During split analysis, a portion of the emissions are introduced onto the GC column while the rest of the sample is discarded. A major challenge faced during this study however, was the simultaneous analysis of n-alkanes and alkylbenzenes. Typically, aliphatics are present at higher abundances in diesel exhaust than aromatics, hence splitting the sample might have risked the alkylbenzenes being below the detection limit. It was thus decided that spitless analysis would be done. If more than one class of analyte is sampled, simultaneous replicate samples can also be collected so different replicate samples can be analysed for different analyte classes. This will also allow for separate optimization of the GC methods for different compound classes to ensure enhanced resolution. This does, however, increase the cost of the study significantly as this would require a larger number of samplers, a larger number of analyses, which in turn leads to longer instrumental analysis time with associated costs.

5.2 Recommendations for future work

The recommendations made focus on further testing, possibly with a larger sample set to gain better understanding of the observed trends in results:

- The question of possible pre-existing HCs on PDMS traps needs to be addressed as low levels of HCs could be detected on some blank traps. A simple study on the HC levels found on newly made traps as compared to traps that have been stored for a period of time prior to sampling could be conducted. Based on these results, an adapted standard protocol could also be developed on the preparation procedure, conditioning method, and storage conditions and/or time of the PDMS samplers to minimise the potential for contamination.
- Analysis of filter samples collected during the second sampling campaign to determine the changes in particulate emissions for different fuels at varying engine operating conditions. These may be compared to the results obtained for gaseous emissions to see if similar trends are observed.
- It was observed that despite having a similar alkylbenzene content, the alkylbenzene emission factors of the EUR10 and SAM10 fuel differed, hence further investigation into the factors that affect these HC emissions is needed. A similar study design to the current one could be used where the effect of various fuel properties and/or engine parameters can be studied in this regard.
- Due to limitations provided by the reference standard chosen for the study, only semi quantitative analysis of the alkylbenzene emissions could be done. In future, quantitative analysis of these HCs as well as other classes of HCs found in the fuel and emissions could be conducted to obtain a complete understanding of how the emission profile of each fuel affects its ozone formation potential.
- The n-alkane emission factors observed during the high speed phase were higher than expected. This was not observed for the alkylbenzene HCs, hence the observed deviation could be due to experimental error. Repeat measurements could be useful to confirm the observed results.

Appendices

Appendix A: Example 2D and 3D chromatograms of test fuel emissions

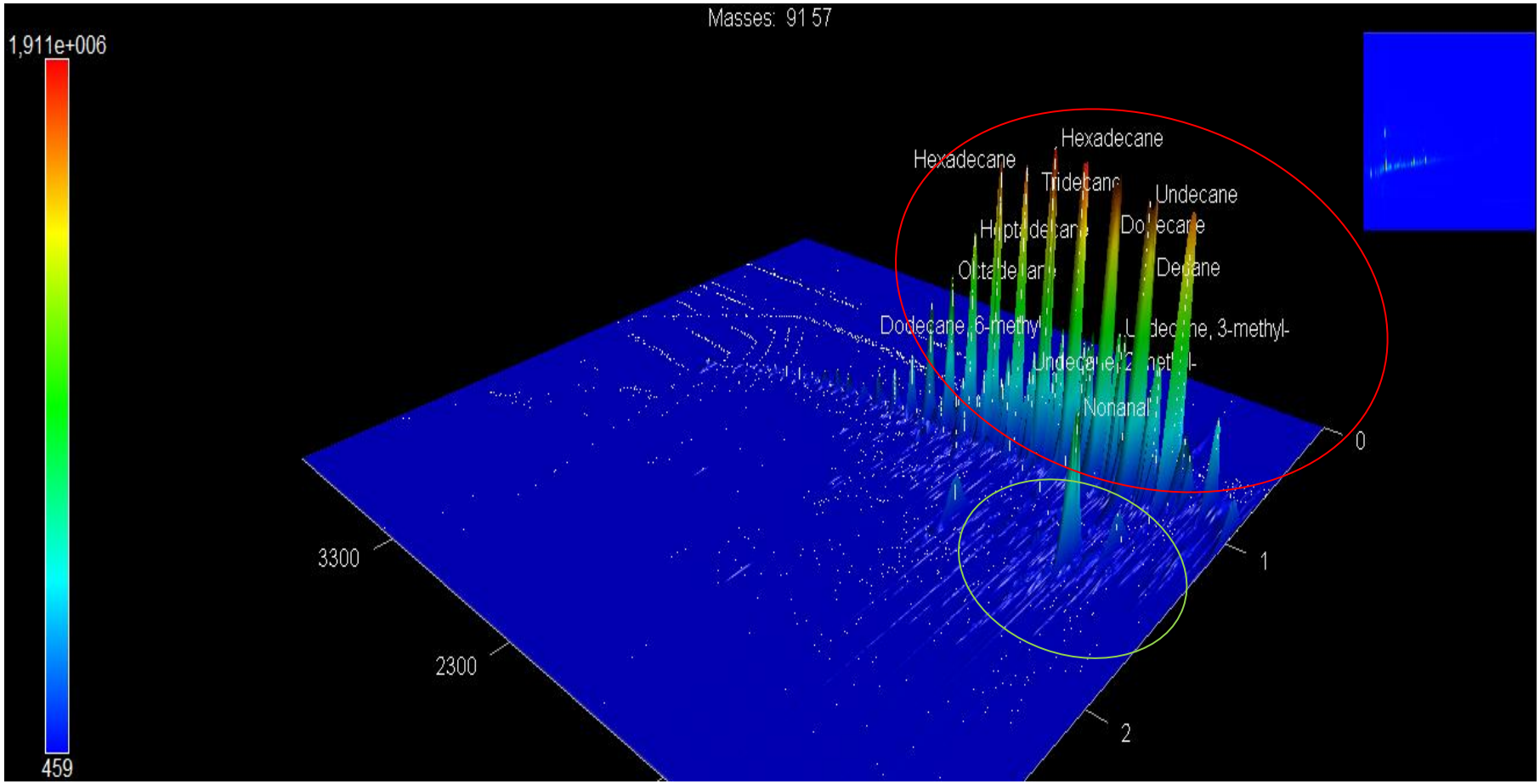

Figure A1 Extracted ion 3D chromatogram (m/z = 57 and 91) showing the n-alkane (red) and alkylbenzene (green) hydrocarbon region from analysis of exhaust emissions from the test engine fueled with PAR10 diesel sampled onto a PDMS trap.

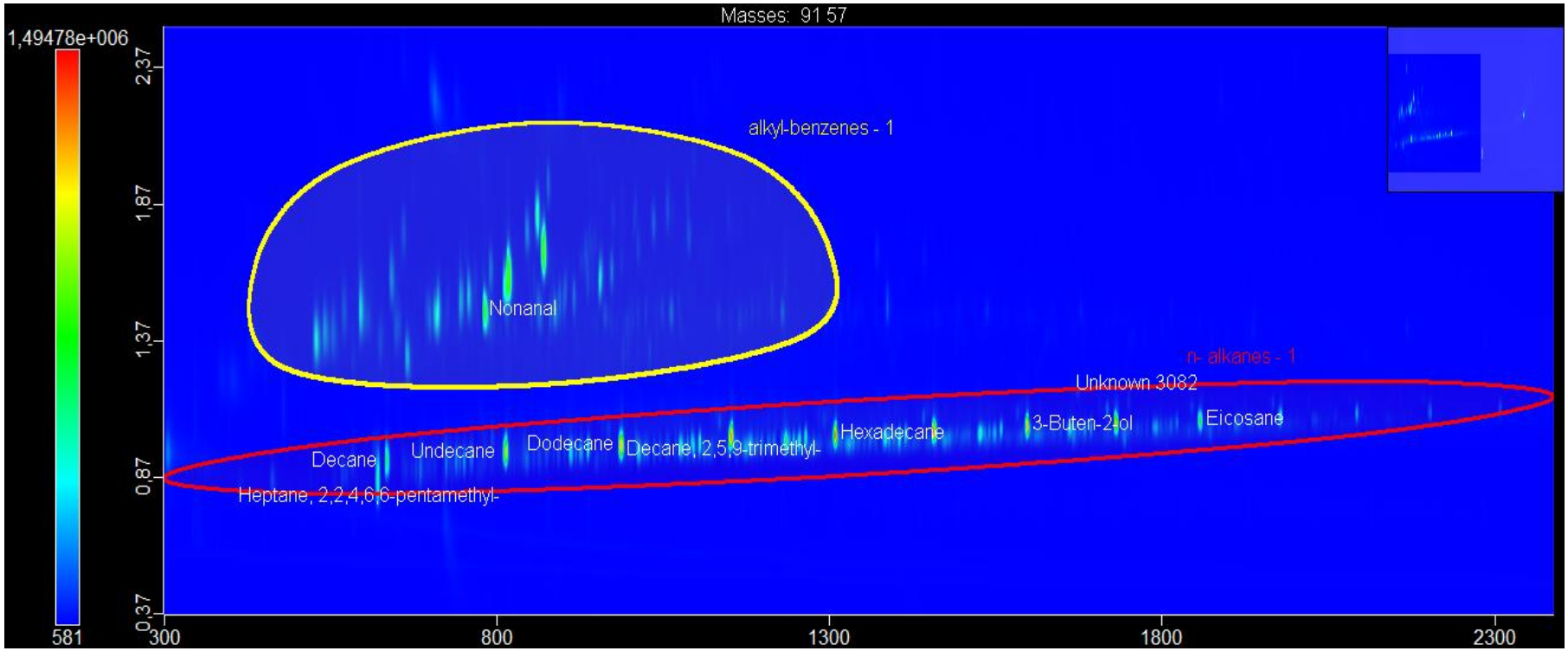

Figure A2 Extracted ion 2D chromatogram (m/z = 57 and 91) showing the n-alkane (red) and alkylbenzene (green) hydrocarbon region from analysis of exhaust emissions from the test engine fueled with PAR10 diesel sampled onto a PDMS trap.

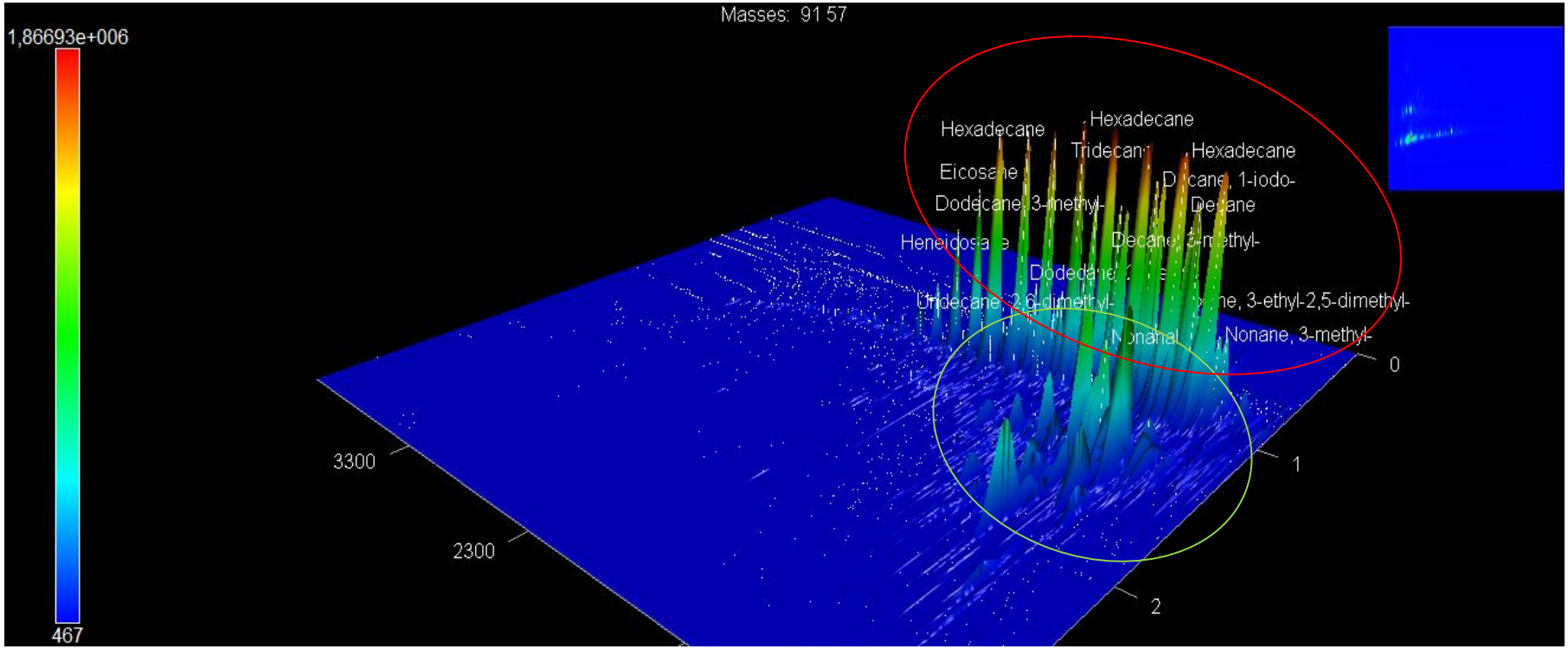

Figure A3 Extracted ion 3D chromatogram (m/z = 57 and 91) showing the n-alkane (red) and alkylbenzene (green) hydrocarbon region from analysis of exhaust emissions from the test engine fueled with SAM10 diesel sampled onto a PDMS trap.

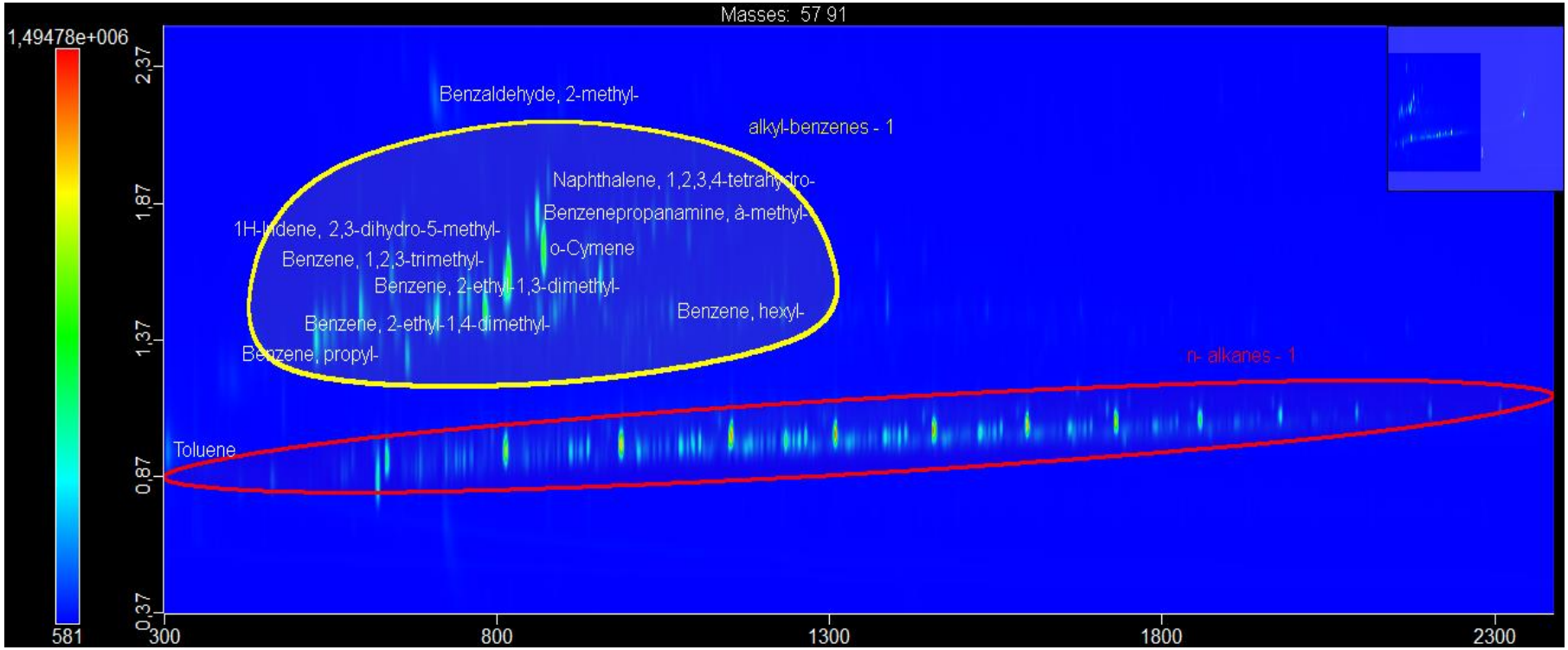

Figure A4 Extracted ion 2D chromatogram (m/z = 57 and 91) showing the n-alkane (red) and alkylbenzene (green) hydrocarbon region from analysis of exhaust emissions from the test engine fueled with SAM10 diesel sampled onto a PDMS trap.

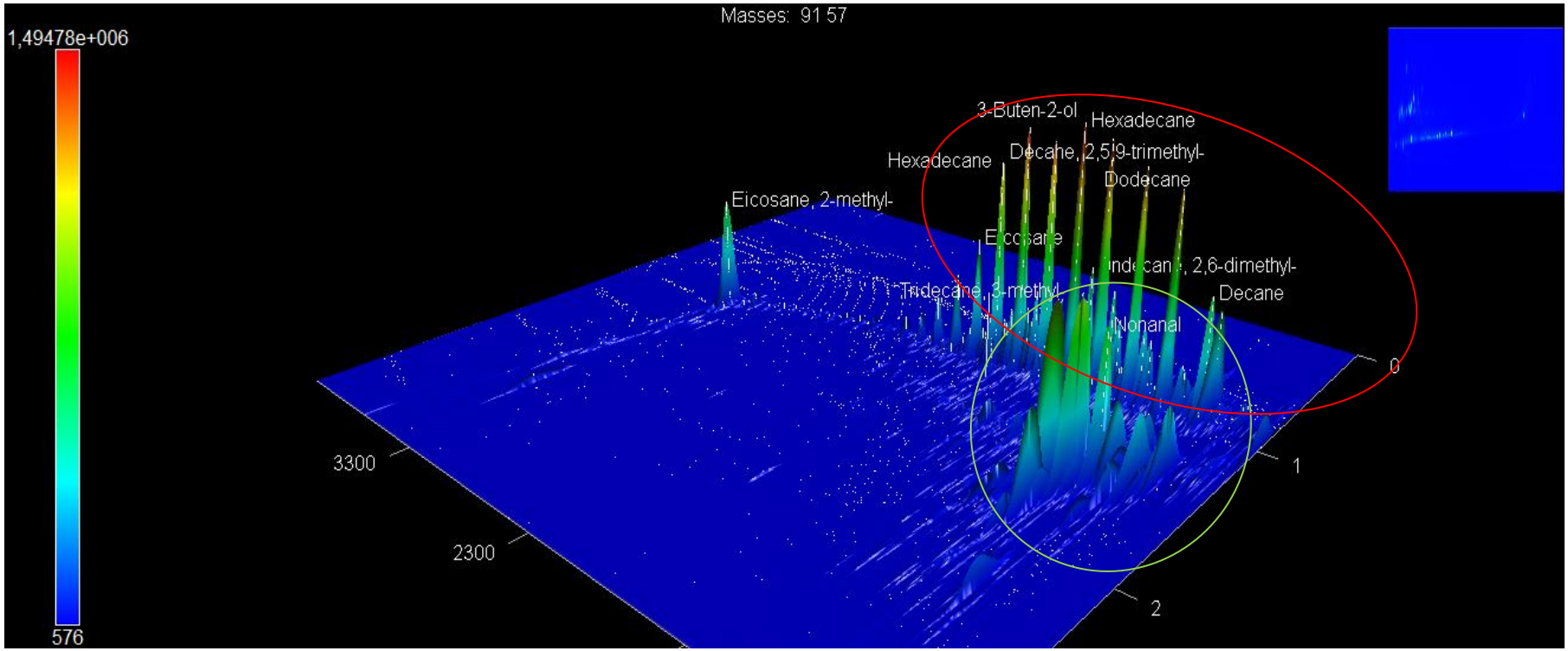

Figure A5 Extracted ion 3D chromatogram (m/z = 57 and 91) showing the n-alkane (red) and alkylbenzene (green) hydrocarbon region from analysis of exhaust emissions from the test engine fueled with EUR10 diesel sampled onto a PDMS trap.

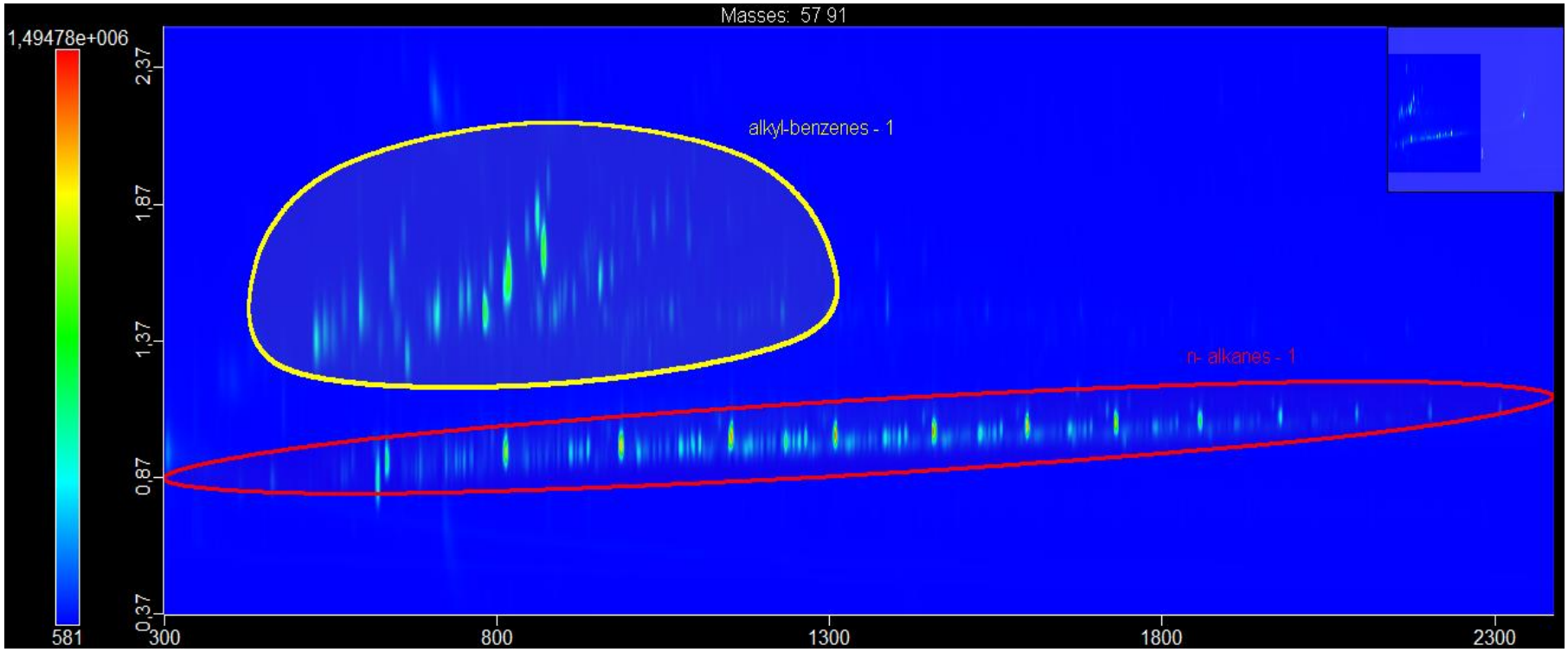

Figure A6 Extracted ion 2D chromatogram (m/z = 57 and 91) showing the n-alkane (red) and alkylbenzene (green) hydrocarbon region from analysis of exhaust emissions from the test engine fueled with EUR10 diesel sampled onto a PDMS trap.

Appendix B: The Unresolved Complex mixture

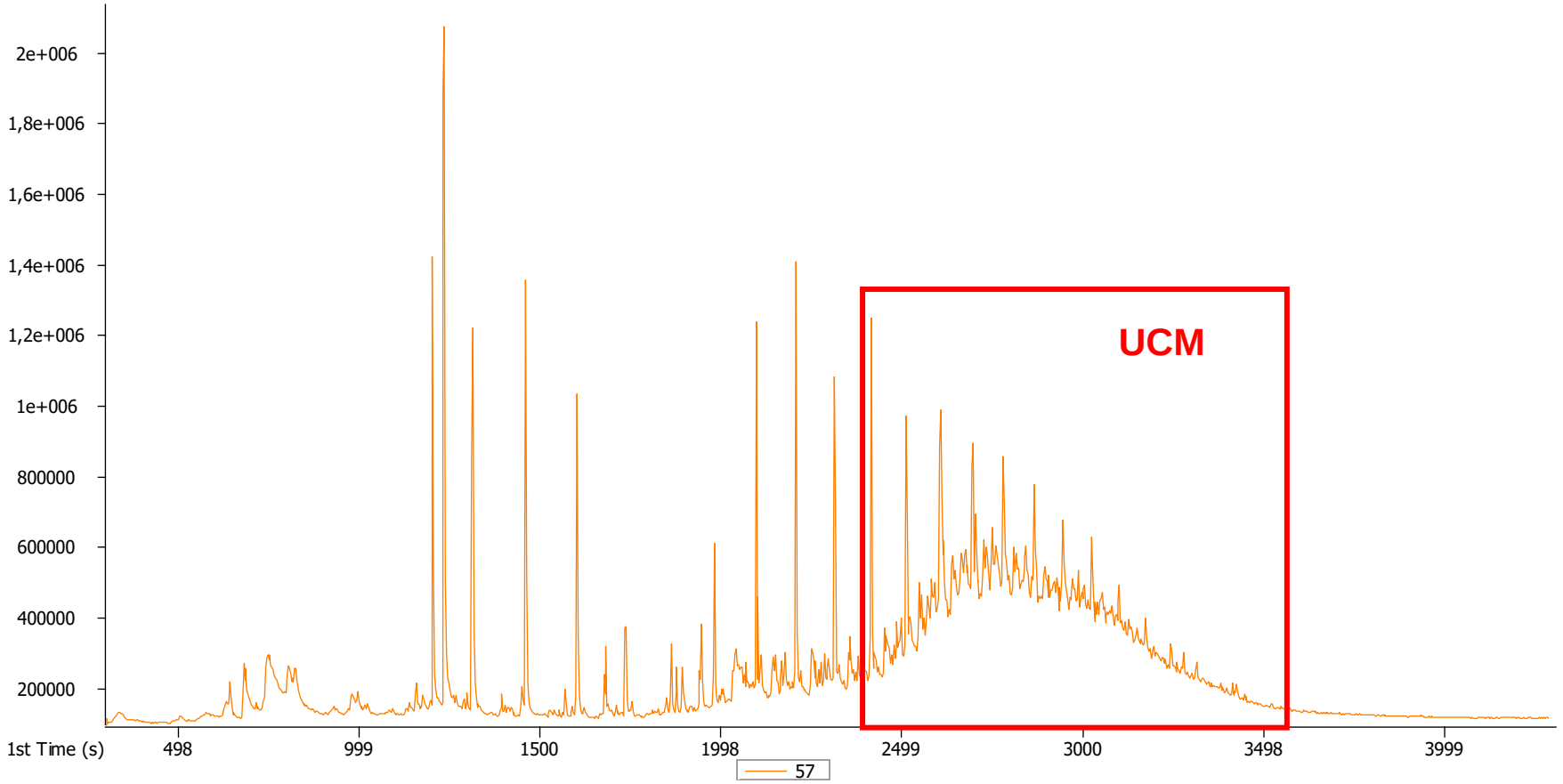

Figure B1 Extracted 1D ion chromatogram (m/z = 57) showing the unresolved complex mixture (UCM) from the analysis of exhaust emissions sampled onto a PDMS trap and speciated using 2D chromatography (SAM10 fuel).
**Sample: SAM PH1CS*

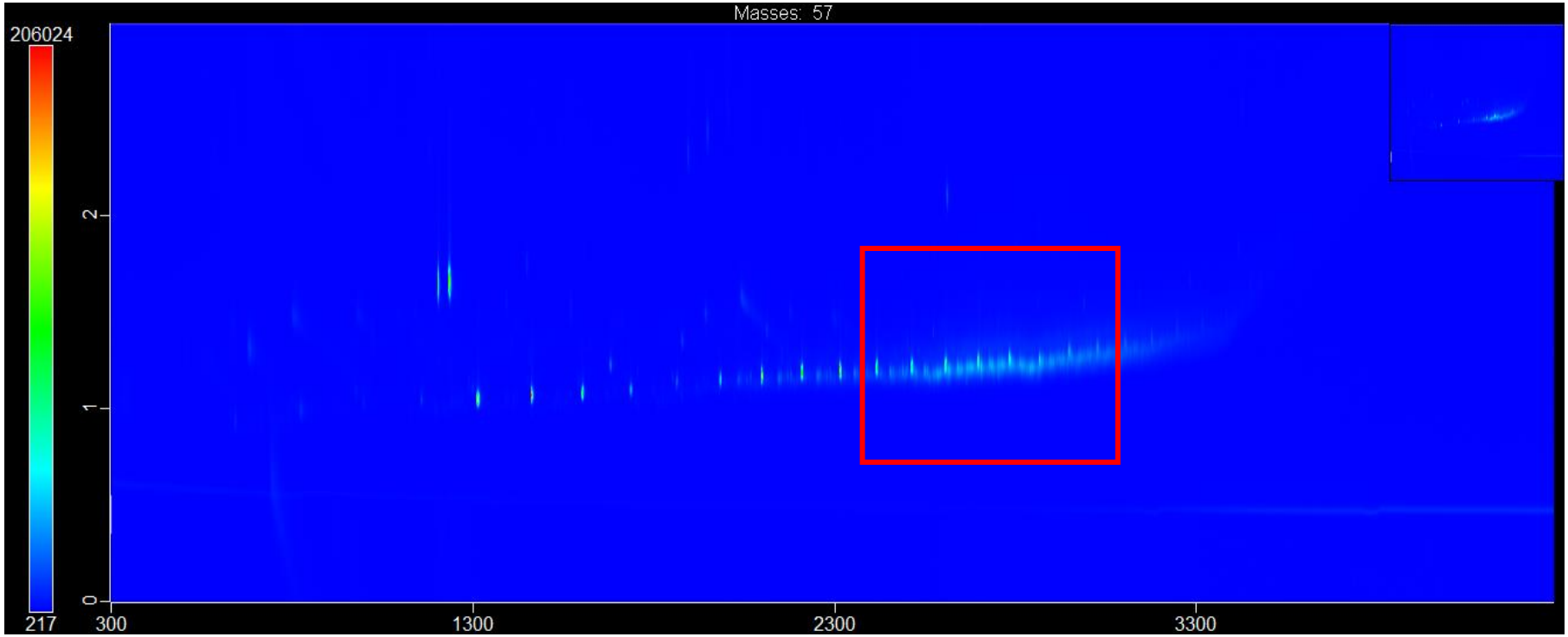

Figure B2 Extracted 2D ion chromatogram (m/z = 57) showing the unresolved complex mixture (UCM) from the analysis of exhaust emissions sampled onto a PDMS trap and speciated using 2D chromatography (SAM10 fuel).
**Sample: SAM PH1CS*

Appendix C: Example sampling information sheet

SAMPLING INFORMATION SHEET

General information

Sampling location	SFAC - Cape Town
Sample name	Cold Start ph1-4 European reference fuel (II)
Sample description	
Date	30/01/2019
Time	10:40

Sampling information

Sampling position	Exit of MOLT mini dilution tunnel after 4-way splitter
Location description	Test cell 5
Trap number & pump used	GR22+GR15 GR23+GR858 GR380+GR GR13+GR16
Pump no	2
Air sampling flow rate	500 mL/mn
Sampling duration	
Dilution ratio	

Conditions at sampling location

Fuel type and specifications European ref fuel	Comments Ph1 0L — 5.061L = 5.06 Ph2 5.061L — 8.453L = 3.392 Ph3 8.453L — 12.243L = 3.79 Ph4 12.243L — 14.932L = 2.689
Height above sea level (m)	
Volumetric ventilation rate (m3/s)	
Air velocity at sampling position (m/s)	
Air velocity (m/s)	
Barometric pressure (kPa) hPa	1013.8
Temparature (°C)	21.4 WB 24.6 °C
Relative humidity (%)	82.9 %

Appendix D: Certificates of analysis

(i) C_8-C_{20} n-alkane standard solution COA

SIGMA-ALDRICH®

3050 Spruce Street, Saint Louis, MO 63103 USA
Email USA: techserv@sial.com Outside USA: eurtechserv@sial.com

Certificate of Analysis

Product Name:	ALKANE STANDARD SOLUTION C_8-C_{20} analytical standard, contains C_8--C_{20}, ~40 mg/L each, in hexane
Product Number:	04070
Batch Number:	BCBS0046V
Brand:	Sigma-Aldrich
CAS Number:	
Formula:	
Formula Weight:	
Quality Release Date:	30 JUN 2016

TEST	SPECIFICATION	RESULT
APPEARANCE (COLOR)	COLORLESS	COLORLESS
APPEARANCE (FORM)	LIQUID	LIQUID
PURITY (GC AREA %)	CONTAINS 13 COMPOUNDS (C8 - C20)	IDENTITY PROOFED, CONTAINS 13 COMPOUNDS (C8 - C20)
DENSITY D20/4	0.659 - 0.661	0.660
REFRACTIVE INDEX N20/D	1.374 - 1.376	1.375

Dr. Claudia Geitner
Manager Quality Control
Buchs, Switzerland

(ii) D_{34}-hexadecane internal standard COA

SIGMA-ALDRICH®

sigma-aldrich.com

3050 Spruce Street, Saint Louis, MO 63103, USA
Website: www.sigmaaldrich.com
Email USA: techserv@sial.com
Outside USA: eurtechserv@sial.com

Certificate of Analysis

Product Name:
Hexadecane-d34 – 98 atom % D

$CD_3(CD_2)_{14}CD_3$

Product Number:	**489603**
Batch Number:	**MBBB9210V**
Brand:	ALDRICH
CAS Number:	15716-08-2
MDL Number:	MFCD00144893
Formula:	C16D34
Formula Weight:	260.65 g/mol
Quality Release Date:	19 AUG 2016

Test	Specification	Result
Appearance (Clarity)	Clear	Clear
Appearance (Color)	Colorless	Colorless
Appearance (Form)	Liquid	Liquid
Purity (GC)	≥ 99 %	99 %
Proton NMR Spectrum	Conforms to Structure	Conforms
D Enrichment	≥ 98	99
Water (by Karl Fischer)	≤ 0.50 %	0.08 %

Greg Abernathy, QC Supervisor
Quality Assurance
Miamisburg, Ohio US

(iii) DHA aromatic standard COA

RESTEK
110 Benner Circle
Bellefonte, PA 16823-8812
Tel: (800)356-1688
Fax: (814)353-1309

www.restek.com

Certificate of Composition

FOR LABORATORY USE ONLY-READ SDS PRIOR TO USE.

This Reference Material is intended for Laboratory Use Only as a standard for the qualitative and/or quantitative determination of the analyte(s) listed.

Catalog No. : 30729 Lot No. : 052731

Description : DHA Aromatics Standard

Container Size : 300 µL Autosampler Vial Pkg Amt : 150 µL

Expiration Date : 12 months unopened* Storage : 4 °C or colder
*From date of shipment.

Manufactured and Tested by : DCG Partnership 1, Ltd.

PEAK #	PEAK TYPE	RET TIME	RT INDEX	ANALYTE	WT, %	MOLE, %	LV, %	SP GR	MOLE WT	BP, °C
1	A6	26.587	654.34	Benzene	8.255	12.408	8.134	0.8846	78.112	80.06
2	A7	41.521	764.00	Toluene	12.342	15.727	12.340	0.8718	92.138	110.61
3	A8	53.708	858.23	Ethylbenzene	8.248	9.121	8.248	0.8717	106.165	136.16
4	A8	54.679	866.27	M-Xylene	3.108	3.437	3.118	0.8688	106.165	139.08
5	A8	54.792	867.19	P-Xylene	1.041	1.151	1.048	0.8656	106.165	138.33
6	A8	57.314	887.28	O-Xylene	3.125	3.456	3.080	0.8845	106.165	144.42
7	A9	60.816	919.95	Isopropylbenzene	2.085	2.037	2.097	0.8666	120.192	152.37
8	A9	63.853	951.46	N-Propylbenzene	3.091	3.019	3.108	0.8670	120.194	159.20
9	A9	64.590	958.85	1-Methyl-3-Ethylbenzene	2.795	2.730	2.800	0.8700	120.194	161.34
10	A9	64.794	960.88	1-Methyl-4-Ethylbenzene	2.070	2.022	2.082	0.8665	120.194	162.01
11	A9	65.328	966.16	1,3,5-Trimethylbenzene	0.422	0.412	0.423	0.8702	120.194	164.74
12	A9	66.385	976.47	1-Methyl-2-Ethylbenzene	1.571	1.535	1.546	0.8857	120.194	165.14
13	A9	67.759	989.59	1,2,4-Trimethylbenzene	2.066	2.018	2.045	0.8807	120.194	169.34
13	A10	67.759	989.59	tert-Butylbenzene	2.058	1.800	2.058	0.8715	134.221	169.11
14	A10	69.214	1004.22	Isobutylbenzene	3.099	2.711	3.148	0.8580	134.221	172.75
15	A10	69.486	1007.55	sec-Butylbenzene	3.090	2.703	3.108	0.8665	134.221	173.29
16	A10	70.339	1017.92	1-Methyl-3-Isopropylbenzene	1.066	0.932	1.073	0.8659	134.221	174.94
17	A10	70.664	1021.84	1-Methyl-4-Isopropylbenzene	4.126	3.609	4.173	0.8618	134.221	177.11
18	A10	71.898	1036.51	1-Methyl-2-Isopropylbenzene	2.806	2.455	2.775	0.8815	134.221	178.32
19	A10	73.003	1049.41	1-Methyl-3-n-Propylbenzene	2.084	1.823	2.098	0.8658	134.221	182.01
20	A10	73.363	1053.56	1-Methyl-4-n-Propylbenzene	2.073	1.813	2.093	0.8633	134.221	183.38
21	A10	73.465	1054.74	N-Butylbenzene	2.077	1.817	2.093	0.8651	134.221	183.26

PEAK #	PEAK TYPE	RET TIME	RT INDEX	ANALYTE	WT, %	MOLE, %	LV, %	SP GR	MOLE WT	BP, °C
22	A10	73.559	1055.82	1,3-Dimethyl-5-Ethylbenzene	0.407	0.356	0.403	0.8807	134.221	183.76
23	A10	74.438	1065.85	1-Methyl-2-n-Propylbenzene	2.148	1.879	2.132	0.8784	134.221	184.93
24	A10	75.257	1075.08	1,4-Dimethyl-2-Ethylbenzene	2.076	1.816	2.049	0.8833	134.221	186.74
25	A10	75.948	1082.76	1,2-Dimethyl-4-Ethylbenzene	0.915	0.800	0.907	0.8792	134.221	189.48
26	A10	77.757	1103.19	1,2-Dimethyl-3-Ethylbenzene	2.152	1.882	2.091	0.8970	134.221	193.91
26	A10	77.757	1103.19	1,3-Dimethyl-2-Ethylbenzene	0.799	0.699	0.778	0.8953	134.221	190.01
27	A10	78.674	1115.43	1,2,4,5-Tetramethylbenzene	0.860	0.752	0.843	0.8895	134.221	196.86
28	A11	78.803	1117.13	2-Methylbutylbenzene	0.118	0.093	0.119	0.8639	148.248	196.11
29	A11	80.130	1134.55	tert-1-Butyl-2-Methylbenzene	2.077	1.645	2.091	0.8660	148.248	200.41
30	A11	81.834	1156.45	Pentylbenzene	2.058	1.630	2.078	0.8633	148.248	205.49
31	A12	83.782	1180.87	tert-1-Butyl-4-Ethylbenzene	2.076	1.502	2.102	0.8610	162.740	206.11
32	A12	86.584	1217.85	1,3,5-Triethylbenzene	2.087	1.510	2.101	0.8659	162.740	215.78
33	A12	88.061	1238.75	1,2,4-Triethylbenzene	1.014	0.734	1.006	0.8788	162.740	219.00
34	A12	89.587	1259.93	Hexylbenzene	5.155	3.730	5.212	0.8622	162.740	226.01
35	A13	94.075	1323.33	tert-1-Butyl-3,4,5-Trimethylbenzene	3.355	2.234	3.401	0.8600	176.300	236.40

IMPORTANT NOTE: RETENTION TIMES VALID ONLY FOR SPECIFIED CONDITIONS.

All chromatograms generated under the following conditions.

Gas Chromatograph:	Agilent 6890 Capillary GC	
Carrier Gas:	Helium Inlet Pressure: 33.7 psig	
Injector:	Temperature at 250° C	
Detector:	FID with a temperature of 250 ° C	
	Hydrogen flow:	40 cc/min
	Oxidant flow:	Air at 450 cc/min
	Makeup gas:	Nitrogen at 10 cc/min
Split Ratio:	300:1	
Column:	Rtx®-5 DHA Tuning Column, 5m x 0.25mm x 1.00µm film (cat.# 10165) Rtx®-DHA-100, 100m x 0.25m x 0.5µm film (cat.# 10148)	
Temperature Program:	Initial Temperature:	35 ° C for 5 minutes
	Ramp 1:	1.5 ° C to 50 ° C
	Hold 1:	5 minutes
	Ramp 2:	2.0 ° C to 200 ° C
	Hold 2:	20 minutes
	Total Run Time:	125 minutes
Sample Size:	Syringe Injection DHA 1uL	

IMPORTANT NOTE: RETENTION ORDER AND TIMES ARE VALID FOR THESE CONDITIONS ONLY.

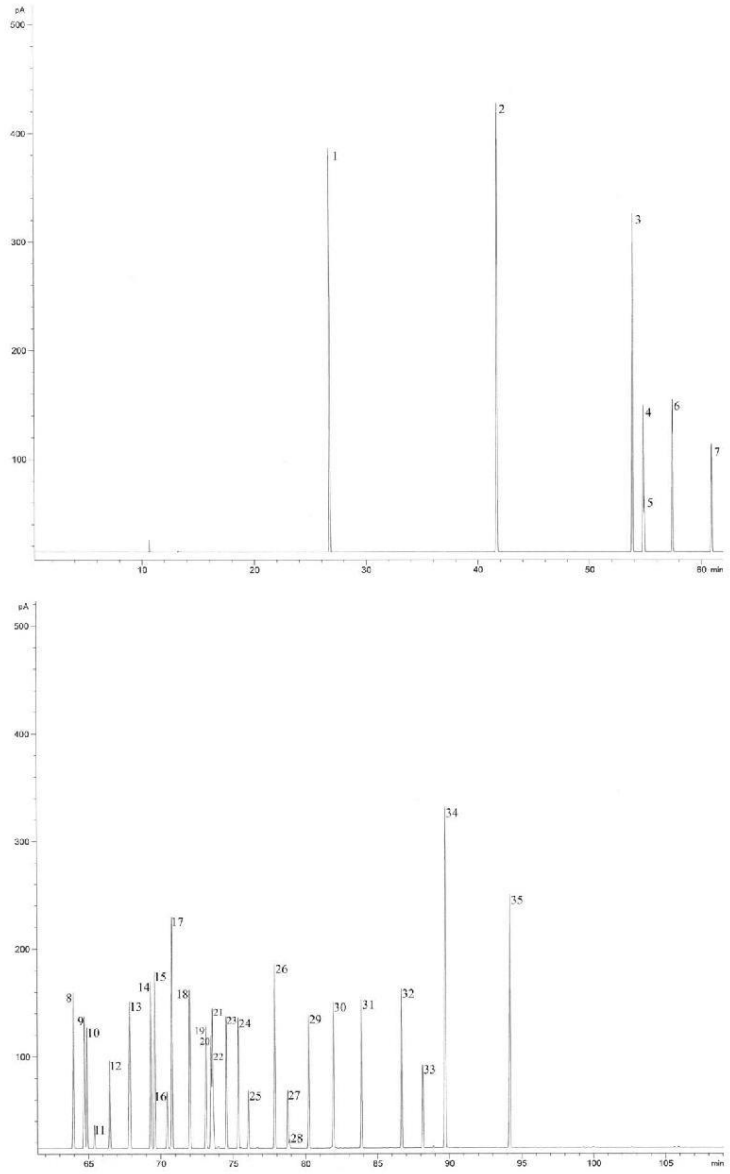
pA
500
400
300
200
100
1
2
3
4
5
6
7
10
20
30
40
50
60 min
pA
500
400
300
200
100
8
9
10
11
12
13
14
15
16
17
18
19
20
21
22
23
24
25
26
27
28
29
30
31
32
33
34
35
65
70
75
80
85
90
95
100
105
min

Appendix E: Calibration curves for PDMS trap

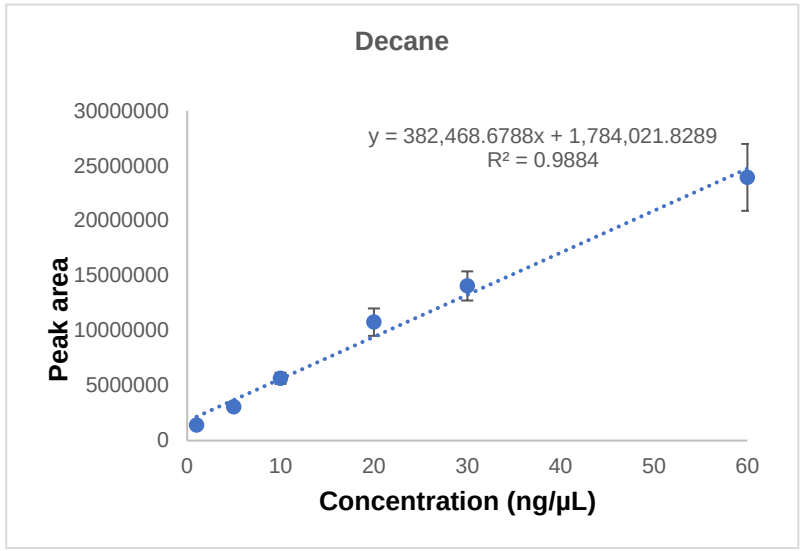

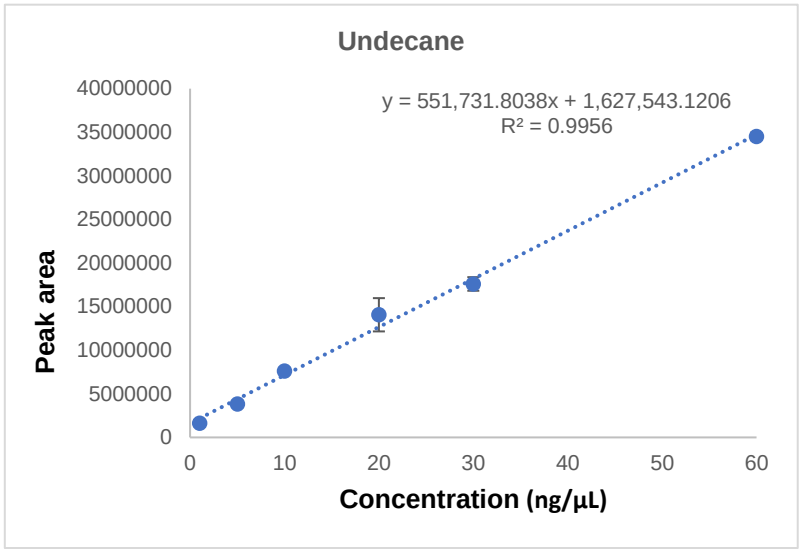

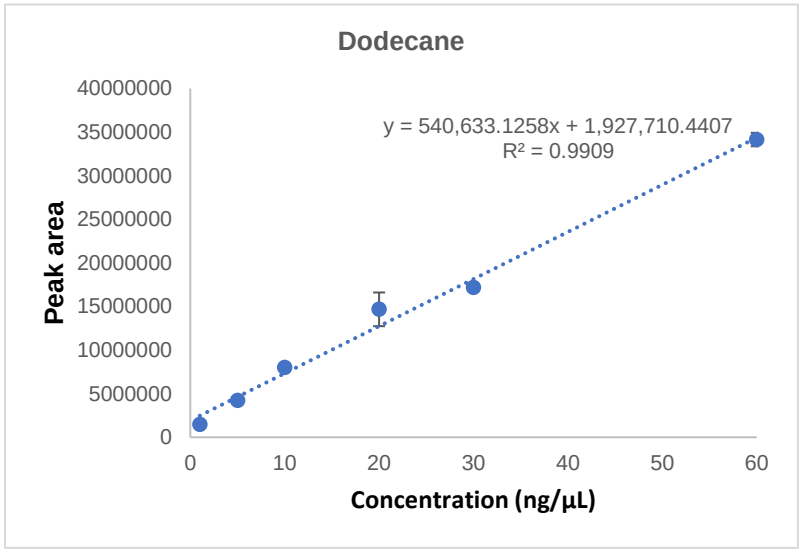

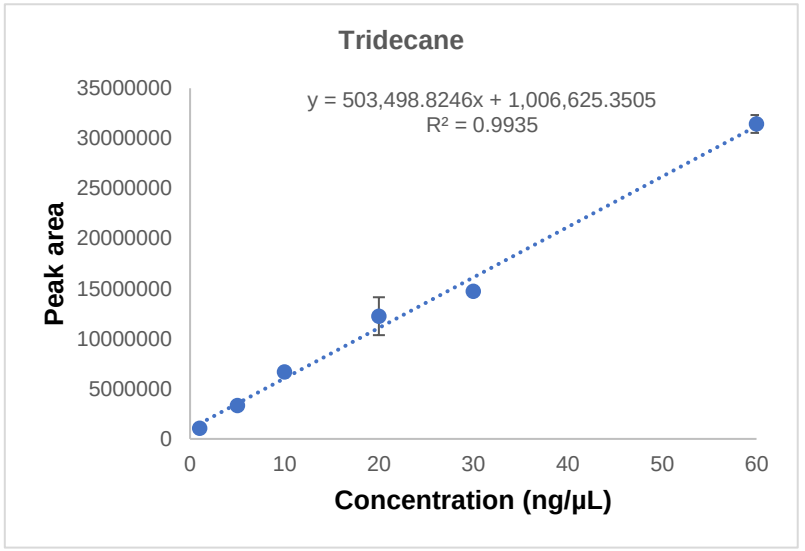

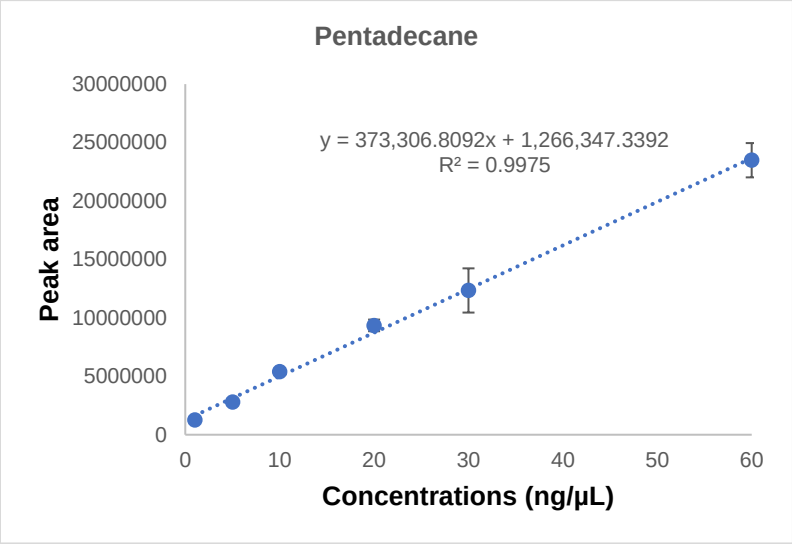
Pentadecane
y = 373,306.8092x + 1,266,347.3392
R² = 0.9975
Peak area
Concentrations (ng/µL)
30000000
25000000
20000000
15000000
10000000
5000000
0
0
10
20
30
40
50
60

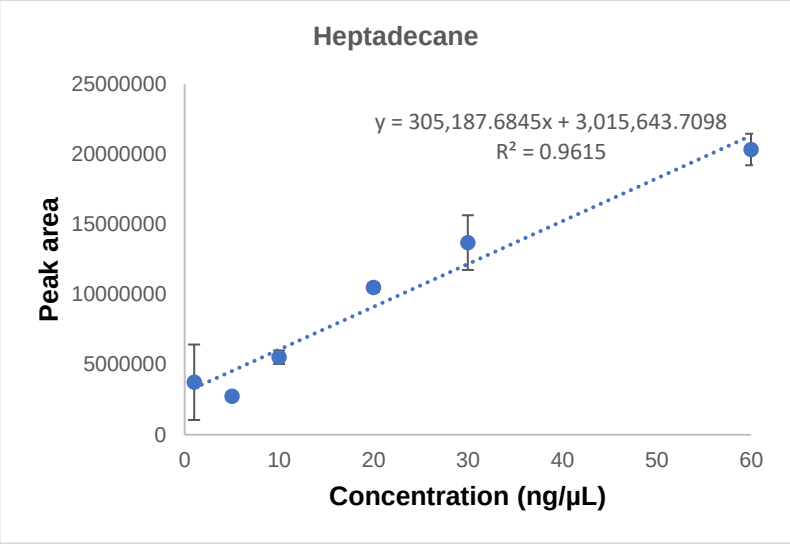
Heptadecane
y = 305,187.6845x + 3,015,643.7098
R² = 0.9615
Peak area
Concentration (ng/µL)
25000000
20000000
15000000
10000000
5000000
0
0
10
20
30
40
50
60

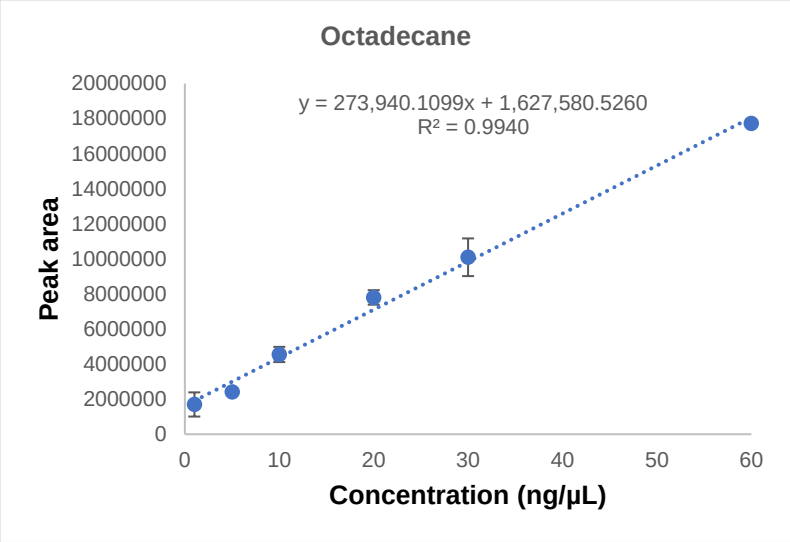
Octadecane
y = 273,940.1099x + 1,627,580.5260
R² = 0.9940
Peak area
Concentration (ng/µL)
20000000
18000000
16000000
14000000
12000000
10000000
8000000
6000000
4000000
2000000
0
0
10
20
30
40
50
60

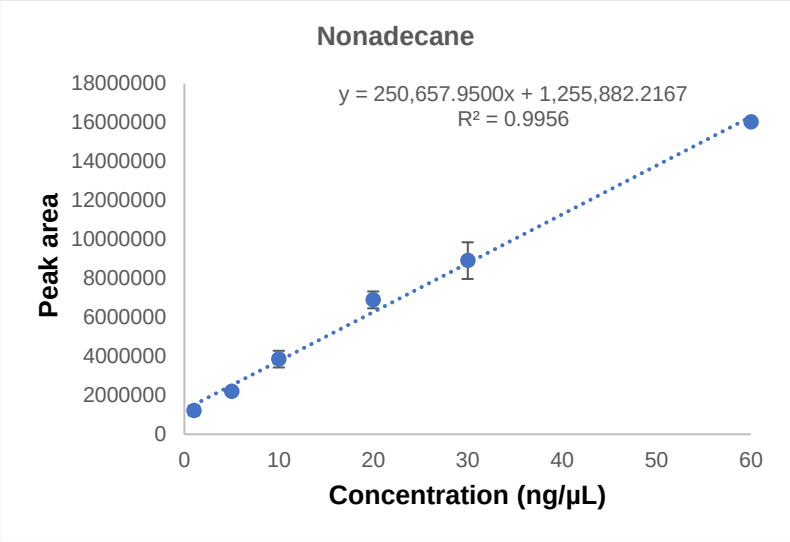
Nonadecane
y = 250,657.9500x + 1,255,882.2167
R² = 0.9956
Peak area
Concentration (ng/µL)
18000000
16000000
14000000
12000000
10000000
8000000
6000000
4000000
2000000
0
0
10
20
30
40
50
60

Appendix F: Poster presentation

Hydrocarbon emissions from diesel engines under different load conditions

AS Mahlangu[1], G Schoonraad[1,2], P Schaberg[3], MC Wattrus[3], C Munyeza[1], C Pretorius[4], PBC Forbes[1]

[1] Department of Chemistry, Faculty of Natural and Agricultural Sciences, University of Pretoria, Pretoria 0002, South Africa.

[2] Processing Laboratory, Impala Platinum Ltd, 123 Bethlehem Drive, Rustenburg 0299, South Africa.

[3] Sasol, Sasol Fuels Application Centre, Bridge Place, Capricorn Park, Cape Town, 7945, South Africa.

[4] Council for Scientific and Industrial Research (CSIR), Meiring Naude Road, Pretoria 0001, South Africa.

UNIVERSITEIT VAN PRETORIA
UNIVERSITY OF PRETORIA
YUNIBESITHI YA PRETORIA

sasol

Introduction

Photochemical smog pollution is produced in the atmosphere from the reaction of nitrogen oxides (NOx) and volatile organic compounds (VOCs), in the presence of ultraviolet sunlight. This complex process occurs in the lower atmosphere (troposphere) and results in the formation of particulate ozone (O_3), the principal component associated with photochemical smog [1]. Hydrocarbons (HCs) are key precursors to photochemical ozone. Studies show that while short-chain HCs are easier to characterise and have been successfully reduced in many developed cities, longer chain HCs, most likely arising from diesel exhaust emissions, are typically not considered as part of air quality strategies [2]. This is mainly due to difficulties in quantitative collection and chemical analysis of these species. During emission speciation studies, these compounds are thus often grouped as an unresolved complex mixture of co-eluting compounds and their contribution to quantitative results is often merely estimated.

In order to circumvent this problem, a method to characterise semi-volatile organic compounds (SVOCs), particularly those emitted by automobile exhaust engines, is required. We therefore conducted an emissions monitoring campaign at a controlled engine test facility to collect and characterise the exhaust emissions from a diesel test engine. HCs from three chemical classes (alkenes, aromatic alkanes and n-alkanes) were successfully characterised. The ozone formation potential of these hydrocarbons was estimated by assigning maximum incremental reactivity (MIR) factors to each compound. MIR factors were developed by Carter [3], and give the impact of each compound on the peak ozone concentration in a system where ozone is being formed under high NOx concentrations, and is most sensitive to hydrocarbon emissions.

Experimental

The exhaust emissions of a Euro 2 compliant 1.6 L Polo TDI test engine, fuelled with a fully synthetic ultra-low sulphur (ULS) diesel fuel were sampled using portable denuder devices [4]. The denuders consisted of 2 multi-channel rubber traps made up of 22 polydimethylsiloxane (PDMS) tubes for collection of the gas phase analytes, and a quartz fibre filter sandwiched between the two traps for collection of particulate matter. (Fig 1). During sampling, one end of the denuder was attached to a battery operated pump, sampling at 500 mL/min for 10 minutes to obtain a total sampling volume of 5 L. An electronic control unit was used to operate the test engine in 5 different operational modes, representing varying torque (power) conditions, including high idle mode. Exhaust emission sampling was done at a distance of 0.3 m from the tailpipe, parallel to the exhaust flow.

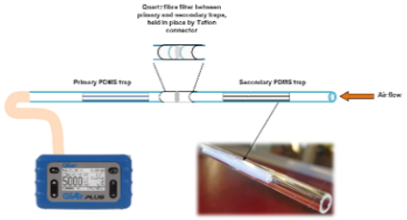

Fig 1: Schematic diagram showing the denuder setup employed during exhaust emission sampling. The bottom right image shows the PDMS trap in more detail.

Thermal desorption coupled with comprehensive gas chromatography–time of flight mass spectrometry (TD–GC × GC–TofMS) was used for sample analysis (Fig 2). Separation was achieved by a Restek Rxi-1MS nonpolar phase 100 % dimethyl polysiloxane column in the first dimension and a Rxi-17Sil MS, midpolar 5 % phenyl 95 % methylsiloxane column in the second dimension. The primary and secondary traps were desorbed directly, while each quartz fibre filter was placed into a clean glass tube and inserted into the thermal desorber such that the end containing the filter was within the heated zone.

Fig 2: Gerstel 3 thermal desorber (a) coupled to a LECO Pegasus 4D GC × GC–TofMS instrument (b).

Identification of n-alkane hydrocarbons was achieved by matching the retention times to those of authentic reference standards as well as mass spectral matching using the NIST MS Search 2.2 mass spectral library (match quality > 80 %).

Results and Discussion

We identified HCs in the samples obtained from sampling the diesel exhaust emissions at high idle mode. Alkanes from octane (n-C8) through to eicosane (n-C20) were found, with lower mass hydrocarbons predominantly present in the traps (Fig 3). A region of high mass compounds beyond n-C20 was seen in most of the samples on both the traps and filters, however was seen at greater intensities on the filters . The compounds found in this region were a series of branched alkanes and were speculated to be arising from lubricant oil due to their high carbon numbers.

The presence of hydrocarbons from other chemical classes that have been shown to contribute to the ozone formation of diesel fuel was also investigated. These compounds were identified by mass spectral matching to the NIST MS Search 2.2 mass spectral library only. Most of the hydrocarbons found, were aromatic hydrocarbons, however alkenes were also seen. All identified hydrocarbons and their MIR factors are listed in Table 1. According to these results, the major contributor to the ozone formation potential of diesel emissions are aromatic compounds with an MIR range of 2.03 – 11.97 g O_3 / g VOC. Alkenes are the second highest contributors with an MIR range of 1.64 – 4.55 g O_3 / g VOC. The n-alkane hydrocarbons seemed to have the least contribution with MIR values < 1 O_3 / g VOC.

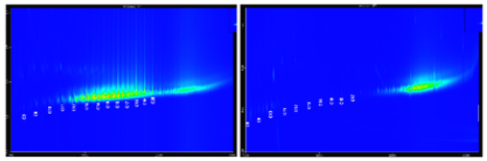

Fig 3: Extracted ion 2D chromatograms (m/z = 57) showing the aliphatic hydrocarbon region from analysis of the gaseous HCs on the primary trap (left) and particle associated HCs on the quartz fibre filter (right) used to sample the diesel engine emissions at high idle.

Table 1: Hydrocarbons identified on the trap and filter used to sample the diesel engine emissions at high idle and their Maximum Incremental Reactivity factors

Hydrocarbon name	% Match	MIR factor (g O_3 / g VOC)	Hydrocarbon name	% Match	MIR factor (g O_3 / g VOC)
Alkanes			Aromatic compounds		
Octane (n-C8)	92	0.90	Ethyl-benzene	97	3.04
Nonane (n-C9)	92	0.78	N-propylbenzene	92	2.03
Decane (n-C10)	95	0.68	N-hexylbenzene	87	4.39
Undecane (n-C11)	96	0.61	Toluene	90	4.00
Dodecane (n-C12)	96	0.55	o-xylene	97	7.64
Tridecane (n-C13)	93	0.50	m-xylene	92	9.75
Tetradecane (n-C14)	95	0.51	p-xylene	97	6.54
Pentadecane (n-C15)	91	0.52	o-ethyltoluene	92	6.59
Hexadecane (n-C16)	91	0.45	m-ethyltoluene	95	7.30
Heptadecane (n-C17)	92	0.42	p-ethyltoluene	81	4.44
Octadecane (n-C18)	94	0.40	Indane	93	3.39
Nonadecane (n-C19)	90	0.38	1,2,3-trimethylbenzene	91	11.97
Eicosane (n-C20)	95	0.36	1,2,4-trimethylbenzene	92	8.87
Alkenes					
Decene	94	2.17			
Undecene	87	1.87			
Dodecene	84	1.64			
Styrene	96	1.73			
Limonene	86	4.55			

Conclusions and Future Work.

- Semi volatile alkenes, n-alkanes and aromatic hydrocarbons were successfully identified in the diesel exhaust samples.
- The MIR factors of the hydrocarbons identified ranged from 0.36-11.97 O3 / g VOC where aromatics > alkenes > n-alkanes.
- The successful use of denuders as well as TD–GC × GC–TofMS illustrates the suitability of these analytical techniques for quantitative collection and analysis of SVOCs. The use of denuder samplers provides an inexpensive, efficient and easy sampling method for use in various air monitoring applications and allows for simultaneous sampling of gas and particle phase SVOCs.
- Full characterisation and quantitation of diesel exhaust emissions from different fuels is still needed to gain a full understanding of the contribution of diesel fuel to photochemical smog formation.

Acknowledgements

The Sasol Fuels Application Centre (SFAC) is acknowledged for their collaboration on the project and resources provided. Financial support from Sasol and the National Research Foundation (NRF) is highly appreciated. Attendance at this conference was funded by the Anatech Instruments Students Sponsorship Program

References

1. Whitten G. The chemistry of smog formation: A review of current knowledge. *Environment International*. 1983;9(6):447-63.
2. Dunmore R, Hopkins J, Lidster R, Lee J, Evans M, Rickard A, et al. Diesel-related hydrocarbons can dominate gas phase reactive carbon in megacities. *Atmospheric Chemistry and Physics*. 2015;15(17):9983-96.
3. Carter W. Updated maximum incremental reactivity scale and hydrocarbon bin reactivities for regulatory applications. Prepared for California Air Resources Board Contract 07-339. College of Engineering, Center for Environmental Research and Technology, University of California, Riverside, California. 2010.
4. Forbes PB, Rohwer ER, Nshenda SA, Zimmermann R, Geldenhuys GJ. Characterisation of atmospheric semi-

Appendix G: Publication

Research article
Characterisation of semi-volatile hydrocarbon emissions from diesel engines

Amanda S. Mahlangu[1], Paul W. Schaberg[2], Mark C. Wattrus[2], Patricia B.C. Forbes[1*]

[1]Department of Chemistry, Faculty of Natural and Agricultural Sciences, University of Pretoria, Pretoria 0002, South Africa, Email: patricia.forbes@up.ac.za, Email: amanda.mahlangu85@gmail.com

[2]Sasol Energy, Sasol Fuels Application Centre, Bridge Place, Capricorn Park, Cape Town, 7945, South Africa

Received: 26 November 2019 - **Reviewed:** 16 January 2020 - **Accepted:** 13 February 2020

https://doi.org/10.17159/caj/2020/30/1.7672

Abstract

Exhaust emissions from diesel vehicles have recently been receiving global attention, due to potential human health effects associated with exposure to emitted pollutants. In addition, a link has recently been established between unburnt hydrocarbon (HC) emissions from diesel engines and photochemical smog. Despite being present at very low concentrations in the exhaust, these HCs may act as precursors in the formation of photochemical smog pollution. While short-chain HCs are easier to characterise and have been successfully reduced in many developed cities, longer chain HCs, most likely arising from diesel exhaust emissions, have been poorly quantified to date, and a limited range of HCs from this source has been studied. In this study, transient cycle tests were conducted to collect exhaust emissions from a Euro 3 compliant, 1.6 L test engine fuelled with three diesel fuels; a highly paraffinic fuel, a South African market fuel and a European reference fuel. Portable denuder samplers were used to collect the emissions and analysis was done by thermal desorption-comprehensive 2D gas chromatography-time of flight mass spectrometry (TD-GC x GC-TofMS). The South African market diesel had the greatest n-alkane emissions, with greater emissions observed in the earlier phases (low and medium phase) of the WLTC test cycle. The total n-alkane emissions for this fuel ranged from 34.80 mg/km - 282.67 mg/km from the low to the extra-high phase. The paraffinic diesel had the second highest n-alkane emissions with the total emissions ranging from 35.43 mg/km – 164.99 mg/km. The European reference diesel had the lowest n-alkane emissions amongst the three fuels, with the total emissions ranging from 22.46 mg/km – 82.56 mg/km. Substituted alkyl-benzenes were also detected in the gas phase emissions from each fuel, however only semi-quantitative analysis of these compounds was conducted. The results showed that long-chain HCs were present at easily detectable concentrations in diesel engine exhaust emissions, which is critical in understanding their contribution to photochemical ozone and informing appropriate mitigation and management strategies.

Keywords

Photochemical smog, hydrocarbons, ozone, diesel exhaust emissions, ozone formation potential, emission factor

Introduction

Exhaust fumes from vehicular emissions are one of the biggest contributors to pollution of the ambient atmosphere, which could be of great concern for South Africa's agricultural sector and in urban environments. Photochemical smog is produced in the atmosphere from the reaction of nitrogen oxides (NO_x) and volatile organic compounds (VOCs), in the presence of ultraviolet sunlight. This complex process occurs in the lower atmosphere (troposphere) and results in the formation of photochemical ozone (O_3), the principal component associated with photochemical smog. The Southern African region is characterised by numerous sources of ozone-forming compounds and presents ideal environmental conditions for O_3 formation. The most significant pollutants from vehicular emissions include nitrogen oxides (NO_x) and HCs which are key precursors to photochemical smog formation. Whilst both diesel and petrol engines contribute to NO_x emissions, until recently the latter was thought to be the primary source of HC emissions in the atmosphere. Characterisation studies on airborne organic compounds in the USA show that there is a significant contribution of semi-volatile organic compounds (SVOCs) emanating from diesel exhaust, to the atmosphere's non-methane organic gas (NMOG) load (Jathar et al., 2014). Gaseous diesel exhaust HCs are composed predominantly of alkanes (straight, branched and cycloalkanes), aromatics (alkyl-benzenes and 2-5 ring polycyclic aromatic hydrocarbons) and alkenes (Gentner et al., 2012, Storey et al., 1999). Although the South African vehicle fleet is dominated by petrol cars, the National Association of Automobile Manufacturers of South Africa (NAAMSA) has reported a steady increase in the popularity of diesel engine models over recent years (Energy, 2017).

SVOCs are described as compounds with an effective saturation concentration (C*) of 0.1 µg m^{-3} – 1000 µg m^{-3} which corresponds to a vapour pressure range of 10^{-8}-10^{-2} Torr (Robinson et al., 2007). These compounds tend to partition between the particulate and gaseous phases at high atmospheric dilution, and thus may participate in gas phase photochemical reactions.

Numerous studies have reported that long term exposure to PM emissions may cause cardiovascular and respiratory diseases, whilst the organic compounds adsorbed onto the surface of PM are toxic and carcinogenic (Reşitoğlu et al., 2015, Kagawa, 2002, Wichmann, 2007). The detrimental health and environmental impacts of photochemical O_3 such as eye irritation, a decline in respiratory function, reduced visibility and damage to crops and vegetation (Laban et al., 2018) has also been reported in literature. According to the South African National Ambient Air Quality Standards for Criteria pollutants (2009 and 2012), the 8-hourly running average standard for O_3 is 120 µg/m^3 (61 ppb), however numerous exceedances have been observed in various regions in South Africa. A study by Zunckel et al. monitored surface ozone outside urban areas in Southern Africa and found that the highest O_3 concentrations were over Botswana and the Mpumalanga Highveld (Zunckel et al., 2004). Both regions had highs between 40 and 60 ppb, however the average concentration in October 2000 was greater than 90 ppb. Gautam et al. speciated diesel exhaust emissions under steady state conditions (Gautam et al., 1996). The ozone formation potential (OFP) of speciated alkyl-benzenes ranged from 0.406 - 0.767 mg O_3/bhp-hr for ethylbenzene and 1,2,4-trimethylbenzene respectively and OFP values of 0.119 mg/bhp-hr and 0.018 mg/bhp-hr were reported for octane and nonane respectively, where bhp-hr is brake horsepower-hour. In another study by Olumayede, the contribution of individual VOCs to photochemical ozone formation in Southern Nigeria was studied (Olumayede, 2014). The following photochemical O_3 formation potentials were reported: 25.7 µg/m^3 for m,p-xylene, 11.02 µg/m^3 for ethylbenzene, 26.43 µg/m^3 for undecane, 18.85 µg/m^3 for 1,2,4-trimethylbenzene and 12.27 µg/m^3 for toluene. It is evident that the contribution of different HC species to O_3 formation varies within chemical classes and between HCs of different classes.

Detailed mechanisms underlying the photochemical conversion of precursor compounds to photochemical ozone have not been elucidated, however, the key elements can be explained using generalized reaction mechanisms. Smog chamber irradiation studies have also been conducted to investigate ozone formation as a function of the initial concentration of its precursors. These studies show that reducing HC and NO_x concentrations simultaneously leads to a decrease in O_3, however, this is less than the decrease observed from HC reduction alone (Glasson, 1981). Thus historically it has been known that by controlling HC levels in the atmosphere, O_3 reduction could be achieved in urban areas (Glasson, 1981). In recent years, VOC emissions have been successfully quantified and reduced in many developed cities, however, research shows that longer chain HCs are typically not considered as part of air quality control strategies. A study was conducted using high resolution measurements to investigate the abundance of diesel related HCs in the atmosphere at an urban background site in London and a comparison of these results to the emission inventory data showed that there is a drastic underestimation of the impact of diesel related emissions on urban air quality (Dunmore et al., 2015).

The challenge faced when characterising SVOCs stems from difficulties in quantitative collection and chemical analysis of these species. Traditional sampling methods for gaseous-particulate phase analytes employ high volume samplers that make use of a glass fibre filter that removes particles from the sample flow, and an adsorbent such as Tenax or polyurethane foam (PUF), to adsorb the gas phase analytes downstream of the filter (Geldenhuys et al., 2015). Although such high volume samplers are robust and easy to use in the field, they exhibit inherent limitations due to the sampling configuration and high volumetric flow rate (Forbes and Rohwer, 2015). Another commonly used sampling method, particularly when conducting engine tests, is collection of dilute exhaust emissions into Tedlar® bags from a constant volume sampler (CVS) and subsequent analysis of emissions by gas chromatography-mass spectrometry (GC-MS). This sampling method is adequate for sampling of VOCs, however, heavier compounds tend to condense on the walls of the sampling bags, which results in errors during quantitative analyses (Newkirk et al., 1993).

Denudation, a sampling technique that has been used extensively for air monitoring applications, eliminates two major limitations suffered by high volume samplers. By removing SVOC gas phase analytes prior to downstream collection of the particulate matter, it prevents adsorption of the gas phase analytes onto particulate matter collected on the filter or onto the filter medium itself. The second artefact relates to volatilisation of the particle phase analyte from the filter. During denudation, a second gas phase sampling device is placed downstream of the filter, which collects any “blow-off” from the filter (Forbes and Rohwer, 2015). Furthermore, denuders allow for collection of diluted exhaust samples, without the need to collect large volumes of samples, as analytes are stripped from the air sample and pre-concentrated onto the sorbent, which later may be extracted or introduced directly into the analytical instrument during analysis.

In this study, an emissions monitoring campaign was conducted to collect and characterise diesel exhaust emissions from a diesel test engine which is a popular model for the passenger car fleet on South African roads. Simulated vehicle exhaust emission testing was conducted at a controlled engine test cell facility using a standard emission test cycle. Cold-start emission tests were performed for three different fuels. Simultaneous sampling of gaseous and particulate exhaust emissions was achieved by using denuder sampling devices with thermal desorption-comprehensive two dimensional gas chromatography-time of flight mass spectrometry (TD-GC x GC-TofMS) analysis. Here we report on these gas phase n-alkane and aromatic hydrocarbon

diesel emissions and their related ozone formation potentials which can be estimated by assigning maximum incremental reactivity (MIR) indices to each compound.

Experimental

Test engine and Test fuels

Simulated vehicle emissions testing was conducted in a test cell (Fig 1) with a Euro 3 compliant, 1.6 L test engine, which was fitted with a close-coupled diesel oxidation catalyst (DOC).

Figure 1: *Test cell setup*

The engine had completed ~137 hours of running on the test bed, under varied operating conditions. A complete set of diagnostic checks were carried out on the engine before testing commenced to ensure that it was performing according to specification. The test engine was coupled to an electrical engine dynamometer which uses a mathematical model to simulate engine operation during emissions testing. Figure 1 shows the test cell setup. Three diesel fuels were selected for testing: a highly paraffinic diesel fuel complying with the European EN15940 specification (PAR10), a South African market fuel complying with the South African SANS 342 specification (SAM10), and a reference fuel complying with the European EN590 specification (EUR10). All of the fuels contained less than 10 ppm sulphur, and were chosen because of their distinct compositional characteristics. The dynamometer details and fuel specifications are listed in Table 1 and Table 2 respectively.

Table 1: *Dynamometer details*

Make and model	Horiba Dynas3 LI350
Rated power and torque	350 kW, 750 Nm
Control system	Horiba SPARC controller and Horiba STARS test automation system

Test cycle

The World Harmonized Light vehicle Test Cycle (WLTC) was used for emissions testing. Figure 2 illustrates a typical speed profile of this test cycle. It consists of four characteristic speed phases (low, medium, high and extra high), and emissions from each phase were collected onto separate samplers.

Table 2: *Fuel properties and composition*

Analysis	Method	Sasol 10ppm	EN590	GTL
Sulfur, mg/kg	ASTM D5453	5	<1	<1
Density, kg/l @ 20 °C	ASTM D4052	0.8163	0.8328	0.7650
Flash Point, °C	ASTM D93	63.9	83.0	57.0
Distillation, °C				
Initial Boiling Point	ASTM D86	176.8	193.1	150.6
5%		187.0	207.1	173.9
10%		192.4	218.1	184.3
50%		232.8	277.0	262.8
90%		333.5	333.0	338.6
95%		368.2	347.9	352.4
Final Boiling Point		389.1	355.6	356.7
Cetane number	ASTM D6890	49.7	53.8	80.0
Viscosity, cSt @ 40°C	ASTM D445/D7042	2.06	2.79	2.20
N-paraffins	GC X GC (mass %)	24.5	9.4	51.9
Branched paraffins		24.1	39.9	47.7
Monocyclic Paraffins		14.0	16.8	0.2
Bi-and polycyclic paraffins		9.2	4.7	0.2
Alkyl benzenes		10.9	13.2	0.0
Cyclic alkylbenzenes		14.9	9.1	0.0
Bi- and polycyclic aromatics		2.3	6.9	0.0
Sum		99.9	100.0	100.0

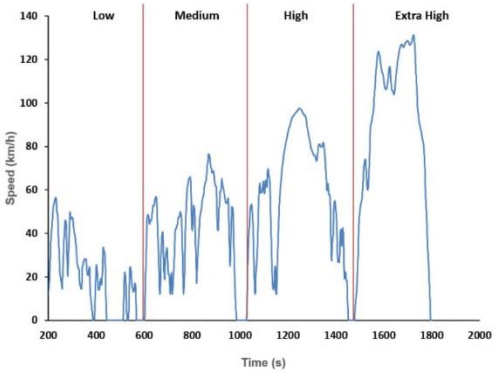

Figure 2: *Speed profile of the WLTC test cycle used during emissions testing.*

Emissions sampling and instrumental analysis

Exhaust gas was drawn directly from the engine's exhaust pipe and fed into a mini dilution tunnel (Horiba MDLT-1303T). The diluted exhaust was sampled onto denuder samplers consisting of a quartz fibre filter sandwiched between two multi-channel polydimethylsiloxane (PDMS) traps (Forbes et al., 2012) via a four-way flow splitter at the exit of the dilution system. Portable sampling pumps (GilAir plus, Sensidyne) were used to draw the diluted exhaust through the denuders at a sampling rate of 500 mL/min. Samples were collected in duplicate for each fuel after which the test fuel was changed.

During fuel change-over the fuel supply system was flushed with approximately 10 litres of the new fuel to remove the remaining old fuel. This was then followed by a 60 min run where the engine was operated at mid-load conditions (50% of full load), at 2500 rpm for an hour. The engine was then pre-conditioned with the new fuel by running the test cycle once, followed by a 20 min run at mid-load conditions, at 2500 rpm once again. The engine was then shut down, and left un-operated overnight, allowing it to stabilize to ambient temperature.

After sampling, each PDMS trap was end capped, wrapped in Al foil and each quartz fibre filter was placed in a clean amber vial. Samples were placed in zip lock bags and refrigerated at -18 °C until analysis using a LECO Pegasus 4D TD-GC x GC-TofMS system with an internal standard mix containing hexadecane-d34, naphthalene-d8 and phenanthrene-d10 in hexane.

Hydrocarbon speciation

Identification of target aromatic and alkane HCs was achieved by matching retention times to those of authentic reference standards (C8-C20 n-alkane standard from Sigma-Aldrich and DHA-aromatic standard from Restek) and calculated retention indices, as well as mass spectral matching using the NIST MS search mass spectral library. Quantitation of n-alkane HCs was achieved by linear regression analysis. Six concentrations (1, 5, 10, 20, 30 and 60 ng/µL) of the C8-C20 alkane standard mix were prepared in hexane (99%, Sigma-Aldrich) and each standard was spiked onto a pre-conditioned trap and analysed in duplicate on the TD-GC x GC-TofMS.

To calculate the emission factor (ng/km) of each n-alkane the mass obtained from calibration (ng) was corrected using dilution factors which were measured continuously during emissions testing.

Results and Discussion

N-alkane gas phase emissions

Transient cycle tests were performed for all three fuels from a cold engine start, over each phase of the WLTC test. Figure 3 shows the relative n-alkane emission factors of each fuel for each phase of the WLTC cycle. The SAM10 diesel had the greatest n-alkane emissions with greater emissions observed in the low phase of the WLTC cycle, and PAR10 diesel had the second highest n-alkane emissions. The EUR10 diesel had the lowest n-alkane emissions amongst the three fuels which may be attributed to its low n-paraffin fuel content, and, potentially its lower volatility. Although PAR10 diesel has the highest n-paraffin fuel content, it had lower n-alkane emissions than the SAM10 diesel. This could be as a result of the high cetane number of this fuel compared to that of the SAM10 fuel. A higher cetane number means the fuel ignites easily which results in better fuel combustion and thus reduction of harmful emissions from unburnt HCs (Ladommatos et al., 1996). A correlation between HC emissions and cetane number has been demonstrated for diesel engine emissions where a reduction in HC emissions was observed with increasing cetane number (Bartlett et al., 1992).

From Figure 3, although unexpectedly higher emissions were observed during the high phase of the WLTC cycle, a general decrease in emissions was observed from the "Low" phase to the "Extra high" phase. This is a result of an increase in the engine and exhaust catalyst temperature which results in improved combustion conditions and catalytic oxidation during engine operation.

Aromatic hydrocarbon gas phase emissions

Semiquantitative analysis of the test fuel emissions was also conducted to identify target aromatic HCs. The target list contained 30 alkyl-benzenes. Figure 4 shows the relative gas phase alkyl-benzene emission factors of each fuel for each phase of the WLTC cycle. It is evident that the EUR10 fuel had the highest alkyl-benzene hydrocarbon emissions, followed by the SAM10 fuel and PAR10 fuel respectively. This trend was highly consistent with the fuel composition, as the EUR10 fuel has the highest alkyl-benzene fuel content and the SAM10 fuel the second highest.

Alkyl-benzene emissions were seen for the PAR10 fuel, although this fuel contains no alkyl-benzenes, thus emissions were suspected to be from residual alkyl-benzene emissions from the previous combustion of other fuels. To further investigate this, a

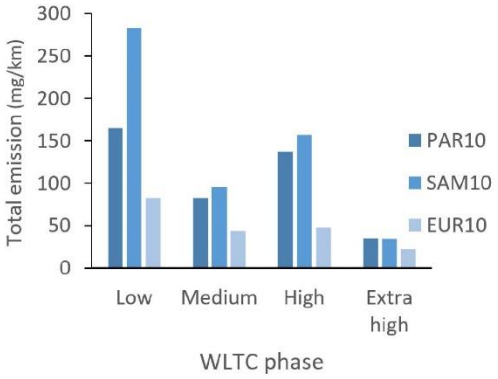

Figure 3: *Relative gas phase n-alkane cold start emissions summed up for each of the WLTC test cycle phases, for each test fuel.*

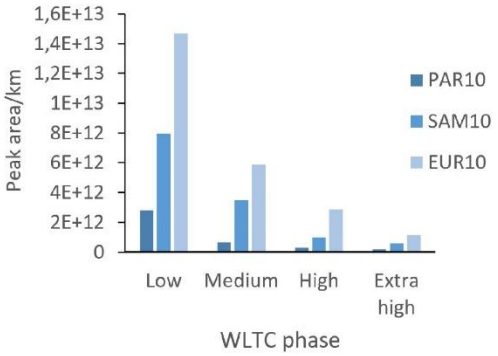

Figure 4: *Relative gas phase alkyl-benzene cold start emissions summed up for each of the WLTC test cycle phases, for each test fuel.*

qualitative analysis of the background samples was conducted. Background samples were taken with the engine switched off, however, the dilution ratio was kept constant to maintain the volume of incoming dilution air. Analysis of these samples confirmed that most of the target alkyl-benzenes were present at low levels in the background air.

Figure 5 shows a comparison of the peak areas of alkyl-benzenes identified in the emissions of the SAM10 fuel as compared to the background air.

Similar compounds to the ones reported in this study were found by other diesel exhaust characterisation studies (Alves et al., 2015, Gentner et al., 2013, Schauer et al., 1999). Comparing the emission factors however can be challenging as the emission factors of hydrocarbons from mobile sources have been shown to depend on engine design, engine operation and fuel composition (Cross et al., 2015), amongst other factors.

Effect of the exhaust after-treatment systems

To meet the increasingly stringent air quality limits regarding

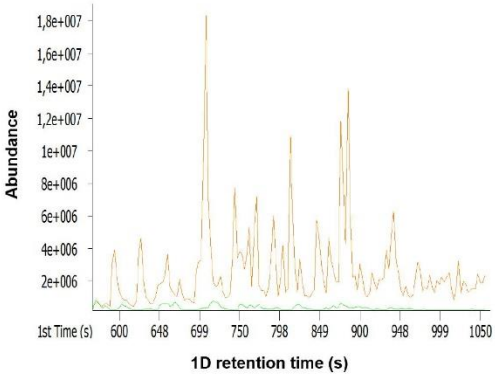

Figure 5: *Example extracted ion chromatograms (m/z = 91) showing the gas phase aromatic hydrocarbon emissions from SAM10 diesel cold start Phase 1 (top) as compared to the background air (bottom).*

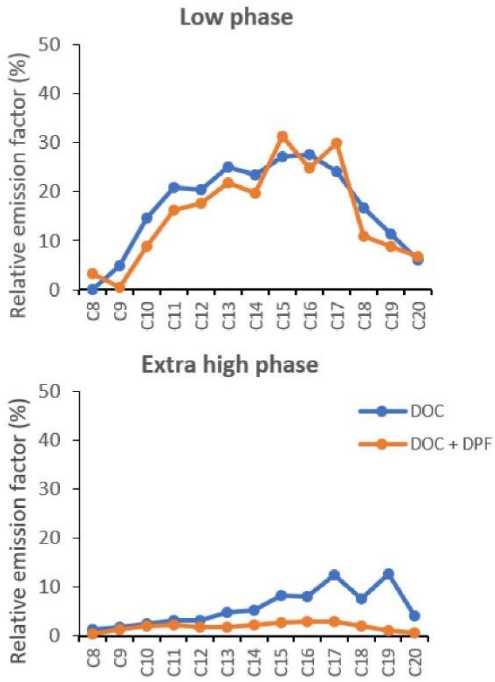

Figure 6: *Preliminary relative gaseous n-alkane emission factors for the DOC and DOC+DPF exhaust after-treatment configurations.*

vehicular exhaust emissions, modern day diesel vehicles have exhaust after-treatment systems, which may include a diesel oxidation catalyst (DOC), diesel particulate filter (DPF) and/or a selective catalytic reduction (SCR) system. To investigate the effect of the exhaust after-treatment system, emissions tests were performed using two configurations: DOC and DOC-DPF. Figure 6 shows the n-alkane relative emission factors for both configurations, during the low phase of the WLTC cycle.

Figure 7: *Quartz fibre filters used to collect particulate emissions for the EUR10 fuel during the low phase of the WLTC test cycle with the DOC only (left) and the DOC-DPF (right) in-line.*

The relative emission factors (%) were determined by expressing the emission factor of each n-alkane relative to that of the n-alkane with the highest emission factor (≡100). The results show a decrease in emissions from the low phase to the extra-high phase, which can be attributed to oxidation of gaseous hydrocarbon emissions by the DOC during high engine temperatures. The results also show lower emissions for the DOC-DPF configuration as compared to the DOC configuration. This was attributed to additional oxidation of HCs by precious metals found within the DPF as well as removal of hydrocarbons adsorbed onto the surface of particulate matter by the DPF.

Figure 7 shows the effective removal of soot and PM by the DPF. These results show the importance of the exhaust after-treatment system, however, the issue remains that optimum functioning of the DOC and regeneration of the DPF requires high engine temperatures which are seldom reached during low-speed city driving conditions.

Ozone formation potentials

The OFPs of the hydrocarbon emissions can be estimated using Carter's MIR indices which give the impact of each compound to the peak ozone concentration in a system where ozone is being formed under high NO_x concentrations, and is most sensitive to HC emissions (Carter 2010). The MIR index of each compound is given as the mass of additional ozone formed per mass of compound added to the emissions (gO_3/gVOC). Thus using the emission factors, the OFP of each compound can then be determined from the product of the emission factor (EFn) and MIR index (MIRn) of each alkane, where n refers to the alkane with n number of carbons (equation 1).

$$\text{OFP}[gO_3/km] = \text{EFn}\,[gVOC/km] \times \text{MIRn}\,[gO_3/gVOC] \quad (1)$$

Photochemical smog occurs predominantly in urban areas, thus phases 1 and 2 (low and medium) cold start emissions were chosen to study the OFP of the different fuels, as they consist of low speeds which are characteristic of urban driving conditions.

The photochemical smog formation potential of n-alkane emissions from each fuel differed. A comparison of the fuel emissions revealed that the SAM10 fuel emitted more ozone forming n-alkane and aromatic HC emissions than the other two fuels. EUR10 diesel had the least n-alkane emissions, however, it had relatively high aromatic HC emissions, which contributed to the OFP of this fuel, as these compounds have large MIR indices. The PAR10 fuel had relatively high n-alkane emissions, which have low MIR factors, although high emission factors would contribute to the OFP of this fuel.

From these results, it is evident that SVOCs arising from diesel emissions have the potential to contribute to photochemical ozone formation in the atmosphere, especially in urban traffic dense areas. The comparison between the test fuels cannot be regarded as conclusive, however, as diesel fuels also contain significant concentrations of branched and cyclic paraffins, which were not quantified in this study.

Conclusion

SVOC exhaust emissions from a diesel engine used in light-duty passenger vehicles were characterised for three fuels. The engine was operated over the WLTC driving cycle consisting of low, medium, high, and extra high speed phases. HC (n-alkane and aromatic) gas phase emissions arising from each fuel were then determined for each phase of the test cycle. The three test fuels showed differing levels of n-alkane and aromatic SVOC emissions, and hence their OFP differed, which could tentatively be explained by the physical and chemical characteristics of the fuels. A general decrease in n-alkane emissions was observed for each fuel when moving from the "Low" to the "Extra high" speed phase of the test cycle, and lower gas phase hydrocarbon emissions were observed in the presence of a DOC and DPF combination. This was attributed to increased engine temperatures which result in improved combustion conditions and optimal functioning of the DOC and DPF. Monitoring of semi-volatile HC emissions may be critical in understanding elevated ozone levels in urban areas, which are often higher than model predictions. This study has illustrated the successful use of denuders and comprehensive 2D gas chromatography with mass spectrometric detection to collect and characterise semi-volatile n-alkane and aromatic emissions from diesel exhaust. Such studies are important in better understanding the tropospheric ozone levels in South Africa and in informing air quality management practices.

Acknowledgements

The Sasol Fuels Application Centre is acknowledged for granting the use of the engine test cell facility and resources provided. Thanks to Mr. David Masemula for construction of PDMS traps and Dr. Yvette Naudé for assistance during instrumental analysis. Financial support from Sasol and the National Research Foundation (NRF) is highly appreciated.

NOTE: An earlier version of this paper was presented at the National Association of Clean Air (NACA) Conference and was published in its Proceedings.

References

Alves, C. A., Lopes, D. J., Calvo, A. I., Evtyugina, M., Rocha, S. & Nunes, T. 2015. Emissions from light-duty diesel and gasoline in-use vehicles measured on chassis dynamometer test cycles. *Aerosol Air Qual. Res*, 15, 99-116.

Bartlett, C., Betts, W., Booth, M., Giavazzi, F., Guttmann, H., Heinze, P. & Mayers, R. 1992. Diesel Fuel Aromatic Content and Its Relationship with Emissions from Diesel Engines. Congawe report no. 92/54.

Carter, W. Updated Maximum Incremental Reactivity Scale and Hydrocarbon Bin Reactivities for Regulatory Applications. 2010. *California Air Resources Board Contract*. 07e339.

Cross, E. S., Sappok, A. G., Wong, V. W. & Kroll, J. H. 2015. Load-dependent emission factors and chemical characteristics of IVOCs from a medium-duty diesel engine. *Environmental Science & Technology*, 49, 13483-13491.

Dunmore, R., Hopkins, J., Lidster, R., Lee, J., Evans, M., Rickard, A., Lewis, A. & Hamilton, J. 2015. Diesel-related hydrocarbons can dominate gas phase reactive carbon in megacities. *Atmospheric Chemistry and Physics*, 15, 9983-9996.

Ratshomo, K. & Nembahe, R. 2017. Overview of the Petrol and Diesel Market in South Africa between 2007 and 2016. Available [Online]: http://www.energy.gov.za/files/media/explained/Overview-of-Petrol-and-Diesel-Market-in-SA-between-2007-and-2016.pdf [Accessed 2019].

Forbes, P. B., Karg, E. W., Zimmermann, R. & Rohwer, E. R. 2012. The use of multi-channel silicone rubber traps as denuders for polycyclic aromatic hydrocarbons. *Analytica Chimica Acta*, 730, 71-79.

Forbes, P. B. & Rohwer, E. R. 2015, Chapter 5: Denuders, in Comprehensive Analytical Chemistry vol. 70: Monitoring of Air Pollutants: Sampling, Sample Preparation and Analytical Techniques, Patricia Forbes (ed.), pp. 153-181, *Elsevier*, Netherlands.

Gautam, M., Gupta, D., El-Gazzar, L., Lyons, D. W. & Popuri, S. 1996. Speciation of heavy duty diesel exhaust emissions under steady state operating conditions. *SAE Transactions*, 2337-2364.

Geldenhuys, G., Rohwer, E. R., Naudé, Y. & Forbes, P. B. 2015. Monitoring of atmospheric gaseous and particulate polycyclic aromatic hydrocarbons in South African platinum mines utilising portable denuder sampling with analysis by thermal desorption–comprehensive gas chromatography–mass spectrometry. *Journal of Chromatography A*, 1380, 17-28.

Gentner, D. R., Isaacman, G., Worton, D. R., Chan, A. W., Dallmann, T. R., Davis, L., Liu, S., Day, D. A., Russell, L. M. & Wilson, K. R. 2012. Elucidating secondary organic aerosol from diesel and gasoline vehicles through detailed characterization of organic carbon emissions. *Proceedings of the National Academy of Sciences*, 109, 18318-18323.

Gentner, D. R., Worton, D. R., Isaacman, G., Davis, L. C., Dallmann, T. R., Wood, E. C., Herndon, S. C., Goldstein, A. H. & Harley, R. A. 2013. Chemical composition of gas-phase organic carbon emissions from motor vehicles and implications for ozone production. *Environmental Science & Technology*, 47, 11837-11848.

Glasson, W. A. 1981. Effect of Hydrocarbon and NO x on Photochemical Smog Formation under Simulated Transport Conditions. *Journal of the Air Pollution Control Association*, 31, 1169-1172.

Jathar, S. H., Gordon, T. D., Hennigan, C. J., Pye, H. O., Pouliot, G., Adams, P. J., Donahue, N. M. & Robinson, A. L. 2014. Unspeciated organic emissions from combustion sources and their influence on the secondary organic aerosol budget in the United States. *Proceedings of the National Academy of Sciences*, 111, 10473-10478.

Kagawa, J. 2002. Health effects of diesel exhaust emissions—a mixture of air pollutants of worldwide concern. *Toxicology*, 181, 349-353.

Laban, T. L., Van Zyl, P. G., Beukes, J. P., Vakkari, V., Jaars, K., Borduas-Dedekind, N., Josipovic, M., Thompson, A. M., Kulmala, M. & Laakso, L. 2018. Seasonal influences on surface ozone variability in continental South Africa and implications for air quality. *Atmospheric Chemistry and Physics*, 18, 15491-15514.

Ladommatos, N., Parsi, M. & Knowles, A. 1996. The effect of fuel cetane improver on diesel pollutant emissions. *Fuel*, 75, 8-14.

Newkirk, M. S., Smith, L. R. & Merritt, P. M. 1993. Heavy-duty diesel hydrocarbon speciation: key issues and technological challenges. *SAE Technical Paper* 932853.

Olumayede, E. G. 2014. Atmospheric volatile organic compounds and ozone creation potential in an urban center of southern Nigeria. *International Journal of Atmospheric Sciences*. Article ID 764948 https://doi.org/10.1155/2014/764948

Reşitoğlu, İ. A., Altinişik, K. & Keskin, A. 2015. The pollutant emissions from diesel-engine vehicles and exhaust aftertreatment systems. *Clean Technologies and Environmental Policy*, 17, 15-27.

Robinson, A. L., Donahue, N. M., Shrivastava, M. K., Weitkamp, E. A., Sage, A. M., Grieshop, A. P., Lane, T. E., Pierce, J. R. & Pandis, S. N. 2007. Rethinking organic aerosols: Semivolatile emissions and photochemical aging. *Science*, 315, 1259-1262.

Schauer, J. J., Kleeman, M. J., Cass, G. R. & Simoneit, B. R. 1999. Measurement of emissions from air pollution sources. 2. C1 through C30 organic compounds from medium duty diesel trucks. *Environmental Science & Technology*, 33, 1578-1587.

Storey, J. M., Domingo, N., Lewis, S. A. & Irick, D. K. 1999. Analysis of semivolatile organic compounds in diesel exhaust using a novel sorption and extraction method. *SAE Technical Paper* 1999-01-3534.

Wichmann, H.-E. 2007. Diesel exhaust particles. *Inhalation Toxicology*, 19, 241-244.

Zunckel, M., Venjonoka, K., Pienaar, J., Brunke, E., Pretorius, O., Koosialee, A., Raghunandan, A. & Van Tienhoven, A. 2004. Surface ozone over southern Africa: synthesis of monitoring results during the Cross border Air Pollution Impact Assessment project. *Atmospheric Environment*, 38, 6139-6147.

UNIVERSITEIT VAN PRETORIA
UNIVERSITY OF PRETORIA
YUNIBESITHI YA PRETORIA

SASOL

Characterisation of semi-volatile hydrocarbon emissions from diesel engines